UNIVERSITY OF CALIFORNIA
Los Angeles

Microbial Regulation of Methane and Redox Dynamics in the Water Column: From a Proterozoic Ocean Analog to Modern Marine Seeps

A dissertation submitted in partial satisfaction of the
requirements for the degree Doctor of Philosophy
in Geochemistry

by

Emily F. Klonicki-Ference

2025

ABSTRACT OF THE DISSERTATION

Microbial Regulation of Methane and Redox Dynamics in the Water Column: From a Proterozoic Ocean Analog to Modern Marine Seeps

by

Emily F. Klonicki-Ference

Doctor of Philosophy in Geochemistry

University of California, Los Angeles, 2025

Professor Tina Irene Treude, Chair

Microbial methane oxidation modulates redox structure, regulates methane flux, and drives carbon cycling in marine environments, with implications for both Earth's biospheric evolution and the functioning of modern ecosystems. This thesis examines water column methanotrophy across environmental settings, from a Proterozoic Ocean analog to modern cold seeps, to address two central questions: (1) What role might methane oxidation have played in influencing oxygen levels and redox balance in Mesoproterozoic oceans? (2) How do environmental regimes, physical transport, and seep dynamics shape water column methanotrophy and its influence on the fate and footprint of methane in modern oceans?

Addressing Question 1, we studied methane oxidation across a steep geochemical gradient in Green Lake, a meromictic, euxinic lake in Fayetteville, New York, used as a Mesoproterozoic Ocean analog. High rates of methanotrophy and sulfate reduction co-occurred below the chemocline, alongside monomethylamine-based methanogenesis. Aerobic methanotrophs, including *Crenothrix* and *Methylacidiphilales*, were likely active in the euxinic waters forming an efficient methane filter, potentially via denitrification or fermentation. A sulfide-dominated redox imbalance limited oxygen intrusion and fueled microbial activity, creating a model for how microbial feedbacks may have modulated oxygen availability and redox stability in early oceans.

For Question 2, contrasting seep environments were explored: low-oxygen sites along the Southern California margin (~400–1000 m) and fully oxygenated seeps in the Gulf of Alaska (~2000–5000 m). In Southern California, aerobic methanotrophs were vertically structured and widespread, with consistent near-seafloor abundance of the particulate methane monooxygenase (*pmoA*) gene. Oxidation was closely coupled to methane and pmoA at Santa Monica Mound but showed weaker associations at Del Mar and Lasuen Knoll. Alaskan sites revealed diverse controls: oxidation tracked methane at Edge, aligned with both methane and pmoA at Shumagin, and persisted at Sanak despite low *pmoA* abundance, possibly reflecting lateral methane transport and tidal influence. Lateral transects across Sanak, Santa Monica, and Del Mar showed oxidation extending beyond seep boundaries, likely shaped by bottom currents. These patterns suggest water column methanotrophy forms a spatially dynamic, functionally cohesive microbial envelope structured by oxygen, methane gradients, and physical transport, mediating carbon flow to support ecosystems across seep and off-seep environments.

The dissertation of Emily Klonicki-Ference is approved.

Craig E. Manning

Edwin Arthur Schauble

Shaily Mahendra

Tina Irene Treude, Committee Chair

University of California, Los Angeles

2025

Table of Contents

List of Figures

List of Tables

Acknowledgments

With my sincerest gratitude, I would like to thank my advisor, Tina Treude, for introducing me to the fields of geomicrobiology and marine biogeochemistry. Under your guidance, I have grown immensely as a scientist and had opportunities I could never imagine. I'm deeply thankful for the intellectual freedom you provided, which allowed me to explore new directions and develop my scientific voice. Your passion, dedication, and meticulous attention to detail (including packing lists) are qualities I greatly admire and hope to carry forward. Your mentorship has shaped both my technical abilities and broader perspective, and I look forward to future opportunities to collaborate in whatever form they may take.

I also wish to thank my thesis committee members Craig Manning, Edwin Schauble, and Shaily Mahendra for their valuable research insights, as well as their thoughtful guidance and support for my professional development. The EPSS community at UCLA, including faculty, researchers, and administrative staff, has played a meaningful role in supporting my time here. I would particularly like to thank Sebastian Krause, Jiarui Liu, George Vetushko, Kira Homola, David Yousavich, De'Marcus Robinson, Jeana Drake, Rhegan Thomason, Max Packebush, and all the brilliant Treude Lab undergraduates for their friendship. I would like to acknowledge those who have offered valuable guidance, mentorship, or contribution throughout the course of my PhD research: Timothy Lyons, Michael McCormick, David Valentine, William Schopf, Lisa Levin, Victoria Orphan, Peter Girguis, Shana Goffredi, the Biotechnology and Planetary Protection Group and my colleagues at NASA JPL. I would like to recognize the contributions of the dedicated crews of the research vessel *Atlantis*, the *Alvin* team, and the funding agencies that supported my research, particularly NASA and the NSF.

I would like to warmly thank the Orphan Lab, whom I had the pleasure of working closely with throughout my PhD. Your friendship, guidance, and patience with all my questions made the experience deeply rewarding and significantly expanded my technical skills. I truly value the time we shared and hope to continue collaborating in the future. I would like to express my sincere gratitude to David Sanchez at the University of Pittsburgh for introducing me to environmental engineering and guiding me through the early stages of my academic journey. Your mentorship helped spark my passion for the field as I began to find my direction as a researcher. I am also grateful to the science educators who inspired me to think big and nurture my scientific curiosity.

I feel especially grateful to my friends who have encouraged me every step of the way. I particularly wish to thank Sierra and Ryan McGlynn, Julie Fornaciari, Ryan Fauver, Paige and Cameron Beichner, Macy Yu, Zachary Margolies, Logan and Gavin Kosko, Ryan and Amy Hendrickson, Marissa Cameron, Lizzie Lust, Taylor Shearer, Alyssa Staniland and Doug Heckman.

Finally, I want to express my heartfelt gratitude to my family; Addy and Kent Truslow, Dominic and Joshua Klonicki, the Ference and Henderson families, Cedar, my extended family, and all my wonderful nieces and nephews Isaac, Evelyn, Owen, Scarlett, and Marina. To my parents, Ann Feyock and Steve Klonicki, your love for children empowered us to pursue our passions, so thank you for the years of unwavering encouragement and support. I am incredibly fortunate to have you both as parents and deeply grateful for the foundation you've given me. To my husband Christian Ference, I hope everyone is lucky enough to have someone in their life who offers the kind of love, care, and support you've given me throughout our journey together. Thank you for all that you do for our family and for removing obstacles so I could pursue my dreams. You continually inspire me to follow my passions and believe in what's possible. I love you immensely and look forward to the many adventures ahead.

Vita/Biographical Sketch

Emily Klonicki-Ference

Education

University of California, Los Angeles 2023

Master of Science in Geochemistry

University of Pittsburgh (Pittsburgh) 2018

Bachelor of Science in Microbiology

Selected Publications

In Review

Klonicki-Ference, E., Waters, T., Jones, C., Hung, C., Diamond, C., McCormick, M., Lyons, T., Treude, T. Microbial Redox Cycling Sustains Euxinia and Limits Methane Escape in a Proterozoic Ocean Analog. *submitted to ISME*.

Published

Liu, J., **Klonicki-Ference, E**., Krause, S. J., & Treude, T. (2024). Iron oxides fuel anaerobic oxidation of methane in the presence of sulfate in hypersaline coastal wetland sediment. Environmental Science & Technology, 59(1), 513-522.

Klonicki-Ference, E. F., Malaska, M. J., Panning, M. P., Waller, S. E., & Gasda, P. J. (2023). Instrumentation for Planetary Exploration. In Handbook of Space Resources (pp. 277-306). Cham: Springer International Publishing.

Dean, Z. S., DiNicola, M., **Klonicki, E**., Roberts, S., Clement, B. G., & Guan, L. (2022). Establishing Sterility Assurance for Bacillus canaveralius 29669 Spores Under High Heat Exposure. Frontiers in Microbiology, 13, 909997.

Hand, K., et al., including **Klonicki, E**., (2022) Science Goals and Mission Architecture of the Europa Lander Mission Concept. Planetary Science Journal. 3 22

Hand, K. et al. including **Klonicki, E**., (2021) Science of the Europa lander mission concept. Bull. AAS **53**, 352.

Field Experience

AT50-24 RV *Atlantis* Gulf of Alaska Methane Seeps, *Alvin* Dive 5278, UCLA	2024
AT50-12 RV *Atlantis* Southern California Methane Seeps, *Alvin* Dive 5197, UCLA	2023
AT50-11 RV *Atlantis* Santa Barabara Basin, *Alvin* Dive 5185, UCLA	2023
Biogeochemical Methane Cycling, Fayetteville Green Lake, New York. UCLA	2022

Selected Awards

Outstanding Student Presentation Award, American Geophysical Union Fall Meeting	2025
Europa Clipper Team Award, NASA Jet Propulsion Laboratory	2025
NSF Graduate Research Fellowship Program, Honorable Mention	2022
Europa Lander Team Award, NASA Jet Propulsion Laboratory	2021; 2022
Outstanding Abstract Award, American Society for Microbiology	2019

Chapter 1: Introduction

1. Sources and sinks of methane

1.1 Overview

While methane (CH_4) is often noted for its role as a potent greenhouse gas (Etminan et al., 2016), it is equally important as a fundamental intermediate in the global carbon cycle. Methane is produced biologically through microbial methanogenesis, thermogenically via the breakdown of organic matter at elevated temperatures and pressures, and abiotically through inorganic water–rock reactions, often involving ultramafic rocks and hydrothermal systems. Natural sources include wetlands, lakes, peatlands, permafrost, and marine sediments, while anthropogenic sources such as ruminant digestion, rice cultivation, fossil fuel extraction, and landfills have contributed to rising atmospheric concentrations (Etiope & Sherwood Lollar, 2013; Saunois et al., 2025). Globally, wetlands are the dominant natural emitter, while geological contributors, including submarine seeps and mud volcanoes, account for a smaller but geochemically significant fraction (Kopf, 2003). Once formed, methane acts as a mobile vector for carbon and energy, fueling microbial metabolism through aerobic and anaerobic oxidation and linking carbon turnover to broader biogeochemical cycles. Beyond Earth, methane has been detected in the atmospheres of Mars and the outer planet moons, where its presence raises questions about the roles of geological versus biological sources and has made it a key target for biosignature detection in both planetary science and exoplanet research (Formisano et al., 2004; Lefevre & Forget, 2009; Webster et al., 2018; Yung et al., 2018). As such, methane not only contributes significantly to Earth's modern biogeochemistry, but likely also played a role in shaping its early biosphere (Catling et al., 2001) and serves as a window into the metabolic potential of other worlds.

1.2 Marine methane cycling

1.2.1 Methane cycling in the sediment

Methane in the ocean originates from a range of geological and biological sources that vary in depth, spatial extent, and temporal persistence. Hydrothermal vents and volcanic centers emit methane through high-temperature alteration of crustal rocks and thermal decomposition of organic matter (Reeves & Fiebig, 2020). Serpentinization of ultramafic rocks produces hydrogen-rich fluids that can drive abiotic methane synthesis via Fischer–Tropsch-type reactions (Etiope, 2017). Gas hydrate deposits, which form under conditions of low temperature and high pressure along continental margins, store vast quantities of methane in solid form and can release it through dissociation triggered by warming or pressure change (Kvenvolden & Claypool, 1988). Microbial activity in anoxic marine sediments, generates substantial methane through the anaerobic degradation of organic matter. Methane produced microbially or geologically in the subsurface can be transported upward and released at the seafloor via focused discharge zones known as methane seeps. These seeps occur across diverse tectonic and sedimentary settings, forming conduits for methane-rich fluids to reach the seafloor and sustain high-biomass communities through chemosynthetic production (Levin, 2005).

Cold seeps, once considered rare and of limited ecological significance, are now recognized as widespread features along continental margins (Judd & Hovland, 2009) and as ecologically important hotspots that influence local biodiversity, biogeochemistry, and carbon cycling (Boetius & Wenzhöfer, 2013; Levin, 2005). Methane discharged at seeps originates from both microbial methanogenesis and deeper thermogenic sources and may also be released from hydrate deposits

that store methane derived from these processes. Fluxes span several orders of magnitude across different systems (Boetius & Wenzhöfer, 2013).

In seep sediments, methane is primarily produced under anoxic conditions via microbial methanogenesis, which utilizes substrates such as carbon dioxide (CO_2), acetate, and methylated compounds.

(Eq. 1) $CO_2 + 4H_2 \rightleftharpoons CH_4 + 2H_2O$

(Eq. 2) $CH_3COOH \rightleftharpoons CH_4 + CO_2$

(Eq. 3) $4CH_3OH \rightleftharpoons 3CH_4 + CO_2 + 2H_2O$

Hydrogenotrophic methanogenesis (Eq. 1) involves the stepwise reduction of carbon dioxide to methane, facilitated by a series of enzymes and redox reactions. Four of the seven enzymatic steps require electron transfer mediated by cofactors such as ferredoxin, coenzyme F_{420}, and coenzyme B (HS-CoB) (Thauer et al., 2008). In the acetoclastic pathway (Eq. 2), acetate (present predominantly as CH_3COO^- in solution) is first converted to acetyl-CoA; its methyl group enters the hydrogenotrophic branch via tetrahydromethanopterin (H_4MPT), while the carbonyl group is oxidized to carbon dioxide (Welte & Deppenmeier, 2014). Methylotrophic methanogenesis (Eq. 3) bypasses intermediate steps by directly transferring a methyl group from methanol or related compounds to HS-CoM, forming methyl-coenzyme M. This intermediate is processed through oxidative and reductive branches that generate carbon dioxide and methane in a roughly 1:3 ratio to balance the electron budget (Vanwonterghem et al., 2016). While all three methanogenic pathways are thermodynamically reversible, only the hydrogenotrophic route has been clearly shown to operate in reverse under natural conditions, typically with electrons transferred to external acceptors rather than producing H_2 (Scheller et al., 2010; Thauer, 2011).

However, in the upper sediment column, methanogenesis is often suppressed due to competition with sulfate-reducing bacteria (SRB), which outcompete methanogens for shared intermediates like hydrogen and acetate because sulfate reduction yields more energy (Kristjansson et al., 1982; Lovley & Klug, 1983). As a result, hydrogenotrophic methanogenesis generally occurs deeper in the sediment column, beneath the sulfate reduction zone, where sulfate is depleted and fermentation byproducts accumulate. Much of the methane produced in sediments is consumed via the anaerobic oxidation of methane (AOM) before it can escape, which serves as the primary biological sink limiting methane release from the seafloor. AOM is typically performed by anaerobic methanotrophic archaea (ANME) in syntrophic partnership with sulfate-reducing bacteria. In this metabolic cooperation, ANME activate and partially oxidize methane and transfer electrons to SRB, which reduce sulfate (SO_4^{2-}), the dominant terminal electron acceptor in marine sediments (Boetius et al., 2000; Knittel & Boetius, 2009; Orphan et al., 2001). The reaction proceeds as:

(Eq. 4) $CH_4 + SO_4^{2-} \rightarrow HCO_3^- + HS^- + H_2O$

where the oxidation of methane with the reduction of sulfate produces bicarbonate (HCO_3^-), hydrogen sulfide (HS^-), and water (H_2O).

This sulfate-driven AOM occurs in the sulfate–methane transition zone (SMTZ), a narrow biogeochemical interface where methane and sulfate gradients converge. In sulfate-poor or metal-rich sediments, alternative electron acceptors such as nitrate (Ettwig et al., 2010), nitrite (Haroon et al., 2013), ferric iron (Fe^{3+}), and manganese oxides (Mn^{4+}) (Beal et al., 2009) can also support AOM. In addition, microbial sulfate reduction in sediments generates hydrogen sulfide, which fuels sulfur-oxidizing microbial mats and supports chemosymbiotic fauna such as tubeworms and bivalves inhabiting the seafloor (Levin, 2005). These processes help structure sedimentary redox gradients,

promote the precipitation of authigenic carbonates, and sustain benthic ecosystems. AOM thus serves as the primary microbial barrier regulating methane flux from sediments into the overlying ocean.

1.2.2 Marine authigenic carbonates

The microbial processes that drive AOM in sediments also promote the precipitation of carbonate minerals. AOM, coupled to sulfate reduction, generates bicarbonate and increases alkalinity, leading to the formation of calcium carbonate ($CaCO_3$) in the presence of calcium ions (Bohrmann et al., 1998; Greinert et al., 2002; Michaelis et al., 2002). These authigenic carbonates frequently accumulate in sediments at or near the SMTZ and can grow upward into the overlying water column, forming prominent features of cold seep environments. Recent studies have shown that seep carbonates not only archive past methane flux but also serve as active habitats for methanotrophic archaea and sulfate-reducing bacteria, contributing directly to *in situ* methane oxidation and continued AOM-linked carbonate formation (Marlow et al., 2014). Hydrogen sulfide produced during AOM can further promote carbonate precipitation and react with metal ions to form sulfide minerals that co-precipitate with carbonate phases, influencing both the structure and geochemistry of the resulting deposits (Karaca et al., 2010).

Over time, these processes lead to the accumulation of carbonate mounds, crusts, and pavements that can persist for thousands of years (Crémière et al., 2016; Kutterolf et al., 2008). These structures act as stable, elevated hard substrates in otherwise soft sediment environments, fostering microbial mats, sessile invertebrates, and ecologically rich benthic communities (Levin, 2005; Suess, 2010). In this way, AOM-linked carbonate formation reinforces the spatial structure, ecological longevity, and geochemical function of seep ecosystems.

1.2.3 Benthic fauna and microbial symbiosis

The chemical gradients created by methane seepage and associated carbonate structures provide habitat for a wide variety of benthic organisms, many of which are tightly linked to microbial processes. Prominent macrofauna at cold seeps, including bathymodiolin mussels (Childress et al., 1986), vestimentiferan tubeworms (Levin, 2005), feather duster worms (Goffredi et al., 2020), ciliates (Pasulka et al., 2017), and sponges (Rubin-Blum et al., 2019), harbor intracellular bacterial symbionts capable of oxidizing methane or reducing sulfur compounds, allowing them to exploit the chemosynthetic energy sources available at the seafloor. These symbiotic associations enable animals to thrive in environments that are rich in reduced compounds but may be depleted in oxygen and photosynthetic inputs. In addition to symbiosis, many benthic invertebrates, including ampharetid polychaetes and gastropods, graze directly on microbial mats composed primarily of sulfur-oxidizing bacteria, incorporating chemosynthetic carbon into broader food webs (Levin et al., 2016; Levin & Michener, 2002).

The stability and elevation provided by authigenic carbonate outcrops allow these communities to persist over long timescales, often developing complex assemblages structured by methane gradients and fluid flow (Cordes et al., 2010). Microbial mats, which may carpet carbonate and sediment surfaces, not only support grazing organisms but also modulate local geochemistry through the oxidation of hydrogen sulfide and methane. The interactions between microbial metabolism, carbonate formation, and chemosynthetic fauna highlight the ecological integration of methane seep systems and their role in sustaining biodiversity, carbon flow, and sediment redox balance.

1.2.4 Water column

While much of the methane produced in sediments is consumed by anaerobic oxidation, a portion escapes or exceeds the capacity of benthic AOM and enters the overlying water column. There, aerobic methane oxidizing bacteria (MOB) oxidize methane using oxygen as a terminal electron acceptor, converting CH_4 to CO_2 and water (Reeburgh, 2007), according to the reaction:

(Eq. 5) $CH_4 + 2O_2 \rightarrow CO_2 + 2H_2O$

These bacteria play a key role in mitigating methane flux to the atmosphere and are widely distributed throughout the marine water column, from oxygenated surface strata to low-oxygen and anoxic zones, depending on local oxygen concentrations, methane availability, and particulate flux (Steinle et al., 2015; Steinle et al., 2017; Tavormina et al., 2008; Thamdrup et al., 2019). Aerobic methane oxidation is catalyzed by methane monooxygenase (MMO), the enzyme that converts methane to methanol which is the rate-limiting first step in this pathway (Grosse et al., 1999). Two forms of MMO exist: particulate MMO (pMMO), a membrane-bound, copper-dependent enzyme expressed by most marine MOB under high-copper conditions, and soluble MMO (sMMO) (Grosse et al., 1999), an iron-containing, cytoplasmic enzyme expressed under copper limitation in some lineages (Chen et al., 2012; Semrau et al., 2010). The presence and expression of these enzymes reflect environmental metal availability and influence the spatial distribution and efficiency of methane oxidation in seawater (**Fig. 1**).

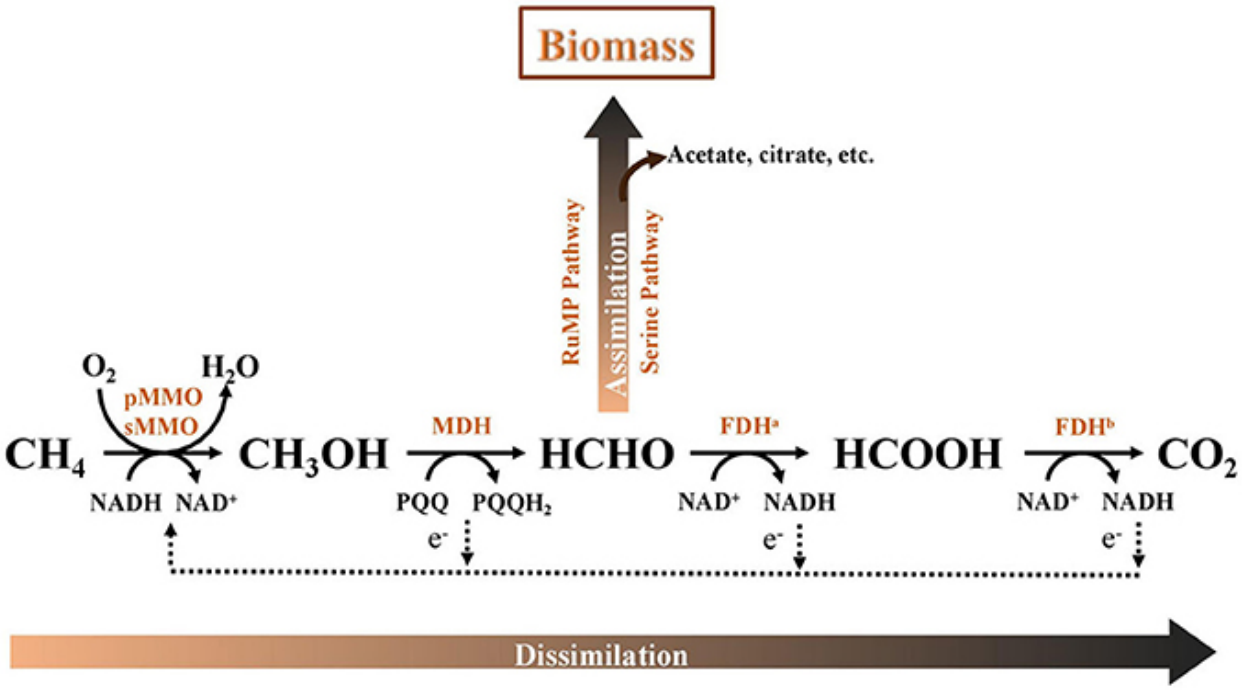

Figure 1. Aerobic methane metabolism in bacterial methanotrophs from (Zhu et al., 2016). Methane (CH_4) is first oxidized to methanol (CH_3OH) by either particulate methane monooxygenase (pMMO) or soluble methane monooxygenase (sMMO), using O_2 and reducing equivalents from NADH. Methanol is then oxidized to formaldehyde (HCHO) via methanol dehydrogenase (MDH), which transfers electrons through pyrroloquinoline quinone (PQQ). Formaldehyde can follow one of two routes: dissimilation through further oxidation to formate (HCOOH) and carbon dioxide (CO_2) via formaldehyde dehydrogenase (FDHa) and formate dehydrogenase (FDHb), or assimilation into biomass via the ribulose monophosphate (RuMP) or serine pathway, generating intermediates such as acetate and citrate. NAD^+/NADH mediate electron flow in the latter oxidation steps.

In addition to their free-living forms, MOB participate in symbiotic associations with a range of marine animals. As described in Section 1.2.3, diverse benthic invertebrates in methane-rich environments host methanotrophic endosymbionts. These bacteria oxidize methane using the

pMMO enzyme, enabling the conversion of methane to methanol and ultimately to biomass that sustains their hosts. Most symbionts belong to the Gammaproteobacteria, particularly the *Methylococcaceae*, and use the ribulose monophosphate (RuMP) pathway for formaldehyde assimilation (Rubin-Blum et al., 2019). Although they occur across a range of redox conditions, symbiotic methanotrophs rely on oxygen as the terminal electron acceptor, supporting methane oxidation in low-oxygen or oxygenated host microenvironments (Petersen & Dubilier, 2009). Through this process, symbiotic MOB effectively transform methane into organic carbon, sustaining animal hosts in environments devoid of photosynthetic input.

Relatively low methane fluxes from sediments can support aerobic methanotrophy in the water column, where these processes shape microbial community composition, influence methane concentrations, and contribute methane-derived carbon to pelagic food webs (Pack et al., 2015; Steinle et al., 2015). Water column methanotrophy may also contribute to oxygen consumption, nutrient regeneration, and the attenuation of methane fluxes to the atmosphere, particularly in low-oxygen zones. While this thesis primarily investigated sediment-derived methane fluxes, surface water methane can also originate from *in situ* microbial production, particularly during periods of high primary productivity. Methanotrophic communities in these surface layers, often associated with phytoplankton blooms, may be stimulated by organic precursors such as dimethylsulfoniopropionate (DMSP), which is released by phytoplankton under bloom conditions (Karl et al., 2008; Klintzsch et al., 2019). Observations from the Arctic Shelf suggest that DMSP can support a coupled cycle of methylotrophic methanogenesis and methane oxidation in oxygenated surface waters, providing an additional pathway for methane turnover in pelagic systems (Damm et al., 2010).

In marine systems, oxygen availability largely governs the activity and vertical distribution of aerobic methanotrophs, which require oxygen as a terminal electron acceptor but can remain active under microaerobic conditions (Reeburgh, 2007; Steinle et al., 2015; Thamdrup et al., 2019). The input of organic matter further shapes oxygen concentrations by fueling heterotrophic respiration, which consumes oxygen and promotes the development of suboxic and anoxic conditions. In sediments, this stratification establishes vertical gradients in the availability of oxygen, methane, and alternative electron acceptors such as sulfate. These gradients govern whether methane is oxidized aerobically at oxic–anoxic interfaces or anaerobically at depth via ANME and SRB (Boetius et al., 2000), in addition to the efficiency at which it is consumed. The depth of oxygen penetration in the sediment, and thus the location of key redox boundaries, is strongly influenced by the oxygen content of the overlying bottom water, which in turn is shaped by physical processes such as mixing, upwelling, and ventilation events (Kämpf & Chapman, 2016).

1.2.5 Defining the methanosphere

The ocean methanosphere encompasses the broader biogeochemical and ecological zone influenced by methane flux, extending beyond the immediate vicinity of seepage (depicted in **Fig. 2**). As discussed in the introduction of this thesis, it integrates the full suite of methane-linked processes and interactions: microbial communities that oxidize methane (Knittel & Boetius, 2009; Reeburgh, 2007), animals that engage in direct symbiosis with methanotrophs or graze on methane-fueled microbial mats (Levin, 2005; Pasulka et al., 2017), and transitional benthic fauna that benefit indirectly from methane through trophic pathways or the colonization of methane-derived authigenic carbonates (Suess, 2010). Though methane emission may be spatially localized, transport processes such as bubble-mediated flux (Jordan et al., 2020), vertical mixing, and lateral

advection expand the footprint of methane and methanotrophic activity (Ussler III et al., 2013). The extent and structure of the methanosphere therefore help define both the fate of methane in the ocean and its ecological footprint, shaping carbon transfer, methane and oxygen gradients, and microbial–metazoan connectivity at local to regional scales.

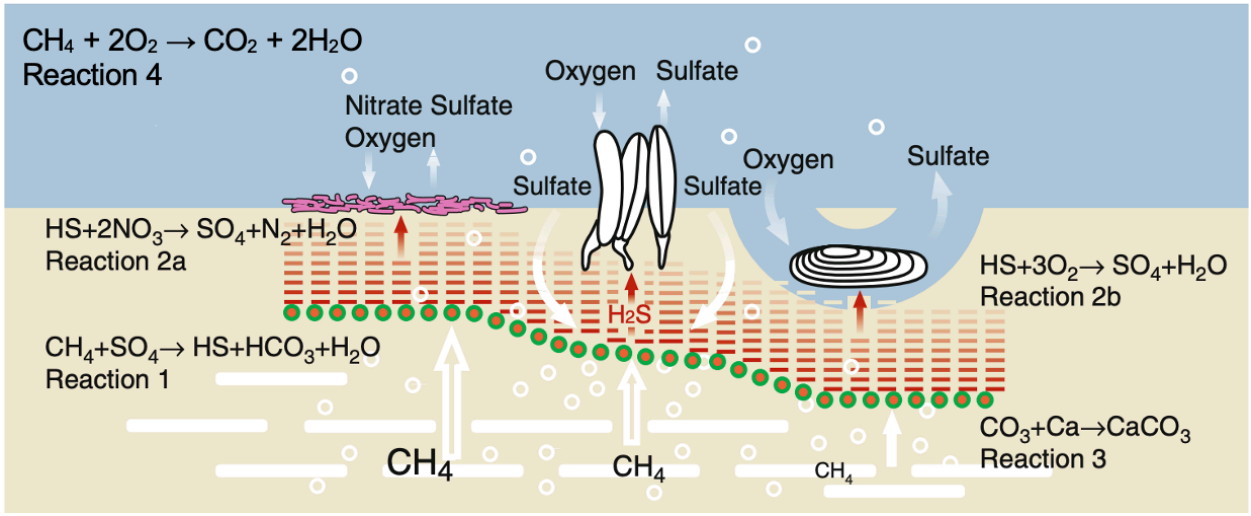

Figure 2. Schematic of key microbial processes in the methanosphere. Methane rising from sediments at varying flux rates fuels AOM by the ANME/SRB microbial consortia (red–green circles), which couple CH_4 oxidation to sulfate reduction (Reaction 1). The resulting hydrogen sulfide (H_2S) diffuses upward and is oxidized by seafloor sulfur oxidizing microbial mats or symbiotic macrofauna using nitrate or oxygen (Reactions 2a, 2b). These processes create localized redox gradients in the sediment and promote calcium carbonate precipitation (Reaction 3), though it is also produced through Reaction 1. Additional CH_4 may escape into the water column and undergo aerobic oxidation by MOB (Reaction 4). Modified from Suess, 2010.

1.3 Metabolic flexibility within methane oxidizing bacteria

While marine cold seeps have yielded critical insights into methane-based ecosystems and anaerobic methane oxidation, methanotrophy has also been extensively studied in freshwater lakes, wetlands, rice paddies, and upland soils, where it serves as a major biological control on methane fluxes to the atmosphere (Conrad, 2009; Hanson & Hanson, 1996). Among these, meromictic and euxinic lakes are particularly informative for examining methane cycling under stratified redox conditions. These environments support both aerobic and anaerobic methanotrophic communities that operate across steep oxygen and chemical gradients, offering valuable perspectives on methane oxidation pathways under diverse geochemical regimes (Crowe et al., 2011; Oswald, Jegge, et al., 2016; Oswald, Milucka, et al., 2016).

MOB exhibit remarkable metabolic plasticity that allows them to adapt to a wide range of environmental conditions. For example, members of the NC10 phylum, such as *Candidatus Methylomirabilis oxyfera*, oxidize methane anaerobically by reducing nitrite through a unique intra-aerobic pathway that generates intracellular oxygen via nitric oxide dismutation (Ettwig et al., 2010; Haroon et al., 2013; He et al., 2016; Wu et al., 2011). In ferruginous and manganiferous environments, certain bacterial communities couple methane oxidation to the reduction of metal oxides such as Fe(III) and Mn(IV) (Sivan et al., 2011). Similarly, quinone-rich humic substances can serve as extracellular electron acceptors under anoxic conditions, enhancing methane removal by facultative methanotrophs (Smemo & Yavitt, 2007). Although aerobic methanotrophs classically use oxygen as a terminal electron acceptor, members of both Type I (Gammaproteobacteria) and Type II (Alphaproteobacteria) lineages have demonstrated the capacity to utilize alternative electron acceptors or carbon substrates under oxygen-limited conditions. Some strains, for example, possess genes involved in denitrification and can reduce nitrate or nitrous oxide (Awala et al., 2024; He et al., 2022), while others, such as acidophilic methanotrophs in the genera *Methylacidiphilum*

and *Methylocella*, are capable of anaerobic growth via nitrous oxide respiration (Awala et al., 2024). Aerobic methanotrophs have also been detected in environments with limited or no detectable oxygen, including meromictic lakes, rice paddies, peatlands, and the deep biosphere (Knief, 2015; Kotelnikova, 2002; Oswald, Jegge, et al., 2016), suggesting they may be capable of sustaining methane oxidation under conditions previously considered unsuitable for aerobic metabolism.

Recent evidence points to fermentation-based methanotrophy as another strategy for MOB survival in reduced environments. For example, *Methylomicrobium* strains have been shown to ferment methane-derived intermediates into organic acids under low-oxygen conditions (Gilman et al., 2017; Kalyuzhnaya et al., 2013), while metagenomic analyses from Lake Zug identified widespread transcription of fermentative genes in MOB under anoxic conditions (Schorn et al., 2024). This metabolic flexibility underscores the diverse physiological strategies methanotrophs use to access methane-derived carbon and energy across steep redox gradients in aquatic systems.

1.4 Global methane budget

Methane plays a dynamic role in the global carbon cycle, with its production and consumption spanning terrestrial ecosystems, aquatic environments (as explored throughout this thesis), and atmospheric processes. Recent estimates place total global emissions between ~575 and 670 Tg CH_4 yr^{-1}, based on top-down and bottom-up approaches, respectively (Saunois et al., 2025) (**Fig. 3**). Approximately 60% of these emissions are anthropogenic, originating from agriculture (e.g., enteric fermentation, rice paddies), fossil fuel systems, landfills, and biomass burning, while the remaining emissions arise from natural sources including wetlands, freshwater systems, geologic seepage, and marine sediments (Kirschke et al., 2013).

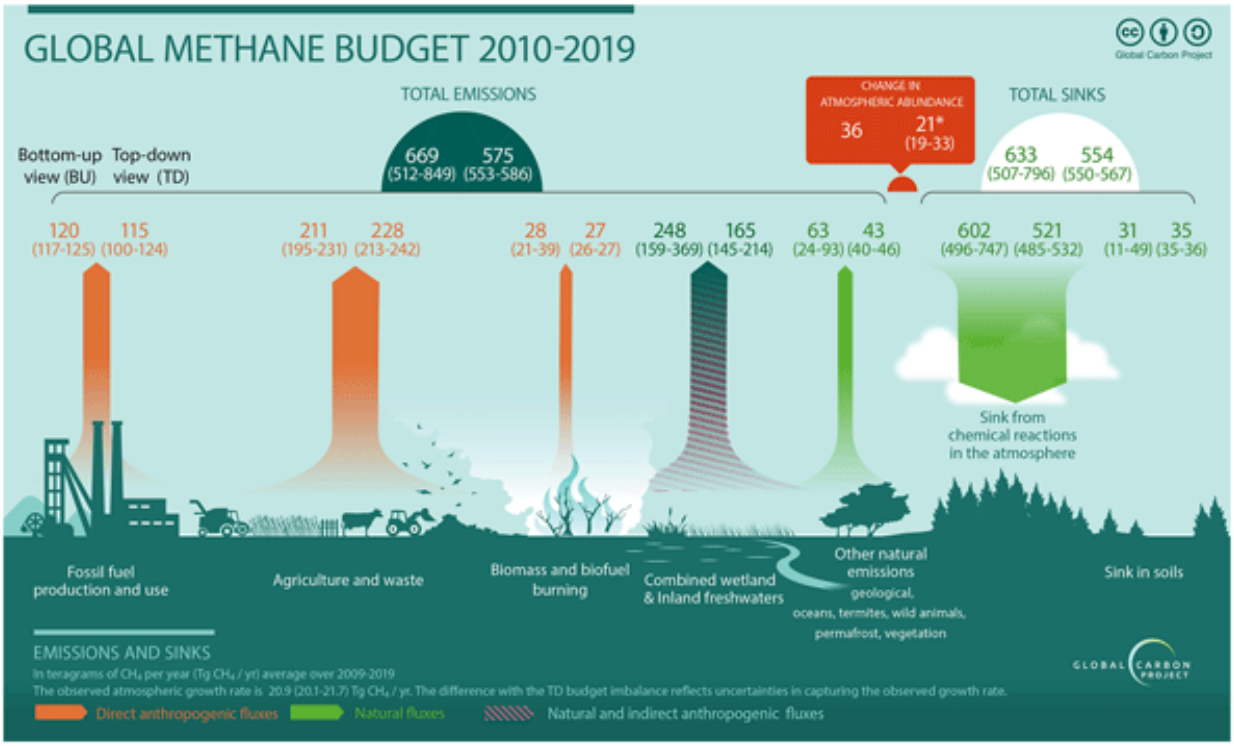

Figure 3. Bottom-up (left) and top-down (right) estimates of methane emissions and sinks from 2010–2019, expressed in Tg CH_4 yr^{-1}. Emission sources include fossil fuels, agriculture and waste, biomass burning, wetlands, and other natural sources. Sinks include atmospheric oxidation and soil uptake. Total emissions and sinks are shown alongside the observed increase in atmospheric methane. Taken from Saunois et al. (2024).

Wetlands represent the largest natural source of methane globally, followed by inland waters such as lakes, rivers, and reservoirs, where microbial methanogenesis is fueled by organic matter degradation under anoxic conditions (Bastviken et al., 2011; Matthews & Fung, 1987). Although the ocean contributes a relatively small fraction of the total CH_4 flux to the atmosphere (~1–5%), large amounts of methane are stored in marine sediments and hydrates (Kvenvolden & Claypool, 1988) and may be mobilized through destabilization or seepage. Atmospheric methane is primarily removed through oxidation by hydroxyl radicals (OH) in the troposphere, which

accounts for roughly 90% of the global sink (Ehhalt, 1974). Other loss pathways include stratospheric photochemistry and microbial oxidation in well-drained upland soils (Conrad, 1996; Saunois et al., 2025).

As microbial methanotrophy acts as a biological filter for methane before it reaches the atmosphere, its activity is a key regulator of net emissions across ecosystems. The balance between methane production and oxidation determines both the magnitude and isotopic signature of atmospheric methane, integrating local microbial processes into the global carbon-climate system. This balance is not only relevant today but also reflects processes that have shaped Earth's biogeochemical evolution over geological time. Understanding how methane cycling operated under low-oxygen conditions in Earth's past, particularly in the Proterozoic Ocean, provides critical context for the origins of complex life, the evolution of redox-sensitive microbial metabolisms, and the regulation of atmospheric composition.

2. Early Earth marine biogeochemistry and methane cycling

Earth's early evolution was shaped by dynamic changes in planetary chemistry, biology, and redox conditions. During the Hadean and Archean eons (4.6 to 2.5 Ga), the atmosphere and oceans were largely anoxic, and microbial life emerged and diversified in the absence of molecular oxygen. The Archean biosphere was likely dominated by anaerobic metabolisms, including methanogenesis, anoxygenic photosynthesis, and fermentation, supported by abundant reduced compounds in Earth's primordial environment (Canfield et al., 2006; Lyons et al., 2024). Redox gradients developed in localized niches, but more widespread oxygenation did not begin until the Great Oxygenation Event (GOE) occurring between ~2.5 and 2.0 Ga. This event marked a fundamental transition from a reducing to an increasingly oxidizing Earth system, with far-reaching

impacts on marine chemistry, atmospheric composition, and microbial evolution (Lyons et al., 2024; Och & Shields-Zhou, 2012). The GOE initiated the oxygenation of surface waters and triggered the emergence of modern biogeochemical cycles, while the deep ocean remained largely anoxic and chemically stratified (**Fig. 4**).

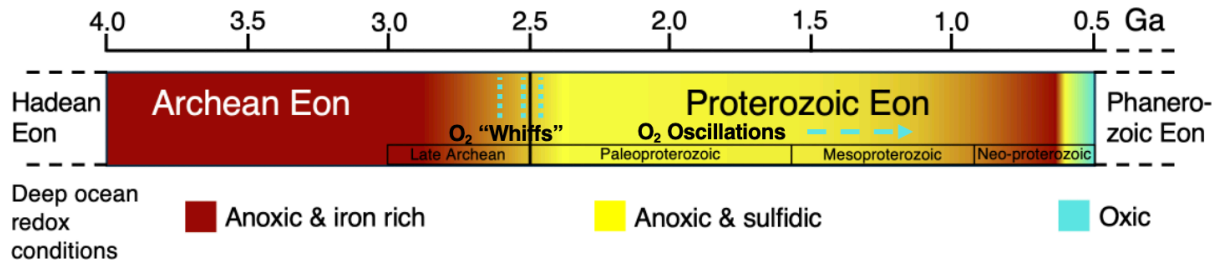

Figure 4. Timeline of hypothesized deep ocean redox conditions from the Hadean to Phanerozoic Eon. The Archean is dominated by anoxic, iron-rich (ferruginous) conditions. Brief oxygen (O_2) "whiffs" occur near the Archean–Proterozoic boundary, followed by fluctuating oxygen levels and the development of sulfidic (euxinic) mid-Proterozoic oceans. Oxic conditions become more widespread only in the late Neoproterozoic and Phanerozoic. Modified from (Camacho et al., 2017).

Following the GOE, the Proterozoic Eon (2.5 to 0.541 Ga) was characterized by persistently low atmospheric oxygen levels, estimated at 1–10% of modern levels (Daines et al., 2017; Diamond & Lyons, 2018; Planavsky et al., 2014; Planavsky et al., 2020). During this time, ocean basins developed strong redox stratification, with oxygenated surface waters overlying deep anoxic layers (Anbar & Knoll, 2002; Planavsky et al., 2011). Ferruginous (Fe(II)-rich) conditions prevailed in many mid-depth and deep-water settings, particularly in basins with low sulfate availability (Poulton & Canfield, 2011). In the mid-to-late Proterozoic, iron and manganese cycling likely played key roles in redox regulation and nutrient transport. Iron and manganese oxides formed in

surface waters via oxygen-mediated or microbial oxidation of the dissolved metals, then settled into deeper anoxic zones where they were reduced, sustaining internal redox shuttles (Lyons & Severmann, 2006; Reinhard et al., 2013). Euxinic conditions also persisted along productive continental margins (Canfield, 1998; Planavsky et al., 2011). Recent models and geochemical records suggest that primary productivity during the Mesoproterozoic (1.6 to 1.0 Ga) was controlled by nutrient levels strongly coupled to marine redox (Lyons et al., 2021; Reinhard, Olson, et al., 2017). Euxinic conditions were impacted by sulfide consumption via anoxygenic photosynthesis (Hamilton et al., 2016; Johnston et al., 2009). During the Mesoproterozoic, these conditions were maintained by microbial sulfate reduction, a process that likely originated in the Archean and later contributed to increased sulfide concentrations (Shen et al., 2001).

In addition, studies have highlighted the impact of Mesoproterozoic euxinia on the nitrogen cycle, demonstrating through both modeling and experimental approaches that copper-limited waters (due to sulfide sequestration) often led to incomplete denitrification, which in turn produced nitrous oxide gas (Buick, 2007; Fennel et al., 2005). Another hypothesis suggests that during the Mesoproterozoic, chemodenitrification involving iron might have been an alternative source of nitrous oxide (Stanton et al., 2018). Meanwhile, feedback from rising atmospheric and upper-ocean molecular oxygen likely facilitated substantial rates of nitrification, including the oxidation of ammonium to nitrate. Recent analyses have documented diagenetic release of the ammonium ion from microbial mats into porewaters, followed by partial oxidation to nitrite or nitrate, which may have further enhanced localized nitrogen availability (Stüeken & Prave, 2022). Moreover, isotopic evidence indicates that biological fixation of molecular nitrogen by molybdenum-dependent nitrogenase was already operative by 3.2 Ga, thereby expanding the pool of bioavailable fixed nitrogen and influencing early biogeochemical cycles (Stüeken et al., 2015). Elevated rates of

denitrification during this interval could have drawn down the reservoir of bioavailable fixed nitrogen and, in turn, constrained production of molecular oxygen (Fennel et al., 2005; Reinhard, Planavsky, et al., 2017). Unfortunately, the scarcity of $\delta^{15}N$ records from the Archean and early Proterozoic limits our ability to quantify rates of nitrogen-species turnover. Available sedimentary $\delta^{15}N$ data reveal a shift from predominantly negative values in the early Archean to positive values in the early Proterozoic, an isotopic fingerprint of increasing microbial denitrification coupled with nitrification feedback (Fennel et al., 2005; Garvin et al., 2009; Stüeken et al., 2016).

While carbon dioxide and water were likely the primary greenhouse gases during the Proterozoic (Kasting & Catling, 2003; Kiehl & Dickinson, 1987), nitrous oxide (Buick, 2007) and methane (Catling et al., 2001; Goldblatt et al., 2006; Hamilton et al., 2016; Pavlov et al., 2000) may have also played a crucial role in regulating the climate once methanogenesis evolved during the Archean around 3.5 Ga (Ueno et al., 2006; Wolfe & Fournier, 2018). However, methane was present on early Earth through abiotic processes before the emergence of biological methanogenesis. For instance, in hydrothermal systems, serpentinization generates hydrogen that reduces carbon dioxide or carbon monoxide to methane (Etiope & Sherwood Lollar, 2013). In addition, large impacts delivered pulses of metallic and ferrous iron which, in the hot, transient, impact-generated atmospheres, first reacted with water vapor to produce molecular hydrogen; that hydrogen subsequently reduced carbon dioxide to methane (Zahnle et al., 2020). Although significant, these atmospheres would have been short-lived, delivering episodic rather than continuous abiotic methane fluxes alongside the steadier outgassing from volcanoes of carbon dioxide. These abiotic sources likely supported a greenhouse contribution that helped stabilize early Earth's climate before biological sources became dominant (Arney et al., 2016; Catling et al., 2001).

Given the low atmospheric oxygen levels during the Mesoproterozoic, biogenic methane cycling in the ocean may have played a role in regulating atmospheric oxygen concentrations (Fakhraee et al., 2019). Anaerobic methanogenesis is regarded as one of the oldest microbial metabolisms, with carbon isotope fractionation measurements (Ueno et al., 2006) and molecular clock estimates (Wolfe & Fournier, 2018) suggesting its existence deep in Earth history during the Archean eon (4 to 2.5 Ga). As abiotic and biogenic methane accumulated, it may have driven the evolution of anaerobic methanotrophy (Catling et al., 2001; Sauterey et al., 2020). While the precise timing of the emergence of anaerobic methane oxidation via nitrate, nitrite, or sulfate reduction remains uncertain, its enzymatic similarity to the reverse process of methanogenesis suggests a potential evolutionary relationship, though whether it preceded or followed biological methanogenesis is unclear, especially given the availability of abiotic methane on early Earth (Nitschke & Russell, 2013). The timing of aerobic methanotrophy is also uncertain; however, isotopic evidence indicates that by 2.72 billion years ago, the initial oxygenation of shallow habitats likely enabled microbial oxidation of methane for energy using oxygen or other electron acceptors. This energy acquisition may have supported the growth of methanotrophic organisms, suggesting that aerobic methanotrophy first emerged in localized niches before becoming more widespread after the Great Oxygenation Event (Eigenbrode & Freeman, 2006). Further, it is believed that aerobic methanotrophs likely evolved from methylotrophs through the lateral gene transfer of methane monooxygenase genes, which is thought to have occurred independently several times (Kang et al., 2019; Khadka et al., 2018; Osborne & Haritos, 2018).

Farther down in the redox ladder within anoxic sediments or anoxic strata of the water column, fermentation functions as a parallel, precursor process. Through the depolymerization of complex organic matter, fermentative microbes produce hydrogen, formate, and acetate, which

serve as the primary electron donors for hydrogenotrophic and acetoclastic methanogens (Schink, 1997). This fermentative 'substrate factory' sustains methane production throughout anoxic zones and concurrently supplies substrates to secondary anaerobic pathways such as sulfate reduction. In doing so, fermentation facilitates vertical coupling of carbon and sulfur cycling across redox gradients. Although direct evidence is limited, several indirect lines suggest fermentation contributed to organic matter turnover under ferruginous and euxinic conditions during the Proterozoic (Canfield et al., 2018) and isotopic studies have begun to clarify its influence on the early Earth carbon cycle (Havig et al., 2017). This interpretation is supported by the modeled environmental context of the time: extensive microbial mat development (Schieber, 1998; Schopf & Klein, 1992) and oxygen-deficient water columns (Lyons et al., 2021; Planavsky et al., 2018; Tang et al., 2016) would have created favorable conditions for anaerobic carbon degradation pathways, including fermentation. Geochemical evidence from the ~1.4 Ga Xiamaling Formation (North China Craton) further supports this scenario, revealing redox-stratified conditions, limited sulfate availability, and elevated organic carbon, conditions that likely favored methanogenesis supported by fermentation as a primary heterotrophic pathway (Diamond et al., 2018; Wang et al., 2017; Zou et al., 2019).

3. Dissertation outlook

This dissertation investigates how water column microbial methane oxidation modulates redox gradients, regulates methane flux, and sustains ecosystems across spatially and temporally distinct aquatic environments. Methane cycling serves as the central thread, with emphasis on how water column methanotrophy contributes to redox stability, ecological structure, and the fate and footprint of methane in both ancient and modern marine systems. While Chapters 3 and 4 focus

explicitly on methane dynamics in the water column of present-day cold seeps, Chapter 2 takes a broader view, integrating sulfur, nitrogen, and carbon cycling to contextualize microbial redox processes in a Proterozoic Ocean analog. Each chapter presents original research, either submitted to a scientific journal or in preparation for submission. Chapter 2 was submitted for peer review, and Chapters 3 and 4 are in preparation for submission. Following the introduction in Chapter 1, this dissertation includes three research chapters (Chapters 2–4), each formatted as a stand-alone manuscript, and concludes with a synthesis chapter (Chapter 5).

Together, these chapters test three central hypotheses:

1. In Proterozoic analog environments, microbial methane oxidation contributed to water column redox stability and may have modulated oxygen availability in low-oxygen oceans.
2. Across modern seep systems, the spatial footprint and ecological influence of water column methanotrophy extends beyond the immediate seep zone, supporting food webs across oxic and suboxic regimes.
3. Physical and chemical factors, including oxygen concentration, methane availability, and transport dynamics, control the activity, extent, and geochemical impact of the methanosphere in the modern ocean.

Chapter 2 examines biogeochemical cycling in Green Lake (Fayetteville, NY), a meromictic, euxinic lake used as an analog for Mesoproterozoic Ocean conditions. Using geochemical profiling, rate measurements, and metagenomics, this chapter investigates how microbial processes, particularly methane oxidation, contributed to redox balance and oxygen availability. Methanotrophy -likely by metabolically versatile aerobic methanotrophs- formed an efficient methane filter, while a sulfide-dominated redox imbalance limited oxygen intrusion and

fueled microbial activity, offering a model for how microbial feedbacks may have modulated oxygen availability and redox stability in early oceans.

Chapter 3 explores methane oxidation in low-oxygen cold seeps along the Southern California margin. By integrating measurements of geochemical parameters (including methane concentrations), microbial indicators (particulate methane monooxygenase (*pmoA)* gene abundance, 16S rRNA community composition), and oxidation rates, this chapter assesses how oxygen availability, organic matter supply, and physical transport shape the spatial extent and ecological influence of the water column methanosphere. Lateral and vertical gradients in oxidation and MOB abundance, together with site-specific correlations between oxidation, methane, and oxygen, support the hypothesis that physical dispersal broadens the biogeochemical influence of seeps. These patterns are consistent with an expanded methanosphere shaped by variable geochemical controls and physical transport, facilitating export of methanotrophic biomass and methane-derived carbon.

Chapter 4 investigates methane oxidation in well-oxygenated waters above deep-sea seeps the Gulf of Alaska. Methane oxidation was primarily governed by methane availability and likely dispersal dynamics. Instances where high methane oxidation occurred despite low *pmoA* gene abundance, indicates microbial persistence under intermittent methane supply potentially driven by physical controls on methane and methanotroph transport through the water column. A horizontal transect revealed that the methanosphere extended beyond vent orifice boundaries, including areas with gas hydrates, with methane and methane oxidation increasing in the direction of observed currents, as also seen in the Southern California seeps described in Chapter 3, influencing water column biogeochemistry and microbial ecology.

The concluding chapter synthesizes these results and emphasizes the broader implications of water column methane-based microbial processes. Water column methanotrophy emerges as a core mechanism of geochemical regulation and carbon cycling, likely shaping Earth's early biosphere, supporting modern benthic-pelagic connectivity, and contributing to broader ecosystem function in cold seep environments. Though not the focus of this thesis, the extended methanosphere may play a critical role in regulating methane budgets in marine systems, with implications for regional carbon cycling and climate feedbacks. As ocean conditions evolve, understanding how microbial community plasticity and physical transport mechanisms govern methane fate will be essential for predicting the resilience and response of marine ecosystems. This work also informs strategies for identifying biosignatures on other planets, where methane and redox disequilibria may offer clues to potential life beyond Earth.

References

Anbar, A. D., & Knoll, A. H. (2002). Proterozoic ocean chemistry and evolution: a bioinorganic bridge? *science*, *297*(5584), 1137-1142.

Arney, G., Domagal-Goldman, S. D., Meadows, V. S., Wolf, E. T., Schwieterman, E., Charnay, B., Claire, M., Hébrard, E., & Trainer, M. G. (2016). The pale orange dot: the spectrum and habitability of hazy Archean Earth. *Astrobiology*, *16*(11), 873-899.

Awala, S. I., Gwak, J.-H., Kim, Y., Jung, M.-Y., Dunfield, P. F., Wagner, M., & Rhee, S.-K. (2024). Nitrous oxide respiration in acidophilic methanotrophs. *Nature communications*, *15*(1), 4226.

Bastviken, D., Tranvik, L. J., Downing, J. A., Crill, P. M., & Enrich-Prast, A. (2011). Freshwater methane emissions offset the continental carbon sink. *science*, *331*(6013), 50-50.

Beal, E. J., House, C. H., & Orphan, V. J. (2009). Manganese-and iron-dependent marine methane oxidation. *science*, *325*(5937), 184-187.

Boetius, A., Ravenschlag, K., Schubert, C. J., Rickert, D., Widdel, F., Gieseke, A., Amann, R., Jørgensen, B. B., Witte, U., & Pfannkuche, O. (2000). A marine microbial consortium apparently mediating anaerobic oxidation of methane. *Nature*, *407*(6804), 623-626.

Boetius, A., & Wenzhöfer, F. (2013). Seafloor oxygen consumption fuelled by methane from cold seeps. *Nature Geoscience*, *6*(9), 725-734.

Bohrmann, G., Greinert, J., Suess, E., & Torres, M. (1998). Authigenic carbonates from the Cascadia subduction zone and their relation to gas hydrate stability. *Geology*, *26*(7), 647-650.

Buick, R. (2007). Did the Proterozoic 'Canfield Ocean'cause a laughing gas greenhouse? In (Vol. 5, pp. 97-100): Wiley Online Library.

Camacho, A., Walter, X. A., Picazo, A., & Zopfi, J. (2017). Photoferrotrophy: remains of an ancient photosynthesis in modern environments. *Frontiers in Microbiology*, *8*, 323.

Canfield, D. E. (1998). A new model for Proterozoic ocean chemistry. *Nature*, *396*(6710), 450-453.

Canfield, D. E., Rosing, M. T., & Bjerrum, C. (2006). Early anaerobic metabolisms. *Philosophical Transactions of the Royal Society B: Biological Sciences*, *361*(1474), 1819-1836.

Canfield, D. E., Zhang, S., Frank, A. B., Wang, X., Wang, H., Su, J., Ye, Y., & Frei, R. (2018). Highly fractionated chromium isotopes in Mesoproterozoic-aged shales and atmospheric oxygen. *Nature Communications*, *9*(1), 2871.

Catling, D. C., Zahnle, K. J., & McKay, C. P. (2001). Biogenic methane, hydrogen escape, and the irreversible oxidation of early Earth. *science*, *293*(5531), 839-843.

Chen, K. H.-C., Wu, H.-H., Ke, S.-F., Rao, Y.-T., Tu, C.-M., Chen, Y.-P., Kuei, K.-H., Chen, Y.-S., Wang, V. C.-C., & Kao, W.-C. (2012). Bacteriohemerythrin bolsters the activity of the particulate methane monooxygenase (pMMO) in Methylococcus capsulatus (Bath). *Journal of inorganic biochemistry*, *111*, 10-17.

Childress, J. J., Fisher, C., Brooks, J., Kennicutt, M., Bidigare, R., & Anderson, A. (1986). A methanotrophic marine molluscan (Bivalvia, Mytilidae) symbiosis: mussels fueled by gas. *Science*, *233*(4770), 1306-1308.

Conrad, R. (1996). Soil microorganisms as controllers of atmospheric trace gases (H2, CO, CH4, OCS, N2O, and NO). *Microbiological reviews*, *60*(4), 609-640.

Conrad, R. (2009). The global methane cycle: recent advances in understanding the microbial processes involved. *Environmental Microbiology Reports*, *1*(5), 285-292.

Cordes, E. E., Cunha, M. R., Galeron, J., Mora, C., Olu-Le Roy, K., Sibuet, M., Van Gaever, S., Vanreusel, A., & Levin, L. A. (2010). The influence of geological, geochemical, and biogenic habitat heterogeneity on seep biodiversity. *Marine Ecology*, *31*(1), 51-65.

Crémière, A., Lepland, A., Chand, S., Sahy, D., Condon, D. J., Noble, S. R., Martma, T., Thorsnes, T., Sauer, S., & Brunstad, H. (2016). Timescales of methane seepage on the Norwegian margin following collapse of the Scandinavian Ice Sheet. *Nature communications*, *7*(1), 11509.

Crowe, S., Katsev, S., Leslie, K., Sturm, A., Magen, C., Nomosatryo, S., Pack, M., Kessler, J., Reeburgh, W., & Roberts, J. (2011). The methane cycle in ferruginous Lake Matano. *Geobiology*, *9*(1), 61-78.

Daines, S. J., Mills, B. J., & Lenton, T. M. (2017). Atmospheric oxygen regulation at low Proterozoic levels by incomplete oxidative weathering of sedimentary organic carbon. *Nature Communications*, *8*(1), 14379.

Damm, E., Helmke, E., Thoms, S., Schauer, U., Nöthig, E., Bakker, K., & Kiene, R. (2010). Methane production in aerobic oligotrophic surface water in the central Arctic Ocean. *Biogeosciences*, *7*(3), 1099-1108.

Diamond, C. W., & Lyons, T. W. (2018). Mid-Proterozoic redox evolution and the possibility of transient oxygenation events. *Emerging Topics in Life Sciences*, *2*(2), 235-245.

Diamond, C. W., Planavsky, N. J., Wang, C., & Lyons, T. W. (2018). What the~ 1.4 Ga Xiamaling Formation can and cannot tell us about the mid-Proterozoic ocean. *Geobiology*, *16*(3), 219-236.

Ehhalt, D. (1974). The atmospheric cycle of methane. *Tellus*, *26*(1-2), 58-70.

Eigenbrode, J. L., & Freeman, K. H. (2006). Late Archean rise of aerobic microbial ecosystems. *Proceedings of the national academy of sciences*, *103*(43), 15759-15764.

Etiope, G. (2017). Abiotic methane in continental serpentinization sites: an overview. *Procedia Earth and Planetary Science*, *17*, 9-12.

Etiope, G., & Sherwood Lollar, B. (2013). Abiotic methane on Earth. *Reviews of Geophysics*, *51*(2), 276-299.

Etminan, M., Myhre, G., Highwood, E. J., & Shine, K. P. (2016). Radiative forcing of carbon dioxide, methane, and nitrous oxide: A significant revision of the methane radiative forcing. *Geophysical Research Letters*, *43*(24), 12,614-612,623.

Ettwig, K. F., Butler, M. K., Le Paslier, D., Pelletier, E., Mangenot, S., Kuypers, M. M., Schreiber, F., Dutilh, B. E., Zedelius, J., & de Beer, D. (2010). Nitrite-driven anaerobic methane oxidation by oxygenic bacteria. *Nature*, *464*(7288), 543-548.

Fakhraee, M., Hancisse, O., Canfield, D. E., Crowe, S. A., & Katsev, S. (2019). Proterozoic seawater sulfate scarcity and the evolution of ocean–atmosphere chemistry. *Nature Geoscience*, *12*(5), 375-380.

Fennel, K., Follows, M., & Falkowski, P. G. (2005). The co-evolution of the nitrogen, carbon and oxygen cycles in the Proterozoic ocean. *American Journal of Science*, *305*(6-8), 526-545.

Formisano, V., Atreya, S., Encrenaz, T., Ignatiev, N., & Giuranna, M. (2004). Detection of methane in the atmosphere of Mars. *science*, *306*(5702), 1758-1761.

Garvin, J., Buick, R., Anbar, A. D., Arnold, G. L., & Kaufman, A. J. (2009). Isotopic evidence for an aerobic nitrogen cycle in the latest Archean. *science*, *323*(5917), 1045-1048.

Gilman, A., Fu, Y., Hendershott, M., Chu, F., Puri, A. W., Smith, A. L., Pesesky, M., Lieberman, R., Beck, D. A., & Lidstrom, M. E. (2017). Oxygen-limited metabolism in the methanotroph Methylomicrobium buryatense 5GB1C. *PeerJ*, *5*, e3945.

Goffredi, S. K., Tilic, E., Mullin, S. W., Dawson, K. S., Keller, A., Lee, R. W., Wu, F., Levin, L. A., Rouse, G. W., & Cordes, E. E. (2020). Methanotrophic bacterial symbionts fuel dense populations of deep-sea feather duster worms (Sabellida, Annelida) and extend the spatial influence of methane seepage. *Science Advances*, *6*(14), eaay8562.

Goldblatt, C., Lenton, T. M., & Watson, A. J. (2006). Bistability of atmospheric oxygen and the Great Oxidation. *Nature*, *443*(7112), 683-686.

Greinert, J., Bohrmann, G., & Elvert, M. (2002). Stromatolitic fabric of authigenic carbonate crusts: result of anaerobic methane oxidation at cold seeps in 4,850 m water depth. *International Journal of Earth Sciences*, *91*, 698-711.

Grosse, S., Laramee, L., Wendlandt, K.-D., McDonald, I. R., Miguez, C. B., & Kleber, H.-P. (1999). Purification and characterization of the soluble methane monooxygenase of the type II methanotrophic bacterium Methylocystis sp. strain WI 14. *Applied and Environmental Microbiology*, *65*(9), 3929-3935.

Hamilton, T. L., Bryant, D. A., & Macalady, J. L. (2016). The role of biology in planetary evolution: cyanobacterial primary production in low-oxygen Proterozoic oceans. *Environmental Microbiology*, *18*(2), 325-340.

Hanson, R. S., & Hanson, T. E. (1996). Methanotrophic bacteria. *Microbiological reviews*, *60*(2), 439-471.

Haroon, M. F., Hu, S., Shi, Y., Imelfort, M., Keller, J., Hugenholtz, P., Yuan, Z., & Tyson, G. W. (2013). Anaerobic oxidation of methane coupled to nitrate reduction in a novel archaeal lineage. *Nature*, *500*(7464), 567-570.

Havig, J. R., Hamilton, T. L., Bachan, A., & Kump, L. R. (2017). Sulfur and carbon isotopic evidence for metabolic pathway evolution and a four-stepped Earth system progression across the Archean and Paleoproterozoic. *Earth-Science Reviews*, *174*, 1-21.

He, R., Wang, J., Pohlman, J. W., Jia, Z., Chu, Y.-X., Wooller, M. J., & Leigh, M. B. (2022). Metabolic flexibility of aerobic methanotrophs under anoxic conditions in Arctic lake sediments. *The ISME journal*, *16*(1), 78-90.

He, Z., Cai, C., Wang, J., Xu, X., Zheng, P., Jetten, M. S., & Hu, B. (2016). A novel denitrifying methanotroph of the NC10 phylum and its microcolony. *Scientific reports*, *6*(1), 32241.

Johnston, D. T., Wolfe-Simon, F., Pearson, A., & Knoll, A. H. (2009). Anoxygenic photosynthesis modulated Proterozoic oxygen and sustained Earth's middle age. *Proceedings of the national academy of sciences*, *106*(40), 16925-16929.

Jordan, S. F., Treude, T., Leifer, I., Janßen, R., Werner, J., Schulz-Vogt, H., & Schmale, O. (2020). Bubble-mediated transport of benthic microorganisms into the water column: Identification of methanotrophs and implication of seepage intensity on transport efficiency. *Scientific reports*, *10*(1), 4682.

Judd, A., & Hovland, M. (2009). *Seabed fluid flow: the impact on geology, biology and the marine environment*. Cambridge University Press.

Kalyuzhnaya, M., Yang, S., Rozova, O., Smalley, N., Clubb, J., Lamb, A., Gowda, G. N., Raftery, D., Fu, Y., & Bringel, F. (2013). Highly efficient methane biocatalysis revealed in a methanotrophic bacterium. *Nature communications*, *4*(1), 2785.

Kämpf, J., & Chapman, P. (2016). *Upwelling systems of the world*. Springer.

Kang, C. S., Dunfield, P. F., & Semrau, J. D. (2019). The origin of aerobic methanotrophy within the Proteobacteria. *FEMS microbiology letters*, *366*(9), fnz096.

Karaca, D., Hensen, C., & Wallmann, K. (2010). Controls on authigenic carbonate precipitation at cold seeps along the convergent margin off Costa Rica. *Geochemistry, Geophysics, Geosystems*, *11*(8).

Karl, D. M., Beversdorf, L., Björkman, K. M., Church, M. J., Martinez, A., & Delong, E. F. (2008). Aerobic production of methane in the sea. *Nature Geoscience*, *1*(7), 473-478.

Kasting, J. F., & Catling, D. (2003). Evolution of a habitable planet. *Annual Review of Astronomy and Astrophysics*, *41*(1), 429-463.

Khadka, R., Clothier, L., Wang, L., Lim, C. K., Klotz, M. G., & Dunfield, P. F. (2018). Evolutionary history of copper membrane monooxygenases. *Frontiers in Microbiology*, *9*, 2493.

Kiehl, J., & Dickinson, R. (1987). A study of the radiative effects of enhanced atmospheric CO2 and CH4 on early Earth surface temperatures. *Journal of Geophysical Research: Atmospheres*, *92*(D3), 2991-2998.

Kirschke, S., Bousquet, P., Ciais, P., Saunois, M., Canadell, J. G., Dlugokencky, E. J., Bergamaschi, P., Bergmann, D., Blake, D. R., & Bruhwiler, L. (2013). Three decades of global methane sources and sinks. *Nature Geoscience*, *6*(10), 813-823.

Klintzsch, T., Langer, G., Nehrke, G., Wieland, A., Lenhart, K., & Keppler, F. (2019). Methane production by three widespread marine phytoplankton species: release rates, precursor compounds, and potential relevance for the environment. *Biogeosciences*, *16*(20), 4129-4144.

Knief, C. (2015). Diversity and habitat preferences of cultivated and uncultivated aerobic methanotrophic bacteria evaluated based on pmoA as molecular marker. *Frontiers in Microbiology*, *6*, 1346.

Knittel, K., & Boetius, A. (2009). Anaerobic oxidation of methane: progress with an unknown process. *Annual review of microbiology*, *63*(1), 311-334.

Kopf, A. J. (2003). Global methane emission through mud volcanoes and its past and present impact on the Earth's climate. *International Journal of Earth Sciences*, *92*, 806-816.

Kotelnikova, S. (2002). Microbial production and oxidation of methane in deep subsurface. *Earth-Science Reviews*, *58*(3-4), 367-395.

Kristjansson, J. K., Schönheit, P., & Thauer, R. K. (1982). Different K s values for hydrogen of methanogenic bacteria and sulfate reducing bacteria: an explanation for the apparent inhibition of methanogenesis by sulfate. *Archives of microbiology*, *131*, 278-282.

Kutterolf, S., Liebetrau, V., Mörz, T., Freundt, A., Hammerich, T., & Garbe-Schönberg, D. (2008). Lifetime and cyclicity of fluid venting at forearc mound structures determined by tephrostratigraphy and radiometric dating of authigenic carbonates. *Geology*, *36*(9), 707-710.

Kvenvolden, K. A., & Claypool, G. E. (1988). *Gas hydrates in oceanic sediment* (2331-1258).

Lefevre, F., & Forget, F. (2009). Observed variations of methane on Mars unexplained by known atmospheric chemistry and physics. *Nature*, *460*(7256), 720-723.

Levin, L. A. (2005). Ecology of cold seep sediments: interactions of fauna with flow, chemistry and microbes. In *Oceanography and marine biology* (pp. 11-56). CRC Press.

Levin, L. A., Baco, A. R., Bowden, D. A., Colaco, A., Cordes, E. E., Cunha, M. R., Demopoulos, A. W., Gobin, J., Grupe, B. M., & Le, J. (2016). Hydrothermal vents and methane seeps: rethinking the sphere of influence. *Frontiers in Marine Science*, *3*, 72.

Levin, L. A., & Michener, R. H. (2002). Isotopic evidence for chemosynthesis-based nutrition of macrobenthos: The lightness of being at Pacific methane seeps. *Limnology and Oceanography*, *47*(5), 1336-1345.

Lovley, D. R., & Klug, M. J. (1983). Sulfate reducers can outcompete methanogens at freshwater sulfate concentrations. *Applied and Environmental Microbiology*, *45*(1), 187-192.

Lyons, T. W., Diamond, C. W., Planavsky, N. J., Reinhard, C. T., & Li, C. (2021). Oxygenation, life, and the planetary system during Earth's middle history: An overview. *Astrobiology*, *21*(8), 906-923.

Lyons, T. W., & Severmann, S. (2006). A critical look at iron paleoredox proxies: New insights from modern euxinic marine basins. *Geochimica et Cosmochimica Acta*, *70*(23), 5698-5722.

Lyons, T. W., Tino, C. J., Fournier, G. P., Anderson, R. E., Leavitt, W. D., Konhauser, K. O., & Stüeken, E. E. (2024). Co-evolution of early Earth environments and microbial life. *Nature Reviews Microbiology*, *22*(9), 572-586.

Marlow, J. J., Steele, J. A., Ziebis, W., Thurber, A. R., Levin, L. A., & Orphan, V. J. (2014). Carbonate-hosted methanotrophy represents an unrecognized methane sink in the deep sea. *Nature communications*, *5*(1), 5094.

Matthews, E., & Fung, I. (1987). Methane emission from natural wetlands: Global distribution, area, and environmental characteristics of sources. *Global Biogeochemical Cycles*, *1*(1), 61-86.

Michaelis, W., Seifert, R., Nauhaus, K., Treude, T., Thiel, V., Blumenberg, M., Knittel, K., Gieseke, A., Peterknecht, K., & Pape, T. (2002). Microbial reefs in the Black Sea fueled by anaerobic oxidation of methane. *science*, *297*(5583), 1013-1015.

Nitschke, W., & Russell, M. J. (2013). Beating the acetyl coenzyme A-pathway to the origin of life. *Philosophical Transactions of the Royal Society B: Biological Sciences*, *368*(1622), 20120258.

Och, L. M., & Shields-Zhou, G. A. (2012). The Neoproterozoic oxygenation event: Environmental perturbations and biogeochemical cycling. *Earth-Science Reviews*, *110*(1-4), 26-57.

Orphan, V. J., House, C. H., Hinrichs, K.-U., McKeegan, K. D., & DeLong, E. F. (2001). Methane-consuming archaea revealed by directly coupled isotopic and phylogenetic analysis. *science*, *293*(5529), 484-487.

Osborne, C. D., & Haritos, V. S. (2018). Horizontal gene transfer of three co-inherited methane monooxygenase systems gave rise to methanotrophy in the Proteobacteria. *Molecular phylogenetics and evolution*, *129*, 171-181.

Oswald, K., Jegge, C., Tischer, J., Berg, J., Brand, A., Miracle, M. R., Soria, X., Vicente, E., Lehmann, M. F., & Zopfi, J. (2016). Methanotrophy under versatile conditions in the water column of the ferruginous meromictic Lake La Cruz (Spain). *Frontiers in Microbiology*, *7*, 1762.

Oswald, K., Milucka, J., Brand, A., Hach, P., Littmann, S., Wehrli, B., Kuypers, M. M., & Schubert, C. J. (2016). Aerobic gammaproteobacterial methanotrophs mitigate methane emissions from oxic and anoxic lake waters. *Limnology and Oceanography*, *61*(S1), S101-S118.

Pack, M. A., Heintz, M. B., Reeburgh, W. S., Trumbore, S. E., Valentine, D. L., Xu, X., & Druffel, E. R. (2015). Methane oxidation in the eastern tropical North Pacific Ocean water column. *Journal of Geophysical Research: Biogeosciences*, *120*(6), 1078-1092.

Pasulka, A. L., Goffredi, S. K., Tavormina, P. L., Dawson, K. S., Levin, L. A., Rouse, G. W., & Orphan, V. J. (2017). Colonial tube-dwelling ciliates influence methane cycling and microbial diversity within methane seep ecosystems. *Frontiers in Marine Science*, *3*, 276.

Pavlov, A. A., Kasting, J. F., Brown, L. L., Rages, K. A., & Freedman, R. (2000). Greenhouse warming by CH4 in the atmosphere of early Earth. *Journal of Geophysical Research: Planets*, *105*(E5), 11981-11990.

Petersen, J. M., & Dubilier, N. (2009). Methanotrophic symbioses in marine invertebrates. *Environmental Microbiology Reports*, *1*(5), 319-335.

Planavsky, N. J., McGoldrick, P., Scott, C. T., Li, C., Reinhard, C. T., Kelly, A. E., Chu, X., Bekker, A., Love, G. D., & Lyons, T. W. (2011). Widespread iron-rich conditions in the mid-Proterozoic ocean. *Nature*, *477*(7365), 448-451.

Planavsky, N. J., Reinhard, C. T., Wang, X., Thomson, D., McGoldrick, P., Rainbird, R. H., Johnson, T., Fischer, W. W., & Lyons, T. W. (2014). Low Mid-Proterozoic atmospheric oxygen levels and the delayed rise of animals. *science*, *346*(6209), 635-638.

Planavsky, N. J., Robbins, L. J., Kamber, B. S., & Schoenberg, R. (2020). Weathering, alteration and reconstructing Earth's oxygenation. *Interface Focus*, *10*(4), 20190140.

Planavsky, N. J., Slack, J. F., Cannon, W. F., O'Connell, B., Isson, T. T., Asael, D., Jackson, J. C., Hardisty, D. S., Lyons, T. W., & Bekker, A. (2018). Evidence for episodic oxygenation in a weakly redox-buffered deep mid-Proterozoic ocean. *Chemical Geology*, *483*, 581-594.

Poulton, S. W., & Canfield, D. E. (2011). Ferruginous conditions: a dominant feature of the ocean through Earth's history. *Elements*, *7*(2), 107-112.

Reeburgh, W. S. (2007). Oceanic methane biogeochemistry. *Chemical reviews*, *107*(2), 486-513.

Reeves, E. P., & Fiebig, J. (2020). Abiotic synthesis of methane and organic compounds in Earth's lithosphere. *Elements: An International Magazine of Mineralogy, Geochemistry, and Petrology*, *16*(1), 25-31.

Reinhard, C. T., Olson, S. L., Schwieterman, E. W., & Lyons, T. W. (2017). False negatives for remote life detection on ocean-bearing planets: lessons from the early Earth. *Astrobiology*, *17*(4), 287-297.

Reinhard, C. T., Planavsky, N. J., Gill, B. C., Ozaki, K., Robbins, L. J., Lyons, T. W., Fischer, W. W., Wang, C., Cole, D. B., & Konhauser, K. O. (2017). Evolution of the global phosphorus cycle. *Nature*, *541*(7637), 386-389.

Reinhard, C. T., Planavsky, N. J., Robbins, L. J., Partin, C. A., Gill, B. C., Lalonde, S. V., Bekker, A., Konhauser, K. O., & Lyons, T. W. (2013). Proterozoic ocean redox and biogeochemical stasis. *Proceedings of the National Academy of Sciences*, *110*(14), 5357-5362.

Rubin-Blum, M., Antony, C. P., Sayavedra, L., Martínez-Pérez, C., Birgel, D., Peckmann, J., Wu, Y.-C., Cardenas, P., MacDonald, I., & Marcon, Y. (2019). Fueled by methane: deep-sea sponges from asphalt seeps gain their nutrition from methane-oxidizing symbionts. *The ISME journal*, *13*(5), 1209-1225.

Saunois, M., Martinez, A., Poulter, B., Zhang, Z., Raymond, P. A., Regnier, P., Canadell, J. G., Jackson, R. B., Patra, P. K., & Bousquet, P. (2025). Global methane budget 2000–2020. *Earth System Science Data*, *17*(5), 1873-1958.

Sauterey, B., Charnay, B., Affholder, A., Mazevet, S., & Ferrière, R. (2020). Co-evolution of primitive methane-cycling ecosystems and early Earth's atmosphere and climate. *Nature Communications*, *11*(1), 2705.

Scheller, S., Goenrich, M., Boecher, R., Thauer, R. K., & Jaun, B. (2010). The key nickel enzyme of methanogenesis catalyses the anaerobic oxidation of methane. *Nature*, *465*(7298), 606-608.

Schieber, J. (1998). Possible indicators of microbial mat deposits in shales and sandstones: examples from the Mid-Proterozoic Belt Supergroup, Montana, USA. *Sedimentary geology*, *120*(1-4), 105-124.

Schink, B. (1997). Energetics of syntrophic cooperation in methanogenic degradation. *Microbiology and molecular biology reviews*, *61*(2), 262-280.

Schopf, J. W., & Klein, C. (1992). *The Proterozoic biosphere: a multidisciplinary study*. Cambridge University Press.

Schorn, S., Graf, J. S., Littmann, S., Hach, P. F., Lavik, G., Speth, D. R., Schubert, C. J., Kuypers, M. M., & Milucka, J. (2024). Persistent activity of aerobic methane-oxidizing bacteria in anoxic lake waters due to metabolic versatility. *Nature communications*, *15*(1), 5293.

Semrau, J. D., DiSpirito, A. A., & Yoon, S. (2010). Methanotrophs and copper. *FEMS microbiology reviews*, *34*(4), 496-531.

Shen, Y., Buick, R., & Canfield, D. E. (2001). Isotopic evidence for microbial sulphate reduction in the early Archaean era. *Nature*, *410*(6824), 77-81.

Sivan, O., Adler, M., Pearson, A., Gelman, F., Bar-Or, I., John, S. G., & Eckert, W. (2011). Geochemical evidence for iron-mediated anaerobic oxidation of methane. *Limnology and Oceanography*, *56*(4), 1536-1544.

Smemo, K. A., & Yavitt, J. B. (2007). Evidence for anaerobic CH 4 oxidation in freshwater peatlands. *Geomicrobiology Journal*, *24*(7-8), 583-597.

Stanton, C. L., Reinhard, C. T., Kasting, J. F., Ostrom, N. E., Haslun, J. A., Lyons, T. W., & Glass, J. B. (2018). Nitrous oxide from chemodenitrification: A possible missing link in the Proterozoic greenhouse and the evolution of aerobic respiration. *Geobiology*, *16*(6), 597-609.

Steinle, L., Graves, C. A., Treude, T., Ferré, B., Biastoch, A., Bussmann, I., Berndt, C., Krastel, S., James, R. H., & Behrens, E. (2015). Water column methanotrophy controlled by a rapid oceanographic switch. *Nature Geoscience*, *8*(5), 378-382.

Steinle, L., Maltby, J., Treude, T., Kock, A., Bange, H. W., Engbersen, N., Zopfi, J., Lehmann, M. F., & Niemann, H. (2017). Effects of low oxygen concentrations on aerobic methane oxidation in seasonally hypoxic coastal waters. *Biogeosciences*, *14*(6), 1631-1645.

Stüeken, E. E., Buick, R., Guy, B. M., & Koehler, M. C. (2015). Isotopic evidence for biological nitrogen fixation by molybdenum-nitrogenase from 3.2 Gyr. *Nature*, *520*(7549), 666-669.

Stüeken, E. E., Kipp, M. A., Koehler, M. C., & Buick, R. (2016). The evolution of Earth's biogeochemical nitrogen cycle. *Earth-Science Reviews*, *160*, 220-239.

Stüeken, E. E., & Prave, A. R. (2022). Diagenetic nutrient supplies to the Proterozoic biosphere archived in divergent nitrogen isotopic ratios between kerogen and silicate minerals. *Geobiology*, *20*(5), 623-633.

Suess, E. (2010). Marine cold seeps. In *Handbook of hydrocarbon and lipid microbiology* (pp. 185-203). Springer.

Suess, E., Bohrmann, G., Von Huene, R., Linke, P., Wallmann, K., Lammers, S., Sahling, H., Winckler, G., Lutz, R. A., & Orange, D. (1998). Fluid venting in the eastern Aleutian subduction zone. *Journal of Geophysical Research: Solid Earth*, *103*(B2), 2597-2614.

Tang, D., Shi, X., Wang, X., & Jiang, G. (2016). Extremely low oxygen concentration in mid-Proterozoic shallow seawaters. *Precambrian Research*, *276*, 145-157.

Tavormina, P. L., Ussler III, W., & Orphan, V. J. (2008). Planktonic and sediment-associated aerobic methanotrophs in two seep systems along the North American margin. *Applied and Environmental Microbiology*, *74*(13), 3985-3995.

Thamdrup, B., Steinsdóttir, H. G., Bertagnolli, A. D., Padilla, C. C., Patin, N. V., Garcia-Robledo, E., Bristow, L. A., & Stewart, F. J. (2019). Anaerobic methane oxidation is an important sink for methane in the ocean's largest oxygen minimum zone. *Limnology and Oceanography*, *64*(6), 2569-2585.

Thauer, R. K. (2011). Anaerobic oxidation of methane with sulfate: on the reversibility of the reactions that are catalyzed by enzymes also involved in methanogenesis from CO2. *Current opinion in microbiology*, *14*(3), 292-299.

Thauer, R. K., Kaster, A.-K., Seedorf, H., Buckel, W., & Hedderich, R. (2008). Methanogenic archaea: ecologically relevant differences in energy conservation. *Nature Reviews Microbiology*, *6*(8), 579-591.

Torres, M. E., McManus, J., Hammond, D., De Angelis, M., Heeschen, K., Colbert, S., Tryon, M., Brown, K., & Suess, E. (2002). Fluid and chemical fluxes in and out of sediments hosting methane hydrate deposits on Hydrate Ridge, OR, I: Hydrological provinces. *Earth and Planetary Science Letters*, *201*(3-4), 525-540.

Ueno, Y., Yamada, K., Yoshida, N., Maruyama, S., & Isozaki, Y. (2006). Evidence from fluid inclusions for microbial methanogenesis in the early Archaean era. *Nature*, *440*(7083), 516-519.

Ussler III, W., Preston, C., Tavormina, P., Pargett, D., Jensen, S., Roman, B., Marin III, R., Shah, S. R., Girguis, P. R., & Birch, J. M. (2013). Autonomous application of quantitative PCR in the deep sea: in situ surveys of aerobic methanotrophs using the deep-sea environmental sample processor. *Environmental science & technology*, *47*(16), 9339-9346.

Vanwonterghem, I., Evans, P. N., Parks, D. H., Jensen, P. D., Woodcroft, B. J., Hugenholtz, P., & Tyson, G. W. (2016). Methylotrophic methanogenesis discovered in the archaeal phylum Verstraetearchaeota. *Nature microbiology*, *1*(12), 1-9.

Wallmann, K., Linke, P., Suess, E., Bohrmann, G., Sahling, H., Schlüter, M., Dählmann, A., Lammers, S., Greinert, J., & von Mirbach, N. (1997). Quantifying fluid flow, solute mixing, and biogeochemical turnover at cold vents of the eastern Aleutian subduction zone. *Geochimica et Cosmochimica Acta*, *61*(24), 5209-5219.

Wang, X., Zhang, S., Wang, H., Canfield, D. E., Su, J., Hammarlund, E. U., & Bian, L. (2017). Remarkable preservation of microfossils and biofilms in Mesoproterozoic silicified bitumen concretions from northern China. *Geofluids*, *2017*(1), 4818207.

Webster, C. R., Mahaffy, P. R., Atreya, S. K., Moores, J. E., Flesch, G. J., Malespin, C., McKay, C. P., Martinez, G., Smith, C. L., & Martin-Torres, J. (2018). Background levels of methane in Mars' atmosphere show strong seasonal variations. *science*, *360*(6393), 1093-1096.

Welte, C., & Deppenmeier, U. (2014). Bioenergetics and anaerobic respiratory chains of aceticlastic methanogens. *Biochimica et Biophysica Acta (BBA)-Bioenergetics*, *1837*(7), 1130-1147.

Wolfe, J. M., & Fournier, G. P. (2018). Horizontal gene transfer constrains the timing of methanogen evolution. *Nature ecology & evolution*, *2*(5), 897-903.

Wu, M. L., de Vries, S., van Alen, T. A., Butler, M. K., Op den Camp, H. J., Keltjens, J. T., Jetten, M. S., & Strous, M. (2011). Physiological role of the respiratory quinol oxidase in the anaerobic nitrite-reducing methanotroph 'Candidatus Methylomirabilis oxyfera'. *Microbiology*, *157*(3), 890-898.

Yung, Y. L., Chen, P., Nealson, K., Atreya, S., Beckett, P., Blank, J. G., Ehlmann, B., Eiler, J., Etiope, G., & Ferry, J. G. (2018). Methane on Mars and habitability: challenges and responses. *Astrobiology*, *18*(10), 1221-1242.

Zahnle, K. J., Lupu, R., Catling, D. C., & Wogan, N. (2020). Creation and evolution of impact-generated reduced atmospheres of early Earth. *The Planetary Science Journal*, *1*(1), 11.

Zhu, J., Wang, Q., Yuan, M., Tan, G.-Y. A., Sun, F., Wang, C., Wu, W., & Lee, P.-H. (2016). Microbiology and potential applications of aerobic methane oxidation coupled to denitrification (AME-D) process: a review. *Water research*, *90*, 203-215.

Zou, C., Zhu, R., Chen, Z.-Q., Ogg, J. G., Wu, S., Dong, D., Qiu, Z., Wang, Y., Wang, L., & Lin, S. (2019). Organic-matter-rich shales of China. *Earth-Science Reviews*, *189*, 51-78.

Chapter 2

Microbial Redox Cycling Sustains Euxinia and Limits Methane Escape in a Proterozoic Ocean Analog

Emily Klonicki-Ference[1], Tanner Waters[2], Christopher Jones[3], Caroline Hung[3], Charles Diamond[3], Michael McCormick[4], Timothy Lyons[3], and Tina Treude[1,5*]

[1]Deptartment of Earth, Planetary, and Space Sciences, University of California, Los Angeles, CA, USA

[2]Institute of the Environmental and Sustainability and The Center for Diverse Leadership in Science, University of California, Los Angeles, CA, USA

[3]Department of Earth Sciences, University of California, Riverside, CA, USA

[4]Department of Biology, Hamilton College, Clinton, NY, USA

[5]Department of Atmospheric and Oceanic Sciences, University of California, Los Angeles, CA, USA

*Correspondence: ttreude@g.ucla.edu

Abstract

Earth's history is marked by ecosystem shifts driven by microbial metabolic innovation in its ancient oceans. Yet, the role of early life in planetary evolution, especially methane's contribution,

remains difficult to resolve. Ancient analog sites, such as stratified euxinic systems, offer an insight into early biogeochemical cycles, reflecting conditions intermittently prevalent within the Proterozoic. Green Lake, a meromictic lake with euxinia below its ~20 m chemocline, was used to study methane, sulfur, and nitrogen cycling via next-generation sequencing, radiotracer incubations, and geochemical flux budgeting. We found high rates of sulfate reduction (396 nmol L^{-1} d^{-1}), methane oxidation (580 nmol L^{-1} d^{-1}), and monomethylamine-based methanogenesis co-occurring in the euxinic water. Methane oxidation was likely driven by metabolically versatile bacterial methanotrophs, including *Crenothrix* and *Methylacidiphilales*, typically aerobic but potentially active here via denitrification or fermentation. Although accounting for only ~4% of total oxygen demand, methanotrophy at the chemocline formed an efficient methane filter, limiting atmospheric flux. Flux calculations of e^- equivalents revealed an oxidant-reductant imbalance dominated by sulfide, maintaining euxinia by preventing oxygen intrusion and fueling microbial redox activity. These sharp redox gradients facilitated tightly coupled methane, nitrogen, and sulfur cycling. Collectively, our results support a model in which euxinia is maintained by vertical fluxes of reductants and microbial redox processes, while methane, though capable of consuming oxygen abiotically, is not the main driver of oxygen drawdown. Such redox architectures could have stabilized Proterozoic Ocean chemistry, limiting greenhouse gas buildup and modulating oxygenation, thus shaping early climate and biosphere evolution.

1. Introduction

Planetary habitability reflects interactions among evolving interior, surface, and atmospheric systems that have shaped life's emergence across Earth's 4.5-billion-year history (Kasting & Catling, 2003). One major inflection point was the Great Oxygenation Event (GOE, ~2.5 to 2.0 Ga), which marked Earth's transition from an anoxic to persistently oxic atmosphere and initiated biogeochemical cycles that still shape global function today (Lyons et al., 2024; Och & Shields-Zhou, 2012). These changes chronical Earth's biospheric evolution and offer a framework for assessing exoplanet habitability.

Post-GOE Proterozoic oxygen levels are estimated to have been 1–10% of present atmospheric concentrations (Daines et al., 2017; Diamond & Lyons, 2018; Planavsky et al., 2020). Oceans likely remained redox-stratified, with anoxic ferruginous waters overlain by weakly oxygenated surface layers (Anbar & Knoll, 2002; Planavsky et al., 2011). Euxinic mid-depth zones presumably persisted along productive continental margins, where Mesoproterozoic primary productivity was regulated by nutrient supply and redox feedbacks (Lyons et al., 2021). Sulfide-driven copper limitation may have inhibited complete denitrification, resulting in nitrous oxide accumulation (Fennel et al., 2005), while iron-mediated chemodenitrification and ammonium release from microbial mats likely further shaped nitrogen availability (Stanton et al., 2018; Stüeken & Prave, 2022). A shift from negative to positive $\delta^{15}N$ values in the isotopic record is consistent with intensified microbial denitrification and coupled nitrification feedbacks (Fennel et al., 2005; Garvin et al., 2009; Stüeken et al., 2016). Although carbon dioxide and water were likely the dominant Proterozoic greenhouse gases (Kasting & Catling, 2003), methane and nitrous oxide may have also contributed (Buick, 2007; Pavlov et al., 2000). Prior to the evolution of biological methanogenesis, episodic abiotic methane production via serpentinization (Etiope & Sherwood

Lollar, 2013) and impact-generated hydrogen in reducing atmospheres (Zahnle et al., 2020) may have sustained a greenhouse effect that stabilized early Earth's climate until biogenic sources became dominant (Catling et al., 2001).

As atmospheric oxygen remained low, the emergence of biogenic methane cycling may have further influenced redox dynamics and climate regulation in Mesoproterozoic oceans (Fakhraee et al., 2019). Anaerobic methanogenesis, among Earth's earliest metabolisms, is supported by isotope and molecular clock data (Ueno et al., 2006; Wolfe & Fournier, 2018) and may have driven the evolution of anaerobic methanotrophy (Catling et al., 2001). Although its exact timing remains uncertain, enzymatic parallels between methanogenesis and methane oxidation suggest a shared origin (Nitschke & Russell, 2013). Aerobic methanotrophy likely emerged in oxygenated surface niches by 2.72 Ga and spread post-GOE via lateral gene transfer (Eigenbrode & Freeman, 2006; Kang et al., 2019).

In modern oxic marine systems, most of the methane flux from the sediment to the water column is sourced in biogenic methane, formed through anaerobic breakdown of organic matter by acetoclastic and hydrogenotrophic methanogenesis (Knittel & Boetius, 2009; Reeburgh, 2007). Anaerobic methanotrophic archaea (ANME) use nitrate (Raghoebarsing et al., 2006), ferric iron, or manganese (Beal et al., 2009) as electron acceptors, or sulfate, often in syntrophy with Desulfobacterota (Boetius et al., 2000). Fermentative microbes produce substrates for methanogens and sulfate reducers (Schink, 1997), linking carbon and sulfur cycling. Methane that escapes or exceeds the capacity of benthic AOM is oxidized by aerobic methanotrophic bacteria in the overlying water column (Reeburgh, 2007). These metabolic interactions may have similarly structured redox conditions and regulated greenhouse gas fluxes in Proterozoic oceans (Canfield et al., 2018; Zou et al., 2019).

To investigate these processes under conditions similar to the Proterozoic, we studied Fayetteville Green Lake (New York), a meromictic lake with euxinia below a ~20.5 m chemocline (**Fig. 1**) (Havig et al., 2015). Its upper mixolimnion experiences seasonal cyanobacterial blooms and carbonate whiting events (Thompson et al., 1990), while sulfate-rich groundwater from gypsum-bearing shale fuels microbial sulfate reduction and anoxygenic phototrophy (Herndon et al., 2018). Sulfate levels (9.5–15.6 mM) exceed Proterozoic estimates (Fakhraee et al., 2019; Kah et al., 2004) but are below modern oceans (28 mM), and methane accumulates in both water column and sediment (Havig et al., 2015). While sulfur cycling is well studied (Block et al., 2021; Zerkle et al., 2010), methane-related microbial activity remains underexplored (Rojas et al., 2021).

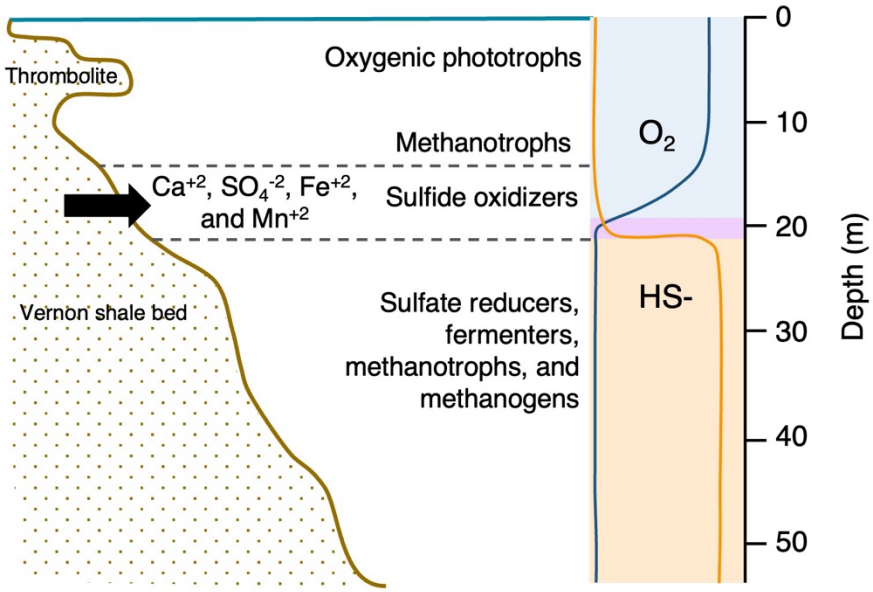

Figure 1. Overview of microbial communities and key geochemical constraints in Fayetteville Green Lake. Black arrow depicts mineral-rich groundwater introduced into the chemocline by the Vernon shale bed. The oxygen and sulfide profiles are denoted on the right, with the magenta coloring representing the suspended purple sulfur bacteria plate at the chemocline. Modified from Hamilton et al., (2016).

Here, we identify methane-cycling mechanisms in the water column, assess microbial oxidation efficiency under euxinic, low-sulfate conditions, and evaluate methane's role in sustaining anoxia. We integrated geochemical analyses, rate measurements, and 16S rRNA gene sequencing to show high rates of sulfate reduction and methane oxidation, with evidence that metabolically versatile methanotrophs such as *Crenothrix* and *Methylacidiphilales* likely drive methane turnover under euxinic conditions. The persistence of euxinia appears to be sustained by microbial redox processes fueled by vertical fluxes of reductants, mostly sulfide, which suppress oxygen intrusion and maintain anoxic conditions.

2. Methods

2.1 Sampling

Samples were collected from Green Lake, Fayetteville, NY, United States at 43.05138° N, 75.96589° W, referred to here as 'Deep Station', where the lake exhibits its deepest depth (53 m). A permit to conduct sampling at Green Lake was obtained from the New York State Office of Parks, Recreation and Historic Preservation.

Temperature, conductivity, pH, turbidity, dissolved oxygen, salinity, and oxidation-reduction potential (ORP) were measured *in situ* using a calibrated YSI EXO2 multi-parameter sonde (YSI Inc.) following the manufacturer's protocol. Water column samples were collected from 10 to 35 m using a Van Dorn-style sampler (WildCo Beta Horizontal Bottle), spanning the oxic mixolimnion, chemocline, and euxinic monimolimnion (**Suppl. Table 1**). Two aluminum rowboats were tethered for station holding, with GPS used to revisit coordinates. Sampling began at 10 m and progressed downward to avoid mixing. At each depth, the sampler was horizontally rinsed

before each of two consecutive hauls: one for geochemical analysis, the other for microbial analysis (16S rRNA sequencing, cell counts).

Upon retrieval, geochemical subsampling prioritized volatiles (methane, total sulfide), followed by nutrients and sulfate. All geochemical samples (except methane) were filtered through 0.45 µm filters to prevent biotic or abiotic alteration. Sulfide was preserved in 4 mL cryovials with 0.5 mL of 20% zinc acetate and 3.5 mL of filtered water. Samples for phosphate, nitrate, and nitrite were preserved in 50 mL aliquots with 20 µL of 20% sodium hydroxide (García-Robledo et al., 2014). Methane was collected in 125 mL glass vials with black stoppers and crimp caps, filled three times to eliminate bubbles before sealing. Samples were stored in a cooler with cold packs (~4 h) prior to refrigeration (~5 °C) or freezing (–20 °C), depending on type and treatment.

On the second sampling day, water for metabolic rate assays (sulfate reduction, methane oxidation, monomethylamine methanogenesis) was collected in triplicate plus one control per depth. Each 30 mL glass crimp vial was filled bubble-free and sealed with non-toxic chlorobutyl stoppers (blue Bellco, 20 mm (Niemann et al., 2015)) and aluminum crimps. Samples were kept cold (4–10 °C) and dark during the 24 h interval between collection and processing at the home laboratory.

2.2 Geochemical analyses of water samples

For methane determination, vials were amended with 7.5 mL 50% NaOH and 2.5 mL air headspace while removing 10 mL of water. Methane partial pressure in the headspace was analyzed via gas chromatography using a Shimadzu GC-2014 with a Haysep-D packed column and flame ionization detector. The column was held at 80 °C, with helium as the carrier gas (12 mL min^{-1}). Methane concentrations were calibrated using Scotty Analyzed Gases (±5% precision) and

calculated using Henry's law and the Bunsen solubility coefficient (Yamamoto et al., 1976) to include both gas and liquid phases.

Sulfate was measured by ion chromatography (Metrohm 761), and total sulfide via spectrophotometry (Cline, 1969). Total alkalinity was determined by titration (Pavlova et al., 2008). Phosphate (Grasshoff et al., 2009), nitrate and nitrite (García-Robledo et al., 2014), as well as ammonium (Grasshoff et al., 2009) were quantified by spectrophotometry. Nitrite was measured directly using a colorimetric azo-dye reaction, while nitrate was first reduced to nitrite using vanadium(III) (García-Robledo et al., 2014). Total values were read in a microplate reader, and nitrate calculated by the difference. Ammonium was quantified using the indophenol (phenol/nitroprusside) method and measured spectrophotometrically following a 1:5 dilution to reduce sulfide interference (Grasshoff et al., 2009).

2.3 Determinations of microbial metabolic rates in water samples

Metabolic *ex situ* rates were determined at the home laboratory using radiolabeled substrates (**Suppl. Table 1**). All incubations were performed at 7 °C (near *in-situ* temperature) and in the dark. Methane oxidation rates were measured using ^{3}H-labeled methane (Bussmann et al., 2015). Samples were incubated for 67 h with 10 µL gaseous ^{3}H-CH_4 (1 kBq, 20 Ci mmol^{-1}; American Radiolabeled Chemicals). Controls received 1 mL of 25% sulfuric acid prior to tracer addition to inhibit microbial activity and account for the higher carbonate content. For total radioactivity, 2 mL subsamples were added to 6 mL scintillation vials with 3 mL Ultima Gold LLT. For ^{3}H-CH_4 converted to ^{3}H-H_2O, additional 2 mL subsamples were bubbled with air for 5 min prior to scintillation fluid addition. All samples were gently inverted and analyzed via liquid scintillation counting.

Methylotrophic methanogenesis was assessed with ^{14}C-labeled monomethylamine (Krause & Treude, 2021). Samples were incubated 11 days with 30 µL tracer (66 kBq, 55 mCi mmol^{-1}), then stopped by pouring into 50 mL crimp vials containing 2 g NaOH pellets (~7% final concentration). Vials were sealed and shaken to halt microbial activity and separate $^{14}CH_4$ (headspace) from ^{14}C-monomethylamine and ^{14}C-inorganic carbon (liquid). An assumed monomethylamine concentration of 100 nM, based on literature (Yang et al., 1994), was used to calculate rates.

Sulfate reduction was measured with ^{35}S-labeled sulfate. Samples were incubated for 10 days with 10 µL carrier-free tracer (1.85 MBq, >1000 Ci mmol^{-1}), then stopped by transferring to 50 mL centrifuge tubes containing 15 mL 20% zinc acetate. Controls received zinc acetate before tracer addition. Samples were stored at –30 °C and analyzed using the cold chromium distillation method (Kallmeyer et al., 2004). Approximately 2 g bentonite clay was added before distillation to form a pellet during centrifugation, facilitating separation of dissolved ^{35}S-sulfate from solid reduced ^{35}S phases.

For all assays (^{3}H, ^{14}C, ^{35}S), samples were considered active if activity exceeded the killed control mean by 3 standard deviations. Values above this threshold were background-corrected by subtracting the killed control mean.

2.4 Microbial cell counts

Formaldehyde-preserved water column samples (final concentration 2%) were vacuum filtered at the home laboratory using a glass filtration tower. Microbial cells were filtered onto a 0.2 µM membrane filter (25 mm Isopore PC Membrane) with a backing filter (25 mm Whatman GF/F Glass Microfiber Filter). Cells were stained with DAPI (4′,6-diamidino-2-phenylindole) and

counted at 1000x oil immersion with an epifluorescence microscope (Zeiss Axio Imager.M2 with APOTOME.2 Zen2.pro software).

2.5 Nucleic acid extraction, amplification of 16S rRNA genes, and sequencing

Water column nucleic acids and negative filter controls were extracted from Sterivex cartridges using a modified DNeasy Blood & Tissue Kit protocol (QIAGEN) optimized for increased eDNA yield (Spens et al., 2017). Library preparation followed a modified protocol (Saito & Doi, 2021). The V3–V4 region of the 16S rRNA gene was amplified using universal bacterial primers 341F (5′-CCTACGGGAGGCAGCAG-3′) (Muyzer et al., 1993) and 806R (5′-GGACTACHVGGGTWTCTAAT-3′) (Caporaso et al., 2011). To target ANME and methanogens, archaeal primers 515f (5′-GTGYCAGCMGCCGCGGTAA-3′) and 926R (5′-CCGYCAATTYMTTTRAGTTT-3′) were used at 18, 20, 22, and 25 m (Parada et al., 2016). PCR was performed using 25 µL reactions: 12.5 µL QIAGEN Multiplex Taq PCR 2× Master Mix, 5 µL each of forward and reverse primer (2 mM), 1 µL sample DNA, and 1.5 µL molecular-grade water. Unique dual indices (Nextera, Illumina) were added in a second 25 µL reaction (12.5 µL Kapa Hifi MasterMix, 5 µL DNA template, 1.25 µL index, 6.25 µL water). Indexing success was confirmed by agarose gel electrophoresis (2% gel, SybrSafe staining). DNA was gel-extracted (QIAquick Gel Extraction Kit), quantified with the Qubit dsDNA Broad Range Assay (Thermo Fisher Scientific), and pooled in equimolar amounts. Sequencing was performed on an Illumina MiSeq 600 platform (2 × 300 bp), with 15% PhiX spike-in, at the University of California, Davis.

2.6 Sequence processing and taxonomic analysis

Paired-end fastq files were processed with DADA2 for amplicon sequence variant (ASV) calling (Callahan et al., 2016) and Cutadapt for primer removal and quality trimming (Martin, 2011). Reads with Q-scores <30 or failing to merge were discarded. Quality-filtered sequences were clustered into OTUs at 97% identity. An average of 87,617 non-chimeric reads was retained per sample. One low-yield sample (22 m, V3–V4; 4,108 reads) was cautiously retained due to taxonomic similarity with adjacent depths. Taxonomy was assigned via the SILVA database (v138.1). Raw reads are archived under BioProject ID PRJNA1261034.

3. Results and Discussion

3.1 Depth-stratified geochemistry and nutrient consumption across the chemocline

In August 2022, a thermocline and chemocline were observed between 18.0 and 20.1 m (**Fig. 2a, b**). In this zone, oxygen concentrations approached the sensor's minimum detection limit of 0 mg L^{-1} (sensor accuracy: ±0.1 mg L^{-1} or 1% of reading, whichever is greater). Below 20.1 m, the sonde consistently reported values at 0 µM and occasionally registered slightly negative readings (**Fig. 2b**), which we interpret as artifacts due to calibration offset. Oxygen was considered effectively absent only when redox potential also dropped below zero. In this profile, redox first became negative at 19.7 m (–5.5 mV) and declined to –372 mV at 40 m. Methane concentrations, while present in lower concentrations above the chemocline (67-185 nM), strongly increased below, reaching 8.7 µM at 35 m (**Fig. 2b**). Total alkalinity peaked at 21 m (6.3 mM), suggesting active biogeochemical processing at this depth, potentially involving multiple anaerobic pathways such as sulfate reduction and methanogenesis. This depth also corresponds to a suspended plate of purple sulfur bacteria (Culver & Brunskill, 1969). These organisms have been estimated to mediate 83% of primary productivity in Green Lake via anoxygenic photosynthesis (Culver & Brunskill, 1969;

Thompson et al., 1990), highlighting the oxic–anoxic interface as a key site of aerobic and anaerobic activity. Turbidity (**Fig. 2a**) and total cell counts (**Fig. 3b**) parallel the alkalinity profile with peaks at 20 m.

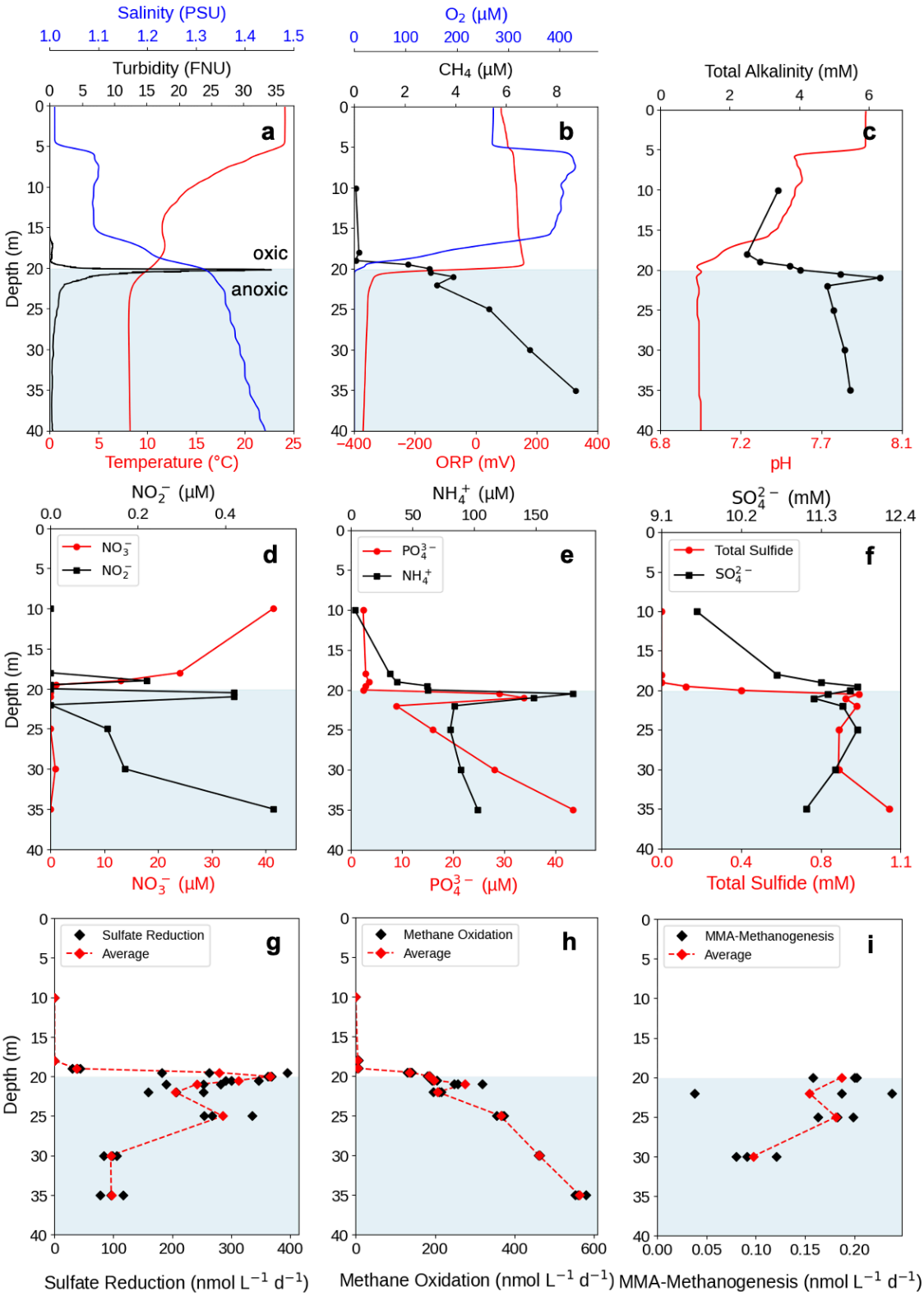

Figure 2. Water column profiles of physical, geochemical and metabolic parameters at the Deep Station (between 10 and 40 m). (**a**) Concentration profiles of salinity (blue), temperature

(red), and turbidity (in Formazin Nephelometric Unit, FNU; black). (**b**) Methane (CH_4) concentrations (black circle) combined with Oxygen Reduction Potential (ORP) (red) and dissolved Oxygen (O_2) (blue). (**c**) Total Alkalinity (black circle) and pH (red) by depth. (**d**) Nitrate (NO_3^-) (red circle) and nitrite (NO_2^-) (black square). (**e**) Phosphate (PO_4^{-3}) (red circle) and ammonium (NH_4^+) (black square). (**f**) Total Sulfide (red circle) and sulfate (SO_4^{-2}) (black square). Rates of (**g**) sulfate reduction, (**h**) methane oxidation, and **i** methanogenesis from monomethylamine. For (**i**), assumed monomethylamine environmental concentration of 100 nM was used to calculate the rates. The chemocline (18.0 to 20.1 m depth), which encompassed the redoxcline, marks the zone where oxygen concentration sharply dropped to 0 µM and the ORP became negative (−5.5 mV). The white background shading in the upper half of the graph corresponds to depths where oxygen was detectable via the sonde and the lower blue shading represents water depths where oxygen was not detected and ORP was negative. Note that NH_4^+ concentrations are likely an underestimation where sulfide is high, caused by sulfide interference in the indophenol blue assay with nitroprusside catalyst, which suppresses color formation and artificially lowers the measured NH_4^+ signal.

Nitrogen and sulfur species varied along the physicochemical gradients, with ammonium concentrations peaking at the chemocline: from 2.6 µM at 10 m to 180 µM at 20.5 m, then decreasing to 103 µM at 35 m. Sulfide increased sharply from 0.12 mM at 19.5 m to 0.93 mM at 20.5 m and 1.1 mM at 35 m, consistent with the redox potential profile (**Fig. 2a, f**). This steep rise in sulfide underscores its role as a key electron donor and highlights the monimolimnion's capacity to sustain microbial reduction processes. Sulfate concentrations ranged from 9.6 mM at 10 m to 11 mM at 35 m, with slightly lower values above the chemocline, likely due to freshwater dilution rather than microbial sulfate reduction. A distinct sulfate decline coincided with the sulfide

maximum and peak sulfate reduction rates, indicating net microbial sulfate consumption and sulfide accumulation, rather than complete recycling within the sulfur pool.

At our shallowest sampling depth (10 m), nitrate reached 40 μM and declined sharply, reaching depletion (0 μM) by 20 m. The steepest drop occurred between 18 and 19.5 m, indicating peak nitrate consumption within the chemocline. Nitrite remained low overall but peaked at 19 m (0.42 μM) and gradually increased to 0.5 μM between 25 and 35 m. These trends reflect active nitrogen cycling under hypoxic to anoxic conditions (18–20 m) and suggest nitrous oxide production via incomplete denitrification, a process active when oxygen falls below 10 μM, as observed near the chemocline. A small increase in nitrate (0.9 μM) and nitrite (0.17 μM) at 30 m supports the presence of a "second chemocline" (Torgersen et al., 1981), likely driven by episodic aquifer discharges transporting nitrate from summer rainfall. Concurrent peaks in alkalinity, ammonium, and phosphate at 30 m indicate organic matter degradation. Anaerobic oxidation of organic material releases ammonium and phosphate and elevates alkalinity via bicarbonate production; these processes are also observed in oxygen minimum zones (Kalvelage et al., 2013).

Phosphate peaked at 20.5 m, decreased at 22 m, and then increased linearly with depth (**Fig. 2e**), mirroring the iron profile in Havig et al. (Havig et al., 2015). Under reducing conditions, ferric iron (Fe^{3+}) is reduced to ferrous iron (Fe^{2+}), destabilizing iron-phosphate minerals and releasing both phosphate and iron into solution. This mechanism is particularly important in anoxic settings, such as sediments and sediment–water interfaces (Dijkstra et al., 2014). Prior work in Green Lake identified elevated dissolved Fe^{2+} concentrations (~1500 nM) below 20.5 m, consistent with biologically or sulfide-driven iron reduction (Havig et al., 2015).

Molar fluxes of key dissolved oxidants (oxygen, nitrate) and reductants (methane, total sulfide, Fe^{2+}, Mn^{2+}, ammonium), along with their electron equivalent (e^- Eq) fluxes, were quantified

across the chemocline to assess methane's role in redox dynamics (**Table 1**). Sulfate was excluded from flux calculations due to its non-linear profile influenced by groundwater and surface inflows (**Fig. 1**); instead, its flux was estimated from sulfate reduction rates (**Fig. 2g**) below the oxygen-depleted zone. For the calculation of solute fluxes we applied Fick's first law of diffusion and included eddy diffusivity (**Eq. 1**), where *J(cc)* is the total solute flux across the chemocline [mol m^{-2} s^{-1}], D_m is the molecular diffusion coefficient of the solute [m^2 s^{-1}], K_z is the eddy diffusivity or turbulent diffusion coefficient [m^2 s^{-1}], *dC* is the change in solute concentration [mol m^{-3}], and *dX* is the diffusion distance [m]. All final fluxes were converted to mmol m^{-2} d^{-1}.

$$J_{(cc)} = -(D_m + K_z)\frac{dC}{dX} \qquad (Eq\ 1)$$

Sulfide contributed the largest reductant flux, substantially exceeding all other measured species. In comparison, NH_4^+ and Mn^{2+} fluxes were one, methane two, and Fe^{2+} three orders of magnitude lower. Expressed as electron equivalents (e^- Eq), the net flux of oxidants and reductants resulted in a surplus of 428 mmol e^- Eq m^{-2} d^{-1}. If this excess consists solely of sulfide and is fully used in anoxygenic photosynthesis by the purple sulfur bacterial plate at the chemocline, it corresponds to a carbon assimilation rate of 469 g C m^{-2} yr^{-1} (based on 4 e^- Eq per CO_2 fixed). This rate is at comparable scale to the 241 g C m^{-2} yr^{-1} reported from ^{14}C-CO_2 incubations at Green Lake in 1966–1967 (Culver & Brunskill, 1969). After validating our preliminary flux estimates against literature values, we found that aerobic methane oxidation contributes ~4% of total oxygen consumption based on electron-equivalent comparisons.

Table 1. Fluxes of solutes and e^- equivalents across the chemocline. For the determination of molecular diffusion fluxes through the thermocline, an average *in-situ* temperature of 10°C, a salinity of 0 PSU, and a porosity of 1 was assumed. All molecular diffusion coefficients (D_m), where

calculated based on Boudreau 1997 (Boudreau, 1997), except for gases. The D_m for CH_4 at 10°C was interpolated using data from Witherspoon et al. 1965 (Witherspoon & Saraf, 1965) and Iversen & Jørgensen 1993 (Iversen & Jørgensen, 1993). The D_m for O_2 was taken from Broecker & Peng 1974 (Broecker & Peng, 1974). For the determination of dX, two end points between a linear concentration change (slope) across the thermocline were used (Top and Bottom Depth). dC is the change in concentration over depth (dX). Mn^{2+} and Fe^{2+} data are from the November 2012 and July 2013 samplings, respectively (Havig et al., 2015). Because eddy diffusivity at the chemocline is currently unknown for Green Lake, we applied a coefficient of 0.01 $cm^2\ s^{-1}$ (Dahl et al., 2010), which was determined for Lake Cadagno, Switzerland, a meromictic sulfidic lake with characteristics similar to Green Lake. Red/Ox indicates the reduction and oxidation reaction from which e^- equivalents (e^- Eq) were derived assuming max use. The e^- Flux was determined by multiplying the solute flux with e^- Eq. Fluxes of oxidants into the chemocline from above are positive, while fluxes of reductants from below are negative. Sum is the sum of all respective fluxes (negative vs. positive). For more details see text.

Solute	**D_m**	**K_z**	**Top Depth**	**Bottom Depth**	**dX**	**dC**	**Solute Flux**	**Red/Ox**	**e^- Eq**	**e^- Flux**
	[10^{-6} $cm^2\ s^{-1}$]	[$cm^2\ s^{-1}$]	[m]	[m]	[cm]	[nmol cm^{-3}]	[mmol $m^{-2}\ d^{-1}$]		[No. of e^-]	[mmol $m^{-2}\ d^{-1}$]
O_2	15.7	0.01	15.50	19.00	350	372	9.20	O_2 red to H_2O	4	36.8
NO_3^-	13.4	0.01	18.00	19.50	150	23.0	1.33	NO_3^- red to NH_4^+	8	10.6
SO_4^{2-}	N/A	N/A	20.00	21.00	100	integrated red rate	0.339	SO_4^{2-} red to HS^-	8	2.71
NH_4^+	13.6	0.01	18.00	20.50	250	-149	-5.15	NH_4^+ ox to NO_3^-	8	-41.2
Mn^{2+}	4.73	0.01	19.25	21.25	200	-58.1	-2.51	Mn^{2+} ox to Mn^{4+}	2	-5.03
Fe^{2+}	4.81	0.01	17.75	20.75	300	-1.97	-0.057	Fe^{2+} ox to Fe^{3+}	1	-0.06
CH_4	11.5	0.01	19.00	21.00	200	-3.86	-0.167	CH_4 ox to CO_2	8	-1.33
HS^-	13.1	0.01	19.00	20.50	150	-934	-53.8	HS^- ox to SO_4^{2-}	8	-431
						Sum Solute Flux:	**-50.9**		**Sum e^- Flux:**	**-428**

3.2 Microbial sulfate and methane turnover

Microbial sulfate reduction peaked at 19.5 m (396 nmol L^{-1} d^{-1}; Fig. 2g), ~0.5 m above the highest total cell counts (**Fig. 3b**). In Green Lake, elevated organic matter, likely from the annual post-whiting die-off of primary producers, may fuel water column sulfate reduction, promoting sulfide accumulation. A similar relationship between organic carbon flux and sulfur cycling is seen in the Black Sea, where decomposing marine snow enhances localized sulfate reduction in euxinic waters (Canfield et al., 1996). These dynamics suggest that episodic organic matter pulses can directly influence the intensity and vertical extent of redox processes in stratified, sulfidic systems. Within the chemocline, cryptic sulfur cycling may occur as a portion of the sulfide produced by microbial sulfate reduction, which is rapidly reoxidized by residual oxygen, nitrate, or metal oxides before reaching detectable concentrations (Canfield et al., 2010). However, given the limited availability of these oxidants, the majority of sulfide is likely processed via anoxygenic photosynthesis. Sulfate reduction (~37 nmol L^{-1} d^{-1}) was detected at 19 m, despite the presence of oxygen (~8 μM), potentially reflecting anoxic micro-niches within organic particles (Raven et al., 2021) or transient anoxia during handling. Together with elevated organic input, these low-oxygen conditions may promote closely linked reductive and oxidative sulfur processes typical of stratified, sulfidic environments.

The persistence of dissolved Fe^{2+} in Green Lake's sulfidic monimolimnion, despite elevated sulfide, has been attributed to continuous microbial iron reduction, limited iron sulfide precipitation, and Fe^{2+} complexation with organic and inorganic ligands (Havig et al., 2015). While some minerals (e.g., greigite, mackinawite) approach saturation, others remain undersaturated, delaying precipitation and allowing Fe^{2+} to persist in solution. Pyrite formation has been shown to occur primarily during sediment diagenesis in the upper 15 cm (Suits & Wilkin, 1998), rather than

in the water column, contributing to Fe^{2+} retention. In contrast to fully oxygenated marine systems, where sulfate reduction is largely confined to sediments, the Black Sea exhibits water column formation of amorphous iron sulfide, greigite, and to a lesser extent pyrite (Canfield et al., 1996; Neretin et al., 2004).

Microbial methane oxidation activity was detectable throughout all sampling depths. While the ^3H-CH_4 tracer does not distinguish between aerobic and anaerobic methane oxidation, the nature of the metabolism can be interpreted in the context of oxygen. Methane oxidation was minimal and likely aerobic above (0.19 nmol L^{-1} d^{-1} at 10 m) and in the upper zone of the chemocline (~5 nmol L^{-1} d^{-1}, at 18 and 19 m) where methane concentrations were low (185 nM and 60 nM, respectively) and oxygen levels >7 µM (**Fig. 2h**). Starting at 19.5 m, oxidation rates increased with methane concentration, reaching the highest rate, 563 nmol L^{-1} d^{-1}, at 35 m, where methane was at its highest (8.7 µM). While methane consumption at 19 m was likely still aerobic (8 µM O_2) the process must have transitioned to anaerobic at 20.5 m and below where oxygen was consistently zero and redox potential was negative.

Notably, microbial methane production from monomethylamine was detected between 20–30 m, overlapping with zones of methane oxidation indicating cryptic methane cycling (Krause & Treude, 2021; Xiao et al., 2017). This process was likely supported by strongly reducing conditions and organic matter input from lysate in the dense bacterial plate. Methane production rates should be interpreted cautiously, as they are based on assumed monomethylamine concentrations and reflect only one methanogenic pathway. Increasing methane concentrations with depth suggest a significant benthic source via upward diffusion (Havig et al., 2015), though *in situ* water column production likely also contributes to overall cycling. As lakes are globally significant methane sources (Bastviken et al., 2004), chemocline-associated methanogenesis highlights the role of

methanotrophs in limiting atmospheric release, reflected in low epilimnetic methane concentrations relative to the monimolimnion. Monomethylamine-based methanogenesis, which does not compete with sulfate reduction, likely occurs in other permanently stratified lakes, supported by taxonomic and isotopic evidence from similar euxinic systems (Biderre-Petit et al., 2019; Oswald et al., 2016).

3.3 Geochemical gradients shape microbial communities driving methane and sulfur cycling

Of the 16S rRNA gene sequences amplified with the V3–V4 primer set, ~99% were assigned to Bacteria and <1% to Archaea. At 10 m (402 μM O_2, 67 nM CH_4, 0.66 mM sulfide), dominant bacterial phyla included Cyanobacteria (44%), Actinobacteria (30%), Proteobacteria (14%), and Bacteroidota (8%). The most abundant classes above the chemocline (10 and 18 m) were Actinobacteria, Cyanobacteriia, Bacteroidia, and Alphaproteobacteria, comprising 84% of the community on average (**Fig. 3a**). Between 20 and 25 m, where oxygen was near or below detection and sulfide concentrations increased, community composition shifted. At 25 m (anoxic, 5.3 μM CH_4, 1.5 mM sulfide), dominant phyla included Bacteroidota (37%), Cyanobacteria (24%), Patescibacteria (13%), and Campylobacterota (10%), with Cyanobacteriia, Chlorobia, Bacteroidia, and Parcubacteria comprising 77% of total 16S reads (**Fig. 3a**). It is important to note that interpreting community composition below the chemocline is complex as settling particles aggregate and integrate microbial populations from shallower depths (Cohen et al., 2023). Sulfur-metabolizing bacteria were detected across all depths. ASVs assigned to sulfur-oxidizing Campylobacterota (families Sulfurimonadaceae and Sulfurovaceae) peaked below the chemocline, consistent with nitrate-reducing and sulfur-oxidizing metabolisms. *Sulfuricurvum*, a facultative sulfur oxidizer, was identified at 20, 22, and 25 m. Purple sulfur bacteria (family Chromatiaceae) were detected primarily at 20 m by 16S rRNA sequencing and visually confirmed by the magenta

pigment observed on filters during geochemical sample filtering, consistent with previous reports of a purple sulfur plate and coinciding with peak cell counts (**Fig. 3b**) (Block et al., 2021).

Sulfate reducers within Desulfobacterota, including Desulfobaccales, were detected at 20 m and below, with peak 16S rRNA abundance at 20 m aligning with maximum sulfate reduction rates. ASVs assigned to *Desulfocapsa thiozymogenes*, capable of both sulfate reduction and sulfur disproportionation (Janssen et al., 1996), were also found at 20 and 25 m. Desulfobacterota (order Syntrophales), detected at the chemocline, are known to oxidize fatty acids syntrophically with methanogens, producing hydrogen or formate that supports hydrogenotrophic methanogens such as *Methanobacterium* (Yan et al., 2024).

Aerobic methanotrophs, including Methylococcales (e.g., *Crenothrix*) and *Methylacidiphilales*, were detected at low relative abundance (<0.01%) across all depths. *Methanofastidiosales*, a methylotrophic methanogen within Euryarchaeota, was identified at 25 m (<0.1%). Despite low 16S rRNA representation, these taxa may still be transcriptionally active (Galambos et al., 2019), suggesting broader vertical activity. V4–V5 region sequencing additionally detected methanogens *Methanoregula* and *Methanobacterium*, along with hydrogen producing bacteria from the *Hydrogenedensaceae* family at 20, 22, and 25 m. *Methanomicrobiales* and *Methanobacterium* include hydrogenotrophic lineages that use H_2 and CO_2 for methanogenesis (Thauer et al., 2008). While their presence in the water column is prominent, their activity remains uncertain due to potential competition with sulfate-reducing bacteria for hydrogen.

Notably, ANME were absent in the reduced, anoxic zone (~20–25 m), while aerobic methane oxidizers like *Crenothrix* and *Methylacidiphilales* were present, highlighting the unexpected dominance of aerobic methanotrophs in a zone typically favorable to anaerobic methane oxidation

(**Table 2**). Further, methanogens potentially capable of reverse methanogenesis, such as *Methanosarcina acetivorans* (Sowers et al., 1984), were also not found.

Table 2. 16S rRNA (V3-V4 and V4-V5 primer sets) percent relative abundances of methane oxidizers and methanogens in the water column by depth. N/A denotes the V4-V5 primer was not used at 10 meters.

			Depth (m)				
Organism	Metabolism	Primer Set	10	18	20	22	25
Crenothrix	Methane Oxidation	V3-V4	0	0.0074	0.018	0	0
Methylacidiphilaceae	Methane Oxidation	V3-V4	0.023	0.0052	0	0	0
Methanofastidiosales	Methanogenesis	V3-V4	0	0	0	0	0.0095
Methanoregula	Methanogenesis	V4-V5	N/A	0	0.041	0.026	0.015
Methanobacterium lacus	Methanogenesis	V4-V5	N/A	0	0.012	0.015	0.012
Methylacidiphilaceae	Methane Oxidation	V4-V5	N/A	0.080	0.0036	0.0033	0
Methanofastidiosales	Methanogenesis	V4-V5	N/A	0	0.011	0.033	0.12
Crenothrix	Methane Oxidation	V4-V5	N/A	0	0	0	0.0043

The detection of methane-oxidizing bacteria as the sole methanotrophs in 16S rRNA sequences, alongside methane oxidation in anoxic waters, suggests that typically aerobic organisms may mediate methane oxidation under anoxia in Green Lake. *Crenothrix* is particularly notable for its ability to grow on methane under nitrate-reducing conditions and its involvement in denitrification, highlighting its distinct role among Gammaproteobacterial methanotrophs (Awala et al., 2024; Hoefman et al., 2014; Oswald et al., 2017). While it remains unclear whether *Crenothrix* can generate and use denitrification intermediates such as nitrite or nitrous oxide when

oxygen and nitrate are depleted, genomic and experimental data suggest it may perform methane oxidation coupled to nitrate reduction (Oswald et al., 2017). Several aerobic methanotrophs harbor genes for denitrification and hydrogen metabolism, and some metabolize alternative substrates like acetate or ethanol (He et al., 2022). Acidophilic methanotrophs, including Methylacidiphilum *(Methylacidiphilales)* and *Methylocella tundrae*, possess *nosZ* genes encoding nitrous oxide reductase and can grow anaerobically via concurrent methane oxidation and nitrous oxide respiration (Awala et al., 2024).

This alternative metabolic strategy may allow bacterial methane oxidation in oxygen-depleted environments. Intra-aerobic methanotrophs, such as *Candidatus Methylomirabilis oxyfera*, oxidize methane via nitrite reduction by internally generating oxygen: nitrite is first reduced to nitric oxide, which then dismutates into nitrogen and oxygen gases, with the oxygen used for methane oxidation (Wu et al., 2011). Aerobic methanotrophs from the Methylomonadaceae and Methylocystaceae families also exhibit metabolic plasticity and may oxidize methane using nitrate, nitrite, or metal oxides under oxygen-limited conditions (Deng et al., 2024). These capabilities suggest alternative energy-conserving mechanisms in anoxic environments for organisms traditionally considered obligate aerobes.

Crenothrix is increasingly reported in methane-rich (up to 1 mM) anoxic freshwater systems, including Lake Rotsee (Cabrol et al., 2020), Lake Zug (Switzerland) (Oswald et al., 2017), and lakes in Northwestern Siberia (Schorn et al., 2024). In Lake Pavin, a permanently stratified, methane-rich lake (up to 4 mM), methanotrophic bacteria including *Methylococcaceae* have been detected, while no evidence of ANME was found (Biderre-Petit et al., 2019). Obligate aerobic methanotrophs (e.g., *Methylocystaceae*, *Methylococcaceae*) are frequently found in hypoxic

(<5 μM O_2) and anoxic environments, including meromictic lakes, rice paddies, peatlands, and the deep biosphere (Guerrero-Cruz et al., 2021).

However, in the absence of nitrous oxide data and with limited nitrite in the monimolimnion, methane oxidation in the euxinic zone may proceed via alternative pathways such as fermentation-based methanotrophy, enabling persistence under strongly reducing conditions lacking typical electron acceptors like oxygen, nitrate, or nitrite. In Lake Zug, *Methylococcales* MOB assimilate methane-derived carbon under hypoxic to anoxic conditions, suggesting fermentation-based methanotrophy possibly coupled with denitrification (Schorn et al., 2024). Supporting this, metagenomic and transcriptomic data show widespread expression of mixed-acid fermentation genes in nearly all MOB bins, indicating fermentative metabolism in anoxic waters (Schorn et al., 2024). Although not yet biochemically confirmed, *Methylomicrobium alcaliphilum* 20Z ferments formaldehyde into organic acids (formate, acetate, succinate, lactate, hydroxybutyrate) under oxygen-limited conditions, producing minimal biomass (Kalyuzhnaya et al., 2013). *M. buryatense* 5GB1C similarly excretes acetate and succinate under micro-oxic conditions (Gilman et al., 2017). These findings highlight fermentation-based methanotrophy as a flexible strategy allowing MOB to persist across steep redox gradients with reduced oxygen dependence. Our results align with Siberian lakes, where *Methylomonadaceae*, *Methylobacter*, and *Crenothrix* dominate methane oxidation in anoxic waters and *mcrA* gene abundance is low, suggesting ANME and methanogens capable of anaerobic methane oxidation play a minor role (Cabrol et al., 2020). We likewise propose *Crenothrix* and *Methylacidiphilales* as the primary methane oxidizers in Green Lake's anoxic zone.

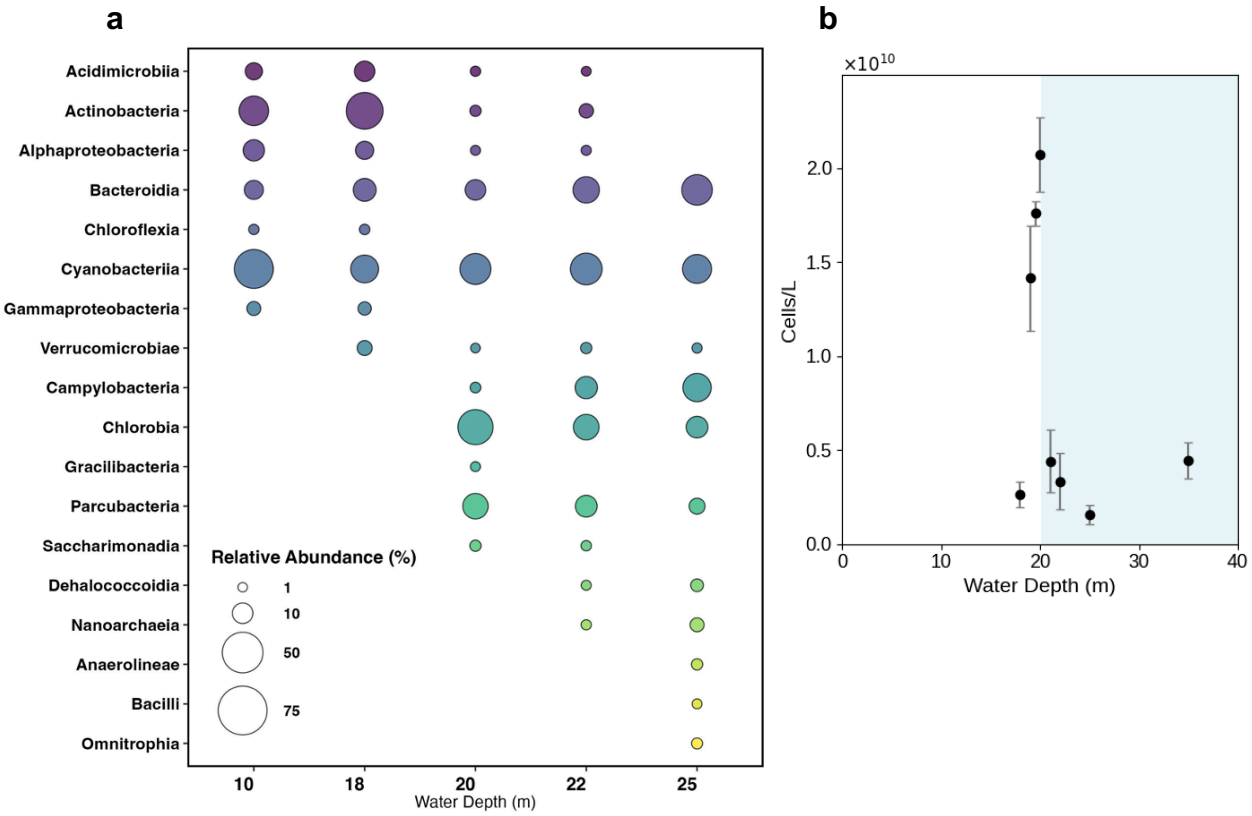

Figure 3. (**a**) 16S rRNA relative abundances of bacterial and archaeal classes above 1% based on 16S RNA gene sequencing (V3–V4 region). The size of the circle corresponds to the percent relative abundance with the legend inset to the figure. (**b**) Total cell counts stained with DAPI (4′,6-diamidino-2-phenylindole). Cell counts were not determined at 10 m. The white background shading in the left half of the graph corresponds to depths where oxygen was detectable via the sonde and the right blue shading represents water depths where oxygen was not detected and ORP was negative.

3.4 Implications for the Proterozoic Ocean

A long-standing hypothesis posits that Earth's oceans experienced a stepwise redox evolution: beginning with pervasive anoxia in the early Proterozoic, followed by the emergence of oxygenated surface waters in the mid to late Proterozoic, and culminating in extensive deep-ocean

ventilation during the Paleozoic. Our observations from Green Lake challenge the simplicity of this narrative, instead highlighting a mosaic of coupled redox processes and microbial interactions that may have sustained localized oxygen sinks and methane barriers under low oxygen and euxinic conditions. Geochemical profiles, metabolic rates, and microbial community data reveal complex coupling among nitrogen, methane, and sulfur cycling. Flux estimates at Green Lake show a net oxygen uptake of 9.2 mmol m^{-2} d^{-1} across the chemocline. Although sulfide (and to some extent nitrogen) fluxes appear largely regulated by anoxygenic photosynthesis in the purple sulfur bacterial mat, oxygen consumption likely results from a mixture of reductant fluxes like sulfide, reduced metals, reduced nitrogen species, and methane. Based on the flux of e- equivalents across the chemocline resulting from methane (-1.33 mmol m^{-2} d^{-1}), the role of methane as an oxygen sink is relatively minor (~4%, **Table 1**). Instead, the combined action of all reductants effectively suppress oxygen accumulation, while methanotrophy limits methane escape to the epilimnion.

By extension, the Mesoproterozoic shallow ocean may have supported similar redox-stratified gradients, where microbial redox cycling created self-reinforcing oxygen sinks and methane barriers. Molecular clocks and geochemical proxies identify this interval as a critical window for convergent microbial innovation under low oxygen (Chen & Strous, 2013; Fakhraee et al., 2019; Lyons et al., 2009). Genomic reconstructions suggest horizontal gene transfer endowed methanotrophs with denitrification and fermentation pathways (Kalyuhznaya et al., 2009), and that the post-GOE fusion of nitric- and nitrous-oxide reductases into cytochrome c oxidase (Castresana et al., 1994) may have enhanced metabolic flexibility at steep redox interfaces. Such innovations likely enabled microbes to exploit variable electron acceptors and persist under fluctuating redox regimes, establishing sharp oxic-sulfidic boundaries where anoxygenic phototrophs could thrive, as observed in Green Lake and Lake Cadagno (Philippi et al., 2021).

Though methane oxidation in the euxinic waters of Green Lake appears linked to characteristically aerobic bacterial taxa, potentially operating through denitrification intermediates or fermentation, such pathways could have persisted in the Proterozoic. Despite lower sulfate levels in Proterozoic oceans, sulfate, as well as iron and manganese oxides, may have served as terminal electron acceptors in localized microenvironments. These could have expanded the range of methane-oxidizing metabolisms, allowing communities to regulate methane flux and redox balance under spatially heterogeneous conditions. Notably, Green Lake maintains high sulfate reduction rates (up to 396 nmol L^{-1} d^{-1}) despite lower sulfate levels than modern marine systems, consistent with isotope- and model-based reconstructions of localized euxinia during this interval (Canfield, 1998; Fakhraee et al., 2019; Lyons et al., 2021; Lyons et al., 2014).

Together, these microbial interactions could have supported spatially heterogeneous and temporally variable oxygen minimum zones, shaped by the balance of oxidants and reductants. Redox-sensitive metal enrichments, sulfur isotope excursions, and iron-sulfur mineralogy in Mesoproterozoic sediments point to the persistence of low-oxygen water masses (Kah et al., 2004; Lyons et al., 2009). As a modern analog, Green Lake highlights the importance of metabolic flexibility in microbial communities, rather than nutrient limitation alone, in regulating Proterozoic oxygenation.

4. Conclusions

Our study demonstrates that even under low-oxygen or euxinic conditions analogous to those predicted for the Mesoproterozoic Ocean, efficient water column methane oxidation, potentially mediated by fermentative methanotrophy or denitrification intermediates, and high microbial sulfate reduction rates co-occurred to suppress methane release and sustain euxinia.

Although methane oxidation accounted for only a small fraction of total oxygen demand, it likely acted as a biological filter, shaping vertical redox structure and limiting methane flux to the atmosphere. These processes contributed to localized anoxia in stratified waters, where microbial and chemical oxygen sinks outpaced resupply. While the Mesoproterozoic is often described as a time of sluggish oxygen production due to nutrient limitation, our findings suggest rapid microbial redox cycling also played a key role in maintaining persistent low-oxygen layers and supporting anaerobic and microaerophilic metabolisms important for greenhouse gas regulation.

Although inconclusive for Green Lake, expansion of photic zone euxinia may have created ecological niches for anoxygenic phototrophic sulfur bacteria capable of coupling sulfide oxidation to nitrogen fixation, potentially influencing nitrogen availability and primary productivity, as observed in Lake Cadagno (Philippi et al., 2021). Over time, such productivity may have contributed to net oxygen accumulation and altered ocean–atmosphere redox balance. These feedbacks raise broader questions about the pathways and electron acceptors involved in methane oxidation, particularly after the emergence of aerobic methanotrophy. By reducing methane emissions and sustaining localized oxygen sinks, microbial processes may have helped buffer redox conditions and modulate greenhouse gas buildup, contributing more actively to climate regulation than previously recognized.

Funding

Funding was provided by the NASA Interdisciplinary Consortia for Astrobiology Research (ICAR) Program issued through the Science Mission Directorate. EK was funded through the ICAR and the US National Science Foundation (Award No.: 2048597). TW was funded by the Eugene-Cota Robles Fellowship, NSF-GRFP, the Switzer Fellowship, R. Eagle and the Center for Diverse Leadership in Science from the David and Lucile Packard Foundation.

Acknowledgements

We thank T. Hughes and the employees at Green Lake State Park for assisting in the permitting process and providing onsite sample processing space. We would also like to thank C. Junium of Syracuse University for hosting sediment core processing and R. Eagle of UCLA for hosting microbial community processing in their respective laboratories. Finally, we would like to thank D. Utter at the California Institute of Technology for guidance on sequencing post-processing.

References

Anbar, A. D., & Knoll, A. H. (2002). Proterozoic ocean chemistry and evolution: a bioinorganic bridge? *science*, *297*(5584), 1137-1142.

Awala, S. I., Gwak, J.-H., Kim, Y., Jung, M.-Y., Dunfield, P. F., Wagner, M., & Rhee, S.-K. (2024). Nitrous oxide respiration in acidophilic methanotrophs. *Nature Communications*, *15*(1), 4226.

Bastviken, D., Cole, J., Pace, M., & Tranvik, L. (2004). Methane emissions from lakes: Dependence of lake characteristics, two regional assessments, and a global estimate. *Global biogeochemical cycles*, *18*(4).

Beal, E. J., House, C. H., & Orphan, V. J. (2009). Manganese-and iron-dependent marine methane oxidation. *science*, *325*(5937), 184-187.

Biderre-Petit, C., Taib, N., Gardon, H., Hochart, C., & Debroas, D. (2019). New insights into the pelagic microorganisms involved in the methane cycle in the meromictic Lake Pavin through metagenomics. *FEMS Microbiology Ecology*, *95*(3), fiy183.

Block, K. R., O'Brien, J. M., Edwards, W. J., & Marnocha, C. L. (2021). Vertical structure of the bacterial diversity in meromictic Fayetteville Green Lake. *MicrobiologyOpen*, *10*(4), e1228.

Boetius, A., Ravenschlag, K., Schubert, C. J., Rickert, D., Widdel, F., Gieseke, A., Amann, R., Jørgensen, B. B., Witte, U., & Pfannkuche, O. (2000). A marine microbial consortium apparently mediating anaerobic oxidation of methane. *Nature*, *407*(6804), 623-626.

Boudreau, B. P. (1997). *Diagenetic models and their implementation* (Vol. 505). Springer Berlin.

Broecker, W. S., & Peng, T.-H. (1974). Gas exchange rates between air and sea. *Tellus*, *26*(1-2), 21-35.

Buick, R. (2007). Did the Proterozoic 'Canfield Ocean'cause a laughing gas greenhouse? In (Vol. 5, pp. 97-100): Wiley Online Library.

Bussmann, I., Matousu, A., Osudar, R., & Mau, S. (2015). Assessment of the radio 3H-CH4 tracer technique to measure aerobic methane oxidation in the water column. *Limnology and Oceanography: Methods*, *13*(6), 312-327.

Cabrol, L., Thalasso, F., Gandois, L., Sepulveda-Jauregui, A., Martinez-Cruz, K., Teisserenc, R., Tananaev, N., Tveit, A., Svenning, M. M., & Barret, M. (2020). Anaerobic oxidation of methane and associated microbiome in anoxic water of Northwestern Siberian lakes. *Science of the Total Environment*, *736*, 139588.

Callahan, B. J., McMurdie, P. J., Rosen, M. J., Han, A. W., Johnson, A. J. A., & Holmes, S. P. (2016). DADA2: High-resolution sample inference from Illumina amplicon data. *Nature methods*, *13*(7), 581-583.

Canfield, D. E. (1998). A new model for Proterozoic ocean chemistry. *Nature*, *396*(6710), 450-453.

Canfield, D. E., Lyons, T. W., & Raiswell, R. (1996). A model for iron deposition to euxinic Black Sea sediments. *American Journal of Science*, *296*(7), 818-834.

Canfield, D. E., Stewart, F. J., Thamdrup, B., De Brabandere, L., Dalsgaard, T., Delong, E. F., Revsbech, N. P., & Ulloa, O. (2010). A cryptic sulfur cycle in oxygen-minimum–zone waters off the Chilean coast. *science*, *330*(6009), 1375-1378.

Canfield, D. E., Zhang, S., Frank, A. B., Wang, X., Wang, H., Su, J., Ye, Y., & Frei, R. (2018). Highly fractionated chromium isotopes in Mesoproterozoic-aged shales and atmospheric oxygen. *Nature Communications*, *9*(1), 2871.

Caporaso, J. G., Lauber, C. L., Walters, W. A., Berg-Lyons, D., Lozupone, C. A., Turnbaugh, P. J., Fierer, N., & Knight, R. (2011). Global patterns of 16S rRNA diversity at a depth of millions

of sequences per sample. *Proceedings of the national academy of sciences*, *108*(supplement_1), 4516-4522.

Castresana, J., Lübben, M., Saraste, M., & Higgins, D. (1994). Evolution of cytochrome oxidase, an enzyme older than atmospheric oxygen. *The EMBO journal*, *13*(11), 2516-2525.

Catling, D. C., Zahnle, K. J., & McKay, C. P. (2001). Biogenic methane, hydrogen escape, and the irreversible oxidation of early Earth. *science*, *293*(5531), 839-843.

Chen, J., & Strous, M. (2013). Denitrification and aerobic respiration, hybrid electron transport chains and co-evolution. *Biochimica et Biophysica Acta (BBA)-Bioenergetics*, *1827*(2), 136-144.

Cline, J. D. (1969). Spectrophotometric determination of hydrogen sulfide in natural waters 1. *Limnology and Oceanography*, *14*(3), 454-458.

Cohen, A. B., Klepac-Ceraj, V., Bidas, K., Weber, F., Garber, A. I., Christensen, L. N., Cram, J. A., McCormick, M. L., & Taylor, G. T. (2023). Deep photoautotrophic prokaryotes contribute substantially to carbon dynamics in oxygen-deficient waters in a permanently redox-stratified freshwater lake. *Limnology and Oceanography*, *68*(1), 232-247.

Culver, D., & Brunskill, G. (1969). Fayetteville Green Lake, New York. V. Studies of primary production and zooplankton in a meromictic marl lake 1. *Limnology and Oceanography*, *14*(6), 862-873.

Dahl, T. W., Anbar, A. D., Gordon, G. W., Rosing, M. T., Frei, R., & Canfield, D. E. (2010). The behavior of molybdenum and its isotopes across the chemocline and in the sediments of sulfidic Lake Cadagno, Switzerland. *Geochimica et Cosmochimica Acta*, *74*(1), 144-163.

Daines, S. J., Mills, B. J., & Lenton, T. M. (2017). Atmospheric oxygen regulation at low Proterozoic levels by incomplete oxidative weathering of sedimentary organic carbon. *Nature Communications*, *8*(1), 14379.

Deng, Y., Liang, C., Zhu, X., Zhu, X., Chen, L., Pan, H., Xun, F., Tao, Y., & Xing, P. (2024). Methylomonadaceae was the active and dominant methanotroph in Tibet lake sediments. *ISME communications*, *4*(1), ycae032.

Diamond, C. W., & Lyons, T. W. (2018). Mid-Proterozoic redox evolution and the possibility of transient oxygenation events. *Emerging Topics in Life Sciences*, *2*(2), 235-245.

Dijkstra, N., Kraal, P., Kuypers, M. M., Schnetger, B., & Slomp, C. P. (2014). Are iron-phosphate minerals a sink for phosphorus in anoxic Black Sea sediments? *PloS one*, *9*(7), e101139.

Eigenbrode, J. L., & Freeman, K. H. (2006). Late Archean rise of aerobic microbial ecosystems. *Proceedings of the national academy of sciences*, *103*(43), 15759-15764.

Etiope, G., & Sherwood Lollar, B. (2013). Abiotic methane on Earth. *Reviews of Geophysics*, *51*(2), 276-299.

Fakhraee, M., Hancisse, O., Canfield, D. E., Crowe, S. A., & Katsev, S. (2019). Proterozoic seawater sulfate scarcity and the evolution of ocean–atmosphere chemistry. *Nature Geoscience*, *12*(5), 375-380.

Fennel, K., Follows, M., & Falkowski, P. G. (2005). The co-evolution of the nitrogen, carbon and oxygen cycles in the Proterozoic ocean. *American Journal of Science*, *305*(6-8), 526-545.

Galambos, D., Anderson, R. E., Reveillaud, J., & Huber, J. A. (2019). Genome-resolved metagenomics and metatranscriptomics reveal niche differentiation in functionally redundant microbial communities at deep-sea hydrothermal vents. *Environmental Microbiology*, *21*(11), 4395-4410.

García-Robledo, E., Corzo, A., & Papaspyrou, S. (2014). A fast and direct spectrophotometric method for the sequential determination of nitrate and nitrite at low concentrations in small volumes. *Marine Chemistry*, *162*, 30-36.

Garvin, J., Buick, R., Anbar, A. D., Arnold, G. L., & Kaufman, A. J. (2009). Isotopic evidence for an aerobic nitrogen cycle in the latest Archean. *science*, *323*(5917), 1045-1048.

Gilman, A., Fu, Y., Hendershott, M., Chu, F., Puri, A. W., Smith, A. L., Pesesky, M., Lieberman, R., Beck, D. A., & Lidstrom, M. E. (2017). Oxygen-limited metabolism in the methanotroph Methylomicrobium buryatense 5GB1C. *PeerJ*, *5*, e3945.

Grasshoff, K., Kremling, K., & Ehrhardt, M. (2009). *Methods of seawater analysis*. John Wiley & Sons.

Guerrero-Cruz, S., Vaksmaa, A., Horn, M. A., Niemann, H., Pijuan, M., & Ho, A. (2021). Methanotrophs: discoveries, environmental relevance, and a perspective on current and future applications. *Frontiers in Microbiology*, *12*, 678057.

Hamilton, T. L., Bryant, D. A., & Macalady, J. L. (2016). The role of biology in planetary evolution: cyanobacterial primary production in low-oxygen Proterozoic oceans. *Environmental Microbiology*, *18*(2), 325-340.

Havig, J. R., McCormick, M. L., Hamilton, T. L., & Kump, L. R. (2015). The behavior of biologically important trace elements across the oxic/euxinic transition of meromictic Fayetteville Green Lake, New York, USA. *Geochimica et Cosmochimica Acta*, *165*, 389-406.

He, R., Wang, J., Pohlman, J. W., Jia, Z., Chu, Y.-X., Wooller, M. J., & Leigh, M. B. (2022). Metabolic flexibility of aerobic methanotrophs under anoxic conditions in Arctic lake sediments. *The ISME journal*, *16*(1), 78-90.

Herndon, E. M., Havig, J. R., Singer, D. M., McCormick, M. L., & Kump, L. R. (2018). Manganese and iron geochemistry in sediments underlying the redox-stratified Fayetteville Green Lake. *Geochimica et Cosmochimica Acta*, *231*, 50-63.

Hoefman, S., van der Ha, D., Boon, N., Vandamme, P., De Vos, P., & Heylen, K. (2014). Niche differentiation in nitrogen metabolism among methanotrophs within an operational taxonomic unit. *BMC microbiology*, *14*, 1-11.

Iversen, N., & Jørgensen, B. B. (1993). Diffusion coefficients of sulfate and methane in marine sediments: Influence of porosity. *Geochimica et Cosmochimica Acta*, *57*(3), 571-578.

Janssen, P. H., Schuhmann, A., Bak, F., & Liesack, W. (1996). Disproportionation of inorganic sulfur compounds by the sulfate-reducing bacterium Desulfocapsa thiozymogenes gen. nov., sp. nov. *Archives of Microbiology*, *166*, 184-192.

Kah, L. C., Lyons, T. W., & Frank, T. D. (2004). Low marine sulphate and protracted oxygenation of the Proterozoic biosphere. *Nature*, *431*(7010), 834-838.

Kallmeyer, J., Ferdelman, T. G., Weber, A., Fossing, H., & Jørgensen, B. B. (2004). A cold chromium distillation procedure for radiolabeled sulfide applied to sulfate reduction measurements. *Limnology and Oceanography: Methods*, *2*(6), 171-180.

Kalvelage, T., Lavik, G., Lam, P., Contreras, S., Arteaga, L., Löscher, C. R., Oschlies, A., Paulmier, A., Stramma, L., & Kuypers, M. M. (2013). Nitrogen cycling driven by organic matter export in the South Pacific oxygen minimum zone. *Nature Geoscience*, *6*(3), 228-234.

Kalyuhznaya, M. G., Martens-Habbena, W., Wang, T., Hackett, M., Stolyar, S. M., Stahl, D. A., Lidstrom, M. E., & Chistoserdova, L. (2009). Methylophilaceae link methanol oxidation to denitrification in freshwater lake sediment as suggested by stable isotope probing and pure culture analysis. *Environmental microbiology reports*, *1*(5), 385-392.

Kalyuzhnaya, M., Yang, S., Rozova, O., Smalley, N., Clubb, J., Lamb, A., Gowda, G. N., Raftery, D., Fu, Y., & Bringel, F. (2013). Highly efficient methane biocatalysis revealed in a methanotrophic bacterium. *Nature Communications*, *4*(1), 2785.

Kang, C. S., Dunfield, P. F., & Semrau, J. D. (2019). The origin of aerobic methanotrophy within the Proteobacteria. *FEMS microbiology letters*, *366*(9), fnz096.

Kasting, J. F., & Catling, D. (2003). Evolution of a habitable planet. *Annual Review of Astronomy and Astrophysics*, *41*(1), 429-463.

Knittel, K., & Boetius, A. (2009). Anaerobic oxidation of methane: progress with an unknown process. *Annual review of microbiology*, *63*(1), 311-334.

Krause, S. J., & Treude, T. (2021). Deciphering cryptic methane cycling: Coupling of methylotrophic methanogenesis and anaerobic oxidation of methane in hypersaline coastal wetland sediment. *Geochimica et Cosmochimica Acta*, *302*, 160-174.

Lyons, T. W., Anbar, A. D., Severmann, S., Scott, C., & Gill, B. C. (2009). Tracking euxinia in the ancient ocean: a multiproxy perspective and Proterozoic case study. *Annual Review of Earth and Planetary Sciences*, *37*(1), 507-534.

Lyons, T. W., Diamond, C. W., Planavsky, N. J., Reinhard, C. T., & Li, C. (2021). Oxygenation, life, and the planetary system during Earth's middle history: An overview. *Astrobiology*, *21*(8), 906-923.

Lyons, T. W., Reinhard, C. T., & Planavsky, N. J. (2014). The rise of oxygen in Earth's early ocean and atmosphere. *Nature*, *506*(7488), 307-315.

Lyons, T. W., Tino, C. J., Fournier, G. P., Anderson, R. E., Leavitt, W. D., Konhauser, K. O., & Stüeken, E. E. (2024). Co-evolution of early Earth environments and microbial life. *Nature Reviews Microbiology*, *22*(9), 572-586.

Martin, M. (2011). Cutadapt removes adapter sequences from high-throughput sequencing reads. *EMBnet. journal*, *17*(1), 10-12.

Muyzer, G., De Waal, E. C., & Uitterlinden, A. (1993). Profiling of complex microbial populations by denaturing gradient gel electrophoresis analysis of polymerase chain reaction-amplified genes coding for 16S rRNA. *Applied and Environmental Microbiology*, *59*(3), 695-700.

Neretin, L. N., Böttcher, M. E., Jørgensen, B. B., Volkov, I. I., Lüschen, H., & Hilgenfeldt, K. (2004). Pyritization processes and greigite formation in the advancing sulfidization front in the Upper Pleistocene sediments of the Black Sea. *Geochimica et Cosmochimica Acta*, *68*(9), 2081-2093.

Niemann, H., Steinle, L., Blees, J., Bussmann, I., Treude, T., Krause, S., Elvert, M., & Lehmann, M. F. (2015). Toxic effects of lab-grade butyl rubber stoppers on aerobic methane oxidation. *Limnology and Oceanography: Methods*, *13*(1), 40-52.

Nitschke, W., & Russell, M. J. (2013). Beating the acetyl coenzyme A-pathway to the origin of life. *Philosophical Transactions of the Royal Society B: Biological Sciences*, *368*(1622), 20120258.

Och, L. M., & Shields-Zhou, G. A. (2012). The Neoproterozoic oxygenation event: Environmental perturbations and biogeochemical cycling. *Earth-Science Reviews*, *110*(1-4), 26-57.

Oswald, K., Graf, J. S., Littmann, S., Tienken, D., Brand, A., Wehrli, B., Albertsen, M., Daims, H., Wagner, M., & Kuypers, M. M. (2017). Crenothrix are major methane consumers in stratified lakes. *The ISME journal*, *11*(9), 2124-2140.

Oswald, K., Jegge, C., Tischer, J., Berg, J., Brand, A., Miracle, M. R., Soria, X., Vicente, E., Lehmann, M. F., & Zopfi, J. (2016). Methanotrophy under versatile conditions in the water

column of the ferruginous meromictic Lake La Cruz (Spain). *Frontiers in Microbiology*, *7*, 1762.

Parada, A. E., Needham, D. M., & Fuhrman, J. A. (2016). Every base matters: assessing small subunit rRNA primers for marine microbiomes with mock communities, time series and global field samples. *Environmental Microbiology*, *18*(5), 1403-1414.

Pavlov, A. A., Kasting, J. F., Brown, L. L., Rages, K. A., & Freedman, R. (2000). Greenhouse warming by CH4 in the atmosphere of early Earth. *Journal of Geophysical Research: Planets*, *105*(E5), 11981-11990.

Pavlova, G. Y., Tishchenko, P. Y., Volkova, T., Dickson, A., & Wallmann, K. (2008). Intercalibration of Bruevich's method to determine the total alkalinity in seawater. *Oceanology*, *48*, 438-443.

Philippi, M., Kitzinger, K., Berg, J. S., Tschitschko, B., Kidane, A. T., Littmann, S., Marchant, H. K., Storelli, N., Winkel, L. H., & Schubert, C. J. (2021). Purple sulfur bacteria fix N2 via molybdenum-nitrogenase in a low molybdenum Proterozoic ocean analogue. *Nature communications*, *12*(1), 4774.

Planavsky, N. J., McGoldrick, P., Scott, C. T., Li, C., Reinhard, C. T., Kelly, A. E., Chu, X., Bekker, A., Love, G. D., & Lyons, T. W. (2011). Widespread iron-rich conditions in the mid-Proterozoic ocean. *Nature*, *477*(7365), 448-451.

Planavsky, N. J., Reinhard, C. T., Isson, T. T., Ozaki, K., & Crockford, P. W. (2020). Large mass-independent oxygen isotope fractionations in mid-Proterozoic sediments: Evidence for a low-oxygen atmosphere? *Astrobiology*, *20*(5), 628-636.

Raghoebarsing, A. A., Pol, A., Van de Pas-Schoonen, K. T., Smolders, A. J., Ettwig, K. F., Rijpstra, W. I. C., Schouten, S., Damsté, J. S. S., Op den Camp, H. J., & Jetten, M. S. (2006). A

microbial consortium couples anaerobic methane oxidation to denitrification. *Nature*, *440*(7086), 918-921.

Raven, M., Keil, R., & Webb, S. (2021). Microbial sulfate reduction and organic sulfur formation in sinking marine particles. *science*, *371*(6525), 178-181.

Reeburgh, W. S. (2007). Oceanic methane biogeochemistry. *Chemical reviews*, *107*(2), 486-513.

Rojas, C. A., De Santiago Torio, A., Park, S., Bosak, T., & Klepac-Ceraj, V. (2021). Organic electron donors and terminal electron acceptors structure anaerobic microbial communities and interactions in a permanently stratified sulfidic lake. *Frontiers in Microbiology*, *12*, 620424.

Saito, T., & Doi, H. (2021). A model and simulation of the influence of temperature and amplicon length on environmental DNA degradation rates: a meta-analysis approach. *Frontiers in Ecology and Evolution*, *9*, 623831.

Schink, B. (1997). Energetics of syntrophic cooperation in methanogenic degradation. *Microbiology and molecular biology reviews*, *61*(2), 262-280.

Schorn, S., Graf, J. S., Littmann, S., Hach, P. F., Lavik, G., Speth, D. R., Schubert, C. J., Kuypers, M. M., & Milucka, J. (2024). Persistent activity of aerobic methane-oxidizing bacteria in anoxic lake waters due to metabolic versatility. *Nature Communications*, *15*(1), 5293.

Sowers, K. R., Baron, S. F., & Ferry, J. G. (1984). Methanosarcina acetivorans sp. nov., an acetotrophic methane-producing bacterium isolated from marine sediments. *Applied and Environmental Microbiology*, *47*(5), 971-978.

Spens, J., Evans, A. R., Halfmaerten, D., Knudsen, S. W., Sengupta, M. E., Mak, S. S., Sigsgaard, E. E., & Hellström, M. (2017). Comparison of capture and storage methods for aqueous macrobial eDNA using an optimized extraction protocol: advantage of enclosed filter. *Methods in Ecology and Evolution*, *8*(5), 635-645.

Stanton, C. L., Reinhard, C. T., Kasting, J. F., Ostrom, N. E., Haslun, J. A., Lyons, T. W., & Glass, J. B. (2018). Nitrous oxide from chemodenitrification: A possible missing link in the Proterozoic greenhouse and the evolution of aerobic respiration. *Geobiology*, *16*(6), 597-609.

Stüeken, E. E., Kipp, M. A., Koehler, M. C., & Buick, R. (2016). The evolution of Earth's biogeochemical nitrogen cycle. *Earth-Science Reviews*, *160*, 220-239.

Stüeken, E. E., & Prave, A. R. (2022). Diagenetic nutrient supplies to the Proterozoic biosphere archived in divergent nitrogen isotopic ratios between kerogen and silicate minerals. *Geobiology*, *20*(5), 623-633.

Suits, N. S., & Wilkin, R. T. (1998). Pyrite formation in the water column and sediments of a meromictic lake. *Geology*, *26*(12), 1099-1102.

Thauer, R. K., Kaster, A.-K., Seedorf, H., Buckel, W., & Hedderich, R. (2008). Methanogenic archaea: ecologically relevant differences in energy conservation. *Nature Reviews Microbiology*, *6*(8), 579-591.

Thompson, J. B., Ferris, F., & Smith, D. A. (1990). Geomicrobiology and sedimentology of the mixolimnion and chemocline in Fayetteville Green Lake, New York. *Palaios*, 52-75.

Torgersen, T., Hammond, D., Clarke, W., & Peng, T. H. (1981). Fayetteville, Green Lake, New York: 3H-3He water mass ages and secondary chemical structure 1, 2. *Limnology and Oceanography*, *26*(1), 110-122.

Ueno, Y., Yamada, K., Yoshida, N., Maruyama, S., & Isozaki, Y. (2006). Evidence from fluid inclusions for microbial methanogenesis in the early Archaean era. *Nature*, *440*(7083), 516-519.

Witherspoon, P., & Saraf, D. (1965). Diffusion of methane, ethane, propane, and n-butane in water from 25 to 43. *The Journal of Physical Chemistry*, *69*(11), 3752-3755.

Wolfe, J. M., & Fournier, G. P. (2018). Horizontal gene transfer constrains the timing of methanogen evolution. *Nature ecology & evolution*, *2*(5), 897-903.

Wu, M. L., de Vries, S., van Alen, T. A., Butler, M. K., Op den Camp, H. J., Keltjens, J. T., Jetten, M. S., & Strous, M. (2011). Physiological role of the respiratory quinol oxidase in the anaerobic nitrite-reducing methanotroph 'Candidatus Methylomirabilis oxyfera'. *Microbiology*, *157*(3), 890-898.

Xiao, K.-Q., Beulig, F., Kjeldsen, K. U., Jørgensen, B. B., & Risgaard-Petersen, N. (2017). Concurrent methane production and oxidation in surface sediment from Aarhus Bay, Denmark. *Frontiers in Microbiology*, *8*, 1198.

Yamamoto, S., Alcauskas, J. B., & Crozier, T. E. (1976). Solubility of methane in distilled water and seawater. *Journal of Chemical and Engineering Data*, *21*(1), 78-80.

Yan, W., Wang, D., Wang, Y., Wang, C., Chen, X., Liu, L., Wang, Y., Li, Y.-Y., Kamagata, Y., & Nobu, M. K. (2024). Metatranscriptomics-guided genome-scale metabolic reconstruction reveals the carbon flux and trophic interaction in methanogenic communities. *Microbiome*, *12*(1), 121.

Yang, X.-H., Scranton, M. I., & Lee, C. (1994). Seasonal variations in concentration and microbial uptake of methylamines in estuarine waters. *Marine Ecology-Progress Series*, *108*, 303-303.

Zahnle, K. J., Lupu, R., Catling, D. C., & Wogan, N. (2020). Creation and evolution of impact-generated reduced atmospheres of early Earth. *The Planetary Science Journal*, *1*(1), 11.

Zerkle, A. L., Kamyshny Jr, A., Kump, L. R., Farquhar, J., Oduro, H., & Arthur, M. A. (2010). Sulfur cycling in a stratified euxinic lake with moderately high sulfate: Constraints from quadruple S isotopes. *Geochimica et Cosmochimica Acta*, *74*(17), 4953-4970.

Zou, C., Zhu, R., Chen, Z.-Q., Ogg, J. G., Wu, S., Dong, D., Qiu, Z., Wang, Y., Wang, L., & Lin, S. (2019). Organic-matter-rich shales of China. *Earth-Science Reviews*, *189*, 51-78.

Supplementary Material: Klonicki et al. Microbial Redox Cycling Sustains Euxinia and Limits Methane Escape in a Proterozoic Ocean Analog

Supplementary Table 1. Summary of sample types collected by depth at the Deep Station in Green Lake. An "X" indicates that the corresponding analysis was performed at that depth. MMA refers to monomethylamine-based methanogenesis.

Depth (m)	Geochemistry	DNA	Cell Counts	Sulfate Reduction	Methane Oxidation	MMA-Methanogenesis
10	X	X		X	X	
18	X	X	X	X	X	
19	X		X	X	X	
19.5	X		X	X	X	
20	X	X	X	X	X	X
20.5	X			X	X	
21	X		X	X	X	
22	X	X	X	X	X	X
25	X	X	X	X	X	X
30	X			X	X	X
35	X		X	X	X	

Chapter 3

Unveiling the Methanosphere: Transport of Methane and Methanotrophs Beyond Visible Seeps in the Southern California Margin

Emily Klonicki-Ference[1*], Daniel R. Utter[2], Kira Homola[1], John S. Magyar[2], Victoria J. Orphan[2], Lisa Levin[3], Tina Treude[1,4*]

[1]Department of Earth, Planetary, and Space Sciences, University of California Los Angeles, Los Angeles, CA, USA

[2]Division of Geological and Planetary Sciences, California Institute of Technology, Pasadena, CA, USA

[3] Scripps Institution of Oceanography, University of California, San Diego, La Jolla, CA, USA

[4]Department of Atmospheric and Oceanic Sciences, University of California Los Angeles, Los Angeles, CA, USA

*Correspondence: Emily Klonicki-Ference, eklonicki@g.ucla.edu; Tina Treude, ttreude@g.ucla.edu

Abstract

Marine methane (CH_4) seeps are dynamic biogeochemical systems that modulate carbon cycling and support high-biomass communities through microbial CH_4 oxidation. While most CH_4 is consumed anaerobically in sediments, a fraction enters the water column, where aerobic methanotrophs form a biological filter limiting CH_4 flux to the atmosphere. However, the extent to

which this microbial activity and CH_4 influence extend beyond visibly active seep zones remains poorly constrained, with implications for deep-sea food webs, biogeochemical gradients, and carbon cycling. We investigated CH_4 dynamics and methanotroph distribution across three seep sites on the Southern California margin (Del Mar, Santa Monica (800 m) Mound, Lasuen Knoll; ~400–1200 m depth). Using radiotracer (^3H-CH_4) incubations, CH_4 concentration profiling, 16S rRNA gene sequencing, and particulate methane monooxygenase (*pmoA*) gene quantification, we sampled vertical and horizontal transects and near-bottom waters via the HOV *Alvin*. CH_4 oxidation was active not only within seep plumes but also in oxygen-depleted off-seep regions, with the highest rate (454 nmol L^{-1} d^{-1}) observed within a CH_4-rich bubble plume. Methanotrophic taxa exhibited vertical structuring, with greater diversity and abundance near the seafloor, while members of the Methylomonadaceae clade IheB2-23 were also detected throughout the water column. *pmoA* gene abundances remained relatively stable across both seep and off-seep waters, suggesting a persistent CH_4-oxidizing potential. Spearman correlation analyses revealed that environmental drivers of oxidation were site-specific, at some sites, oxidation correlated positively with CH_4 and negatively with O_2, while at others, O_2 availability appeared to enhance oxidation, highlighting geochemical gradients as key but variable controls. These findings support an expanded "methanosphere," a CH_4-influenced microbial zone shaped by physical transport and environmental gradients. This system may facilitate the lateral export of methanotrophic biomass and CH_4-derived carbon, extending the ecological reach of seep ecosystems and linking local CH_4 cycling to broader deep-sea biogeochemistry.

1. Introduction

Although once regarded as rare and biologically limited, deep-sea methane (CH_4) seeps are now increasingly recognized as critical ecosystems that provide services supporting the health and functioning of broader deep-sea communities (Boetius & Wenzhöfer, 2013; Levin, 2005; L. A. Levin et al., 2016; Sibuet & Roy, 2002; Thurber et al., 2014; Treude et al., 2011). Distributed widely along continental margins (Judd & Hovland, 2009), these dynamic environments may play a far more expansive ecological role than previously understood, with implications that extend beyond the boundaries of seep-specific habitats. Cold seeps form where CH_4 is released from subsurface sources via microbial methanogenesis and abiotic processes such as hydrothermal alteration of organic-rich sediments and the dissociation of gas hydrates. These discharges fuel high-biomass communities sustained by chemosynthesis, fundamentally altering local biodiversity and geochemistry (Levin, 2005; Paull et al., 1984; Suess, 2010; Tunnicliffe et al., 2003). The resulting ecosystems are structured by CH_4-oxidizing and chemosynthetic microorganisms, along with a range of fauna that indirectly rely on CH_4-derived carbon (Levin, 2005).

Within seep sediments and associated authigenic carbonates, the anaerobic oxidation of CH_4 (AOM) is tightly coupled to sulfate (SO_4^{2-}) reduction, mediated by syntrophic consortia of anaerobic methanotrophic (ANME) archaea and sulfate-reducing bacteria (SRB) (Boetius et al., 2000; Orphan et al., 2001). This microbial process acts as a significant biological filter, limiting the efflux of CH_4 to the overlying ocean and atmosphere (Hinrichs & Boetius, 2002; Knittel & Boetius, 2009; Treude et al., 2003). The hydrogen sulfide (H_2S) generated through AOM supports dense microbial mats composed of sulfur-oxidizing bacteria and sustains a diverse assemblage of chemosymbiotic invertebrates, such as tubeworms and bivalves (Cavanaugh, 1983).

CH_4 that escapes or exceeds the capacity of sedimentary AOM is oxidized aerobically by methanotrophic bacteria in the overlying water column (Reeburgh, 2007), according to the reaction:

$$CH_4 + 2O_2 \rightarrow CO_2 + 2H_2O$$

CH_4-oxidizing bacteria (MOB), which are phylogenetically diverse and metabolically adaptable, play a central role in mitigating CH_4 emissions from the ocean. MOB occur throughout the marine water column, from well-oxygenated surface waters to low-oxygen (O_2) and even anoxic zones, depending on environmental conditions such as CH_4 availability, O_2 concentration, and particle flux (Reeburgh, 2007; Steinle et al., 2015; Tavormina et al., 2010; Thamdrup et al., 2019). These bacteria catalyze CH_4 oxidation using methane monooxygenase (Kemnitz et al., 2020), the enzyme responsible for the conversion of CH_4 to methanol, the first and rate-limiting step of CH_4 oxidation. MMO exists in two forms: particulate methane monooxygenase (pMMO), a membrane-bound, copper-dependent enzyme that is widely distributed and typically expressed under high-copper conditions, and soluble methane monooxygenase (sMMO), a cytoplasmic, iron-containing enzyme that is expressed under copper-limiting conditions in some methanotrophs (Kalyuzhnaya et al., 2013; Semrau et al., 2010). Most marine MOB encode and express pMMO, which is considered the dominant form of methane monooxygenase among methanotrophs in seawater.

Beyond their free-living forms, MOB also establish symbiotic relationships with protozoan and metazoan hosts. Such symbioses are well documented in CH_4-rich settings like cold seeps and hydrothermal vents, where MOB occur as endosymbionts in bathymodiolin mussels (Childress et al., 1986), vestimentiferan tubeworms (Levin, 2005), feather duster worms (Goffredi et al., 2020), ciliates (Pasulka et al., 2017), and sponges (Rubin-Blum et al., 2019). In these partnerships, MOB supply CH_4-derived organic carbon to their hosts, enabling persistence in CH_4-rich environments that are depleted in photosynthetic carbon sources. Even minimal CH_4 flux from sediments to the

water column supports benthic chemosynthetic processes, while methanotrophs in the overlying water oxidize CH_4 across broad spatial and vertical gradients, shaping both local and regional carbon cycles (Damm et al., 2010).

Beyond their role in structuring benthic and symbiotic communities, CH_4 seeps may influence water column processes at broader spatial scales. CH_4 that escapes from sediments can fuel aerobic methanotrophy above the seafloor, altering O_2/CH_4 gradients, shaping microbial community structure, and potentially supporting pelagic food webs through the transfer of CH_4-derived carbon (Damm et al., 2010; Steinle et al., 2015; Thamdrup et al., 2019). These microbial processes may contribute to nutrient regeneration, localized O_2 consumption, and the attenuation or buffering of CH_4 fluxes to the atmosphere, particularly in low-O_2 environments. Such dynamics may extend beyond the immediate seep zone, affecting adjacent off-seep ecosystems by altering microbial community composition and biogeochemical conditions. The extent to which these microbial processes support ecosystem function is regulated by environmental gradients, notably O_2 availability and organic matter input. O_2 availability directly governs the activity and niche space of aerobic methanotrophs, which require O_2 as a terminal electron acceptor (Boetius & Wenzhöfer, 2013). In O_2-limited zones, aerobic MOB may operate at reduced rates or be outcompeted by anaerobic communities. While SO_4^{2-} is typically abundant in marine settings, organic matter input influences the vertical structure of O_2 concentration by fueling heterotrophic respiration. This, in turn, determines O_2 penetration depth and the location of sulfate-reducing zones, which are critical for AOM (Jørgensen & Kasten, 2006). Consequently, organic matter input modulates the spatial overlap between CH_4 and available electron acceptors, shaping the overall efficiency and pathway of CH_4 consumption in seep systems (Egger et al., 2017).

In contrast to deeper CH_4 seeps such as those along the Aleutian margin, where organic matter delivery to the seafloor is limited and bottom waters are well oxygenated (~160 μM O_2) (Jahnke, 2010; Wallmann et al., 1997), bathyal CH_4 seeps along the Southern California Borderland (~450–1050 m) are defined by elevated organic input and substantially lower O_2 concentrations (<23 μM) (Grupe et al., 2015). These environmental conditions support distinct CH_4-driven biogeochemical regimes. Multiple active seep sites occur along faulted basins and ridges of the Southern California Borderland (Hein et al., 2006; Maloney et al., 2015), where CH_4-rich fluids migrate upward and sustain communities of bacterial mats, carbonate crusts, clams, and tubeworms (Grupe et al., 2015; L. Levin et al., 2016). In this setting, CH_4 oxidation in the water column plays a central role in shaping geochemical gradients and microbial community composition. Variability in seepage intensity, seafloor topography, and local biogeochemistry may further influence aerobic CH_4 oxidation, the redistribution of methanotrophic communities, and geochemical processes such as carbonate precipitation and dissolution (Marlow et al., 2014; Sulpis et al., 2021).

These interactions define a spatially diffuse yet biogeochemically distinct methanosphere, a CH_4-influenced zone that extends beyond visible seep structures. Within the Southern California Borderland, the methanosphere may be expanded by physical processes such as bubble transport, plume dynamics, and lateral advection, which redistribute CH_4 and methanotrophic microbes into adjacent off-seep habitats (Jordan et al., 2019; Ussler III et al., 2013). Understanding these transport pathways is essential for defining the ecological footprint of cold seeps and quantifying their role in deep-sea carbon cycling.

Despite increasing recognition of CH_4 seeps as dynamic deep-sea ecosystems, the extent to which seep-derived CH_4 and associated microbial communities influence off-seep environments remains poorly constrained. Most studies have focused on benthic or near-seep dynamics, leaving

open questions about how far CH_4 and methanotrophs are transported into surrounding waters, and how this dispersal affects microbial activity, geochemical gradients, and adjacent ecosystems beyond the seep center. While some seep-associated mobile fauna, such as red crabs, exhibit variable incorporation of CH_4-derived carbon (Turner et al., 2020), direct evidence for CH_4-derived carbon assimilation by organisms residing exclusively in off-seep habitats remains limited.

To address these gaps, we tested the following hypotheses:

1. CH_4 concentrations and methanotroph indicators (e.g., *pmoA* gene abundance, community composition) decrease with distance from active seep zones but remain elevated relative to background levels within the sampled off-seep area.
2. Lower O_2 and higher organic matter concentrations enhance CH_4 oxidation rates and support greater methanotroph abundance in the water column.
3. Physical transport processes, such as bottom current and bubble-mediated dispersal, contribute to the redistribution of CH_4 and CH_4-oxidizing microbes into adjacent off-seep waters.

This study was conducted during a June–July 2023 expedition aboard the R/V *Atlantis*, where we investigated the spatial extent and structure of the water column methanosphere, defined here as the zone influenced by seep-derived CH_4 in terms of microbial activity, geochemical gradients, and faunal associations. We focused on three active CH_4 seeps along the Southern California Borderland margin, Del Mar (~1000 m), Santa Monica Mound (~800 m), and Lasuen Knoll (~400 m), selected to represent a range of water depths, bottom-water O_2 concentrations, and regional current regimes at the time of sampling. Lasuen Knoll, in particular, lies closer to the photic zone and coastal productivity sources, while the others reflect more bathyal conditions. All sites

exhibited ongoing seepage and supported characteristic seep-associated fauna, including microbial mats and chemosynthetic megafauna. We used vertical, horizontal, and point water column sampling via a CTD-rosette system and instruments mounted on the human-occupied vehicle *Alvin*. CH_4 concentrations and oxidation rates (^3H-CH_4 tracer method) were paired with 16S rRNA gene sequencing and quantification of the *pmoA gene*. Our results reveal strong spatial variation in microbial community structure, metabolic activity, and CH_4 geochemistry within and beyond seep sites. Notably, we found that CH_4 and methanotroph signatures extended beyond the visible seep zones, and that CH_4 oxidation occurred across a range of O_2 conditions.

2. Methods

2.1 Study Areas

2.1.1 Del Mar Seep

The Del Mar Seep, ~30 km off Del Mar, California, at 1020–1040 m depth, is positioned within strike-slip faults at the lower edge of the Santa Monica Basin oxygen minimum zone (OMZ) boundary (Maloney et al., 2015; Ryan et al., 2012). Overlaid with low-O_2 (~17 μM O_2; (Grupe et al., 2015) bearing water, benthic fauna and sediments are influenced by sharp gradients in O_2, H_2S, and organic carbon (Maloney et al., 2015). The seep varies in localized CH_4 fluxes, with a relatively inactive eastern edge, indicated by disarticulated, sparse clam beds and lack of bacterial mat or active gas venting (Maloney et al., 2015). In the western region, carbonate outcrops and chemosynthetic fauna dominate (Maloney et al., 2015). Specifically, previous expeditions to the seep have identified authigenic carbonate boulders, dense bacterial mats and clam beds, tubeworm clusters, and *Bathysiphon filiformis* tube fields (Grupe et al., 2015). Additionally, lower mean faunal $\delta^{13}C$ values were observed in samples collected closer to the seep (<200 m), indicating that

chemosynthetically derived carbon may support elevated animal biomass beyond the central seep zone (Grupe et al., 2015).

2.1.2 Santa Monica Mound

The Santa Monica (800 m) Mound, referred to hereafter as Santa Monica Mound, lies in the Santa Monica Basin at ~800 m water depth, an area characterized by strong CH_4-rich seepage, the presence of gas hydrates, and blister-like seafloor deformation (Hein et al., 2006; Maloney et al., 2015; Paull et al., 2008). Periodic sampling and *in situ* surveys have documented persistent CH_4 bubbling and vigorous fluid flow across the 800 m mound (Paull et al., 1984). Located within the Santa Monica Basin OMZ, the semi-enclosed hydrography can restrict bottom-water exchange, leading to O_2 depletion (<3 μM O_2; (Kemnitz et al., 2020)) that enhances CH_4 oxidation and restricts benthic communities (Grupe et al., 2015; Heintz et al., 2012). Specifically, in the basin it was found that methanotrophic activity increases with restricted water circulation, peaking near the 737 m sill depth, where O_2-depleted waters support a psychrotolerant methanotrophic community (Heintz et al., 2012). At a nearby seep in the Santa Monica Basin, aragonite shells of potential chemosymbiotic bivalves exhibited pronounced ^{13}C depletion (−12‰ to −19‰ $\delta^{13}C$), consistent with incorporation of CH_4-derived carbon. Authigenic carbonate recovered from sediment cores was even more ^{13}C-depleted (−46‰ to −58‰ $\delta^{13}C$), indicating that carbon from AOM was the primary source (Hein et al., 2006).

2.1.3 Lasuen Knoll

Lasuen Knoll is positioned within the Palos Verdes Fault Zone, a tectonically complex region that facilitates vertical fluid migration and supports the development of CH_4-rich habitats

(Fisher et al., 2004; Thompson & Francis, 2019). Seismic mapping suggests that Lasuen Knoll is a pop-up structure at ~670 m depth at its base linked to a restraining stepover of the Palos Verdes Fault, with dextral shear transferring southeast through faults like Carlsbad Ridge and Coronado Bank (Thompson & Francis, 2019). As a relatively uncharacterized CH_4 cold seep, it is not known how CH_4 flux and activity vary spatially, or how it is influenced by faulting and localized overpressure zones. An exploratory dive by the Schmidt Ocean Institute was conducted in 2018 with the ROV SuBastian which visually identified carbonate outcrops, CH_4 bubbles, and potential CH_4 seep-associated fauna.

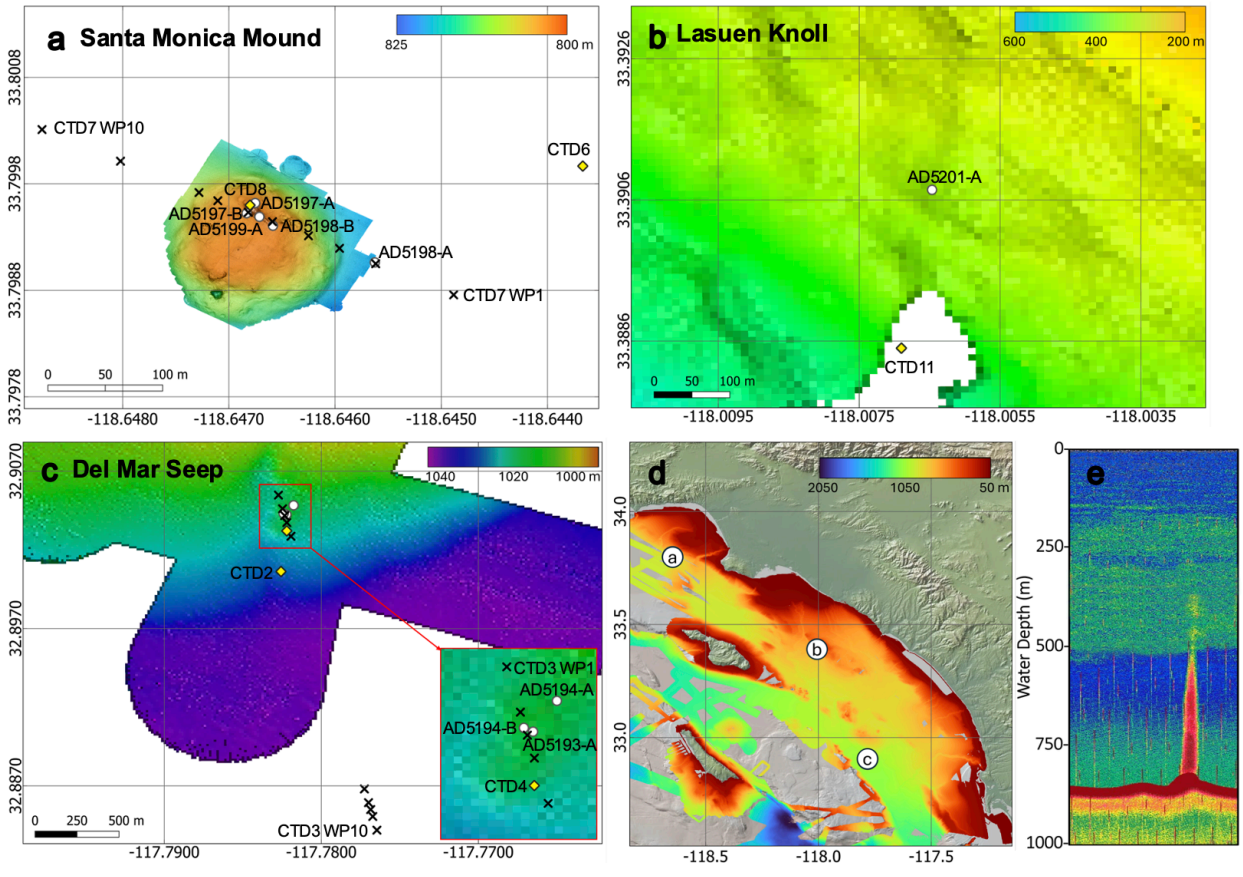

Figure 1. Bathymetric maps of (**a**) the Santa Monica Mound, (**b**) Lasuen Knoll, and (**c**) Del Mar Seep (northwest and ~1km away southeast seep regions), with (**d**) showing site locations within the

Southern California Borderland. High-resolution seafloor mapping of Santa Monica Mound was carried out by the Monterey Bay Aquarium Research Institute (MBARI, n.d.) and archived in the Marine Geoscience Data System. Bathymetric data for Del Mar and Lasuen Knoll were acquired via hydroacoustic surveys to identify and characterize active CH_4 seepage, including CH_4 bubble plumes. Knudsen 3.5 kHz sub-bottom profiling, Kongsberg EM124 multibeam, and Kongsberg EK80 wideband echo sounding systems were used to resolve subseafloor, seafloor, and water column features, respectively. Nighttime survey data informed dive planning for the HOV *Alvin* and guided vertical and horizontal CTD cast deployments the following day. Sampling stations from R/V *Atlantis* include vertical CTD casts (yellow diamonds) and horizontal CTD cast waypoints (black 'X'). Labeled waypoints include WP1 and WP10, with WP2–WP9 ordered sequentially between. HOV *Alvin* dive locations are indicated by white circles. (**e**) EK80 backscatter profile of a CH_4 bubble plume observed at CTD8 and WP6 (CTD7) during cruise AT50-12.

2.2 Sample collection

Sampling was conducted over two weeks during the AT50-12 expedition (July 16–29) aboard the R/V *Atlantis* using the HOV *Alvin* and a CTD/Rosette system for water column profiling and collection. Water samples were collected from various depths, spanning the surface to near-seafloor, across three CH_4 seep sites (Del Mar, Santa Monica, and Lasuen Knoll) using a rosette equipped with 23 × 10 L Niskin bottles (Ocean Test Equipment, Inc., Fort Lauderdale, Florida). A Seabird Scientific pumped CTD system was mounted on a rosette frame outfitted with Niskin bottles and sensors to continuously measure conductivity (SBE4), temperature (SBE3), pressure (SBE9), dissolved O_2 (SBE43), fluorescence (FLNTURTD), and light transmission (C-Star). Salinity and density were calculated from conductivity and temperature, respectively, and depth

was inferred from pressure. All sensors were calibrated prior to deployment according to manufacturer instructions.

Vertical CTD casts were deployed over active seep sites selected based on available information, which varied by location and included real-time EK80 acoustic backscatter data, multibeam seafloor mapping, and/or prior observations from *Alvin* dives. Horizontal CTD transects targeted both active features and surrounding background areas (no visible seep associated fauna, microorganisms, or structures), with the CTD rosette maintained approximately 5 m above the seafloor. For each cast, the ship maintained dynamic positioning using acoustic beacons to remain on station despite prevailing currents. Niskin bottles were only fired after the rosette stabilized at the target location to ensure representative sampling and to minimize current-related offsets. At the Del Mar site, a noticeable gap in horizontal sampling reflects the transit between two spatially distinct, acoustically active seep features (the northwest and southeast region identified through bathymetry).

Samples collected by *Alvin* were obtained via Niskin bottles mounted on the submersible's basket. Sample locations were chosen based on either previously known coordinates (e.g., colonization arrays deployed during the WF05-21 expedition with the R/V *Western Flyer* and ROV *Doc Ricketts* (May 2021)) or observations of gas bubble releases (EK80 or *Alvin* observation) and chemosynthetic habitats during the dive. To prevent sediment contamination, Niskin bottles were triggered while the vehicle hovered approximately 0.5 m above the seafloor, just prior to contact and or after the observed current removed resuspended sediment. For all sampling events, water from each Niskin bottle was subsampled in the following order: (1) CH_4 concentration, (2) CH_4 oxidation rate, and (3) DNA preservation. A complete list of CTD casts and *Alvin* sample metadata is provided in **Table 1** with the horizontal CTD cast waypoint metadata outlined in **Suppl. Table 1.**

All depths are reported as meters below sea level, with “surface waters” defined as 1–5 m depth and “bottom waters” as 5–10 m above the seafloor.

Table 1. Summary of sampling events with Niskin bottles, including seep location, specific site characteristics (such as dominant seep organisms or gas releases), *Alvin* Dive/CTD no., sampling date, sampling start time (*Alvin*: Niskin closure, CTD: start of cast/transect), and geographic coordinates (latitude and longitude). Asterisks (*) indicate that multiple coordinates were recorded for CTD transects, which can be found in **Suppl. Table 1.** The abbreviations used are as follows: DMS for Del Mar Seep, SMM for Santa Monica Mound, and LK for Lasuen Knoll.

Site	Dive/CTD No.	Total Water Depth (m)	Latitude (dec. deg.)	Longitude (dec. deg.)	Sampling Date (UTC)	Sampling Start Time (UTC)	Site Characteristic
DMS	AD5193-A	1022	32.9042	-117.7822	2023-07-17	16:50	crabs, carbonate
	CTD 2	1044	32.8339	-117.7826	2023-07-17	22:45	frenulate worms
	AD5194-A	1022	32.9048	-117.7818	2023-07-18	17:30	brittle stars, snails
	AD5194-B	1019	32.9043	-117.7824	2023-07-18	20:30	carbonate, orange sulfur mat
	CTD 3	1031*	*	*	2023-07-19	1:00	on-seep
	CTD 4	1036	32.9032	-117.7822	2023-07-19	23:50	across seep transect
SMM	AD5197-A	802	33.7996	-118.6468	2023-07-21	17:00	CH_4 bubbles, orange and white sulfur mat, carbonate
	AD5197-B	800	33.7995	-118.6468	2023-07-21	20:00	symbiotic clams
	CTD 6	827	33.7999	-118.6437	2023-07-22	3:30	off-seep
	AD5198-A	816	33.7991	-118.6456	2023-07-22	16:00	symbiotic clams, white sulfur mat
	AD5198-B	801	33.7994	-118.6466	2023-07-22	19:30	carbonate ledge, ampharetid worm bed
	CTD 7	807*	*	*	2023-07-23	3:40	across seep transect
	AD5199-A	800	33.7995	-118.6467	2023-07-23	16:30	CH_4 plume, carbonate, orange sulfur mat
	CTD 8	800	33.7996	-118.6468	2023-07-24	02:20	CH_4 plume
LK	CTD 11	387	33.3885	-118.0069	2023-07-26	3:30	on-seep
	AD5201-A	310	33.3907	-118.0065	2023-07-26	15:45	no obvious seep features

2.3 CH_4 Concentration

Water column CH_4 samples were collected in 100 mL glass vials sealed with grey stoppers and crimp caps, filling each vial three times to eliminate bubbles before final sealing. Vials for CH_4 determination were injected with 7.5 mL of 50% NaOH and a 2.5 mL air headspace while a total volume of 10 ml water sample was removed. The partial pressure of CH_4 in the headspace was subsequently analyzed via gas chromatography. Specifically, a Shimadzu Gas Chromatograph (GC-2014) was used, equipped with a Haysep-D packed column and a flame ionization detector. The column temperature was set to 80 °C, and helium served as the carrier gas at a flow rate of 12 mL per minute. CH_4 concentrations were calibrated using CH_4 standards (Scotty Analyzed Gases), with a precision of ±5%. Sulfate samples were analyzed via ion chromatography (Metrohm 761). Water column CH_4 concentrations were calculated using Henry's law and the Bunsen solubility coefficient (Yamamoto et al., 1976) to account for CH_4 in both the gas and liquid phase of the preserved samples.

2.4 Radiotracer incubations for the determinations of microbial CH_4 oxidation

Water column CH_4 oxidation samples were collected in 30 mL glass vials sealed with non-toxic chlorobutyl stoppers (blue Bellco stoppers, 20 mm, (Niemann et al., 2015)) filling each vial three times to eliminate bubbles before final sealing. CH_4 oxidation rates were determined onboard through *ex situ* incubations with tritium-labelled CH_4 (^3H-CH_4) applying established methods (Steinle et al., 2015; Bussmann et al., 2015). Samples (triplicates) were incubated between 35 and 88 hours (depending on sample set) with 10 µL gaseous ^3H-CH_4 (~2 kBq, specific activity 20 Ci/mmol, American Radiolabeled Chemicals, USA). Control samples were injected with 100 µL of 25% H_2SO_4 prior to radiotracer injection to stop microbial activity. To determine the total

radioactivity of the sample, the crimped vials were opened, and a 2 mL subsample was pipetted into a 6 mL scintillation vial and filled with 3 mL of Ultima Gold LLT scintillation cocktail from Perkin Elmer. For the determination of ^3H-CH_4 that was metabolized to ^3H-H_2O, 2 mL from the incubation was subsampled into an additional 6 mL scintillation vial and bubbled with air for 5 minutes to remove ^3H-CH_4 prior to the addition of the scintillation cocktail. Both subsamples were mixed by gentle inversion and counted onboard in a PerkinElmer Tri-Carb liquid scintillation counter. The *in-situ* temperatures of the samples ranged from ~4 to 20°C. Due to the availability of only a single incubator, all samples were incubated at 6 °C. in the dark. To correct for abiotic tracer turnover, the reported rate values are at least the mean tracer turnover in the killed controls plus one standard deviation of the killed-control value. Assuming first-order kinetics, the rate constant (k) was determined using the following equation:

$$k = \frac{^3H - H_2O}{[(^3H - H_2O \ + \ ^3H - CH_4) \ \cdot \ t]}$$

In this equation, ^3H-H_2O refers to the amount of tritiated water produced (in counts per minute, cpm), ^3H-CH_4 represents the remaining unoxidized tritiated CH_4 (cpm), and t is the incubation duration in days. CH_4 turnover time was calculated as the inverse of the fractional turnover rate ($1/k$), equivalent to the CH_4concentration divided by the oxidation rate (r_{ox}) ($[CH_4]/r_{ox}$), under the assumption of prolonged water mass residence with limited mixing (Heintz et al., 2012).

CH_4 oxidation rates (r_{ox}) were calculated again assuming first-order kinetics, using the fractional turnover rate multiplied by the CH_4 concentration (nM). Rates were determined with the following equation:

$$\mathrm{r_{ox}} = \mathrm{k} \cdot \ [CH_4]$$

2.5 DNA Extraction

Seawater was collected into pre-rinsed 1.5 L polycarbonate bottles and stored at 6 °C until filtration. Microbial biomass was collected by filtering the samples using a peristaltic pump through 0.22 µm Sterivex filters (Millipore, Cat. No. SVGP0150). Filters were immediately frozen after filtration for downstream molecular analyses. Genomic DNA was extracted from Sterivex filters using a modified phenol–chloroform procedure followed by purification on Zymo silica spin columns (part C1006). Briefly, each filter was sealed, and 1.8 mL of filter-sterilized lysis buffer (containing 50 mM EDTA, 50 mM Tris–Cl [pH 8], 0.75 M sucrose, and 0.01% Tween 20) was injected into the cartridge. Lysozyme (40 µL; 50 mg mL^{-1}) was then added, and the filter was incubated at 37 °C for 45 min under rotation. 50µL of Proteinase K (800 U mL^{-1}) and 150 µL of 20% SDS were added to achieve a final SDS concentration of ~1%, followed by incubation at 55°C for 2 hr. The lysate was transferred to a polypropylene tube, and total nucleic acids were extracted via successive phenol–chloroform–isoamyl alcohol (25:24:1) extractions at 65°C, with centrifugation steps (10 min at 16,000 × g) to separate the aqueous and organic phases. Residual phenol was removed through an additional chloroform–isoamyl alcohol wash, and DNA was precipitated with 0.4 vol of 5 M NaCl and 0.8 vol of isopropanol. The precipitated DNA was bound to Zymo Spin-Away columns by repeated loading at 6,000 × g for 1 min, washed with 70% ethanol, and eluted in nuclease-free water or 10 mM Tris. Final DNA extracts were stored at −80 °C until further analysis.

2.6 PCR and Illumina MiSeq sequencing of the 16s rRNA gene

The V4-V5 region of the 16S rRNA gene was amplified using 515F and 926R (Parada, 2016) archaeal/bacterial primers with Illumina adapters (515F 5’-

TCGTCGGCAGCGTCAGATGTGTATAAGAGACAG-GTGYCAGCMGCCGCGGTAA-3’; 926R 5’-GTCTCGTGGGCTCGGAGATGTGTATAAGAGACAG-CCGYCAATTYMTTTRAGTTT-3’). PCR reactions were completed with Q5 Hot Start High-Fidelity 2x Master Mix (New England Biolabs, USA) in 15 μL reaction volumes according to manufacturer’s directions with the following cycle parameters: 2 min at 98C followed by 31 cycles of 98◦C for 10s, 54◦C for 20s, 72◦C for 20s, with an extra final elongation step of 72°C for 2 min. PCR samples were pooled and barcoded with Illumina Nextera XT index 2 primers that include unique 8-bp barcodes (P5 5’-AATGATACGGCGACCACCGAGATCTACAC-XXXXXXXX-TCGTCGGCAGCGTC-3’; P7 5’-CAAGCAGAAGACGGCATACGAGAT-XXXXXXXX-GTCTCGTGGGCTCGG-3’) using Q5 Hot Start with 3 μL pooled PCR product added to a 30 μL reaction volume, annealed at 66°C, and cycled 11 times. Products were run on 1.5% agarose gel and quantified by band intensity. Barcoded PCR products were combined in equimolar amounts and 300uL of this combined sample was run on 1.5% low melt agarose gel and purified with Promega’s Wizard SV Gel and PCR Clean-up System, Promega#A9281. Sample was sequenced by Laragen (Culver City, CA, USA) using MiSeq Reagent Kit v3 (600-cycle) #MS-102-3003 on Illumina’s MiSeq platform with the addition of 15-20% PhiX.

2.7 Sequence processing and taxonomic analysis

The Illumina-sequenced paired-end fastq files were processed using DADA2 for amplicon sequence variant (ASV) calling (Callahan et al., 2016) based on developer recommendations and Cutadapt v3.4 for sequence quality trimming and primer removal (Martin, 2011). Reads that did not assemble in the overlapping region or that failed to meet the q-score threshold of 30 were removed from subsequent analyses. See supplements for additional information on read retention

and all parameters used during DADA2. Taxonomy was assigned to 16S rRNA sequences via alignment to SILVA Train Set v138.2 amended with plastid sequences annotated with host taxonomy (Eitel et al., 2024). Raw reads were deposited in the NCBI's Sequence Read Archive (SRA).

2.8 Quantitative PCR

For the qPCR assays, each 10 µL reaction consisted of 5 µL Phusion SYBR® Green PCR Master Mix (BioRad), 0.5 µL (0.5 µM) each primer, 3.5 µL PCR-grade H_2O and 0.5 µL of DNA (concentration pre-determined through Qubit™ dsDNA Quantification, High Sensitivity Assay Kit). Duplicate bacterial pmoA assays were run using water column specific primers wcpmoA189f and wcpmoA661r (Tavormina et al., 2008) and the following cycling parameters: 98◦C for 2 min followed by 40 cycles of 98◦C for 10s, 52◦C for 20s, 72◦C for 30s, detection, then a melt curve from 65◦C to 95◦C in 0.5C increments, plate reading every 5s. Standard curves were constructed with 10-fold dilutions of PCR products from 0 (negative control) to 10^6 gene copies total DNA from extracted *Methylomonas* sp. LW13 cells.

3. Results

3.1 Physical properties and biogeochemical characteristics of the water column

Hydrographic profiles revealed pronounced vertical gradients in temperature, salinity, and density across all sites, shaped by strong upper-ocean stratification and well-defined pycnoclines (**Fig. 2a–d**). At Del Mar Seep (CTD4, 1035 m), a sharp pycnocline occurred between ~50–150 m, where temperature dropped rapidly from ~18 to 8 °C, salinity increased from ~33.1 to ~34.1 PSU, and density rose from ~1023 to ~1027.5 kg m^{-3}. Below this zone, gradients were more gradual,

reaching 3.9 °C, 34.48 PSU, and 1032.2 kg m^{-3} near the seafloor. Similar stratification was observed at Santa Monica Off-seep (CTD6, 820 m) and Santa Monica Mound (CTD8, 799 m), with strong thermoclines and haloclines in the upper ~100–150 m, followed by more linear deep-water gradients. Near-bottom values converged around 5.3 °C, 34.38 PSU, and ~1030.8–1030.9 kg m^{-3}. The shallower Lasuen Knoll site (CTD11, 382 m) showed a compressed but still distinct pycnocline from ~25–100 m, with temperature declining from ~19.6 to ~10 °C, salinity increasing from ~33.2 to 34.2 PSU, and density rising from ~1023.7 to 1028.4 kg m^{-3}.

Optical profiles revealed vertical structure in fluorescence and beam transmission at all sites (**Fig. 2e–h**). At Del Mar Seep (CTD4, 1035 m), a sharp subsurface fluorescence peak (1.29 µg L^{-1}) was observed at 33 m, with values declining steeply through the upper ~100 m and tapering more gradually to 0.034 µg L^{-1} near the seafloor. Beam transmission was at 95.8% at the surface, decreased to 92.4% at 34 m below sea level, then increased to ~97% by 800 m with a slight decline in the bottom 100 m, marking the presence of a benthic nepheloid layer. Similar fluorescence profiles were observed at Santa Monica off-seep (CTD6, 820 m), where a 1.29 µg L^{-1} peak occurred at 41 m, decreasing steadily to 0.041 µg L^{-1} at depth. Transmission increased to ~96.5% but also dipped slightly near the bottom. At Santa Monica Mound (CTD8, 799 m), fluorescence peaked at 0.81 µg L^{-1} at 34 m, with a similar decline to 0.040 µg L^{-1} at depth. Transmission followed the same pattern, increasing from 92.3% to ~96.2% with a small downturn near the seafloor. Lasuen Knoll (CTD11, 382 m) exhibited the highest surface fluorescence (1.82 µg L^{-1} at 34 m), declining steadily to 0.021 µg L^{-1} at depth, with beam transmission increasing from 92.0% to 96.8% before also decreasing slightly near bottom.

Dissolved CH_4 and O_2 profiles varied in magnitude across seep sites but generally showed similar vertical structure (**Fig. 2i–l**). Near-surface CH_4 concentrations exceeded atmospheric

equilibrium at all sites, with values ranging from 33 to 99 nM in the upper 3 m. These elevated surface concentrations may reflect upward transport from depth, localized seep influence, or *in situ* CH_4 production in oxygenated surface waters. At Del Mar Seep (CTD4), CH_4 peaked at 131 nM at 1026 m and was 47 nM at 3 m. O_2 decreased from 231.5 µM at the surface to a minimum of 9.2 µM at 715 m, then increased slightly to 22.7 µM at 1035 m. This O_2 pattern, surface maximum, subsurface decline, and deep minimum, reflects typical midwater structure shaped by air-sea equilibration, photosynthetic production, and midwater respiration. Santa Monica off-seep (CTD6) exhibited the highest CH_4 concentration in the dataset, reaching 797 nM at 804 m; this deep value was confirmed by three replicate headspace measurements. Surface CH_4 was 99 nM at 2 m. O_2 declined from 232.8 µM at the surface to 3.9 µM at 820 m. At Santa Monica Mound (CTD8), CH_4 peaked at 293 nM at 798 m, with 82 nM at 3 m. O_2 ranged from 253.4 µM at the surface to 3.5 µM at 799 m; this cast intersected the EK80 CH_4 plume. At Lasuen Knoll (CTD11), CH_4 increased from 33 nM at 3 m to a maximum of 214 nM at 360 m, then declined to 127 nM at 382 m. O_2 concentrations decreased from 236.7 µM at the surface to 32.1 µM at 378 m. The relatively higher deep O_2 at Lasuen reflects the shallower sampling depth and less intense depletion compared to deeper sites.

CH_4 oxidation rates varied across sites and depths and were generally elevated near CH_4 concentration maxima and within O_2-limited strata (**Fig. 2m–p**). At Del Mar Seep (CTD4), oxidation peaked at 0.34 nmol L^{-1} d^{-1} at 1005 m, with measurable activity at the surface (up to 0.15 nmol L^{-1} d^{-1} at 2 m). These depths corresponded to CH_4 concentrations between 75–131 nM and O_2 levels ranging from 22.7 µM near the bottom to a minimum of 9.2 µM at 715 m. At Santa Monica off-seep (CTD6), oxidation reached 1.50 nmol L^{-1} d^{-1} at 804 m, where CH_4 was 797 nM and O_2 was 3.9 µM. Average oxidation across 804–819 m ranged from 0.50 to 1.18 nmol L^{-1} d^{-1}. At

Santa Monica Mound (CTD8), oxidation rates were highest overall, reaching 4.98 nmol L^{-1} d^{-1} at 791 m where CH_4 was 235 nM and O_2 was 3.5 µM. Lasuen Knoll (CTD11) showed lower oxidation activity, peaking at 0.76 nmol L^{-1} d^{-1} at 201 m at CH_4 concentrations of 62 nM and a minimum O_2 of 32.1 µM. In all cases, peak CH_4 oxidation occurred 13 to 30 m above the seafloor, rather than at the deepest sampling depth, which was itself ~5 m above bottom. These maxima generally aligned with elevated CH_4 concentrations and reduced O_2 levels. At Lasuen Knoll, the oxidation maximum was located much higher in the water column, at 201 m (~186 m above the seafloor).

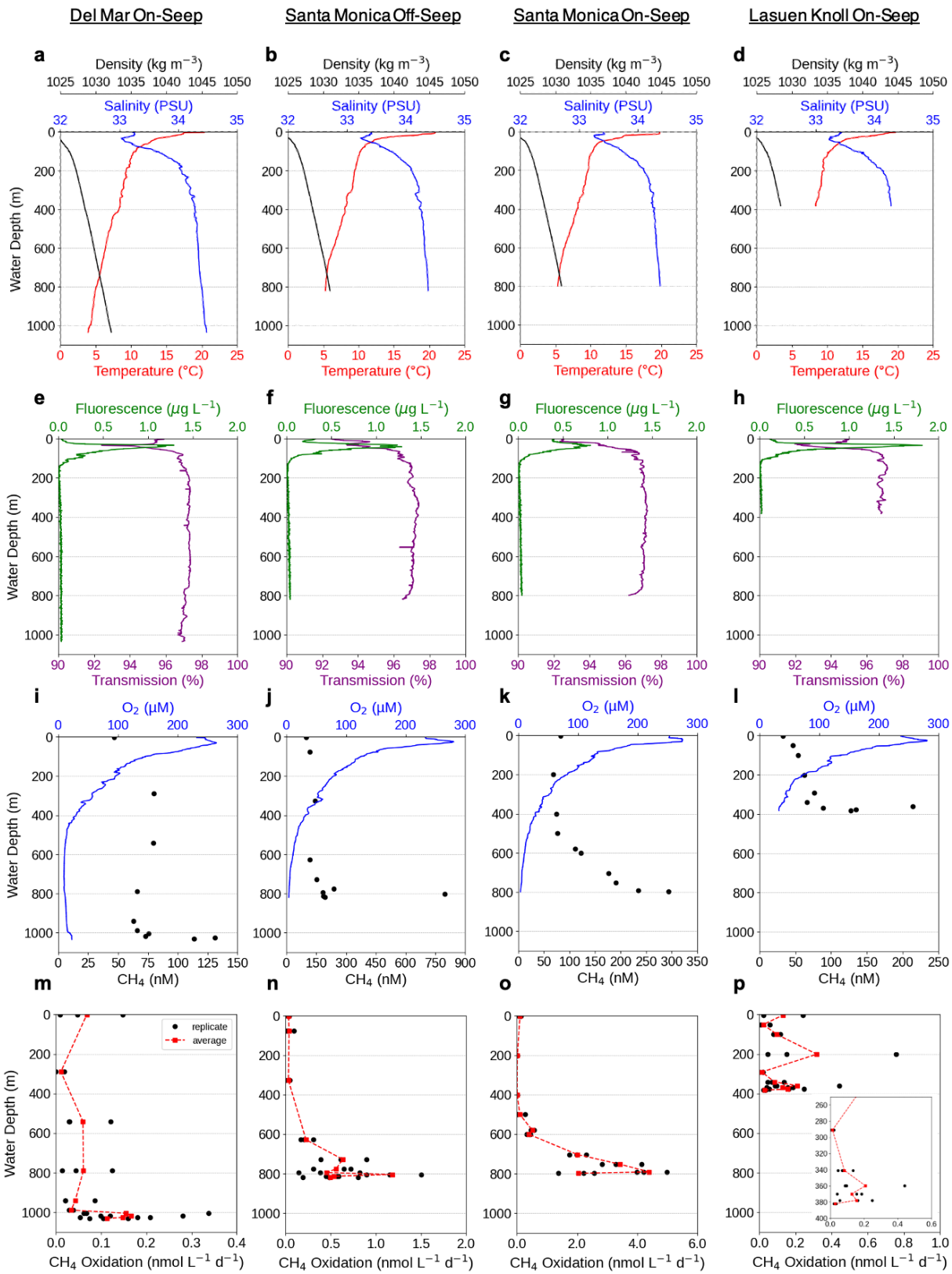

Figure 2. Vertical profiles of hydrographic and biogeochemical parameters in the water column at

the Del Mar (left panels; seafloor at 1036 m), Santa Monica off-seep (center-left panels; seafloor at 827 m), Santa Monica Mound on-seep (center-right panels; seafloor at 800 m), and Lasuen Knoll (right panels; seafloor at 387 m) seep sites. Panels (**a–d**) show density (black, top x-axis), salinity (blue, top x-axis), and temperature (red, bottom x-axis). Panels (**e–h**) show chlorophyll-a fluorescence (green, bottom x-axis), reported in μg L^{-1} as a proxy for phytoplankton biomass, and beam transmission (magenta, top x-axis). Panels (**i–l**) show dissolved CH_4 concentrations (black circles, left x-axis) and dissolved O_2 (blue, right x-axis). Panels (**m–p**) display CH_4 oxidation rates measured in triplicate (black circles), with average rates shown as red squares connected by dashed lines. Note the differences in x-axis scales among CH_4 and CH_4 oxidation variables, and depth in the inset of **Fig. 2p**. All data were collected from vertical CTD casts (casts 4, 6, 8, and 11, respectively) at the sites indicated in **Table 1** and **Fig. 1** on the Southern California margin.

CH_4 oxidation rates and dissolved CH_4 concentrations fluctuated across a horizontal transect sampled 5 m above the seafloor across Del Mar Seep (~2.4 km track; **Fig. 3a**). Oxidation was highest at WP1 (0 m along track; up to 2.56 nmol L^{-1} d^{-1}) at the northwestern end of the transect, where CH_4 was 92.4 nM and O_2 was 17.9 μM. Rates declined at WP2 and WP3 (0.29 and 0.36 nmol L^{-1} d^{-1} at 102 and 150 m; CH_4: 77.0 nM), with WP3 corresponding to the center of the northwestern seep site. Beyond 200 m across the track, oxidation remained lower (0.16–0.20 nmol L^{-1} d^{-1}; CH_4: 64.9–80.9 nM), with the lowest rates and concentrations observed between WP6 and WP10 (0.07–0.20 nmol L^{-1} d^{-1}; 42.7–66.6 nM). A modest increase at WP8 (2284 m along track; 0.19 nmol L^{-1} d^{-1}; 55.0 nM) likely reflects the southeastern seep site, which was identified through high-resolution bathymetric mapping. O_2 concentrations across the transect ranged from ~16 to 22 μM. These patterns highlight the spatial heterogeneity of CH_4 oxidation across the seep

field and indicate that peak water column microbial activity does not necessarily coincide with areas of strongest visible seep signs (e.g., carbonates, sulfur bacteria mats).

At Santa Monica Mound, CH_4 oxidation rates and concentrations varied across a ~400 m transect sampled 5 m above the seafloor (800–816 m water depth; CTD7; **Fig. 3b**). The CH_4 plume was centered at WP6 (193 m across the track), and a directional bottom current inferred from plume curvature in sonar data. WP1 and WP2 (0 and 73 m across the track respectively) were located off-mound to the southeast, while WP9 and WP10 (317 and 399 m across the track respectively) were off-mound to the northwest. WP3 through WP8 (112–245 m across the track) spanned the mound crest and encompassed the visibly active seepage zone. CH_4 oxidation was moderate off-mound at WP1 and WP2 (1.46 and 1.33 nmol L^{-1} d^{-1}; CH_4: 141.6 and 147.4 nM) and increased across the mound crest (1.27–2.61 nmol L^{-1} d^{-1}; CH_4: 107.9–194.4 nM). WP3 marked a local CH_4 maximum (194.4 nM; 1.75 nmol L^{-1} d^{-1}), and WP6 intersected the sonar-detected CH_4 plume (192.4 nM; 2.29 nmol L^{-1} d^{-1}). The highest oxidation rate occurred at WP10 (3.54 nmol L^{-1} d^{-1}), followed by elevated activity at WP9. O_2 ranged from ~3.3 to 4.0 μM across the transect. Overall, oxidation increased from WP1 to WP10, with peak activity observed at off-mound sites beyond the visibly active seep zone similar to the Del Mar transect.

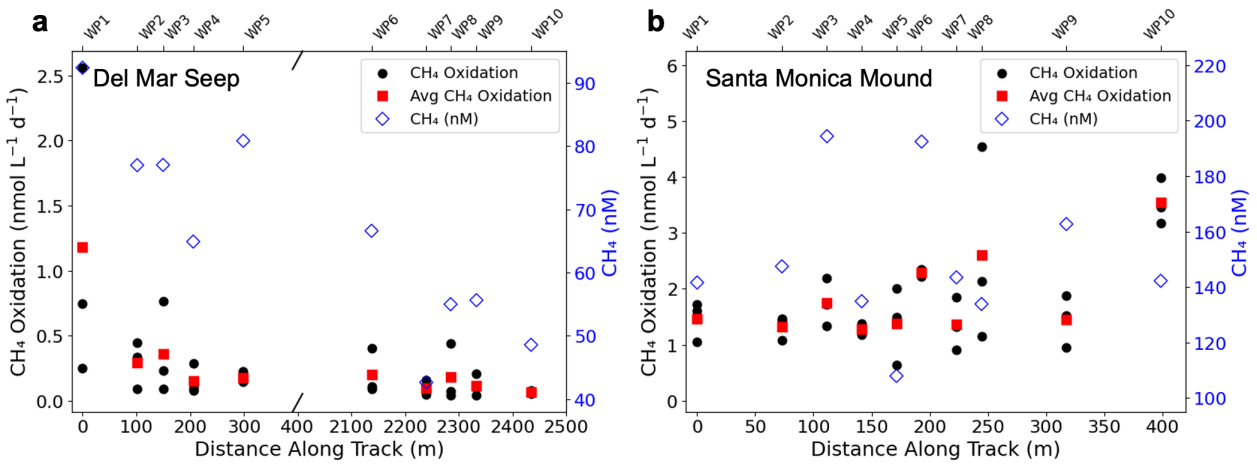

Figure 3. Both (**a**) and (**b**) represent a near seafloor (5 m above) lateral transect of methane concentration and CH4 oxidation rates across (**a**) Del Mar Seep (WP3) and a potential new seep location identified through bathymetric mapping (WP8) (CTD3), and (**b**) Santa Monica Mound (WP1–10; CTD7). CH_4 oxidation (black circles) and average CH_4 oxidation (red squares) are shown on the left y-axes; dissolved CH_4 concentrations (blue diamonds) on the right y-axes. Panel (**a**) shows a broken x-axis to accommodate distant sampling locations. At Santa Monica Mound, the CH_4 plume detected by EK80 echosounder data was centered near WP6, and the bottom current was inferred to flow from WP1 toward WP10. Note the distinct x-axis scales in each panel. See text for details.

3.2. Methanotrophic activity in the near-seafloor water column

Water column samples near the seafloor (0.5 m above bottom) were collected using the *Alvin* submersible. The ^3H-CH_4 *ex situ* incubations revealed a wide range of CH_4 oxidation rates, indicating substantial spatial heterogeneity across sites (**Table 2**). At Del Mar Seep (~1,020 m), three stations (AD5193-A, AD5194-A, AD5194-B) within 200 m of the seep center showed moderate CH_4 oxidation (0.31–0.64 nmol L^{-1} d^{-1}) and concentrations (74–190 nM). AD5193-A was

sampled above seep carbonates colonized by crabs, while AD5194-A featured brittle stars and snails. AD5194-B was positioned adjacent to a patch of orange sulfur bacteria mat. Although faunal composition and mat presence varied, CH_4 levels and oxidation rates remained within a similar range.

In contrast, Santa Monica Mound (~800–816 m) exhibited greater variability across five stations. AD5197-A, located near white and orange sulfur mats and carbonate outcrops with intermittent CH_4 bubbling, had elevated CH_4 (1.3×10^4 nM) and an intermediate oxidation rate (52 nmol L^{-1} d^{-1}). AD5197-B, sampled from a chemosymbiotic clam bed lacking mat and carbonate cover, showed lower CH_4 (109 nM) and oxidation (0.32 nmol L^{-1} d^{-1}). AD5198-A (off-mound) and AD5198-B had moderate CH_4 concentrations (149–183 nM) and oxidation rates (0.20–0.77 nmol L^{-1} d^{-1}), corresponding to patchy mat and carbonate habitats. The highest values occurred at AD5199-A, sampled within an intense CH_4 bubble plume (EK80-detected; **Fig. 1e**), with a CH_4 concentration of 2.5×10^5 nM and an oxidation rate of 454 nmol L^{-1} d^{-1}. This station also had extensive sulfur mat cover and carbonate substrate.

At Lasuen Knoll (~310 m), the single station AD5201-A lacked visible seep structures but showed signs of recent slope disturbance. CH_4 concentration was 133 nM, and oxidation was 0.84 nmol L^{-1} d^{-1}, values consistent with low-intensity seepage in the absence of visible seep structures**.** Overall, CH_4 oxidation and concentrations varied both within and among seep fields, including measurable methanotrophic activity at sites lacking strong visual indicators of seepage such as sulfur bacteria mat or carbonates.

Table 2. Summary of *Alvin* sampling stations for Del Mar Seep (DMS), Santa Monica Mound (SMM), and Lasuen Knoll (LK) including the average CH_4 oxidation rates, corresponding CH_4 concentrations and environmental features.

Location	Niskin ID	CH_4 (nM)	Avg CH_4 Oxidation (nmol L^{-1} d^{-1})	Standard Deviation (± nmol L^{-1} d^{-1})	Site Characteristic
DMS	AD5193-A	190	0.31	0.38	crabs, carbonate
	AD5194-A	85	0.64	0.75	brittle stars, snails
	AD5194-B	74	0.64	0.17	carbonate, orange sulfur mat
SMM	AD5197-A	1.3×10^4	52	24	CH_4 bubbles, orange and white sulfur mat, carbonate
	AD5197-B	109	0.32	0.13	symbiotic clams
	AD5198-A	149	0.20	0.13	symbiotic clams, white sulfur mat
	AD5198-B	183	0.77	0.24	carbonate ledge, ampharetid worm bed
	AD5199-A	2.5×10^5	454	121	CH_4 plume, carbonate, orange sulfur mat
LK	AD5201-A	133	0.84	0.73	no obvious seep features

3.3 Rate constant and CH_4 turnover times

CH_4 oxidation rate constants (k) and corresponding turnover times were calculated from a subset of Niskin bottles collected during vertical CTD casts at Del Mar Seep (CTD4), Santa Monica Mound (CTD8), and Lasuen Knoll (CTD11), as well as paired *Alvin* Niskin samples. Results from selected depths are presented in **Table 3**. The full dataset for each vertical CTD cast is listed in **Suppl. Table 2.** Turnover times varied by site and depth, ranging from as short as 0.32 years to as long as 19.3 years. At Del Mar Seep, turnover times ranged from 1.73 years near the surface (2 m depth) to 0.32 years above the seafloor at AD5194-A. A midwater sample at 290 m showed the longest turnover time (19.3 years), corresponding to a CH_4 minimum and elevated O_2. At Santa Monica Mound, turnover was relatively fast at the surface (2.18 years at 2 m) and above the seafloor (0.40–1.47 years), with slower turnover observed at 200 m (10.1 years). At Lasuen Knoll, turnover times ranged from 0.48 to 11.9 years, with the longest value at 382 m and shorter turnover times

both near the surface and above the seafloor. Across all three sites, shorter CH_4 turnover times were typically observed near the seafloor and surface, while slower turnover occurred at intermediate depths.

Table 3. Depth-dependent measurements of O_2, CH_4, CH_4 oxidation rate constants (k), and resulting turnover times for Del Mar Seep (DMS), Santa Monica Mound (SMM), and Lasuen Knoll (LK). (*) denotes the O_2 concentration and temperature are estimated from the vertical CTD profile at the corresponding depth and site (CTD4 for DMS, CTD8 for SMM, and CTD11 for LK).

Location	CTD/Niskin ID	Water depth (m)	O_2 (μM)	CH_4 (nM)	Temp (°C)	Rate constant (k)	Turnover Time (y)
DMS	4	2	237	21	20.4	1.6×10^{-3}	1.73
DMS	4	290	58	36	8.95	1.4×10^{-4}	19.3
DMS	4	1031	22	51	3.96	8.4×10^{-4}	3.15
DMS	AD5194-A	1022	20*	39	3.96*	8.3×10^{-3}	0.321
SMM	8	2	260	37	19.8	1.3×10^{-3}	2.18
SMM	8	200	103	31	3.69	2.7×10^{-4}	10.1
SMM	8	798	3.3	132	5.30	6.8×10^{-3}	0.404
SMM	AD5199-A	799	3.3*	9.8×10^{4}	5.30*	1.9×10^{-3}	1.47
LK	11	3	243	15	19.6	4.2×10^{-3}	0.719
LK	11	201	75	28	9.52	4.9×10^{-3}	0.563
LK	11	382	33.0	57.36	8.36	2.3×10^{-4}	11.9
LK	AD5201-A	310.432	46*	60	8.8*	5.7×10^{-3}	0.477

3.4 Microbial community composition in the water column

Analysis of 16S rRNA gene sequences from water column samples collected above the seep sites, from the euphotic zone to near-bottom waters, revealed that the dominant bacterial and

archaeal taxa included Thermoplasmatota, Crenarchaeota, Proteobacteria, Cyanobacteria, and Planctomycetota. While Thermoplasmatota was the most prevalent overall, the relative distributions of these phyla varied by seep site and water column depth (e.g., ~18% at Del Mar Seep, ~43% at Santa Monica Mound, and ~36% at Lasuen Knoll for Thermoplasmatota average relative abundance). Notably, Proteobacteria, including Oceanospirillales_7, Alteromonadales, Thiomicrospirales, and Arenicellales, were particularly well represented in mid- and deepwater samples, consistent with the broad metabolic versatility characteristic of this phylum. In surface waters, the phototrophic primary producers within the order Synechococcales were highly abundant, accounting for 77% of the microbial community at Del Mar Seep and 60% at Santa Monica Mound, suggesting a significant contribution of cyanobacterial primary production (Fig. 4). Flavobacteriales was the second most abundant order in the surface water at Del Mar Seep (3.7%) and Santa Monica Mound (4.8%). Members of this group are known for their role in the decomposition of organic matter and utilizing dissolved organic carbon from phytoplankton blooms (Pontiller et al., 2022). Archaeal orders including Marine Group II (Thermoplasmatota) and Nitrosopumilales (Crenarchaeota) were the dominant taxa in most samples. The prevalence of Nitrosopumilales, an order characterized by ammonia-oxidizing archaea, aligned with their near absence in surface waters above the OMZ. Among bacterial orders, Oceanospirillales_7 was abundant in mid- and deep-water samples at Del Mar Seep and detected at lower abundances Santa Monica Mound and Lasuen Knoll. Nitrincolaceae, the predominant family found within Oceanospirillales_7, are heterotrophic bacteria that include many known alkane oxidizers and play a role in organic matter degradation, sulfur compound metabolism, and nitrogen cycling (Liu et al., 2019). Flavobacteriales, in addition to its presence in the surface water, was prevalent throughout the water column of Del Mar seep and in near the seafloor of Santa Monica Mound (AD5198-A;

20.7% relative abundance) and Lasuen Knoll (AD5201). Thiomicrospirales, an order containing many sulfur-oxidizing bacteria, was abundant in deep samples across all three seep sites, including Lasuen Knoll with the highest relative abundance in the bottom waters of Santa Monica Mound (11.3%). In contrast to other microbial groups associated with hypoxic and anoxic environments, such as ammonia- or nitrite-oxidizing taxa, Thiomicrospirales exhibited a more restricted vertical distribution, with peak abundances occurring in deeper water. Orders that contain methanotrophs (e.g., Burkholderiales) did not show a noticeable increase at active seepage sites. However, any such signal was likely obscured by the presence of non-methanotrophic members within the order.

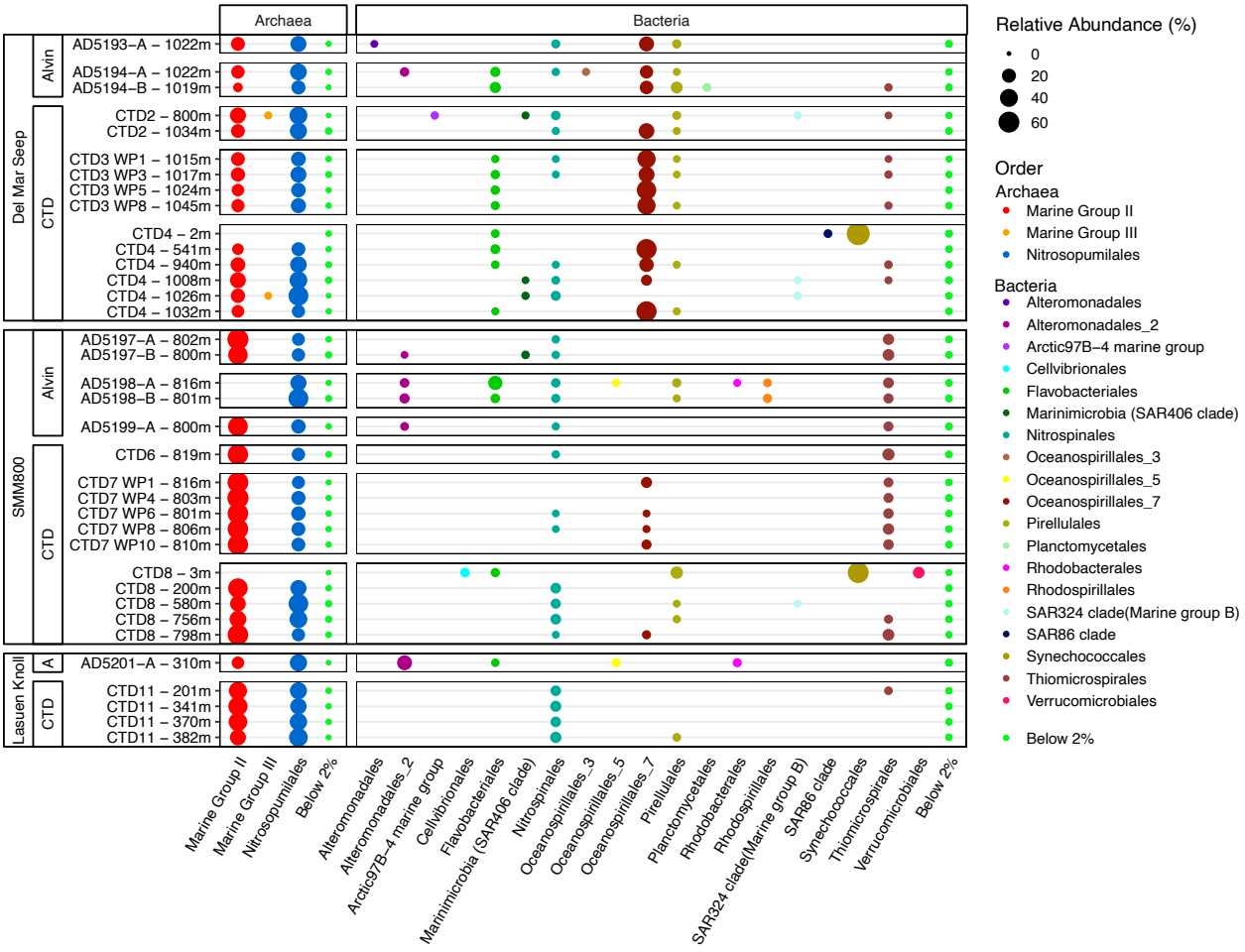

Figure 4. Microbial community composition from CTD and *Alvin* Niskin samples from Del Mar Seep, Santa Monica Mound, and Lasuen Knoll. Dot size shows the relative abundance (%) of microbial orders (columns, colors) in samples (rows). Samples are grouped by site (major grouping), collection strategy (CTD or *Alvin*, middle grouping), and deployment (minor groups). Only orders reaching at least 2% abundance in at least one sample are shown. Taxonomy follows SILVA conventions (e.g., Oceanospiralles_3).

Taxonomic genera typically associated with aerobic CH_4 oxidation and methylotrophy were detected at low relative abundances (<0.5%) but were consistently present across multiple bottom water samples (**Fig. 5**). The most abundant methanotroph across the seep sites, IheB2-23 (Methylomonadaceae), was particularly prevalent above Santa Monica Mound, with peak abundance observed in the deepest samples from CTD6 (819 m) and along the CTD7 horizontal transect, where WP8 (~72 m down current from the EK80 CH_4 plume at WP6) exhibited the highest relative abundance. Though, this group was also detected at high abundances throughout the water column, including the CH_4 minimum zone of CTD8.

Regarding horizontal methanotroph distribution, the 16S rRNA abundance of methanotrophs remained relatively stable across the 400 m transect at Santa Monica Mound, with consistently low but detectable levels across the waypoints. In contrast, along the horizontal transect across Del Mar Seep (CTD3), aerobic methanotrophs were only detected at WP1 (off-seep), potentially indicating a more restricted distribution. Interestingly, the sample with the highest diversity, AD5194-B (CH_4 74 nM), was collected above an active seep habitat at Del Mar Seep, where carbonate rocks and an orange sulfur bacteria mat were observed. The second most diverse assembly was noted in AD5199-A (CH_4 2.5 x 10^5 nM), which was taken within the Santa Monica

Mound EK80 CH_4 plume. Notably, no methanotrophs were detected in the water overlying Lasuen Knoll based on 16S rRNA gene sequencing, suggesting that known methanotrophic taxa were present at levels below the detection limit of the method. However, positive CH_4 oxidation was measured across these depths, indicating ongoing microbial activity. This discrepancy likely reflects the limitations of amplicon sequencing in detecting low abundance but metabolically active community members, as transcriptional activity can be disproportionately higher than their representation in the 16S rRNA amplicon pool (Galambos et al., 2019). Alternatively, it is plausible that methane oxidation in this context is catalyzed by a group not yet recognized as methanotrophic. The radiotracer incubations confirm that methanotrophs were still present and active at Lasuen Knoll but not captured by the sequencing approach used in this study.

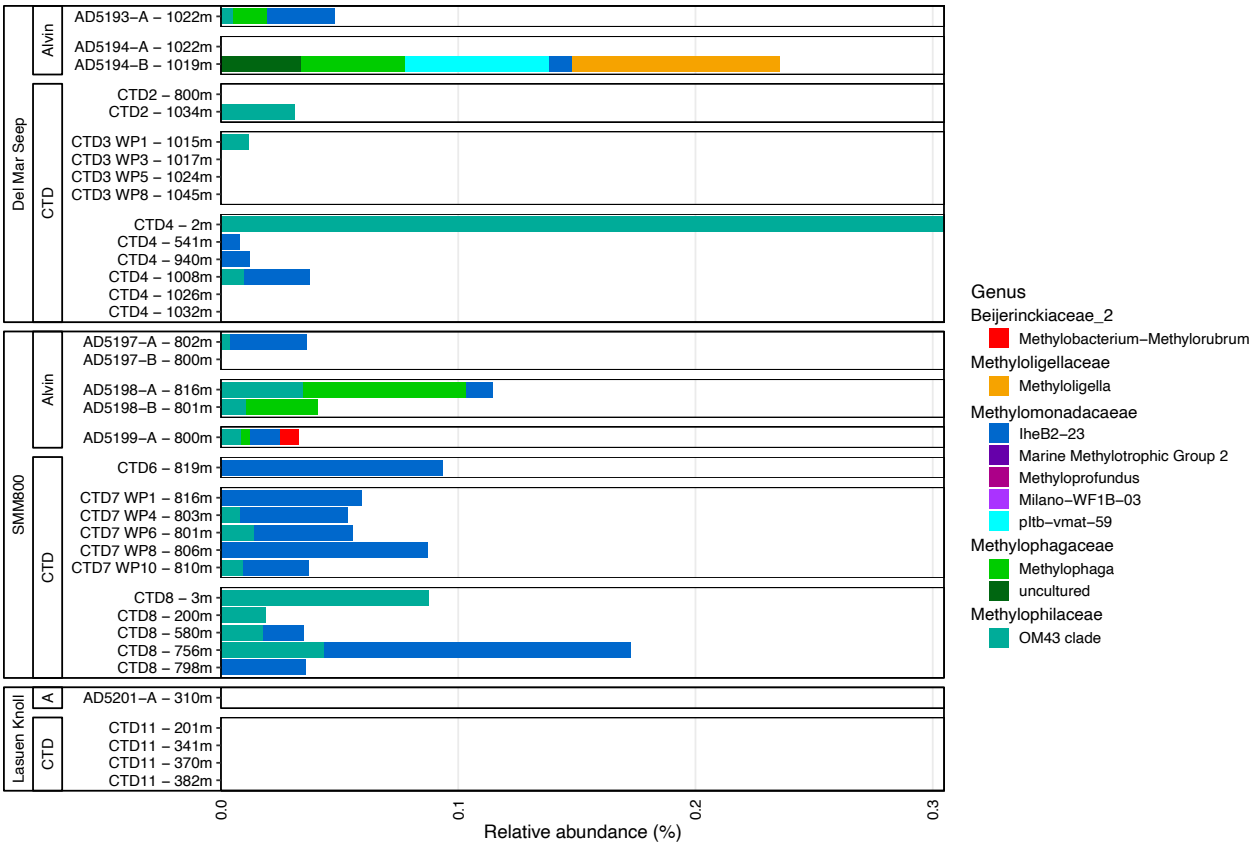

Figure 5. Relative percent abundance of select methanotrophic and methylotrophic genera in samples collected from the water column (CTD and *Alvin* Dives). Relative abundance (x-axis, %) is shown as a stacked bar plot for genera (colored bars) for samples (y-axis) in which this collective of genera reached at least 0.01% abundance. Samples are grouped by site (major grouping), collection strategy (CTD or *Alvin*, middle grouping), and deployment (minor groups). In this figure, all members of Methylomonadaceae are canonical aerobic methanotrophs (Orata et al., 2018). By contrast, *Methylobacterium–Methylorubrum*, *Methyloligella*, the OM43 clade (Methylophilaceae), and most Methylophagaceae (e.g., *Methylophaga*) are methylotrophs; note, however, that some Methylophagaceae lineages in this study possess a divergent *pmoCAB* operon that may confer methane-oxidizing potential (Mayr et al., 2025). Although not shown, the related genus *Methyloceanibacter* (Methyloligellaceae) can encode sMMO and behave as a methanotroph (Vekeman et al., 2016).

3.5 Quantitative PCR analysis

Vertical CTD casts and *Alvin* Niskin samples at Del Mar Seep, Santa Monica Mound, and Lasuen Knoll revealed strong depth-related patterns in *pmoA* gene abundance, with higher values concentrated near deeper seep-influenced waters and lower abundances in midwater and surface layers (**Fig. 6**). At Del Mar, the highest *pmoA* abundance was detected between 800 and 1,034 m, where values ranged from 5.82 log copies L^{-1} at 800 m to 5.57 log copies L^{-1} at 1,034 m. In contrast, shallower depths displayed lower gene abundance, with 4.65 log copies L^{-1} in the surface water, however, *pmoA* gene abundance remained steady through the CH_4 minima with 5.59 log copies L^{-1} at 540 m. *Alvin* Niskin samples in Del Mar exhibited more pronounced variability, with AD5193-A and AD5194-A yielding moderate values (4.53–4.70 log copies L^{-1}), whereas AD5194-B, while in an active environment, showed a significantly lower abundance of 2.50 log copies L^{-1}, suggesting potential localized differences in methanotrophic community density near active seepage. Santa Monica Mound exhibited a similar depth-related pattern, with *pmoA* values peaking between 752 and 816 m (5.84–6.05 log copies L^{-1}), while surface waters had the lowest abundance (3.49 log copies L^{-1}). In the CH_4 minima, the concentration remained at 5.84 log copies L^{-1}. *Alvin* samples from seep-associated areas showed moderate variability, with AD5198-B recording the highest abundance (5.30 log copies L^{-1}), while AD5198-A (4.77 log copies L^{-1}) and AD5197-B (4.42 log copies L^{-1}) were slightly lower, potentially reflecting differences in seep intensity or population drift from bottom currents. At Lasuen Knoll, *pmoA* abundance ranged from 5.12 to 5.32 log copies L^{-1}, with the highest value recorded at 341 m (5.32 log copies L^{-1}) and the lowest at AD5201-A (4.99 log copies L^{-1}). Although no DNA samples were taken in the surface water at Lasuen Knoll, *pmoA* data suggests that the MOB population is distributed throughout the majority of the water

column similar to Del Mar Seep and Santa Monica Mound, with moderate *pmoA* abundance at midwater and near the seafloor.

Horizontal CTD transects across the Del Mar Seep and Santa Monica Mound highlight the ubiquity of pmoA in microbial communities over distances up to ~2.4km from active seep (**Fig. 6**). Along the Del Mar transect (water depths between 1,015 and 1,045 m), *pmoA* gene abundance remained relatively stable over short distances, with WP1 and WP3 (~150 m apart) containing similar values of 5.25 and 5.46 log copies L^{-1}, respectively. At WP5, ~150 m from WP3, *pmoA* abundance was stable at 5.45 log copies L^{-1}. At WP8 (~1988 m from WP5), *pmoA* gene abundance remained stable at 5.29 log copies L^{-1}. Given the narrow range observed across sites and the potential limits of detection sensitivity, this suggests minimal variation in methanotroph abundance across this portion of the transect. At Santa Monica Mound (water depth between 801 to 816 m), horizontal variability in *pmoA* gene abundance was similarly minimal over short distances and exhibited slight fluctuations across the broader seep field. At WP1 (816 m depth) had a *pmoA* value of 5.88 log copies L^{-1} and WP4 (~142 m apart) the *pmoA* concentration slightly increased to 6.05 log copies L^{-1}, the highest recorded at this site. WP6, the location of the vigorous CH_4 bubble plume in the EK80, reached a *pmoA* gene abundance of 5.91 log copies L^{-1}. WP8 (~52 m from WP6) retained similarly high values (5.93 log copies L^{-1}). These findings suggest that methanotrophic community density remains relatively consistent across short distances (≤100 m), with periphery stations such as WP1 at Del Mar (CTD3), WP1 at Santa Monica Mound (CTD7), and the off-seep CTD6 site at Santa Monica showing comparable *pmoA* abundance to nearby on-seep locations. Slight increases in gene copy number were observed in areas of higher CH_4 bubble release, such as WP6 and WP8. Collectively, the vertical and horizontal distributions of *pmoA* gene abundance suggest that the MOB population is highest in deeper waters near active seeps and remains relatively

stable over short horizontal distances while exhibiting some variation across larger spatial scales. A horizontal CTD transect was not conducted for Lasuen Knoll.

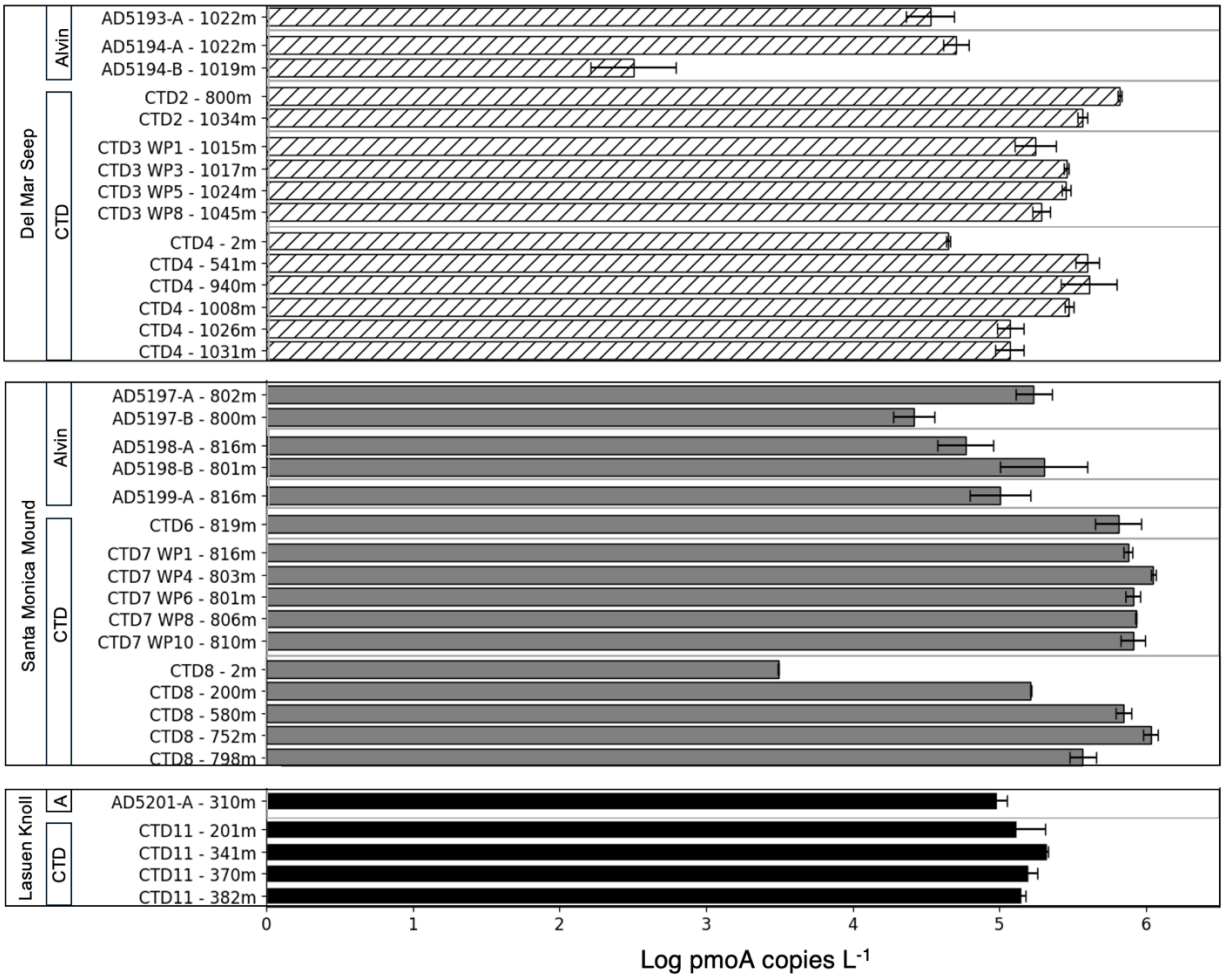

Figure 6. Log-transformed qPCR-derived abundances of the particulate methane monooxygenase gene (pmoA) in water samples collected at Del Mar (striped bars), Santa Monica Mound (gray bars), and Lasuen Knoll (black bars). Each horizontal bar represents the $\log_{10}$ pmoA copy number per liter for a given sample (labeled by depth, Waypoint (WP), or *Alvin* cast), illustrating the distribution of CH_4-oxidizing microbial populations across depths and seep sites in the Southern

California margin. Samples are grouped by site (major grouping), collection strategy (CTD or *Alvin* (A), middle grouping), and deployment (minor groups). Error bars represent the standard deviation.

4. Discussion

4.1 CH_4 and methanotroph transport beyond the seep

Our observations indicate that both CH_4 and methanotrophs are transported vertically beyond visibly active seep areas (>200 m). Vertical transport within the water column could be conducted via gas bubbles (Jordan et al., 2019; Jordan et al., 2020) and other physical processes including turbulent mixing and seasonal upwelling (Hickey, 1992; Leifer et al., 2006; Pohlman et al., 2017). Elevated CH_4 oxidation rates were consistently detected 10–30 m above the seafloor across the three seep sites (**Fig. 2m-p**) paired with slight increases (~0.5 log) in *pmoA* gene copy numbers. Most evidently, the EK80 bubble plume at Santa Monica Mound extended to approximately 400 m, which aligned with the CH_4 concentration profile shown in **Fig. 2k** and CH_4 oxidation in **Fig. 2o**. It remains unclear whether methanotrophs residing near the seafloor influence microbial community composition in the overlying water column at these sites. However, *pmoA* gene copy numbers remained relatively stable from the bottom waters up to 200 m depth at both Del Mar and Santa Monica Mound.

Horizontal transects revealed spatial patterns in CH_4 oxidation that suggest physical transport influences methanotroph distribution across seep systems. At Del Mar Seep, average CH_4 oxidation rates increased from WP10 toward WP1, with intermediate values near active seepage sites such as WP3 and WP8. This pattern may reflect redistribution of CH_4 and methanotrophs by a bottom current flowing northwest along the transect which generally aligns with mean circulation pattern in the Southern California Bight (Hickey, 1992). A similar oxidation gradient was observed

at Santa Monica Mound, where rates increased from WP1 to WP10, consistent with a westward current inferred from CH_4 plume morphology. Although CH_4 concentrations were more variable due to localized seepage, the directional oxidation signal was maintained. These results suggest that bottom currents may extend the spatial reach of CH_4 oxidation, and thus the methanosphere, beyond visibly active seep zones. At Haakon Mosby Mud Volcano, low CH_4 oxidation rates were attributed to strong bottom currents that displaced CH_4 before microbial communities could respond (Sauter et al., 2006). As currents also impact CH_4 release and vary on an hourly time scale from tides and passing eddies (van Aken et al., 1995), it is difficult to constrain comprehensive CH_4 oxidation without time series sampling. A similar mechanism may help explain elevated oxidation at peripheral stations such as WP1 at Del Mar and WP10 at Santa Monica, where CH_4 and methanotrophs appear to be redistributed laterally from active seeps. On broader scales, circulation-driven dilution and water mass mixing can suppress oxidation by altering CH_4 availability and methanotroph standing stocks, as shown in Arctic shelf systems (Steinle et al., 2015). In the Santa Barbara Basin, an enclosed system comparable to the Santa Monica Basin, episodic bottom water renewal due to springtime upwelling disrupts persistent low-O_2 conditions, with consequences for CH_4 retention and microbial activity (Qin et al., 2022). Collectively, these transport processes modulate methanotroph dispersal and CH_4 oxidation, expanding the footprint of the methanosphere beyond active seep zones.

4.2 Inter- and intra-seep heterogeneity of CH_4, CH_4 oxidation, and community composition

CH_4 seep environments in the Southern California Borderland exhibited pronounced spatial heterogeneity, both within individual seeps and across sites. At Del Mar Seep (~1020 m), low-O_2 bottom waters (as low as 9.2 μM) coincided with moderate CH_4 concentrations (74–190 nM) and

oxidation rates (0.31–0.64 nmol L^{-1} d^{-1}). These conditions, coupled with variable faunal and mat cover, suggest a dynamic environment potentially shaped by organic matter input and limited bottom water ventilation. In contrast, Santa Monica Mound (~800 m) exhibited vigorous CH_4 bubbling, plume formation, and lower bottom water O_2 (~3–4 µM), alongside elevated CH_4 concentrations and oxidation rates (up to 2.61 nmol L^{-1} d^{-1} near the mound, and 454 nmol L^{-1} d^{-1} within the bubble plume). The semi-enclosed hydrography of the Santa Monica Basin may promote CH_4 retention and shape the vertical structure and persistence of methanotrophic communities in the overlying water column. These site-level contrasts support previous findings that circulation patterns and O_2 concentrations modulate CH_4 transport and oxidation efficiency (Hein et al., 2006; Heintz et al., 2012; Paull et al., 2008; Steinle et al., 2015), expanding the functional extent of CH_4 cycling without necessarily altering the underlying seepage dynamics.

At the Lasuen Knoll site (~310 m), located along an active tectonic structure, *Alvin* observations documented recent seafloor disturbance, including slumped sediment and displacement along the knoll's cliff face, consistent with a submarine slide. While no vigorous venting was observed during the dive, partially buried sulfur bacteria mats suggested prior seepage activity. The site's water column CH_4 and CH_4 oxidation profiles were variable, and O_2 concentrations were elevated (~30–32 µM) relative to the conditions observed at deeper seep sites. These features may reflect episodic or spatially diffuse seepage, potentially linked to tectonic forcing or slope instability that intermittently opens migration pathways for CH_4. However, in areas with variable or no visible signs of seepage, activity at the time of sampling appeared limited, though measurable methanotrophic oxidation suggests recent or low-level CH_4 input to the water column. Additional surveys and time-series observations will be necessary to resolve the temporal variability of CH_4 release and associated microbial responses at this location.

These contrasts, specifically differences in bottom water O_2 concentration, CH_4 availability, and vertical water column structure across seep sites, highlight the role of localized geochemical and physical gradients in shaping the dynamics of CH_4 transport and oxidation in the water column. Such environmental variability also appears to structure methanotrophic communities. For example, deep-water samples at both Del Mar and Santa Monica Mound contained greater methanotrophic diversity and abundance near the seafloor, while members of the Methylomonadaceae clade IheB2-23 were also detected throughout the water column. These observations underscore how environmental conditions across and within seep sites influence not only the magnitude of CH_4 oxidation but also the stratification and dispersal of key methanotrophic lineages.

Oxidation rates in marine water columns span several orders of magnitude, from $<1 \times 10^{-2}$ to $>1 \times 10^{3}$ nmol L^{-1} d^{-1}, with the highest rates measured in active CH_4 plumes and or in hypoxic environments (Mau et al., 2013; Rogener et al., 2021; Steinle et al., 2015; Steinle et al., 2017). CH_4 oxidation rate (4.54×10^{2} nmol L^{-1} d^{-1}) measured at Santa Monica Mound (station AD5199-A) falls among the upper end of values reported for CH_4-enriched marine systems. This elevated activity coincided with a vigorous bubble plume and high CH_4 concentrations, in stark contrast to nearby peripheral sites (e.g., AD5197-B), where CH_4 levels and oxidation rates were markedly lower. In contrast, at Del Mar, two visibly active habitats (AD5193-A and AD5193-B) showed notable intra-site differences. AD5193-A exhibited CH_4 concentrations of 190 nM, 4.5 log pmoA copies L^{-1}, and an oxidation rate of 0.31 nmol L^{-1} d^{-1}, while AD5194-B displayed lower CH_4 concentrations (74 nM) and pmoA levels (2.5 log copies L^{-1}) but a higher oxidation rate (0.64 nmol L^{-1} d^{-1}) and greater methanotroph/methylotroph diversity. Molecular analyses further underscore this heterogeneity, revealing distinct microbial assemblages that vary with seep intensity, geochemical gradients, and

physical habitat structure. Moreover, small-scale differences in fluid flow and geological heterogeneity create niche environments that drive localized microbial diversification and patchy higher trophic distributions (Cordes et al., 2010; Levin et al., 2003).

4.3 CH_4 turnover and environmental controls

To better understand how environmental conditions shape microbial CH_4 oxidation, the turnover times were calculated using measured oxidation rate constants (k) from selected vertical CTD casts and *Alvin*-collected water samples across all three seep sites (**Table 4**). These depth-resolved turnover estimates provide insight into how CH_4 oxidation dynamics respond to vertical gradients in CH_4 concentration, O_2 availability, and proximity to active seepage.

At Del Mar Seep, short turnover near the surface and above the seafloor contrasted with much slower turnover at midwater depths, consistent with CH_4 depletion zones where oxidation is limited. At Santa Monica Mound, turnover patterns similarly tracked CH_4 and O_2 gradients. The rapid surface turnover despite low CH_4 concentrations and high O_2 suggests cryptic CH_4 cycling, possibly linked to the breakdown of methylated compounds (Krause & Treude, 2021; Xiao et al., 2017; Xiao et al., 2018). During the summer sampling period, CH_4 production in surface waters could be driven by the breakdown of methylated compounds such as dimethylsulfoniopropionate (DMSP), a common byproduct of phytoplankton productivity, which may fuel aerobic CH_4 production by methylotrophic bacteria (Damm et al., 2010). Turnover slowed at midwater depths (~10.1 years), consistent with a 'CH_4 desert,' then accelerated again near the seafloor, with turnover times of 0.40 years at CTD8 and 1.47 years at AD5199-A, sampled within the CH_4 plume, where CH_4 peaked (~293 nM) and O_2 was lowest (~3.3 μM). These patterns echo findings from Eckernförde Bay, where CH_4 oxidation was enhanced under low O_2 but with limited carbon

assimilation (Steinle et al., 2017), highlighting the role of both seep-derived and *in situ* CH_4 supply in regulating turnover.

Lasuen Knoll showed a similar depth-dependent trend, with the slowest turnover at mid-depth (382 m), while surface and near-bottom waters supported more rapid oxidation. Despite higher O_2 concentrations at this shallower site, oxidation appeared to remain closely tied to CH_4 availability, reinforcing that CH_4 supply, not just O_2 limitation, drives turnover. This aligns with prior studies from the Santa Monica Basin (Heintz et al., 2012; Ward & Kilpatrick, 1993), where short turnover times tracked zones of elevated CH_4 flux. Moreover, small-scale O_2 and CH_4 gradients may generate microsites of high methanotrophic activity, fueling local biomass production and trophic transfer (Thurber et al., 2013). Environmental factors such as temperature (Fuchs et al., 2016), methanotroph abundance (Tavormina et al., 2013), and carbon quality likely further modulate turnover rates, contributing to the spatial heterogeneity of CH_4 oxidation in seep-influenced water columns.

To further identify the environmental factors regulating the CH_4 oxidation rate constant (k) and turnover time, a Spearman Rank Correlation analysis was conducted across the three seep sites (**Fig. 7**). The analysis incorporated the most complete available environmental data from CTD4, CTD8, and CTD11, including measurements of CH_4, O_2, temperature, fluorescence (as a proxy for primary productivity), and *pmoA* gene concentration (log copies L^{-1}). Details are provided in **Suppl. Table 2**. As CH_4 oxidation characteristically follows first-order kinetics, CH_4 concentration inherently governs the reaction rate. However, variability in the rate constant (k) reflects differences in how efficiently methanotrophic communities can convert available CH_4 under prevailing environmental conditions. This efficiency is shaped by factors such as approximate MOB abundance (pmoA), O_2 availability, and potentially organic carbon export from the surface ocean.

Therefore, observed differences in *k* across sites reflect broader ecological and geochemical constraints on CH_4 oxidation.

At Del Mar Seep (**Fig. 7a**), *k* displayed only moderate correlations with environmental variables, despite measurable CH_4 concentrations. Although a positive correlation with CH_4 (ρ = 0.49) is expected from first-order kinetics, the weak association between *k* and pmoA, and the negative correlation with O_2, suggest that physical processes like mixing or seep patchiness may limit the extent to which CH_4 availability translates into active oxidation. The modest positive correlation between fluorescence and *k* (ρ = 0.26) implies a potential indirect link between surface productivity and methanotrophic activity, but the overall pattern indicates that oxidation is not tightly coupled to any single environmental driver. These results highlight that CH_4 presence alone is not sufficient to ensure high oxidation rates.

At Santa Monica Mound (**Fig. 7b**), *k* showed strong positive correlations with CH_4 (ρ = 0.90), pmoA (ρ = 0.70), and fluorescence (ρ = 0.80), suggesting a system where CH_4 availability, approximate MOB abundance, and surface productivity are all elevated and co-aligned. The strong negative correlation with O_2 (ρ = –0.70) is consistent with enhanced oxidation under low-O_2 conditions, as expected within the Santa Monica Basin OMZ where bottom-water O_2 concentrations fall below 3 μM. Turnover time was inversely correlated with both CH_4 and pmoA, indicating that areas of high CH_4 supply and methanotroph presence correspond to faster CH_4 turnover. Together, these patterns reflect a well-integrated seep system with high CH_4 oxidation capacity.

At Lasuen Knoll (**Fig. 7c**), k was strongly correlated with CH_4 (ρ = 1.00) and O_2 (ρ = 0.80), and moderately with pmoA (ρ = 0.60), suggesting that CH_4 oxidation here is more O_2-dependent than at the other sites. Located at shallower depth (~450 m), this site lies outside the OMZ and experiences higher baseline O_2 availability. The positive correlation with O_2 implies that aerobic

CH_4 oxidation is not O_2-limited and may be enhanced under these conditions. Fluorescence was only weakly associated with *k*, suggesting surface productivity plays a minimal role in regulating methanotrophy here. Turnover time correlations were generally weaker, possibly reflecting the influence of variable seepage intensity or recent slope disturbance.

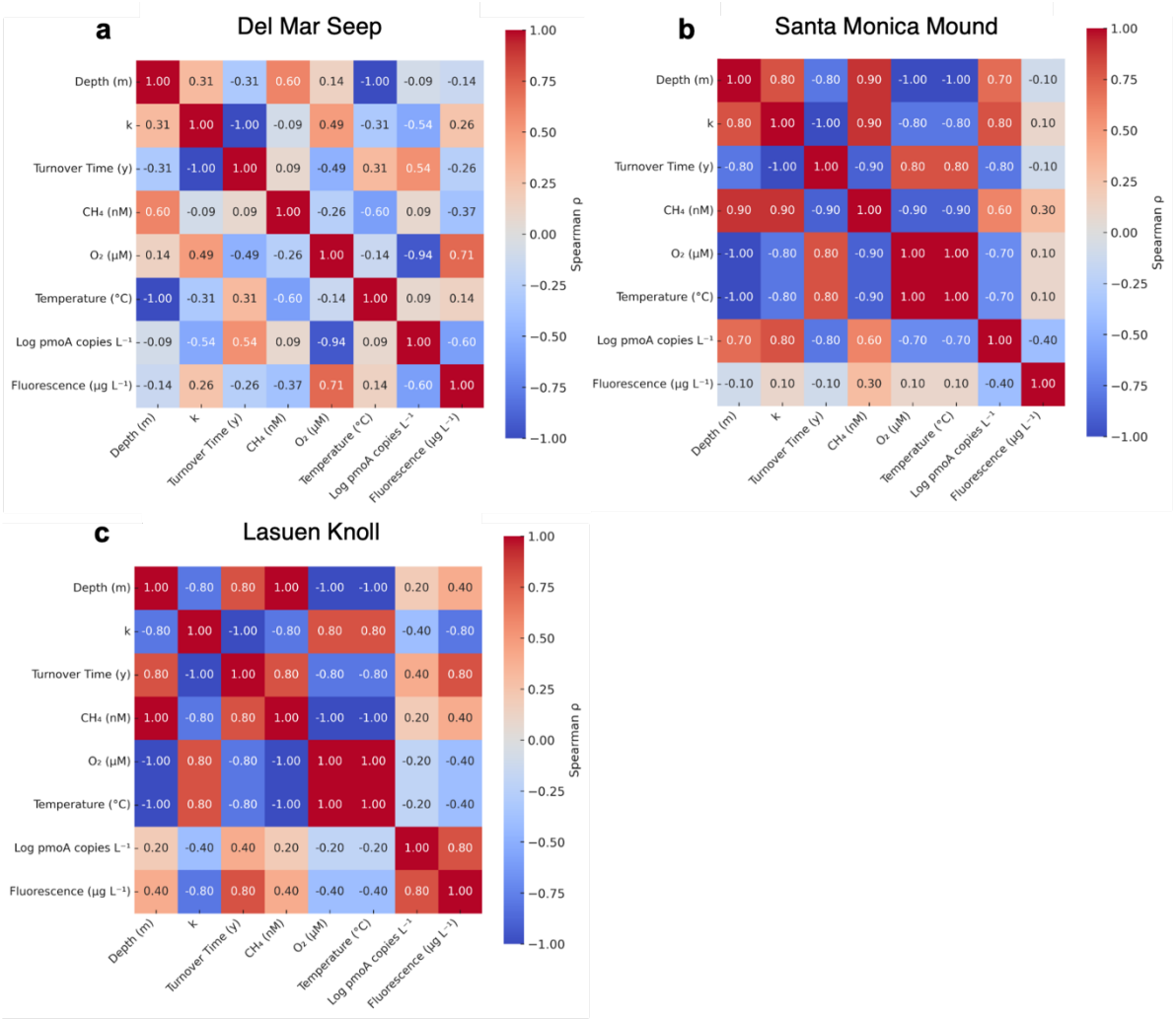

Figure 7. Spearman correlation heatmaps showing relationships among environmental and chemical variables at three CH_4 seep sites: (**a**) Del Mar Seep, (**b**) Santa Monica Mound, and (**c**) Lasuen Knoll. Correlation matrices include depth, CH_4 oxidation rate constant (*k*), turnover time, methane (CH_4), oxygen (O_2), temperature, *pmoA* gene concentration (log copies L^{-1}), and

fluorescence (proxy for primary productivity). Warmer colors (red) represent stronger positive correlations, while cooler colors (blue) represent stronger negative correlations. Note that Spearman's rank correlation detects monotonic associations but does not imply causality and may be sensitive to outliers or small sample sizes.

4.4 Ecological significance of the methanosphere

Our results provide new insight into the spatial extent and ecological significance of the methanosphere, which encompasses both discrete seep features and the surrounding water column where CH_4 oxidation and MOB may extend beyond the immediate seep environment. As discussed, the transect data from Del Mar Seep and Santa Monica Mound (**Fig. 3**) show measurable CH_4 oxidation rates extending over several hundred meters from the seep source, with positive rates observed potentially up to 1 km away. The directional CH_4 transport observed at Santa Monica Mound, combined with oxidation activity across the transect, supports the view that the methanosphere is not a static feature but a dynamic microbial envelope shaped by physical circulation and spatial biogeochemical gradients.

Elevated *pmoA* gene concentrations in the water column, particularly at Santa Monica Mound, indicate that MOB are distributed at least hundreds of meters beyond the immediate seep environment, consistent with diffuse CH_4 enrichment and favorable O_2 conditions. These observations are consistent with prior work showing that aerobic methanotrophs can persist in CH_4-enriched waters removed from direct benthic sources (Steinle et al., 2015) and that their abundance can respond dynamically to CH_4 gradients (Tavormina et al., 2013). Collectively, these findings support an expanded view of the methanosphere as a spatially diffuse, responsive microbial system that contributes significantly to CH_4 turnover in the water column and may influence adjacent biogeochemical regimes (Damm et al., 2010; Reeburgh, 2007).

Although direct measurements of MOB biomass were not made, *pmoA* gene concentrations enable a first-order approximation. Based on published estimates of ~1–2 *pmoA* gene copies per cell (Kolb et al., 2003) and ~10 fg C per cell (Cermak et al., 2017) the observed gene abundances correspond to high nanogram to potentially microgram-scale MOB carbon per liter in some water column samples. Given average bottom current velocities of 5–10 cm s^{-1} in the Santa Monica Basin (Hickey et al., 2003), this suspended microbial biomass could be advected several kilometers per day. Such dispersal may allow methanotrophs to persist in CH_4-poor environments by maintaining low-activity states until CH_4 becomes available, thereby expanding their ecological range and response potential (Reis et al., 2024). Importantly, this advected MOB biomass represents a small but potentially steady microbial carbon source to surrounding heterotrophic food webs. Methanotrophic cells may be consumed by mixotrophic protists, suspension feeders, or benthic filter feeders outside active seep zones, linking water column CH_4 oxidation to broader trophic and carbon cycling processes (Boetius & Wenzhöfer, 2013; de Angelis & Lee, 1994; Pernthaler, 2005). Together, these results suggest that the methanosphere may function not only as a water column CH_4 sink but also as a vector of microbial biomass, connecting seep-associated production to adjacent ecosystems.

4.5 Surface water CH_4 oxidation and implications for cryptic CH_4 cycling

While not as pronounced as the CH_4 oxidation rates near the seafloor, our results reveal active methanotrophy in surface waters despite low ambient CH_4 concentrations. Quantitative PCR analyses confirmed the presence of aerobic methanotrophs in these waters; however, none were identified through 16S sequencing. Methanotrophy may be stimulated by organic precursors like DMSP released during periods of elevated primary productivity (Damm et al., 2010; Karl et al.,

2008; Klintzsch et al., 2019). Specifically, during a summer phytoplankton bloom in the Artic Shelf, an *in situ* cycle of CH_4 production and consumption was observed, and an inverse correlation between DMSP and CH_4 suggested that DMSP might serve as a potential substrate for methylotrophic methanogenesis in surface waters (Damm et al., 2010). The enrichment of cyanobacterial taxa (e.g., Synechococcales) in our surface CTD samples further supports the idea that phytoplankton-derived substrates may enhance methanotrophic activity in the upper water column.

Previous studies have shown that while CH_4 concentrations in the surface ocean are typically low, the surface can still act as a significant CH_4 sink, meaning it serves as a net zone of CH_4 removal through rapid microbial oxidation by specialized communities (Hartmann et al., 2020). The dynamic spatial and temporal variability of CH_4 in oxic surface waters, combined with rapid microbial turnover times (**Table 3**), suggests that these environments are more biogeochemically active than traditionally assumed. Rather than reflecting direct interactions with primary producers, CH_4 oxidation in surface waters likely responds to CH_4 produced during microbial degradation of organic matter derived from phytoplankton productivity (Mao et al., 2024; Perez-Coronel & Michael Beman, 2022). This CH_4 may be rapidly oxidized *in situ* by aerobic methanotrophs, consistent with previously described cryptic CH_4 cycling (Krause & Treude, 2021; Xiao et al., 2017; Xiao et al., 2018). Our findings suggest that surface methanotrophy not only contributes to the biological CH_4 filter but may also support the persistence and dispersal of methanotrophic communities across dynamic oceanic habitats. These insights are important for predicting how future shifts in oceanographic conditions may alter CH_4 cycling and ecosystem function, with implications for both regional biogeochemistry and global carbon budgets.

5. Conclusion

Our study refines the concept of the methanosphere by demonstrating that aerobic CH_4 oxidation and MOB extend well beyond the boundaries of visibly active seepage, with important implications for the fate and footprint of CH_4 in the ocean. Across three distinct seep environments, Santa Monica Mound, Del Mar Seep, and Lasuen Knoll, we observed elevated *pmoA* gene concentrations, CH_4 oxidation activity potentially from seep sources over 1 km away, and directional CH_4 transport through vertical and horizontal processes (e.g., bubble-mediated, bottom currents). These patterns suggest that the methanosphere is not a fixed or localized zone, but a spatially distributed and environmentally responsive microbial system shaped by CH_4 availability, physical transport, and O_2 gradients in the water column.

Site-specific analyses revealed that the drivers of CH_4 oxidation vary depending on local environmental conditions. At Santa Monica Mound, high CH_4 flux, low O_2 concentrations, and elevated MOB abundance support tightly coupled and efficient CH_4 oxidation. In contrast, Del Mar Seep shows weaker coupling between CH_4 and MOB activity, likely due to more variable mixing and higher background O_2 levels. At Lasuen Knoll, a positive correlation between CH_4 oxidation and O_2 points to O_2 availability as a key control, possibly influenced by its shallower depth and episodic fluid flow. Despite these differences, Del Mar seep and Santa Monica Mound exhibit evidence of MOB biomass extending horizontally beyond seep boundaries, suggesting a broader ecological footprint for these communities.

Importantly, the methanosphere functions as a vector for microbial biomass and CH_4-derived carbon export. First-order estimates based on *pmoA* concentrations and regional current velocities indicate that MOB carbon might possibly be transported several kilometers per day. This

advected biomass may support heterotrophic food webs outside of seep zones, linking CH_4 oxidation to broader ecological processes. In this way, the methanosphere serves not only as a CH_4 sink, but also as a microbial and biogeochemical interface between seeps and surrounding ecosystems. In a warming ocean, with regions characterized by lower O_2 levels and higher CH_4 concentrations, the adaptive capacity of methanotrophic communities may still support CH_4 oxidation, including in sites with low ambient CH_4, and can seed new habitats with CH_4-oxidizing communities. This extended methanosphere likely plays a critical role in regulating CH_4 budgets in marine ecosystems, with significant implications for regional carbon cycling and broader climate feedback. As ocean conditions continue to change, understanding the integration of microscale and macroscale processes will be essential for predicting how these ecosystems respond and adapt to shifting biogeochemical regimes.

Funding

This project was supported by the U.S. National Science Foundation (Award Nos. 2048597 to T.T., 2048720 to L.A.L., 2048666 to V.J.O., 2205998 to K.H., and 2126631 to D.U.). We would like to thank UNOLS, the crew of R/V *Atlantis*, the HOV *Alvin* team, and the shipboard scientific party for their logistical, technical, and scientific support during expedition AT50-12.

Acknowledgements

We thank the captain and crew of the *R/V Atlantis*, the *Alvin* operations team, the Shipboard Scientific Services Group (SSSGs), and the supporting personnel from the Woods Hole Oceanographic Institution (WHOI) for their outstanding support during the AT50-12 cruise. Their expertise and dedication were essential to the success of this research. We are also thankful to Y. Li

for her assistance with night operations and water filtration. We also gratefully acknowledge S. Connon at the California Institute of Technology for her invaluable guidance in microbial sample processing.

References

Boetius, A., Ravenschlag, K., Schubert, C. J., Rickert, D., Widdel, F., Gieseke, A., Amann, R., Jørgensen, B. B., Witte, U., & Pfannkuche, O. (2000). A marine microbial consortium apparently mediating anaerobic oxidation of methane. *Nature*, *407*(6804), 623-626.

Boetius, A., & Wenzhöfer, F. (2013). Seafloor oxygen consumption fuelled by methane from cold seeps. *Nature Geoscience*, *6*(9), 725-734.

Callahan, B. J., McMurdie, P. J., Rosen, M. J., Han, A. W., Johnson, A. J. A., & Holmes, S. P. (2016). DADA2: High-resolution sample inference from Illumina amplicon data. *Nature methods*, *13*(7), 581-583.

Cavanaugh, C. M. (1983). Symbiotic chemoautotrophic bacteria in marine invertebrates from sulphide-rich habitats. *Nature*, *302*(5903), 58-61.

Cermak, N., Becker, J. W., Knudsen, S. M., Chisholm, S. W., Manalis, S. R., & Polz, M. F. (2017). Direct single-cell biomass estimates for marine bacteria via Archimedes' principle. *The ISME journal*, *11*(3), 825-828.

Childress, J. J., Fisher, C., Brooks, J., Kennicutt, M., Bidigare, R., & Anderson, A. (1986). A methanotrophic marine molluscan (Bivalvia, Mytilidae) symbiosis: mussels fueled by gas. *Science*, *233*(4770), 1306-1308.

Cordes, E. E., Cunha, M. R., Galeron, J., Mora, C., Olu-Le Roy, K., Sibuet, M., Van Gaever, S., Vanreusel, A., & Levin, L. A. (2010). The influence of geological, geochemical, and biogenic habitat heterogeneity on seep biodiversity. *Marine Ecology*, *31*(1), 51-65.

Damm, E., Helmke, E., Thoms, S., Schauer, U., Nöthig, E., Bakker, K., & Kiene, R. (2010). Methane production in aerobic oligotrophic surface water in the central Arctic Ocean. *Biogeosciences*, *7*(3), 1099-1108.

de Angelis, M. A., & Lee, C. (1994). Methane production during zooplankton grazing on marine phytoplankton. *Limnology and Oceanography*, *39*(6), 1298-1308.

Egger, M., Hagens, M., Sapart, C. J., Dijkstra, N., van Helmond, N. A., Mogollón, J. M., Risgaard-Petersen, N., van der Veen, C., Kasten, S., & Riedinger, N. (2017). Iron oxide reduction in methane-rich deep Baltic Sea sediments. *Geochimica et Cosmochimica Acta*, *207*, 256-276.

Eitel, E. M., Utter, D., Connon, S., Orphan, V. J., & Murali, R. (2024). CABO-16S: A Combined Archaea, Bacteria, Organelle 16S database for amplicon analysis of prokaryotes and eukaryotes in environmental samples. *bioRxiv*, 2024.2010. 2023.619938.

Fisher, M. A., Normark, W. R., Langenheim, V. E., Calvert, A. J., & Sliter, R. (2004). The offshore Palos Verdes fault zone near san Pedro, southern California. *Bulletin of the Seismological Society of America*, *94*(2), 506-530.

Fuchs, A., Lyautey, E., Montuelle, B., & Casper, P. (2016). Effects of increasing temperatures on methane concentrations and methanogenesis during experimental incubation of sediments from oligotrophic and mesotrophic lakes. *Journal of Geophysical Research: Biogeosciences*, *121*(5), 1394-1406.

Galambos, D., Anderson, R. E., Reveillaud, J., & Huber, J. A. (2019). Genome-resolved metagenomics and metatranscriptomics reveal niche differentiation in functionally redundant microbial communities at deep-sea hydrothermal vents. *Environmental Microbiology*, *21*(11), 4395-4410.

Goffredi, S. K., Tilic, E., Mullin, S. W., Dawson, K. S., Keller, A., Lee, R. W., Wu, F., Levin, L. A., Rouse, G. W., & Cordes, E. E. (2020). Methanotrophic bacterial symbionts fuel dense populations of deep-sea feather duster worms (Sabellida, Annelida) and extend the spatial influence of methane seepage. *Science Advances*, *6*(14), eaay8562.

Grupe, B. M., Krach, M. L., Pasulka, A. L., Maloney, J. M., Levin, L. A., & Frieder, C. A. (2015). Methane seep ecosystem functions and services from a recently discovered southern California seep. *Marine Ecology*, *36*, 91-108.

Hartmann, J. F., Günthel, M., Klintzsch, T., Kirillin, G., Grossart, H.-P., Keppler, F., & Isenbeck-Schröter, M. (2020). High spatiotemporal dynamics of methane production and emission in oxic surface water. *Environmental science & technology*, *54*(3), 1451-1463.

Hein, J. R., Normark, W. R., McIntyre, B. R., Lorenson, T. D., & Powell, C. L. (2006). Methanogenic calcite, 13C-depleted bivalve shells, and gas hydrate from a mud volcano offshore southern California. *Geology*, *34*(2), 109-112.

Heintz, M., Mau, S., & Valentine, D. (2012). Physical control on methanotrophic potential in waters of the Santa Monica Basin, Southern California. *Limnology and Oceanography*, *57*(2), 420-432.

Hickey, B. M. (1992). Circulation over the Santa Monica-San Pedro basin and shelf. *Progress in Oceanography*, *30*(1-4), 37-115.

Hickey, B. M., Dobbins, E., & Allen, S. E. (2003). Local and remote forcing of currents and temperature in the central Southern California Bight. *Journal of Geophysical Research: Oceans*, *108*(C3).

Hinrichs, K.-U., & Boetius, A. (2002). The anaerobic oxidation of methane: new insights in microbial ecology and biogeochemistry. *Ocean margin systems*, 457-477.

Jahnke, R. A. (2010). Global synthesis1. In *Carbon and nutrient fluxes in continental margins: A global synthesis* (pp. 597-615). Springer.

Jordan, S., Treude, T., Leifer, I., Schulz-Vogt, H., & Schmale, O. (2019). Bubble Shuttle: A bubble-mediated bentho-pelagic transport mechanism of methanotrophs and a first study at the Coal

Oil Point seep field to identify the controlling parameters. EGU General Assembly Conference Abstracts,

Jordan, S. F., Treude, T., Leifer, I., Janßen, R., Werner, J., Schulz-Vogt, H., & Schmale, O. (2020). Bubble-mediated transport of benthic microorganisms into the water column: Identification of methanotrophs and implication of seepage intensity on transport efficiency. *Scientific reports*, *10*(1), 4682.

Jørgensen, B. B., & Kasten, S. (2006). Sulfur cycling and methane oxidation. In *Marine geochemistry* (pp. 271-309). Springer.

Judd, A., & Hovland, M. (2009). *Seabed fluid flow: the impact on geology, biology and the marine environment*. Cambridge University Press.

Kalyuzhnaya, M., Yang, S., Rozova, O., Smalley, N., Clubb, J., Lamb, A., Gowda, G. N., Raftery, D., Fu, Y., & Bringel, F. (2013). Highly efficient methane biocatalysis revealed in a methanotrophic bacterium. *Nature communications*, *4*(1), 2785.

Karl, D. M., Beversdorf, L., Björkman, K. M., Church, M. J., Martinez, A., & Delong, E. F. (2008). Aerobic production of methane in the sea. *Nature Geoscience*, *1*(7), 473-478.

Kemnitz, N., Berelson, W. M., Hammond, D. E., Morine, L., Figueroa, M., Lyons, T. W., Scharf, S., Rollins, N., Petsios, E., & Lemieux, S. (2020). Evidence of changes in sedimentation rate and sediment fabric in a low-oxygen setting: Santa Monica Basin, CA. *Biogeosciences*, *17*(8), 2381-2396.

Klintzsch, T., Langer, G., Nehrke, G., Wieland, A., Lenhart, K., & Keppler, F. (2019). Methane production by three widespread marine phytoplankton species: release rates, precursor compounds, and potential relevance for the environment. *Biogeosciences*, *16*(20), 4129-4144.

Knittel, K., & Boetius, A. (2009). Anaerobic oxidation of methane: progress with an unknown process. *Annual review of microbiology*, *63*(1), 311-334.

Kolb, S., Knief, C., Stubner, S., & Conrad, R. (2003). Quantitative detection of methanotrophs in soil by novel pmoA-targeted real-time PCR assays. *Applied and Environmental Microbiology*, *69*(5), 2423-2429.

Krause, S. J., & Treude, T. (2021). Deciphering cryptic methane cycling: Coupling of methylotrophic methanogenesis and anaerobic oxidation of methane in hypersaline coastal wetland sediment. *Geochimica et Cosmochimica Acta*, *302*, 160-174.

Leifer, I., Luyendyk, B. P., Boles, J., & Clark, J. F. (2006). Natural marine seepage blowout: Contribution to atmospheric methane. *Global Biogeochemical Cycles*, *20*(3).

Levin, L., Girguis, P. R., German, C. R., Brennan, M. L., Tüzün, S., Wagner, J., Smart, C., Kruger, A., Inderbitzen, K., & Le, J. (2016). Exploration and discovery of methane seeps and associated communities in the California Borderland. *Oceanography*, *29*(1), 40-43.

Levin, L. A. (2005). Ecology of cold seep sediments: interactions of fauna with flow, chemistry and microbes. In *Oceanography and Marine Biology* (pp. 11-56). CRC Press.

Levin, L. A., Baco, A. R., Bowden, D. A., Colaco, A., Cordes, E. E., Cunha, M. R., Demopoulos, A. W., Gobin, J., Grupe, B. M., & Le, J. (2016). Hydrothermal vents and methane seeps: rethinking the sphere of influence. *Frontiers in Marine Science*, *3*, 72.

Levin, L. A., Ziebis, W., Mendoza, G. F., Growney, V. A., Tryon, M. D., Brown, K. M., Mahn, C., Gieskes, J. M., & Rathburn, A. E. (2003). Spatial heterogeneity of macrofauna at northern California methane seeps: influence of sulfide concentration and fluid flow. *Marine Ecology Progress Series*, *265*, 123-139.

Liu, J., Zheng, Y., Lin, H., Wang, X., Li, M., Liu, Y., Yu, M., Zhao, M., Pedentchouk, N., & Lea-Smith, D. J. (2019). Proliferation of hydrocarbon-degrading microbes at the bottom of the Mariana Trench. *Microbiome*, *7*, 1-13.

Maloney, J. M., Grupe, B. M., Pasulka, A. L., Dawson, K. S., Case, D. H., Frieder, C. A., Levin, L. A., & Driscoll, N. W. (2015). Transpressional segment boundaries in strike-slip fault systems offshore southern California: implications for fluid expulsion and cold seep habitats. *Geophysical Research Letters*, *42*(10), 4080-4088.

Mao, Y., Lin, T., Li, H., He, R., Ye, K., Yu, W., & He, Q. (2024). Aerobic methane production by phytoplankton as an important methane source of aquatic ecosystems: Reconsidering the global methane budget. *Science of the Total Environment*, *907*, 167864.

Marlow, J. J., Steele, J. A., Ziebis, W., Thurber, A. R., Levin, L. A., & Orphan, V. J. (2014). Carbonate-hosted methanotrophy represents an unrecognized methane sink in the deep sea. *Nature communications*, *5*(1), 5094.

Martin, M. (2011). Cutadapt removes adapter sequences from high-throughput sequencing reads. *EMBnet. journal*, *17*(1), 10-12.

Mau, S., Blees, J., Helmke, E., Niemann, H., & Damm, E. (2013). Vertical distribution of methane oxidation and methanotrophic response to elevated methane concentrations in stratified waters of the Arctic fjord Storfjorden (Svalbard, Norway). *Biogeosciences*, *10*(10), 6267-6278.

Mayr, M. J., Parra, S. A., Connon, S. A., Narayanan, A. K., Murali, R., Cremiere, A., & Orphan, V. J. (2025). Distinct Microbial Communities Within and On Seep Carbonates Support Long-term Anaerobic Oxidation of Methane and Novel pMMO Diversity. *bioRxiv*, 2025.2002. 2004.636526.

Niemann, H., Steinle, L., Blees, J., Bussmann, I., Treude, T., Krause, S., Elvert, M., & Lehmann, M. F. (2015). Toxic effects of lab-grade butyl rubber stoppers on aerobic methane oxidation. *Limnology and Oceanography: Methods*, *13*(1), 40-52.

Orata, F. D., Meier-Kolthoff, J. P., Sauvageau, D., & Stein, L. Y. (2018). Phylogenomic analysis of the gammaproteobacterial methanotrophs (order Methylococcales) calls for the reclassification of members at the genus and species levels. *Frontiers in Microbiology*, *9*, 3162.

Orphan, V. J., House, C. H., Hinrichs, K.-U., McKeegan, K. D., & DeLong, E. F. (2001). Methane-consuming archaea revealed by directly coupled isotopic and phylogenetic analysis. *science*, *293*(5529), 484-487.

Pack, M. A., Heintz, M. B., Reeburgh, W. S., Trumbore, S. E., Valentine, D. L., Xu, X., & Druffel, E. R. (2015). Methane oxidation in the eastern tropical North Pacific Ocean water column. *Journal of Geophysical Research: Biogeosciences*, *120*(6), 1078-1092.

Pasulka, A. L., Goffredi, S. K., Tavormina, P. L., Dawson, K. S., Levin, L. A., Rouse, G. W., & Orphan, V. J. (2017). Colonial tube-dwelling ciliates influence methane cycling and microbial diversity within methane seep ecosystems. *Frontiers in Marine Science*, *3*, 276.

Paull, C. K., Hecker, B., Commeau, R., Freeman-Lynde, R., Neumann, C., Corso, W., Golubic, S., Hook, J., Sikes, E., & Curray, J. (1984). Biological communities at the Florida Escarpment resemble hydrothermal vent taxa. *Science*, *226*(4677), 965-967.

Paull, C. K., Normark, W. R., Ussler III, W., Caress, D. W., & Keaten, R. (2008). Association among active seafloor deformation, mound formation, and gas hydrate growth and accumulation

within the seafloor of the Santa Monica Basin, offshore California. *Marine Geology*, *250*(3-4), 258-275.

Perez-Coronel, E., & Michael Beman, J. (2022). Multiple sources of aerobic methane production in aquatic ecosystems include bacterial photosynthesis. *Nature communications*, *13*(1), 6454.

Pernthaler, J. (2005). Predation on prokaryotes in the water column and its ecological implications. *Nature Reviews Microbiology*, *3*(7), 537-546.

Pohlman, J. W., Greinert, J., Ruppel, C., Silyakova, A., Vielstädte, L., Casso, M., Mienert, J., & Bünz, S. (2017). Enhanced CO2 uptake at a shallow Arctic Ocean seep field overwhelms the positive warming potential of emitted methane. *Proceedings of the National Academy of Sciences*, *114*(21), 5355-5360.

Pontiller, B., Martínez-García, S., Joglar, V., Amnebrink, D., Pérez-Martínez, C., González, J. M., Lundin, D., Fernández, E., Teira, E., & Pinhassi, J. (2022). Rapid bacterioplankton transcription cascades regulate organic matter utilization during phytoplankton bloom progression in a coastal upwelling system. *The ISME journal*, *16*(10), 2360-2372.

Qin, Q., Kinnaman, F. S., Gosselin, K. M., Liu, N., Treude, T., & Valentine, D. L. (2022). Seasonality of water column methane oxidation and deoxygenation in a dynamic marine environment. *Geochimica et Cosmochimica Acta*, *336*, 219-230.

Reeburgh, W. S. (2007). Oceanic methane biogeochemistry. *Chemical reviews*, *107*(2), 486-513.

Reis, P. C., Tsuji, J. M., Weiblen, C., Schiff, S. L., Scott, M., Stein, L. Y., & Neufeld, J. D. (2024). Enigmatic persistence of aerobic methanotrophs in oxygen-limiting freshwater habitats. *The ISME journal*, *18*(1), wrae041.

Rogener, M. K., Hunter, K. S., Rabalais, N. N., Roberts, B. J., Bracco, A., Stewart, F. J., & Joye, S. B. (2021). Pelagic denitrification and methane oxidation in oxygen-depleted waters of the Louisiana shelf. *Biogeochemistry*, *154*, 231-254.

Rubin-Blum, M., Antony, C. P., Sayavedra, L., Martínez-Pérez, C., Birgel, D., Peckmann, J., Wu, Y.-C., Cardenas, P., MacDonald, I., & Marcon, Y. (2019). Fueled by methane: deep-sea sponges from asphalt seeps gain their nutrition from methane-oxidizing symbionts. *The ISME journal*, *13*(5), 1209-1225.

Ryan, H. F., Conrad, J. E., Paull, C., & McGann, M. (2012). Slip rate on the San Diego Trough fault zone, Inner California Borderland, and the 1986 Oceanside earthquake swarm revisited. *Bulletin of the Seismological Society of America*, *102*(6), 2300-2312.

Sauter, E. J., Muyakshin, S. I., Charlou, J.-L., Schlüter, M., Boetius, A., Jerosch, K., Damm, E., Foucher, J.-P., & Klages, M. (2006). Methane discharge from a deep-sea submarine mud volcano into the upper water column by gas hydrate-coated methane bubbles. *Earth and Planetary Science Letters*, *243*(3-4), 354-365.

Semrau, J. D., DiSpirito, A. A., & Yoon, S. (2010). Methanotrophs and copper. *FEMS microbiology reviews*, *34*(4), 496-531.

Sibuet, M., & Roy, K. O.-L. (2002). Cold seep communities on continental margins: structure and quantitative distribution relative to geological and fluid venting patterns. In *Ocean margin systems* (pp. 235-251). Springer.

Steinle, L., Graves, C. A., Treude, T., Ferré, B., Biastoch, A., Bussmann, I., Berndt, C., Krastel, S., James, R. H., & Behrens, E. (2015). Water column methanotrophy controlled by a rapid oceanographic switch. *Nature Geoscience*, *8*(5), 378-382.

Steinle, L., Maltby, J., Treude, T., Kock, A., Bange, H. W., Engbersen, N., Zopfi, J., Lehmann, M. F., & Niemann, H. (2017). Effects of low oxygen concentrations on aerobic methane oxidation in seasonally hypoxic coastal waters. *Biogeosciences*, *14*(6), 1631-1645.

Suess, E. (2010). Marine cold seeps. In. Springer.

Sulpis, O., Jeansson, E., Dinauer, A., Lauvset, S. K., & Middelburg, J. J. (2021). Calcium carbonate dissolution patterns in the ocean. *Nature Geoscience*, *14*(6), 423-428.

Tavormina, P. L., Ussler III, W., Joye, S. B., Harrison, B. K., & Orphan, V. J. (2010). Distributions of putative aerobic methanotrophs in diverse pelagic marine environments. *The ISME journal*, *4*(5), 700-710.

Tavormina, P. L., Ussler III, W., Steele, J. A., Connon, S. A., Klotz, M. G., & Orphan, V. J. (2013). Abundance and distribution of diverse membrane-bound monooxygenase (C u-MMO) genes within the C osta R ica oxygen minimum zone. *Environmental Microbiology Reports*, *5*(3), 414-423.

Thamdrup, B., Steinsdóttir, H. G., Bertagnolli, A. D., Padilla, C. C., Patin, N. V., Garcia-Robledo, E., Bristow, L. A., & Stewart, F. J. (2019). Anaerobic methane oxidation is an important sink for methane in the ocean's largest oxygen minimum zone. *Limnology and Oceanography*, *64*(6), 2569-2585.

Thompson, M., & Francis, R. D. (2019). Tectonic Evolution of the Palos Verdes Fault–Lasuen Knoll Segment, Offshore Southern California.

Thurber, A. R., Levin, L. A., Rowden, A. A., Sommer, S., Linke, P., & Kröger, K. (2013). Microbes, macrofauna, and methane: a novel seep community fueled by aerobic methanotrophy. *Limnology and Oceanography*, *58*(5), 1640-1656.

Thurber, A. R., Sweetman, A. K., Narayanaswamy, B. E., Jones, D. O., Ingels, J., & Hansman, R. (2014). Ecosystem function and services provided by the deep sea. *Biogeosciences*, *11*(14), 3941-3963.

Treude, T., Boetius, A., Knittel, K., Wallmann, K., & Jørgensen, B. B. (2003). Anaerobic oxidation of methane above gas hydrates at Hydrate Ridge, NE Pacific Ocean. *Marine Ecology Progress Series*, *264*, 1-14.

Treude, T., Kiel, S., Linke, P., Peckmann, J., & Goedert, J. L. (2011). Elasmobranch egg capsules associated with modern and ancient cold seeps: a nursery for marine deep-water predators. *Marine Ecology Progress Series*, *437*, 175-181.

Tunnicliffe, V., Juniper, S. K., & Sibuet, M. (2003). Reducing environments of the deep-sea floor. *Ecosystems of the World*, 81-110.

Turner, P. J., Ball, B., Diana, Z., Fariñas-Bermejo, A., Grace, I., McVeigh, D., Powers, M. M., Van Audenhaege, L., Maslakova, S., & Young, C. M. (2020). Methane seeps on the US Atlantic margin and their potential importance to populations of the commercially valuable deep-sea red crab, Chaceon quinquedens. *Frontiers in Marine Science*, *7*, 75.

Ussler III, W., Preston, C., Tavormina, P., Pargett, D., Jensen, S., Roman, B., Marin III, R., Shah, S. R., Girguis, P. R., & Birch, J. M. (2013). Autonomous application of quantitative PCR in the deep sea: in situ surveys of aerobic methanotrophs using the deep-sea environmental sample processor. *Environmental science & technology*, *47*(16), 9339-9346.

van Aken, H. M., Budeus, G., & Hähnel, M. (1995). The anatomy of the Arctic frontal zone in the Greenland Sea. *Journal of Geophysical Research: Oceans*, *100*(C8), 15999-16014.

Vekeman, B., Kerckhof, F. M., Cremers, G., De Vos, P., Vandamme, P., Boon, N., Op den Camp, H. J., & Heylen, K. (2016). New Methyloceanibacter diversity from North Sea sediments

includes methanotroph containing solely the soluble methane monooxygenase. *Environmental microbiology*, *18*(12), 4523-4536.

Wallmann, K., Linke, P., Suess, E., Bohrmann, G., Sahling, H., Schlüter, M., Dählmann, A., Lammers, S., Greinert, J., & von Mirbach, N. (1997). Quantifying fluid flow, solute mixing, and biogeochemical turnover at cold vents of the eastern Aleutian subduction zone. *Geochimica et Cosmochimica Acta*, *61*(24), 5209-5219.

Ward, B., & Kilpatrick, K. (1993). Methane oxidation associated with mid-depth methane maxima in the Southern California Bight. *Continental Shelf Research*, *13*(10), 1111-1122.

Welte, C., & Deppenmeier, U. (2014). Bioenergetics and anaerobic respiratory chains of aceticlastic methanogens. *Biochimica et Biophysica Acta (BBA)-Bioenergetics*, *1837*(7), 1130-1147.

Xiao, K.-Q., Beulig, F., Kjeldsen, K. U., Jørgensen, B. B., & Risgaard-Petersen, N. (2017). Concurrent methane production and oxidation in surface sediment from Aarhus Bay, Denmark. *Frontiers in microbiology*, *8*, 1198.

Xiao, K. Q., Beulig, F., Røy, H., Jørgensen, B. B., & Risgaard-Petersen, N. (2018). Methylotrophic methanogenesis fuels cryptic methane cycling in marine surface sediment. *Limnology and Oceanography*, *63*(4), 1519-1527.

Yamamoto, S., Alcauskas, J. B., & Crozier, T. E. (1976). Solubility of methane in distilled water and seawater. *Journal of Chemical and Engineering Data*, *21*(1), 78-80.

Supplementary Material: Klonicki et al. Unveiling the Methanosphere: Transport of Methane and Methanotrophs Beyond Visible Seeps in the Southern California Margin

Supplementary Table 1. Geographic coordinates, depths, and two-dimensional distances between sequential waypoints for two surveyed locations: DMS (CTD3) and SMM (CTD7). The last waypoint in each section does not have a distance to the next waypoint, as it is the final point in the survey sequence.

Location	Waypoint	Latitude (dec. deg.)	Longitude (dec. deg.)	Depth (m)	Distance to next Waypoint (m)
DMS	1	32.9055	-117.7827	1015	101.6
DMS	2	32.9046	-117.7825	1018	48.1
DMS	3	32.9042	-117.7823	1018	56.2
DMS	4	32.9037	-117.7822	1007	93.1
DMS	5	32.9029	-117.7819	1024	1836.7
DMS	6	32.8868	-117.7773	1045	103.7
DMS	7	32.8859	-117.7770	1045	45.3
DMS	8	32.8855	-117.7769	1045	48.1
DMS	9	32.8851	-117.7767	1045	101.6
DMS	10	32.8842	-117.7765	1045	N/A
SMM	1	33.7988	-118.6449	816	72.9
SMM	2	33.7991	-118.6456	812	38.7
SMM	3	33.7992	-118.6460	809	29.9
SMM	4	33.7993	-118.6463	803	29.9
SMM	5	33.7994	-118.6466	800	21.6
SMM	6	33.7995	-118.6468	801	29.9
SMM	7	33.7996	-118.6471	805	21.6
SMM	8	33.7997	-118.6473	806	72.9
SMM	9	33.8000	-118.6480	810	81.2
SMM	10	33.8003	-118.6488	810	N/A

Supplementary Table 2. Environmental and microbiological characteristics at different depths across the three seep sites: Santa Monica Mound (SMM), Del Mar Seep (DMS), and Lasuen Knoll (LK). Variables include depth, first-order rate constant (k), methane turnover time, methane (CH_4) and oxygen (O_2) concentrations, temperature, pmoA gene copy abundance (log scale), and fluorescence as a proxy for microbial biomass.

Site	Depth (m)	*k*	Turnover Time (y)	CH_4 (nM)	O_2 (µM)	Temp. °C	Log copies pmoA L^{-1}	Fluorescence (µg L^{-1})
SMM	2	0.001256	2.18	82	253	19.8	3.49	0.3989
SMM	200	0.000272	10.1	68	82	9.62	5.21	0.0084
SMM	400	0.000156	17.5	74	28	8.15	N/A	0.0244
SMM	500	0.001282	2.14	77	18	7.21	N/A	0.0261
SMM	580	0.004633	0.591	111	11	6.42	5.84	0.0373
SMM	600	0.003128	0.876	122	11	6.33	N/A	0.0351
SMM	703	0.011327	0.242	172	5.9	5.63	N/A	0.0343
SMM	752	0.01777	0.154	191	5.4	5.50	6.03	0.0372
SMM	791	0.018501	0.148	235	3.8	5.32	N/A	0.0417
SMM	798	0.006782	0.404	293	3.5	5.31	5.57	0.0443
DMS	2	0.001588	1.73	47	231	20.35	4.65	0.043
DMS	290	0.000142	19.3	80	56	8.95	N/A	0.016
DMS	541	0.000491	5.58	79	12	6.72	5.560	0.0212
DMS	790	0.001025	2.67	66	10	5.19	N/A	0.0355
DMS	940	0.000428	6.41	63	14	4.49	5.61	0.0379
DMS	989	0.000509	5.38	66	15	4.35	N/A	0.026
DMS	1008	0.002133	1.28	75	20	4.13	5.47	0.0402
DMS	1017	0.002624	1.04	73	22	3.97	5.07	0.0329
DMS	1026	0.001065	2.57	131	22	3.96	5.07	0.0389
DMS	1031	0.000869	3.15	113	23	3.96	N/A	0.0341
LK	3	0.003812	0.719	33	232	20.4	N/A	0.1178
LK	51	0.000525	5.22	47	233	12.8	N/A	0.7355
LK	101	0.001743	1.57	54	145	10.6	N/A	0.1266
LK	201	0.004869	0.563	62	95	9.30	5.12	0.0116
LK	291	0.000188	14.6	76	56	8.94	N/A	0.0227
LK	341	0.001174	2.33	66	45	8.47	5.32	0.0255
LK	360	0.000909	3.01	214	39	8.46	N/A	0.0217
LK	370	0.001412	1.94	89	35	8.46	5.20	0.0202
LK	378	0.001152	2.38	135	36	8.43	N/A	0.0204

Chapter 4

Methane Oxidation and the Distribution of Methane-Oxidizing Bacteria above Cold Seeps in the Eastern Aleutian Subduction Zone

Emily Klonicki-Ference[1*], Daniel R. Utter[2], Kira Homola[1], John S. Magyar[2], Victoria J. Orphan[2], Lisa Levin[3], Tina Treude[1,4*]

[1]Department of Earth, Planetary, and Space Sciences, University of California Los Angeles, Los Angeles, CA, USA

[2]Division of Geological and Planetary Sciences, California Institute of Technology, Pasadena, CA, USA

[3] Scripps Institution of Oceanography, University of California, San Diego, La Jolla, CA, USA

[4]Department of Atmospheric and Oceanic Sciences, University of California Los Angeles, Los Angeles, CA, USA

*Correspondence: Emily Klonicki-Ference, eklonicki@g.ucla.edu; Tina Treude, ttreude@g.ucla.edu

Abstract

Cold seeps along the eastern Aleutian subduction zone in the Gulf of Alaska fuel benthic ecosystems through microbial methane (CH_4) consumption, yet the structure and controls of water column CH_4 oxidation in these deep, cold waters remain poorly resolved. During a May–June 2024 expedition with the R/V *Atlantis* and HOV *Alvin*, we studied CH_4 and its bacterial oxidation from surface to

seafloor above three deep seep sites (2000–5000 m): Edge, Shumagin, and Sanak, by combining radiotracer incubations with pmoA gene and 16S rRNA profiling. CH_4 oxidation occurred throughout the water column, with peak rates (1–242 nmol L^{-1} d^{-1}) in near-seafloor *Alvin* samples and 0.1–0.25 nmol L^{-1} d^{-1} in CTD rosette samples 10–30 m above bottom. Rates varied by site and depth. CH_4 oxidation in surface waters, coinciding with an algal bloom, suggests cryptic cycling via *in situ* production and consumption. Methanotroph communities varied with depth: diversity and abundance were greatest near the seafloor, while the Gammaproteobacterial lineage Milano-WF1B-03 persisted throughout the water column. A ~325 m near-bottom CTD transect at Sanak revealed lateral gradients in CH_4 and oxidation aligned with bottom currents, with oxidation highest near hydrate-bearing gas vents and at the off-seep distal end. These findings show that aerobic CH_4 oxidation peaks near the seafloor to ~30 m above but extends laterally and vertically beyond active seepage. Oxidation was detected even where methanotroph gene abundance was low, potentially indicating the influence of lateral CH_4 transport and tidal currents. The methanosphere thus emerges as a dynamic and spatially diffuse microbial system shaped by CH_4 availability and physical transport processes.

1. Introduction

In and around active cold seeps along continental margins, where methane (CH_4) diffuses through sediments and enters the water column, diverse microbial and faunal communities are connected to CH_4 via methanotrophy, symbioses, and food webs fueled by CH_4-derived carbon (Levin, 2005; Paull et al., 1984; Suess, 2010; Tunnicliffe et al., 2003). Cold seeps are dynamic environments characterized by continuous physical, chemical, and biological fluxes (i.e., biomass turnover by microbes and fauna) that sustain these complex networks of CH_4-based interactions. This biologically active domain is here termed the 'methanosphere': a spatially expansive zone spanning seep sediments and adjacent waters, where CH_4 influences benthic animal communities and drives microbial activity throughout the water column. The methanosphere is foundationally sustained by microbial processes: in sediments, the anaerobic oxidation of CH_4 by syntrophic archaea and sulfate-reducing bacteria acts as a biological filter that mitigates CH_4 release (Boetius et al., 2000; Orphan et al., 2001), while the hydrogen sulfide (H_2S) produced during AOM fuels sulfur-oxidizing microbial mats and their symbiotic invertebrates (Boetius et al., 2000). When CH_4 diffuses from the sediments into the overlying water, it undergoes aerobic oxidation by methane-oxidizing bacteria (MOB), which occur as free-living cells in the water column (Kalyuzhnaya et al., 2019) or sometimes in association with benthic invertebrates (e.g., sponges and clams) (Childress et al., 1986; Goffredi et al., 2020; Levin, 2005; Pasulka et al., 2017; Rubin-Blum et al., 2019).

Together, these microbial processes not only regulate CH_4 and its emission into the water column and atmosphere but also shape the physical and biological architecture of seep ecosystems. AOM contributes to the precipitation of authigenic carbonates (Bohrmann et al., 1998; Greinert et al., 2002), which accumulate into mounds, crusts, and pavements that can persist for thousands of

years (Crémière et al., 2016; Kutterolf et al., 2008). These structures provide stable, elevated substrate in otherwise unconsolidated sediments, fostering the establishment of microbial mats, sessile invertebrates, and complex benthic communities. In doing so, AOM-linked carbonate formation reinforces both the spatial structure and ecological longevity of seep habitats (Levin, 2005; Suess, 2010).

MOB extend the methanosphere vertically by forming a biologically active layer within the water column. As the primary consumers of CH_4, MOB assimilate CH_4-derived carbon into biomass, which can then enter benthic and pelagic food webs; although the overall magnitude of MOB contribution to deep ocean carbon cycling remains to be quantified (Crespo-Medina et al., 2014; Grey, 2016). Recent studies have highlighted the role of MOB in mediating carbon transport from CH_4 into higher trophic levels, particularly in O_2-deficient zones where CH_4 oxidation may constitute an important organic carbon input (Steinle et al., 2017; Thamdrup et al., 2019). MOB biomass colonizes surfaces such as sediment particles (Tavormina et al., 2008), authigenic carbonates (Cordova-Gonzalez et al., 2023), and microbial mats (Paul et al., 2017); grazers can then acquire this biomass either by directly grazing on those surfaces or by ingesting aggregates mobilized during resuspension events, linking microbial CH_4 oxidation to macrofaunal energy pathways (Deines et al., 2007).

Supported by diffuse CH_4 fluxes and oxygen gradients, MOB have been shown to persist well beyond active seepage, mediating CH_4 oxidation across broad spatial and vertical gradients (Steinle et al., 2015). Observations of elevated MOB abundance and activity more than a kilometer from visibly active seep sites reveal a dynamic methanosphere that spans from the sediment–water interface through the overlying water column (Pasulka et al., 2017; Tavormina et al., 2008; Ussler III et al., 2013); this thesis, chapter 3). As ocean warming and shifting circulation patterns intensify

the physical and biogeochemical drivers of CH_4 release, oxidation, and transport (Ciais et al., 2014), it becomes increasingly important to characterize these processes across a range of settings; from shallow, organic-rich, and oxygen-poor to deep, organic-poor, and oxygen-rich seeps.

To address the spatial extent, controls, and dynamics of the water column methanosphere, we conducted the first of two ecological expeditions on CH_4 seep microbial and faunal symbioses in summer 2023 at shallower (~400–1,000 m), low-O_2 CH_4 seeps in the Southern California Borderland (this thesis, chapter 3). The expedition revealed that aerobic CH_4 oxidation and MOB communities extend beyond visibly active seepage, dispersing laterally and vertically throughout the water column. Across geochemically distinct sites, elevated *pmoA* gene abundance and CH_4 oxidation activity were detected more than 1 km from observed active seep sources. We propose that the observed distribution may be influenced by localized CH_4 flux, vertical O_2 gradients, and physical transport processes, such as bottom-water circulation and bubble-mediated transfer of CH_4 and microbes. MOB communities responded dynamically to these gradients, showing high oxidation rates under low-O_2, high-CH_4 conditions, and more spatially dispersed, lower-intensity activity in regions with likely greater mixing or episodic seepage. In addition to modulating CH_4 availability, MOB biomass may be transported kilometers via water currents, potentially subsidizing heterotrophic food webs beyond seep boundaries. These findings underscore the role of aerobic methanotrophy not merely as a CH_4 sink, but as a mobile, ecosystem-shaping process that broadens the functional footprint of cold seeps.

Deeper (2000-5000 m) cold seeps in the Gulf of Alaska reside in low-temperature, high-pressure, fully oxygenated (~160 μM) waters with expected minimal organic matter flux (~0.17 mol C_{org} y^{-1}) along the Aleutian margin (Elvert et al., 2000; Jahnke, 2010; Suess et al., 1998; Wallmann et al., 1997). Active fluid venting (Wallmann et al., 1997), vent-associated biota (Levin

& Mendoza, 2007; Wallmann et al., 1997), and authigenic calcium carbonate and barite precipitates have been documented bordering the eastern Aleutian Trench (Greinert et al., 2002; Suess et al., 1998). These seep sites are oxygenated, providing the O_2 required for aerobic CH_4 oxidation, and receive minimal input of photosynthetically derived organic matter. Consequently, microbial productivity and faunal biomass depend primarily on *in situ* chemosynthetic processes (CH_4 and H_2S oxidation) rather than on surface-delivered organic carbon (Conrad, 2009; Jørgensen & Boetius, 2007; Reeburgh, 2007). Cold temperatures can slow enzymatic activity and reduce CH_4 oxidation rates relative to warmer settings (Fuchs et al., 2016). At the same time, abundant O_2 supports aerobic metabolism; together, cold, O_2-rich conditions may select for psychrophilic, O_2-tolerant MOB assemblages distinct from those in warmer, hypoxic seep environments (Hanson & Hanson, 1996; Reeburgh, 2007). These deep, oxygenated seeps provide a valuable framework for assessing how variations in O_2 availability govern CH_4 oxidation rates and structure the water column methanosphere. Understanding these dynamics will also improve predictions of methanosphere responses to future changes in ocean oxygenation.

In the present study, we propose the following hypotheses: (1) CH_4 concentrations and methanotroph indicators (e.g., *pmoA* abundance, community composition, activity) decrease with distance from active seep zones but remain elevated above background in off-seep waters, reflecting a broad methanosphere in fully oxygenated deep settings. (2) In high-O_2 waters, CH_4 oxidation rates and methanotroph abundance are primarily governed by CH_4 availability and transport, with little influence from ambient O_2 variability across sites.

During a May–June 2024 research expedition aboard the R/V, we conducted the second and final expedition of the series to investigate the spatial extent and dynamics of the overlaying water column of the methanosphere at deep, fully oxygenated (Edge and Shumagin) CH_4 seeps along the eastern Aleutian subduction zone in the Gulf of Alaska. Building on insights gained from our earlier work on shallower Southern California Borderland seeps, the expedition combined measurements of CH_4 concentrations and ^3H-CH_4 incubations with 16S rRNA next-generation sequencing and the quantification of the particulate methane monooxygenase gene (pmoA). Samples were collected via vertical and horizontal CTD transects and targeted dives with human occupied vehicle *Alvin*. Our results reveal pronounced spatial and vertical heterogeneity in CH_4 concentrations, oxidation rates, and methanotroph distributions, demonstrating active CH_4 turnover not only in deep bottom waters but also in surface layers with minimal ambient CH_4. By assessing how O_2 availability, particle flux, and lateral/vertical transport combine to shape these gradients, we show how the water column methanosphere is sculpted in deep, O_2-rich settings, with implications for marine carbon cycling and ecosystem connectivity.

2. Methods

2.1. Study Areas

2.1.1 Sanak

The Sanak Seep is a recently discovered cold seep site located along the Aleutian margin near Sanak Island. First detected in May 2023 during NOAA's Seascape Alaska 1 expedition (Cuellar, 2023), the site was confirmed and further characterized on July 18, 2023, during Seascape Alaska 3 Dive 04 (Hoy, 2023). The seep lies at a depth of approximately 2,100 meters and features active CH_4 bubble plumes, exposed gas hydrates, and extensive chemosynthetic communities.

Observations included dense aggregations of tubeworms, chemosynthetic vesicomyid clams, and ampharetid polychaetes, as well as outcropping, CH_4-derived authigenic carbonates. These biological and geochemical features indicate sustained fluid flow and a biologically active, CH_4-rich environment.

2.1.2 Shumagin

The Shumagin CH_4 cold seep system is located along the eastern Aleutian subduction zone near the Shumagin Islands. Situated at depths near approximately 4,850 meters, the site lies within a tectonically active region where subduction of the Pacific Plate beneath the Aleutian Arc generates faulting and deformation that drive tectonically induced fluid flow (Wallmann et al., 1997). The cold seep was first documented during R/V SONNE cruises SO97 and SO110, which identified widespread CH_4 venting along the margin, including concentrated discharge at fault-controlled fluid escape sites within the Shumagin sector (Suess et al., 1998; Wallmann et al., 1997). Specifically, elevated CH_4 concentrations in both bottom waters and surface layers were documented, providing evidence for CH_4 transfer into the water column and potential CH_4 oxidation (Suess et al., 1998; Wallmann et al., 1997). Regarding benthic communities, active CH_4 seepage was observed alongside dense chemosynthetic communities and the presence of authigenic carbonates (primarily composed of Mg-calcite and aragonite, $\delta^{13}C$ values between -42.7‰ and -50.8‰ PDB) was confirmed through sediment sampling (Greinert et al., 2002; Suess et al., 1998). Siboglinid frenulate worms (formerly known as pogonophorans), vestimentiferan tubeworms, and large aggregations of vesicomyid bivalves, exhibited tissue $\delta^{13}C$ values of –55.82‰ to –67.37‰, reliance on methanotrophy to support these communities (Suess et al., 1998).

2.1.3 Edge

The easternmost of the three seep sites, the Edge CH_4 seep system, is located along the eastern Aleutian subduction zone at depths near 5,000 meters and was first documented during R/V SONNE cruises SO97 and SO110 (Suess et al., 1998; Wallmann et al., 1997). Similar to the Shumagin seep, Edge is structurally controlled by faulting and deformation associated with the subduction of the Pacific Plate beneath the North American Plate, which facilitates CH_4-rich fluid migration through fault-controlled pathways (Suess et al., 1998; Wallmann et al., 1997). As at Shumagin, CH_4 concentrations were elevated in both bottom and surface waters (Suess et al., 1998). Dense vesicomyid clam and siboglinid worm colonies (159–200 m^{-2}) as well as authigenic carbonates sampled from sediments with negative $\delta^{13}C$ values indicative of deep-sourced fluids, have been documented at Edge (Suess et al., 1998; Wallmann et al., 1997).

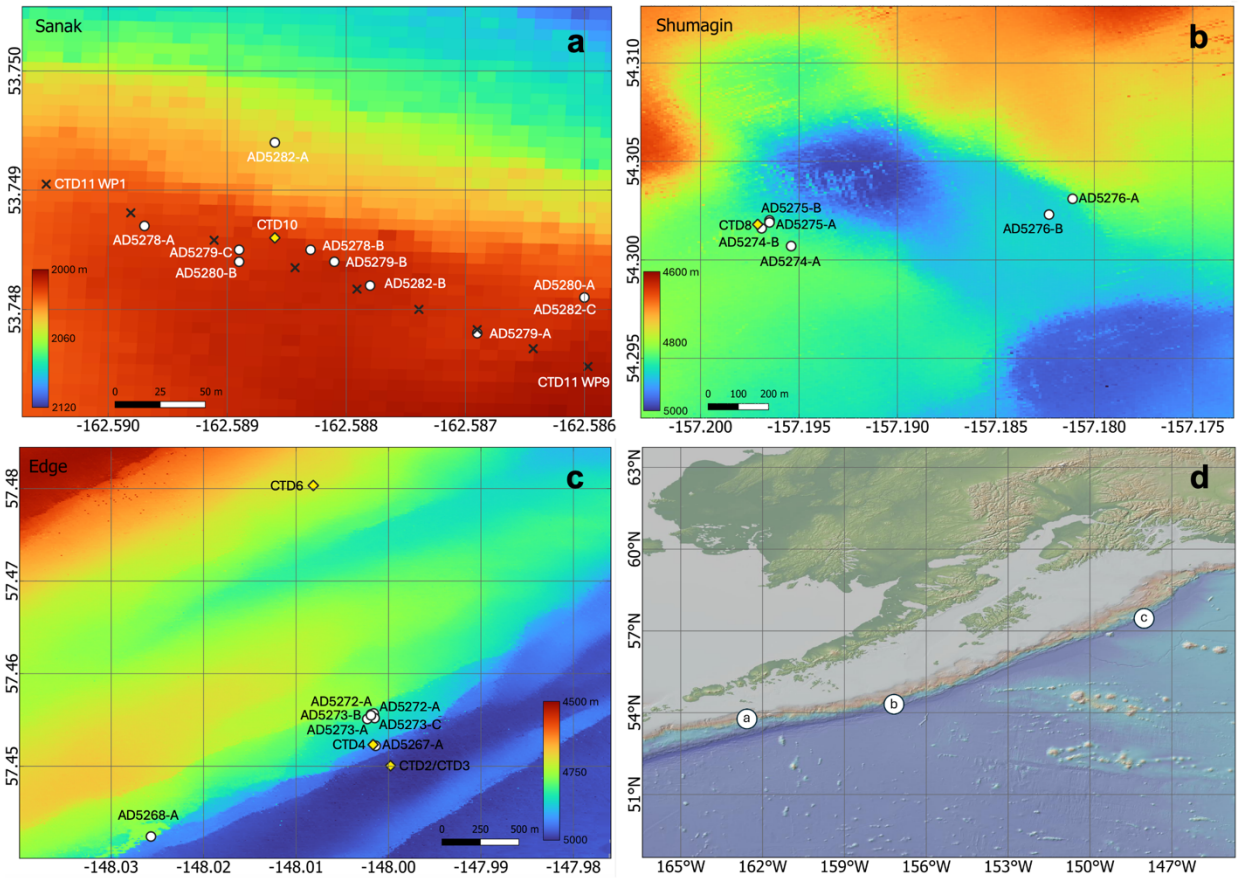

Figure 1. Bathymetric maps of (**a**) Sanak, (**b**) Shumagin, and (**c**) Edge CH_4 seeps with an overview of the site locations along the Aleutian Margin in panel (**d**). Sub-bottom profiling was performed using a Kongsberg EM124 multibeam (3.5 kHz) to document seafloor features. Nighttime survey data informed dive planning for the HOV *Alvin* and guided vertical and horizontal CTD cast deployments the following day. Sampling stations from R/V *Atlantis* include vertical CTD casts (yellow diamonds) and horizontal CTD cast waypoints (black 'X'). Labeled waypoints include WP1 and WP9, with WP2–WP8 ordered sequentially between. HOV *Alvin* dive locations are indicated by white circles.

2.2 Sample collection

Water column sampling and profiling was conducted over two weeks during the AT50-24 expedition (May 15th – June 7th) aboard the R/V *Atlantis* using the HOV *Alvin* and a CTD/Rosette system. Water samples were collected from surface to near-seafloor at all three CH_4 seep sites using Niskin-bottle rosettes (Ocean Test Equipment, Inc., Fort Lauderdale, FL): a 12 × 10 L configuration for Edge and Shumagin to accommodate the cable-tension limits at these depths, and a 23 × 10 L configuration for Sanak. A Seabird Scientific pumped CTD system was mounted on the rosette frames outfitted with Niskin bottles and sensors to continuously measure conductivity (SBE4), temperature (SBE3), pressure (SBE9), dissolved O_2 (SBE43), and light transmission (C-Star) and chlorophyll-a fluorescence (WET Labs ECO-AFL). Fluorescence data were only collected at Sanak, as rosette size constraints prevented installation of the fluorometer at the other sites. Salinity and density were calculated from conductivity and temperature, respectively, and depth was inferred from pressure. All sensors were calibrated prior to the expedition.

Vertical CTD casts were deployed above active seep sites and inactive off-seep locations selected based on available information, such as real-time EK80 acoustic backscatter data, multibeam seafloor mapping, and/or prior observations of seep-associated organisms and features from *Alvin* dives. At all three seep sites, vertical CTD/rosette casts were conducted to profile the water column above areas of active seepage. At Sanak, we additionally conducted a horizontal near-bottom CTD transect spanning active vent zones and off-seep background areas, with water collected at multiple waypoints along the direction of bottom current flow. To achieve this, the CTD/rosette was maintained approximately 5 meters above the seafloor and towed horizontally along the transect that extended from the background area, across the seep site, and back into the background area. During CTD/rosette casts, the ship followed a pre-defined set of coordinates using

dynamic positioning, a computer-controlled thruster system that uses satellite and/or acoustic transponder inputs to maintain or adjust the vessel's location. A CTD-mounted acoustic beacon was used to track the position of the CTD package relative to the ship, allowing real-time monitoring of its trajectory during movement between waypoints for the horizontal transect at Sanak. Niskin bottles were triggered after the rosette stabilized, following the ship's arrival at a new waypoint. To ensure representative sampling and minimize current-related offsets, the CTD was gently raised and lowered within a 5-meter vertical range at the target depth to flush the bottles.

Samples collected by *Alvin* were obtained via Niskin bottles mounted on the submersible's basket. Sample locations were chosen based on either previously known coordinates from literature (e.g., (Suess et al., 1998; Wallmann et al., 1997)) or *in situ* observations of gas bubble releases and chemosynthetic habitats during the dive. To prevent sediment contamination, Niskin bottles were triggered while the vehicle hovered approximately 0.5 m above the seafloor, just prior to contact and or following landing on the seafloor after the observed current removed resuspended sediment. For all sampling events, water from each Niskin bottle (CTD and Alvin) was subsampled in the following order: (1) CH_4 concentration, (2) CH_4 oxidation rate, and (3) DNA preservation. For an overview of water column samples, see **Table 1** with the horizontal CTD cast waypoint metadata outlined in **Suppl. Table 1.** All depths are reported as meters below sea level, with "surface waters" defined as 1–5 m depth and "bottom waters" as 5–10 m above the seafloor.

Table 1. Summary of *Alvin* dives and CTD casts at three CH_4 seep sites. Columns list the site name, *Alvin* Dive or CTD identifier, total water depth (m), latitude and longitude (decimal degrees), sampling date, sampling start time (*Alvin*: Niskin closure; CTD: cast or tow-yo start), and site characteristics (e.g., dominant seep fauna or gas releases for on-seep; off-seep locations lacked

typical seep features). Asterisks (*) indicate that the CTD11 transect recorded multiple coordinates and depths (see **Suppl. Table 1**).

Site	Dive/CTD No.	Total Water Depth (m)	Latitude (dec. deg.)	Longitude (dec. deg.)	Sampling Date (UTC)	Sampling Start Time (UTC)	Site Characteristic
Edge	CTD2	4974	57.4501	-147.9998	2024-05-17	05:12:00	on-seep, (Suess et al., 1998)
	AD5267-A	4908	57.4522	-148.0014	2024-05-17	21:40:00	off-seep, non-carbonate rock with zooanthids
	CTD3	4975	57.4501	-147.9998	2024-05-18	04:00:00	on-seep
	CTD4	4893	57.4523	-148.0017	2024-05-19	22:40:00	off-seep, over non-carbonate rock with zooanthids
	AD5268-A	4863	57.4424	-148.0257	2024-05-20	21:50:00	on-seep. frenulate bed
	CTD6	4724	57.4803	-148.0081	2024-05-23	04:50:00	off-seep, second ridge feature (Suess et al., 1998)
	AD5272-A	4815	57.4556	-148.0019	2024-05-24	23:47:00	on-seep, frenulates
	AD5272-B	4817	57.4557	-148.0016	2024-05-25	00:43:00	on-seep, clam bed
	AD5273-A	4813	57.4551	-148.0023	2024-05-25	19:09:00	on-seep, Suess et al., 1998)
	AD5273-B	4812	57.4555	-148.0019	2024-05-25	20:34:00	on-seep, clam bed
	AD5273-C	4820	57.4552	-148.0015	2024-05-25	21:41:00	off-seep, inactive
Shumagin	AD5274-A	4820	54.3007	-157.1954	2024-05-27	20:17:00	on-seep, clam bed, frenulate bed
	AD5274-B	4838	54.3016	-157.1969	2024-05-27	22:47:00	on-seep, clam bed on a hillside
	AD5275-A	4859	54.3019	-157.1965	2024-05-28	21:52:00	on-seep, frenulate bed
	AD5275-B	4865	54.3020	-157.1965	2024-05-28	22:45:00	on-seep, clam bed
	CTD8	4827	54.3018	-157.1971	2024-05-29	04:50:00	on-seep, clam bed
	AD5276-A	4854	54.3031	-157.1811	2024-05-29	20:59:00	on-seep, clam bed
	AD5276-B	4874	54.3023	-157.1823	2024-05-29	10:06:00	off-seep
Sanak	AD5277-A	2014	53.7485	-162.5889	2024-05-30	19:35:00	on-seep, carbonates, tubeworms
	AD5278-A	2019	53.7487	-162.5897	2024-05-31	19:12:00	on-seep, carbonates
	AD5278-B	2018	53.7485	-162.5883	2024-05-31	20:23:00	on-seep, carbonates
	AD5279-A	2017	53.7478	-162.5869	2024-06-01	18:31:00	on-seep, gas hydrate, orange sulfur bacteria mat, tubeworms
	AD5279-B	2014	53.7484	-162.5881	2024-06-01	19:37:00	on-seep, carbonates, tubeworms, *Hymedesmia*
	AD5279-C	2014	53.7484	-162.5889	2024-06-01	21:36:00	on-seep, orange sulfur bacteria mat, tubeworms, clam bed
	CTD10	2017	53.7486	-162.5886	2024-06-02	02:20:00	on-seep, gas hydrate, carbonates, tube worms, white bacterial mat, CH_4 plume
	AD5280-A	2020	53.7481	-162.5860	2024-06-02	18:11:00	large carbonate mound
	AD5280-B	2015	53.7484	-162.5889	2024-06-02	22:26:00	on-seep, gas hydrate, tubeworms
	CTD11	2007*	*	*	2024-06-03	04:18:00	tow-yo across Sanak seep including non-seep peripheries
	AD5282-A	2046	53.7494	-162.5886	2024-06-05	18:55:00	on-seep, clam bed
	AD5282-B	2010	53.7482	-162.5878	2024-06-05	20:23:00	on-seep, orange sulfur bacteria mat
	AD5282-C	2017	53.7481	-162.586	2024-06-05	21:55:00	on-seep, carbonates

2.3 CH_4 Concentration

Water column CH_4 samples were collected in 125 mL glass vials sealed with grey stoppers and crimp caps, filling each vial three times to eliminate bubbles before final sealing. Vials for CH_4 determination were injected with 7.5 mL of 50% NaOH and a 2.5 mL air headspace while a total volume of 10 ml water sample was removed. The amount of CH_4 in the headspace was subsequently analyzed via gas chromatography. Specifically, a Shimadzu Gas Chromatograph (GC-2014) was used, equipped with a Haysep-D packed column and a flame ionization detector. The column temperature was set to 80 °C, and helium served as the carrier gas at a flow rate of 12 mL per minute. CH_4 concentrations were calibrated using CH_4 standards (Scotty Analyzed Gases), with a precision of ±5%. Water column CH_4 concentrations were calculated using Henry's law and the Bunsen solubility coefficient (Yamamoto et al., 1976) to account for CH_4 in both the gas and liquid phase of the preserved samples.

2.4 Radiotracer incubations for the determinations of microbial CH_4 oxidation

Water column CH_4 oxidation samples were collected in 30 mL glass vials sealed with non-toxic chlorobutyl stoppers (blue Bellco stoppers, 20 mm, (Niemann et al., 2015)) filling each vial three times to eliminate bubbles before final sealing. CH_4 oxidation rates were determined onboard through *ex situ* incubations with tritium-labelled CH_4 (^3H-CH_4) applying established methods (Bussmann et al., 2015; Steinle et al., 2015). Samples (triplicates) were incubated between 36 and 105 hours (the exact duration for each sample set was determined by workflow constraints) with 10 µL gaseous ^3H-CH_4 (~2 kBq, specific activity 20 Ci/mmol, American Radiolabeled Chemicals, USA). Control samples were injected with 100 µL of 25% H_2SO_4 prior to radiotracer injection to stop microbial activity. To determine the total radioactivity of the sample, the crimped vials were

opened, and a 2 mL subsample was pipetted into a 6 mL scintillation vial and filled with 3 mL of Ultima Gold LLT scintillation cocktail from Perkin Elmer. For the determination of ^{3}H-CH_4 that was metabolized to ^{3}H-H_2O, 2 mL from the incubation was subsampled into an additional 6 mL scintillation vial and bubbled with air for 5 minutes to remove ^{3}H-CH_4 prior to the addition of the scintillation cocktail. Both subsamples were mixed by gentle inversion and counted onboard in a PerkinElmer Tri-Carb liquid scintillation counter. The *in-situ* temperatures of the samples ranged from 1.5 to 6°C. Due to the availability of only a single incubator, all samples were incubated at 5 °C in the dark. To correct for abiotic tracer turnover, the reported rate values are at least the mean tracer turnover in the killed controls plus one standard deviation of the killed-control value. Assuming first-order kinetics, the rate constant (k) was determined using the following equation:

$$k = \frac{^{3}H - H_2O}{[(^{3}H - H_2O \; + \; ^{3}H - CH_4) \; \cdot \; t]}$$

In this equation, ^{3}H-H_2O refers to the amount of tritiated water produced (in counts per minute, cpm), ^{3}H-CH_4 represents the remaining unoxidized tritiated CH_4 (cpm), and t is the incubation duration in days. CH_4 turnover time was calculated as the inverse of the fractional turnover rate ($1/k$), equivalent to the CH_4 concentration divided by the oxidation rate (r_{ox}) ($[CH_4]/r_{ox}$), under the assumption of prolonged water mass residence with limited mixing (Heintz et al., 2012).

CH_4 oxidation rates (r_{ox}) were calculated again assuming first-order kinetics, using the fractional turnover rate multiplied by the CH_4 concentration (nM). Rates were determined with the following equation:

$$r_{ox} = k \cdot [CH_4]$$

2.5 DNA Extraction

Seawater was collected into pre-rinsed 1.5 L polycarbonate bottles and stored at 6 °C until filtration. Microbial biomass was collected by filtering the samples using a peristaltic pump through 0.22 µm Sterivex filters (Millipore, Cat. No. SVGP0150). Filters were immediately frozen after filtration for downstream molecular analyses. Genomic DNA was extracted from Sterivex filters using a modified phenol–chloroform procedure followed by purification on Zymo silica spin columns (part C1006). Briefly, each filter was sealed, and 1.8 mL of filter-sterilized lysis buffer (containing 50 mM EDTA, 50 mM Tris–Cl [pH 8], 0.75 M sucrose, and 0.01% Tween 20) was injected into the cartridge. Lysozyme (40 µL; 50 mg mL^{-1}) was then added, and the filter was incubated at 37 °C for 45 min under rotation. 50µL of Proteinase K (800 U mL^{-1}) and 150 µL of 20% SDS were added to achieve a final SDS concentration of ~1%, followed by incubation at 55°C for 2 hr. The lysate was transferred to a polypropylene tube, and total nucleic acids were extracted via successive phenol–chloroform–isoamyl alcohol (25:24:1) extractions at 65°C, with centrifugation steps (10 min at 16,000 × g) to separate the aqueous and organic phases. Residual phenol was removed through an additional chloroform–isoamyl alcohol wash, and DNA was precipitated with 0.4 vol of 5 M NaCl and 0.8 vol of isopropanol. The precipitated DNA was bound to Zymo Spin-Away columns by repeated loading at 6,000 × g for 1 min, washed with 70% ethanol, and eluted in nuclease-free water or 10 mM Tris. Final DNA extracts were stored at −80 °C until further analysis.

2.6 PCR and Illumina MiSeq sequencing of the 16s rRNA gene

The V4-V5 region of the 16S rRNA gene was amplified using 515F and 926R (Parada, 2016) archaeal/bacterial primers with Illumina adapters (515F 5'-TCGTCGGCAGCGTCAGATGTGTATAAGAGACAG-GTGYCAGCMGCCGCGGTAA-3'; 926R 5'-GTCTCGTGGGCTCGGAGATGTGTATAAGAGACAG-CCGYCAATTYMTTTRAGTTT-3'). PCR reactions were completed with Q5 Hot Start High-Fidelity 2x Master Mix (New England Biolabs, USA) in 15 μL reaction volumes according to manufacturer's directions with the following cycle parameters: 2 min at 98C followed by 31 cycles of 98°C for 10s, 54°C for 20s, 72°C for 20s, with an extra final elongation step of 72°C for 2 min. PCR samples were pooled and barcoded with Illumina Nextera XT index 2 primers that include unique 8-bp barcodes (P5 5'-AATGATACGGCGACCACCGAGATCTACAC-XXXXXXXX-TCGTCGGCAGCGTC-3'; P7 5'-CAAGCAGAAGACGGCATACGAGAT-XXXXXXXX-GTCTCGTGGGCTCGG-3') using Q5 Hot Start with 3 μL pooled PCR product added to a 30 μL reaction volume, annealed at 66°C, and cycled 11 times. Products were run on 1.5% agarose gel and quantified by band intensity. Barcoded PCR products were combined in equimolar amounts and 300uL of this combined sample was run on 1.5% low melt agarose gel and purified with Promega's Wizard SV Gel and PCR Clean-up System, Promega#A9281. Sample was sequenced by Laragen (Culver City, CA, USA) using MiSeq Reagent Kit v3 (600-cycle) #MS-102-3003 on Illumina's MiSeq platform with the addition of 15-20% PhiX.

2.7 Sequence processing and taxonomic analysis

The Illumina-sequenced paired-end fastq files were processed using DADA2 for amplicon sequence variant (ASV) calling (Callahan et al., 2016) based on developer recommendations and

Cutadapt v3.4 for sequence quality trimming and primer removal (Martin, 2011). Reads that did not assemble in the overlapping region or that failed to meet the q-score threshold of 30 were removed from subsequent analyses. See supplements for additional information on read retention and all parameters used during DADA2. Taxonomy was assigned to 16S rRNA sequences via alignment to SILVA Train Set v138.2 amended with plastid sequences annotated with host taxonomy (Eitel et al., 2024). Raw reads were deposited in the NCBI's Sequence Read Archive (SRA).

2.8 Quantitative PCR

For the qPCR assays, each 10 µL reaction consisted of 5 µL Phusion SYBR® Green PCR Master Mix (BioRad), 0.5 µL (0.5 µM) each primer, 3.5 µL PCR-grade H_2O and 0.5 µL of DNA (concentration pre-determined through Qubit™ dsDNA Quantification, High Sensitivity Assay Kit). Duplicate bacterial pmoA assays were run using water column specific primers wcpmoA189f and wcpmoA661r (Tavormina et al., 2008) and the following cycling parameters: 98◦C for 2 min followed by 40 cycles of 98◦C for 10s, 52◦C for 20s, 72◦C for 30s, detection, then a melt curve from 65◦C to 95◦C in 0.5C increments, plate reading every 5s. Standard curves were constructed with 10-fold dilutions of PCR products from 0 (negative control) to 10^6 gene copies total DNA from extracted *Methylomonas* sp. LW13 cells.

3. Results

3.1. Physical and Biogeochemical Properties of the Water Column

All sites exhibited similar vertical trends in temperature, salinity, and density over overlapping depth ranges (**Fig. 2a–d, Fig. 3a**). Density profiles generally increased linearly with depth, driven primarily by hydrostatic pressure, with minor surface variations influenced by salinity. Temperature showed moderate decreases typical of subpolar regions, declining approximately from ~6 °C at the surface to ~1.5–1.9 °C at depth. Salinity increased slightly from around 32 to about 34.6–34.7 PSU. These patterns reflect the presence of similar water masses across the sites, with cold, saline, and dense bottom water underlying slightly fresher, warmer surface layers, consistent with subpolar North Pacific conditions.

Beam transmission profiles (**Fig. 2e–h**, **Fig. 3b**) showed moderate attenuation near the surface and slight declines close to the seafloor, likely reflecting the influence of surface particle production and benthic nepheloid layers, respectively. Transmission remained high through most of the water column at Edge and Shumagin, with only minor near-bottom decreases. In contrast, Sanak (CTD10) exhibited a more pronounced drop in beam transmission near the seafloor, consistent with elevated particle concentrations likely associated with a phytodetritus snowstorm observed during *Alvin* dives at that site (described below). Fluorescence was elevated both in surface waters, peaking at 10.87 μg L^{-1} at 14 m depth likely reflecting an ongoing phytoplankton bloom, and near the bottom, where a slight increase in fluorescence coincided with the low-transmission layer, suggesting the presence of organic material.

Dissolved O_2 profiles (**Fig. 2g–i**, **Fig. 3c**) were broadly similar across all sites, displaying a characteristic subpolar structure with high concentrations near the surface (~314–340 μM), a

midwater oxygen minimum zone (OMZ) around 650–860 m (lowest values ~14–17 μM), and concentrations increasing again beneath the OMZ.

In contrast, CH_4 distributions exhibited strong site-specific variability. At Edge On-Seep (CTD2/3), CH_4 concentrations displayed three distinct peaks: in surface waters (30 nM at ~10 m), at mid-depth (44 nM ~2000 m; near the base of the OMZ), and close to the seafloor (associated with active seepage). This layered structure suggests multiple CH_4 sources, including surface water CH_4 cycling, *in situ* water column production or accumulation at mid-depth, and sediment-derived seepage at the seafloor. CH_4 at Edge Off-Seep (CTD4) also peaked near the bottom (47 nM at 4883 m), while a similar profile at the Off-Seep (CTD6) (second ridge (Suess et al., 1998)) showed 43 nM at 4693 m. At Shumagin (CTD8), concentrations were elevated at both surface (23 nM at 4 m) and bottom (59 nM at 4800 m), though sparse midwater data limit further resolution. Sanak (CTD10) displayed the highest CH_4 concentration within 100 m of the seafloor across all profiles, with a pronounced near-bottom maximum of 322 nM at 1991 m, consistent with intense CH_4 seepage and vertical dispersal.

Vertical profiles of CH_4 oxidation (**Fig. 2j–l, Fig. 3d**) revealed detectable activity at all stations, with depth distributions varying by site. Oxidation was present in surface and near-surface waters (≤50 m) across multiple casts, with rates on the order of 10^{-3} to 10^{-2} nmol L^{-1} d^{-1}, indicating active turnover even in low-CH_4 environments. At Edge On-Seep (CTD2/3), oxidation was not detected at 11 m (8.6 nM CH_4), but activity was evident at 50 m. The highest average oxidation rate occurred at 2000 m (44 nM CH_4), where it reached 2.9 $\times 10^{-2}$ nmol L^{-1} d^{-1} which was positioned near the base of the OMZ. No activity was detected between 3000 and 4000 m, but oxidation resumed near the seafloor. At Edge Off-Seep (CTD4), oxidation rates ranged from 3.5×10^{-3} nmol L^{-1} d^{-1} at ~20 m (22 nM CH_4) to a peak of 3.09×10^{-2} nmol L^{-1} d^{-1} at 4883 m (47 nM

CH_4), ~10 m above the bottom. The ridge site (CTD6) exhibited similar structure, with rates between 2.1×10^{-3} nmol L^{-1} d^{-1} at 101 m (7.2 nM CH_4) and a maximum of 1.1×10^{-2} nmol L^{-1} d^{-1} at 4693 m (43 nM CH_4). At Shumagin (CTD8), oxidation was up to 1.0×10^{-2} nmol L^{-1} d^{-1} at 20.8 m (49 nM CH_4), increasing to 1.1×10^{-1} nmol L^{-1} d^{-1} at 4501 m (50 nM CH_4) which was ~320 m above the seafloor. Sanak (CTD10) exhibited the highest oxidation rate observed across all sites, 2.46×10^{-1} nmol L^{-1} d^{-1} at 1991 m (322 nM CH_4), coinciding with the deep CH_4 maximum. Replicate variability differed by site, with noticeable spread near peak depths at CTD2/3 and CTD8. Oxidation maxima frequently occurred within 10–30 m of the seafloor, suggesting localized stimulation by near-bottom CH_4 availability, although this pattern was not observed at all stations.

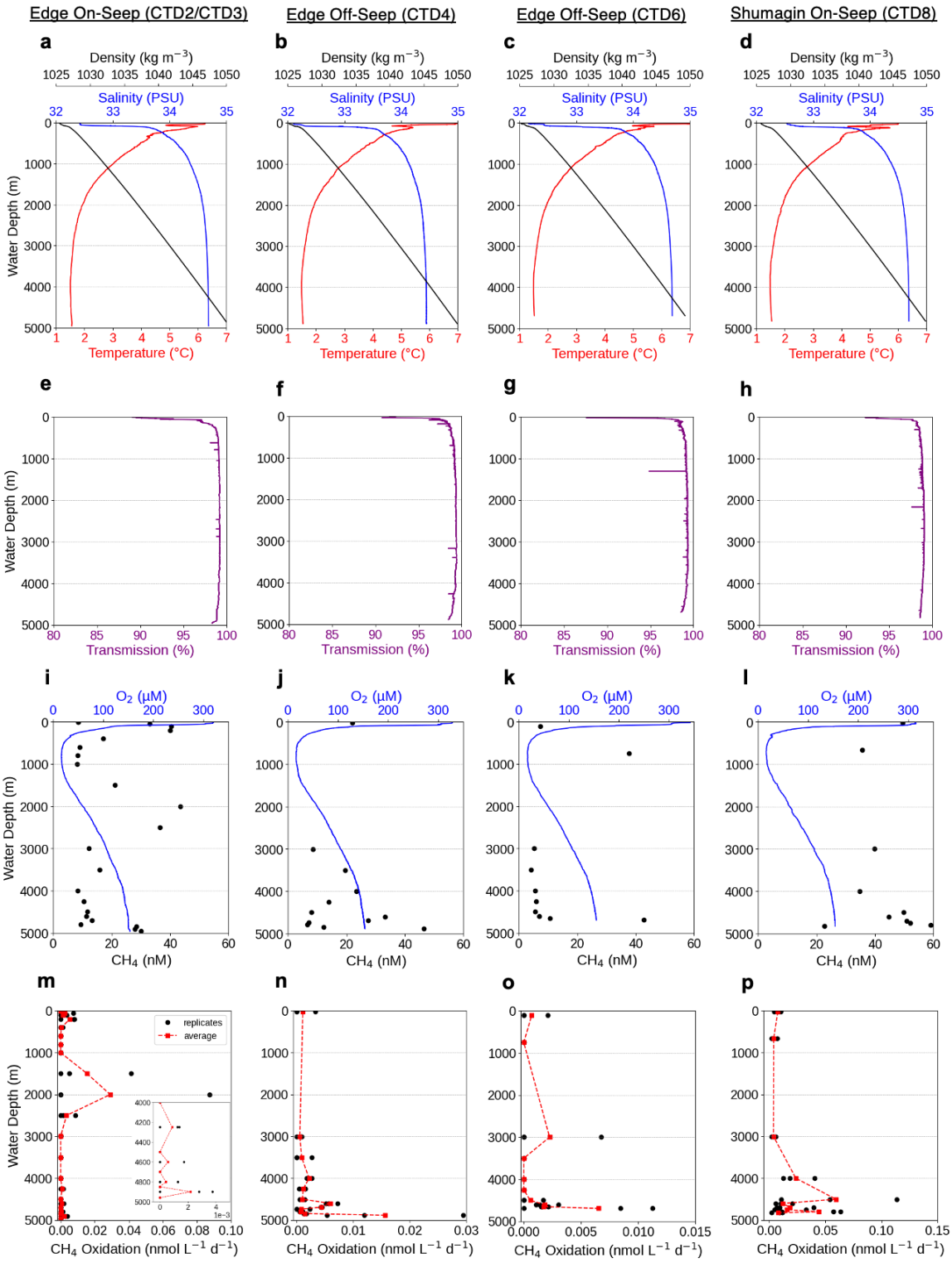

Figure 2. Hydrographic and biogeochemical profiles at the Edge (left three columns) and Shumagin (rightmost column) seep sites in the Gulf of Alaska. Panels (**a–d**) show profiles of density (black,

top x-axis), salinity (blue, middle x-axis), and temperature (red, bottom x-axis); (**e–h**) show beam transmission (purple, bottom x-axis); (**i–l**) show dissolved CH4 concentrations (black circles, bottom x-axis) and dissolved O_2 concentrations (blue line, top x-axis); and (**m–p**) show CH4 oxidation rates (black circles) and average CH4 oxidation rates (red squares connected by dashed lines). Panel m includes a zoomed inset of near-seafloor values. CTD casts 2 and 3 were conducted at the same geographic location over the Edge seep site (seafloor at 4974 m); CTD4 (seafloor at 4893 m) was located at the AD5267 site; CTD6 (seafloor at 4724 m) was positioned over the second ridge feature; and CTD8 (seafloor at 4827 m) sampled the Shumagin seep site. See **Table 1** for station metadata.

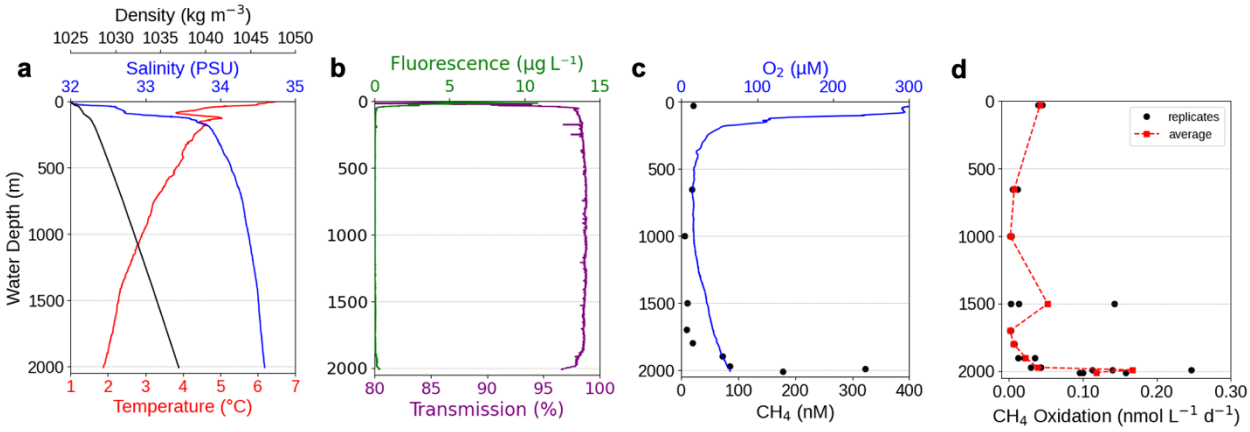

Figure 3. Hydrographic and biogeochemical profiles at the Sanak seep site (CTD10; seafloor at 2017 m). (**a**) Density (black, top x-axis), salinity (blue, middle x-axis), and temperature (red, bottom x-axis). (**b**) Beam transmission (purple, bottom x-axis) and fluorescence (green, top axis). (**c**) Dissolved CH_4 concentrations (black circles, bottom x-axis) and dissolved O_2 concentrations (blue line, top x-axis). (**d**) CH_4 oxidation rates (black circles) and average CH_4 oxidation rates (red squares connected by dashed lines), with a zoomed inset highlighting near-seafloor values. See **Table 1** for station metadata.

At the Sanak seep site, CH_4 oxidation rates and CH_4 concentrations were determined across a ~325 m horizontal transect during CTD11 (**Fig. 4**), with Niskin bottles above the seafloor at depths between 1,999 and 2,019 m. Dissolved O_2 concentrations remained consistent across all waypoints, ranging from 62 to 64 μM (data not shown). A directional bottom current from WP1 towards WP9 was noted during sampling, which may have influenced the distribution of both CH_4 and microbial oxidation. WP1 (off-seep) and WP2 (seep periphery) showed relatively modest CH_4 concentrations of 36 and 31 nM, and CH_4 oxidation activity (3.1×10^{-3} to 1.3×10^{-2} nmol L^{-1} d^{-1}) respectively. WP3 through WP7 represented the central portion of the transect and showed moderate CH_4 concentrations (35–99 nM) and oxidation rates ranging from 3.6×10^{-3} to 8.5×10^{-2} nmol L^{-1} d^{-1}. The presence of gas hydrates at WP3 and WP5, combined with elevated CH_4 and active oxidation, suggests (in addition to high-density seep associated fauna including tubeworms) ongoing seepage in this region. WP9 (off-seep) displayed the highest CH_4 concentration (181 nM) and CH_4 oxidation (1.39 nmol L^{-1} d^{-1}). CH_4 generally increased from WP1 towards WP 9 in the direction of an observed bottom current. Overall, CH_4 oxidation rates remained moderate along the transect, with an increase near the distal end of the track (WP9).

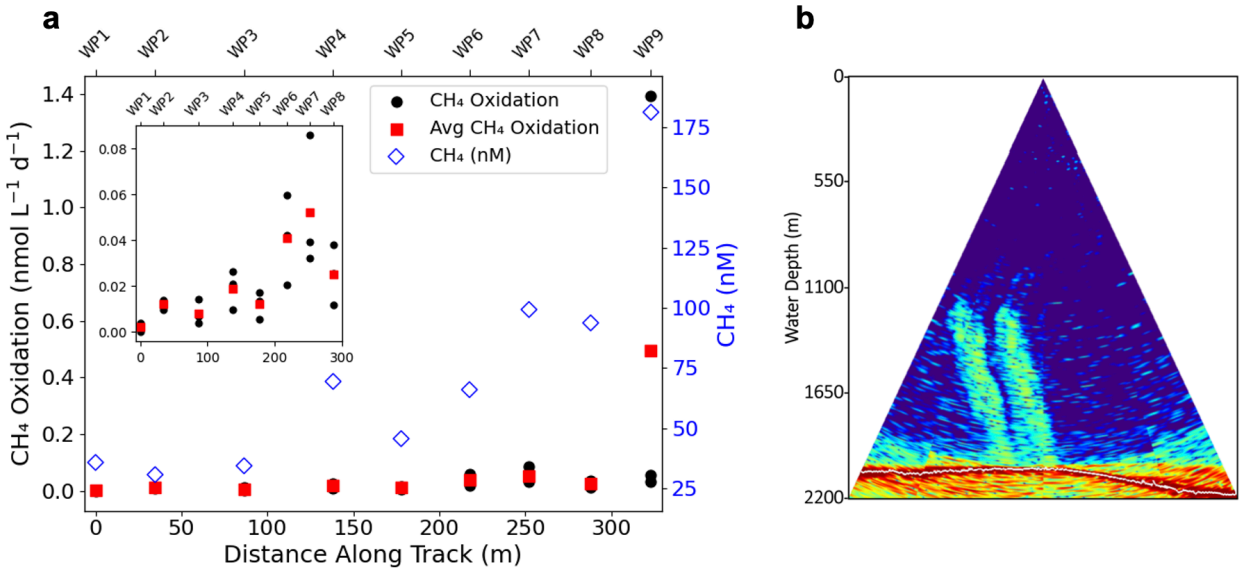

Figure 4. (**a**) Near seafloor (5 m above) lateral transect of CH_4 concentration and CH4 oxidation across the Sanak seep area (53.7491° N, 162.5891° W to 53.7476° N, 162.5859° W), spanning off-seep (WP1, WP9), periphery (WP2, WP8), and on-seep (WP3–WP7) locations. CH_4 oxidation rates are shown as black circles (individual replicates) and red squares (averages) on the left y-axis, while dissolved CH_4 concentrations (blue diamonds) are plotted on the right y-axis. All data were collected from CTD11. Inset is a close-up of CH_4 oxidation (black circles) and average CH_4 oxidation (red squares) through WP8. (**b**) Corresponding EM124 multibeam image of the same transect, showing gas plumes rising from the seafloor, consistent with gas hydrates observed with *Alvin* at WP3 and WP5. Data for (**a**) were collected from CTD11. Waypoint coordinates are provided in **Suppl. Table 1**.

3.2 Methanotrophic activity in the near-seafloor water column

Water column samples near the seafloor (0.5 m above the bottom) were collected using the *Alvin* submersible. The ^3H-CH_4 *ex situ* incubations revealed a wide range of CH_4 oxidation rates and concentrations across the three seep fields, indicating substantial spatial heterogeneity

(**Table 2**). At the Edge site (~4,812–4,908 m), seven stations displayed low CH_4 concentrations (5.4–53.0 nM) and oxidation rates ranging from 0 to 3.9×10^{-2} nmol L^{-1} d^{-1}. CH_4 oxidation was undetectable at AD5272-B, a clam bed site, while the highest occurred at AD5273-C (3.89×10^{-2} nmol L^{-1} d^{-1}), an inactive off-seep location with 51.0 nM CH_4. AD5272-A, located at a site with short frenulates, had the highest CH_4 concentration (53.0 nM) and an intermediate oxidation rate (2.12×10^{-2} nmol L^{-1} d^{-1}).

Shumagin Seep (~4,820–4,874 m) displayed intermediate CH_4 concentrations (11.0–70.0 nM) and oxidation rates ranging from 8.25×10^{-4} to 2.31×10^{-2} nmol L^{-1} d^{-1}. The highest oxidation was recorded at AD5276-B (2.31×10^{-2} nmol L^{-1} d^{-1}), an off-seep site, while the lowest occurred at AD5274-A (8.25×10^{-4} nmol L^{-1} d^{-1}), located at Suess Seep among clams and frenulates. CH_4 concentrations were generally low, consistent with background water column conditions or weak, spatially dispersed fluid flow not visibly associated with active seep features. In contrast, Sanak Seep (~2,010–2,046 m) exhibited both elevated CH_4 concentrations (78–2.2 x 10^4 nM) and oxidation rates (8.6 x 10^{-2} – 242 nmol L^{-1} d^{-1}) across eleven stations. The highest CH_4 concentration and oxidation rate were both recorded at AD5279-A (2.2 x 10^4 nM CH_4, 242 nmol L^{-1} d^{-1}), a gas hydrate site, which was significantly higher than what was captured from the CTD11 tow-yo at WP3 and WP5. Other stations with high CH_4 concentrations (e.g., AD5282-B at 1.7 x 10^3 nM) showed oxidation rates ranging from 0.123 to 12.0 nmol L^{-1} d^{-1}, indicating that substantial methanotrophic activity co-occurred with visible seep structures including bacterial mats, carbonate outcrops, and gas hydrates.

Table 2. Summary of *Alvin* sampling stations for Edge, Shumagin, and Sanak including the average CH_4 oxidation rates, corresponding CH_4 concentrations and environmental features.

Location	Niskin ID	CH_4 (nM)	Avg CH_4 Oxidation (nmol L^{-1} d^{-1})	Standard Deviation (± nmol L^{-1} d^{-1})	Site Characteristic
Edge	AD5267-A	6.7	1.6×10^{-3}	2.37×10^{-4}	off-seep, non-carbonate rock with zooanthids
	AD5268-A	5.4	3.5×10^{-3}	3.04×10^{-3}	on-seep, frenulate bed
	AD5272-A	53	2.1×10^{-2}	2.33×10^{-3}	on-seep, frenulates
	AD5272-B	34	0	0.00	on-seep, clam bed
	AD5273-A	25	9.2×10^{-3}	3.02×10^{-3}	on-seep, (Suess et al., 1998)
	AD5273-B	36	1.7×10^{-2}	1.48×10^{-2}	on-seep, clam bed
	AD5273-C	51	3.9×10^{-2}	6.74×10^{-2}	off-seep, inactive
Shumagin	AD5274-A	41	8.2×10^{-4}	1.43×10^{-3}	on-seep, clam bed, frenulate bed
	AD5274-B	15	2.5×10^{-3}	2.60×10^{-4}	on-seep, clam bed on a hillside
	AD5275-A	18	1.7×10^{-3}	2.92×10^{-4}	on-seep, frenulate bed
	AD5275-B	70	5.5×10^{-3}	9.98×10^{-4}	on-seep, clam bed
	AD5276-A	11	5.2×10^{-3}	1.57×10^{-3}	on-seep, clam bed
	AD5276-B	16	2.3×10^{-2}	7.83×10^{-3}	off-seep
Sanak	AD5277-A	705	0.12	4.01×10^{-2}	on-seep, carbonates, tubeworms
	AD5278-A	542	1.9	2.3×10^{-1}	on-seep, carbonates
	AD5278-B	78	8.6×10^{-2}	8.6×10^{-2}	on-seep, carbonates
	AD5279-A	2.2×10^{4}	242	2.24×10^{0}	on-seep, gas hydrate, carbonates, tube worms
	AD5279-B	3.5×10^{3}	12	3.24×10^{0}	on-seep, carbonates, tubeworms, Hymedesmia
	AD5279-C	593	1.4	2.50×10^{-1}	on-seep, orange sulfur bacteria mat, tubeworms, clam bed
	AD5280-A	735	1.4	1.89×10^{-1}	large carbonate mound
	AD5280-B	703	0.51	1.80×10^{-1}	on-seep, gas hydrate, tubeworms
	AD5282-A	111	0.12	8.86×10^{-2}	on-seep, clam bed
	AD5282-B	1.7×10^{3}	1.7	1.07×10^{0}	on-seep, orange sulfur bacteria mat
	AD5282-C	2.0×10^{3}	1.2	3.73×10^{-1}	on-seep, carbonates

3.3 Rate constant and turnover times

CH_4 oxidation rate constants (k) and corresponding turnover times were calculated from a subset (samples that contained data for all tested parameters) of Niskin bottles collected during vertical CTD casts at Edge (CTD2/3), Shumagin (CTD8), and Sanak (CTD10), as well as paired *Alvin* Niskin samples. Results from selected depths are presented in **Table 3** The full dataset for each vertical CTD cast is listed in **Suppl. Table 2.** Across all three sites, CH_4 turnover times varied

with depth and location, ranging from 0.24 to 35.4 years. The shortest turnover times were generally observed near the seafloor, particularly at stations influenced by seepage, while slower turnover characterized intermediate depths. At Edge, turnover times ranged from 19.7 years in midwaters (200 m) to 35.4 years near the bottom (4901 m), with a shorter turnover time of 4.86 years observed in the *Alvin* bottle AD5267-A (4908 m) above inactive rock. At Shumagin, turnover times spanned 3.66 to 29.8 years, with the fastest values recorded at 4800 and 4000 m and the slowest in midwater at 3001 m. *Alvin* Niskin AD5274-B (4838 m), sampled above a clam bed, exhibited a turnover time of 9.39 years. At Sanak, CH_4 turnover times were among the shortest, ranging from 1.38 years near the surface (30 m) to 0.24 years at the seep-influenced *Alvin* station AD5279-A (2017 m) above a gas hydrate outcrop. Mid- and bottom water samples at Sanak displayed intermediate turnover values (5.20–8.46 years).

Table 3. Depth-dependent measurements of O_2, CH_4, CH_4 oxidation rate constants (*k*), and resulting turnover times for Edge, Shumagin, and Sanak.

Location	CTD/Niskin ID	Water depth (m)	O_2 (µM)	CH_4 (nM)	Temp (°C)	Rate constant (k)	Turnover Time (y)
Edge	2	11	320	8.6	6.23	0	N/A
Edge	3	200	73.4	73	4.85	$1.39x10^{-4}$	19.7
Edge	3	1000	17.4	17	3.01	0	N/A
Edge	2	4250	143	10	1.51	$8.50x10^{-5}$	32.2
Edge	2	4901	150	28	1.56	$7.73x10^{-5}$	35.4
Edge	AD5267-A	4908	151*	6.7	1.56*	$5.64x10^{-4}$	4.86
Shumagin	8	20	314	49	6.00	$1.55x10^{-4}$	17.7
Shumagin	8	660	16.4	36	3.51	$1.17x10^{-4}$	23.4
Shumagin	8	3001	112	40	1.59	$9.20x10^{-5}$	29.8
Shumagin	8	4000	144	35	1.48	$6.54x10^{-4}$	4.19
Shumagin	8	4800	154	59	1.53	$7.49x10^{-4}$	3.66
Shumagin	AD5274-B	4838	154*	15	1.53*	$2.92x10^{-4}$	9.39
Sanak	10	30	312	21	5.79	$1.98x10^{-3}$	1.38
Sanak	10	651	14.7	19	6.95	$4.03x10^{-3}$	6.80
Sanak	10	1001	16.6	5.4	2.00	$3.81x10^{-3}$	7.19
Sanak	10	1800	54.3	20	2.07	$3.24x10^{-3}$	8.46
Sanak	10	1991	63.2	63	1.89	$5.23x10^{-3}$	5.20
Sanak	AD5279-A	2017	64.4*	2.2×10^4	1.88*	$1.14 x10^{-2}$	0.241

*The O_2 concentration and temperature are estimated from the vertical CTD profile at the nearest corresponding depth and site (CTD2 Edge, CTD8 for Shumagin, and CTD10 for Sanak).

3.4 Microbial community composition in the water column

16S rRNA gene sequences were analyzed from water column samples collected above CH_4 seep sites, spanning the euphotic zone to near-bottom depths. Across the three Alaska seep sites, the dominant bacterial and archaeal taxa included Proteobacteria, Planctomycetota, Cyanobacteria, Crenarchaeota, and Bacteroidota. Microbial community composition was strongly structured by depth. In surface waters, Pirellulales (Planctomycetota), Flavobacteriales (Bacteroidota), and Synechococcales (Cyanobacteria) were the most abundant. At Edge Seep, Pirellulales accounted for ~23% of the community, followed by Flavobacteriales at ~20%, and Synechococcales at ~19%. Enterobacterales dominated the surface at Shumagin Seep with ~50% relative abundance, while Synechococcales and Pirellulales followed at ~15% and 8.7%, respectively. These patterns reflect the presence of phototrophic and heterotrophic taxa adapted to light-rich, nutrient-fluctuating surface environments.

In contrast, deep samples showed a marked shift toward archaeal and facultative anaerobic lineages. At Shumagin and Sanak seeps, Nitrosopumilales (Crenarchaeota), a group of ammonia-oxidizing archaea, dominated with relative abundances of ~33% and ~38%, respectively. Enterobacterales was also prominent in the deep, reaching ~15% at Shumagin and ~14% at Sanak. *Marine Group II* was not among the top three most abundant orders in these samples, suggesting variability in archaeal community structure across seeps. At Edge Seep, the deepest samples (4812–4908 m) were characterized by Enterobacterales (~19%), Pseudomonadales (~14%), and a lower but consistent abundance of Enterobacterales at 8.1%, suggesting taxonomic heterogeneity within this order.

The microbial community composition reflected strong vertical stratification, with phototrophic and bloom-associated taxa like Synechococcales and Flavobacteriales confined to the

surface, while nitrifiers (Nitrosopumilales) and facultative heterotrophs (Enterobacterales, Pseudomonadales) dominated deeper waters. These patterns underscore the influence of light availability, organic matter flux, and geochemical conditions in structuring microbial communities at Alaska cold seeps.

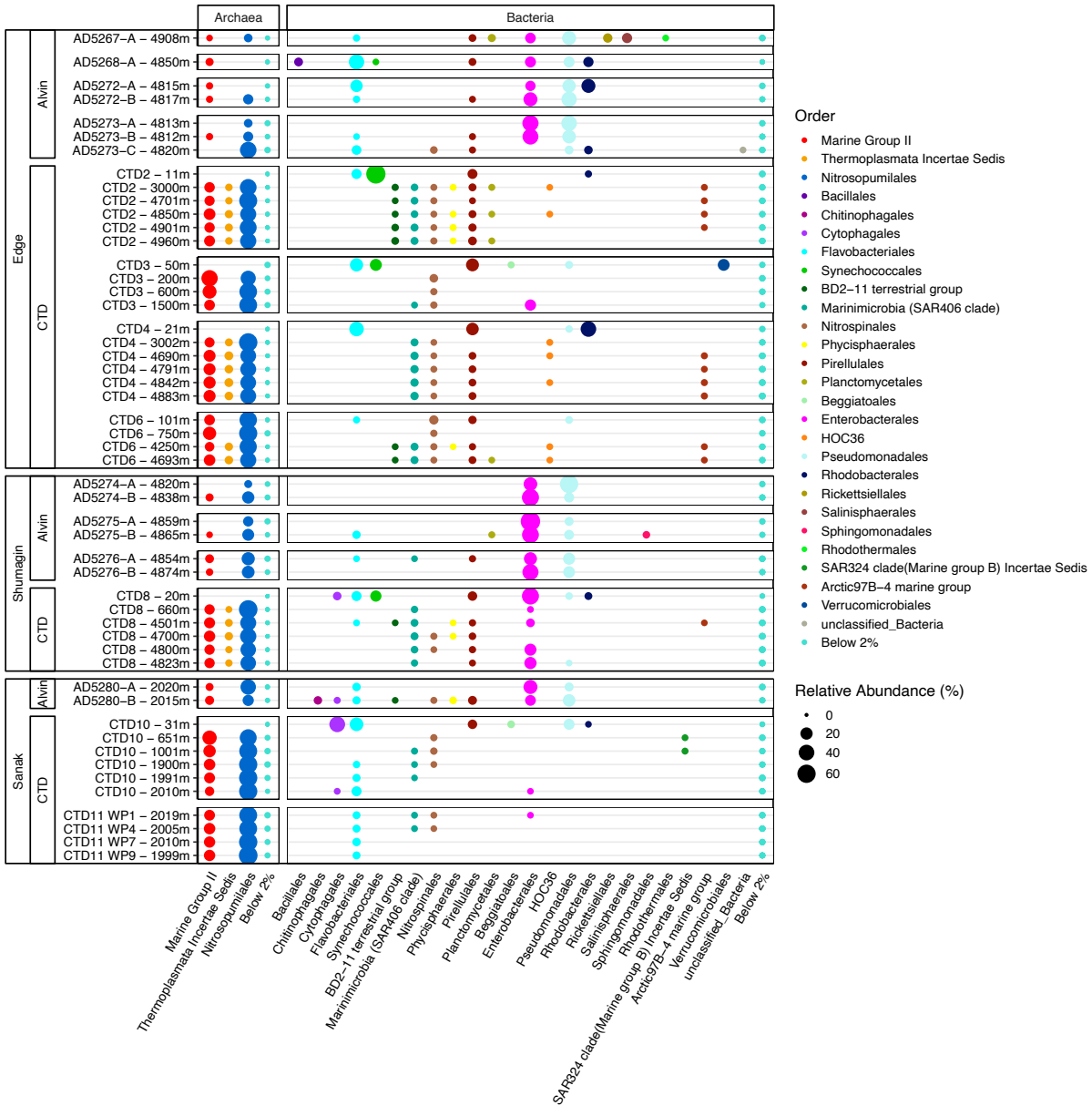

Figure 5. Microbial community composition from CTD and *Alvin* Niskin samples from Edge, Shumagin, and Sanak cold seeps. Dot size shows the relative abundance (%) of microbial orders

(columns, colors) in samples (rows). Samples are grouped by site (major grouping), collection strategy (CTD or *Alvin*, middle grouping), and deployment (minor groups). Only orders reaching at least 2% abundance in at least one sample are shown. Taxonomy follows SILVA conventions.

Taxonomic genera typically associated with aerobic CH_4 oxidation and methylotrophy were detected at low relative abundances (<0.3%) but were consistently present across multiple bottom water samples (**Fig. 6**). The most abundant methanotroph, IheB2-23 (Methylomonadaceae), reached its highest relative abundance in deep *Alvin* bottles at Shumagin (AD5274-A, 4820 m, 0.12%) and in the deep CTD10 cast at Sanak (1900 m, 0.10%). An additional aerobic methanotroph, Milano-WF1B-03, was largely restricted to the deepest CTD casts, including Shumagin CTD8 (4700 m) and Edge CTD4 (4791 m).

Along the Sanak CTD11 horizontal tow-yo transect, the relative abundances of IheB2-23 (0.03–0.06%) remained uniform over the ~325 m track, with no discernible enrichment near hydrate-associated sites (WP3 and WP5). Milano-WF1B-03 similarly maintained low, stable abundances (<0.05%) across all sequenced waypoints, indicating that proximity to gas hydrates did not drive elevated methanotroph concentrations. Despite their limited representation, reproducible trends emerged across Edge, Shumagin, and Sanak: IheB2-23 was the dominant deepwater methanotroph yet persisted at depth, Milano-WF1B-03 was primarily confined to the deepest horizons, and MOB were present in off-seep waters.

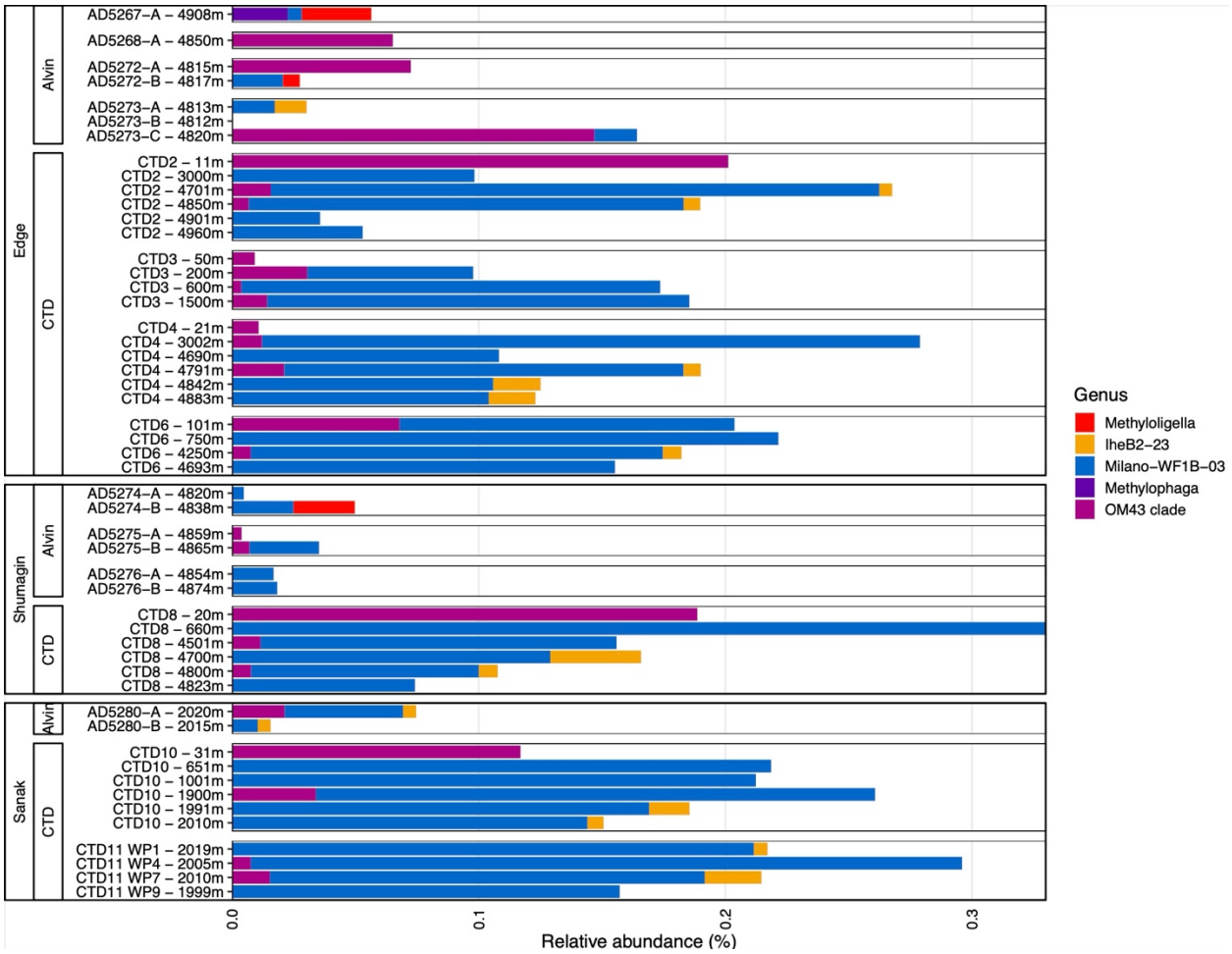

Figure 6. Relative abundance of select methanotrophic and methylotrophic genera. Relative abundance (x-axis, %) is shown as a stacked bar plot for genera (colored bars) for samples (y-axis) in which this collective of genera reached at least 0.01% abundance. Samples are grouped by site (major grouping), collection strategy (CTD or *Alvin*, middle grouping), and deployment (minor groups). In this figure, *Methyloligella* (Takeuchi et al., 2014), *Methylophaga* (Janvier et al., 1985), and the OM43 clade (Jimenez-Infante et al., 2016) represent methylotrophic lineages. *Methylophaga* and OM43 (family Methylophilaceae) are not known to oxidize CH_4. *Methyloligella* is also methylotrophic, though related genera like *Methyloceanibacter* may encode sMMO (Vekeman et al., 2016). IheB2–23 and Milano–WF1B–03 belong to Methylomonadaceae, a family of documented aerobic methanotrophs (Orata et al., 2018).

3.5 Quantitative PCR analysis

Vertical CTD casts and *Alvin* Niskin samples at Edge, Shumagin, and Sanak revealed distinct depth-related patterns in *pmoA* gene abundance, with higher values generally concentrated near the seafloor and lower abundances in surface waters (**Fig. 7**). At Edge, the highest *pmoA* gene abundance was observed at AD5273-A (4813 m), located at the TV Grab-66 site (Suess et al., 1998) near patchy clam beds, with 6.05 log copies L^{-1}. Other *Alvin* samples at this site displayed a range of values depending on habitat context. For example, AD5272-A (short frenulates) showed 3.00 log copies L^{-1} and at AD5268-A (frenulate bed) it was 3.03 log copies L^{-1}, while AD5272-B increased to 5.85 log copies L^{-1} (clam bed). The lowest abundance was detected in surface waters (CTD4 at 21 m) with just 0.37 log copies L^{-1}. Overall, *pmoA* abundance at Edge increased with depth, with higher values observed in samples over seep-associated habitats.

At Shumagin, gene abundances were similarly depth-structured but reached the highest overall values of the study. The peak abundance (6.86 log copies L^{-1}) occurred in AD5274-B (4838 m), collected over a clam bed on a hillside. Other *Alvin* samples associated with frenulates or clam beds (e.g., AD5275-B, 5.63 log copies L^{-1}; AD5274-A, 5.42 log copies L^{-1}) also displayed consistently high values. Inactive sites such as AD5276-B had slightly lower values than the peak abundance (5.60 log copies L^{-1}). In contrast, surface waters (CTD8 at 20 m) showed very low gene abundance (0.10 log copies L^{-1}), reinforcing the deep-water localization of MOB activity at this site. At Sanak, *pmoA* gene abundance peaked in AD5279-B (2014 m, 5.51 log copies L^{-1}), a site featuring an orange bacterial mat, tubeworms, and clams. Other moderate-abundance sites included AD5280-A (a large carbonate mound, 4.18 log copies L^{-1}) and AD5282-C (carbonates, 4.94 log copies L^{-1}). In contrast, *Alvin* bottles at gas hydrate sites (AD5279-A and AD5280-B) showed lower abundances (5.26 and 3.29 log copies L^{-1}, respectively). The lowest values were again observed in

surface waters, such as CTD10 at 31 m (1.86 log copies L^{-1}). These results suggest that while MOB abundance at Sanak is highest in association with bacterial mats and carbonate features, gas hydrate sites may not necessarily correspond with elevated *pmoA* gene abundance.

A horizontal CTD transect across Sanak (CTD11) revealed relatively stable *pmoA* gene abundance over a ~325 m across-seep distance, with no pronounced enrichment near known gas hydrate features. Gene abundance at WP1 (2019 m; off-seep) and WP9 (1999 m; off-seep) was 4.93 and 4.97 log copies L^{-1}, respectively, while intermediate waypoints WP4 (2005 m) and WP7 (2010 m) yielded 5.05 and 4.39 log copies L^{-1}. While WP3 and WP5 (not sampled for DNA) overlay visible gas hydrate outcrops, stations adjacent to them showed no evidence of elevated methanotroph gene abundance. Collectively, these data reveal a consistent pattern across all three seep fields: *pmoA* gene abundance increases with depth and is often highest in proximity to seep-associated fauna or microbial mats. However, not all chemosynthetic features correspond with elevated gene abundance, particularly in gas hydrate areas. The Sanak transect further suggests that methanotroph populations are depth-structured and relatively stable across short horizontal distances, with little spatial clustering near hydrate outcrops.

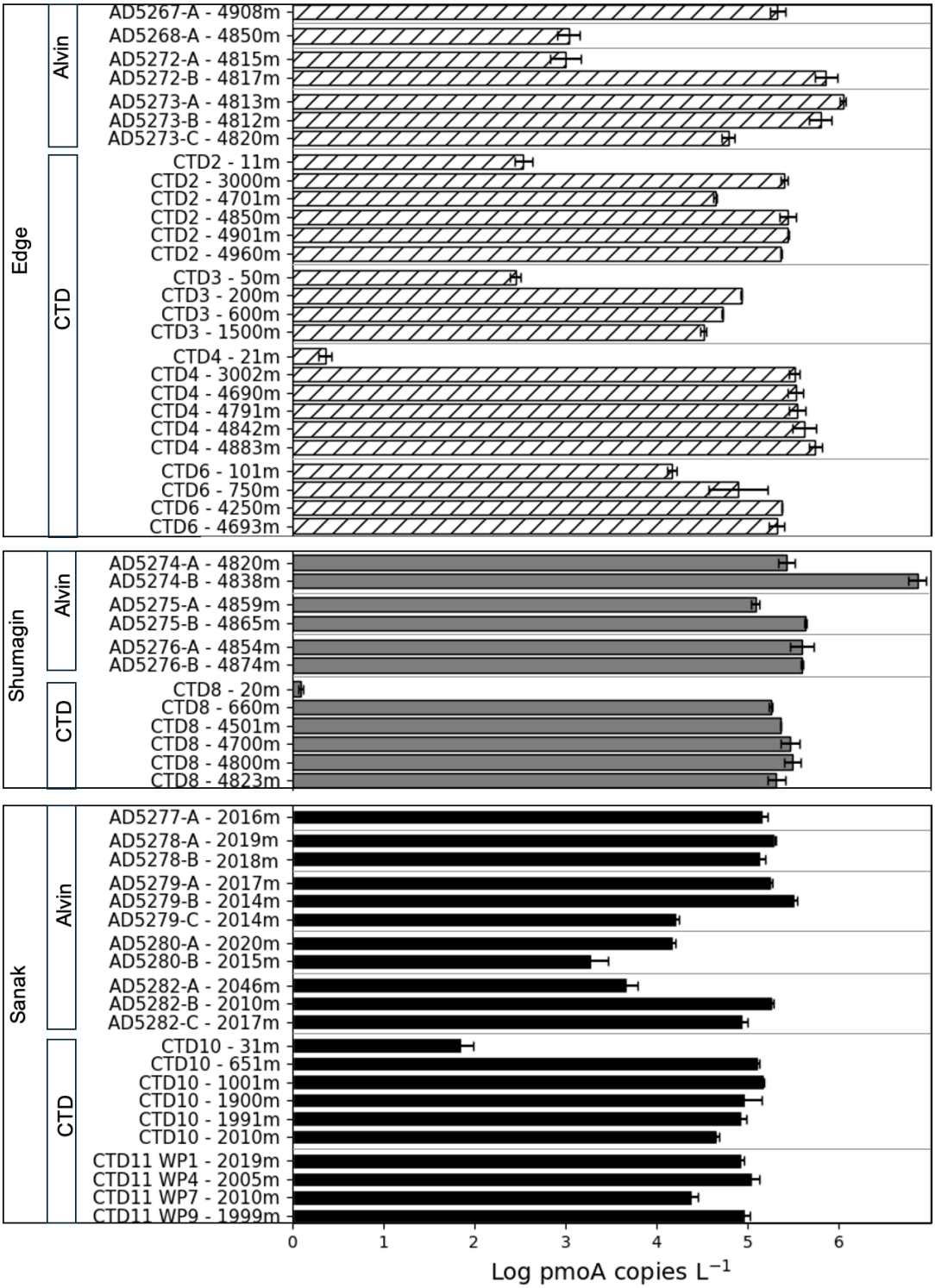

Figure 7. Log-transformed qPCR-derived abundances of the particulate methane monooxygenase gene (pmoA) in water samples collected at Edge (striped bars), Shumagin (gray bars), and Sanak (black bars). Each horizontal bar represents the $\log_{10}$ pmoA copy number per liter for a given sample

(labeled by depth, Waypoint (WP), or *Alvin* cast), illustrating the distribution of CH_4-oxidizing microbial populations across depths and seep sites in the Aleutian margin. Samples are grouped by site (major grouping), collection strategy (CTD or *Alvin* (A), middle grouping), and deployment (minor groups). Error bars represent the standard deviation.

4. Discussion

4.1 CH_4 and methanotroph transport beyond the seep

Our observations indicate that both CH_4 and methanotrophs are transported upward and laterally from visibly active seep areas, with microbial activity detectable throughout the lower water column. At Sanak, vertical CH_4 transport is likely enhanced by bubble plumes rising from the seafloor (Jordan et al., 2019; Jordan et al., 2020), consistent with visual observations, EK80 detection, and the presence of exposed gas hydrates. In contrast, no bubble plumes were observed at Edge or Shumagin, and only moderate CH_4 concentrations were detected in the water column. At these sites, CH_4 redistribution in the water column is likely influenced by physical processes such as turbulent mixing and regional circulation (Leifer et al., 2006; Pohlman et al., 2017; Steinle et al., 2015). However, differences in sediment-side flux regimes are critical for explaining observed CH_4 concentrations in the water column. For instance, at Edge and Shumagin, the absence of bubble plumes or sulfur bacteria mats and the presence of clam beds suggest moderate, advective CH_4 fluxes where AOM is relatively efficient, limiting CH_4 escape from the sediments. In contrast, elevated water column CH_4 at Sanak likely reflects greater upward CH_4 flux, including from bubble plumes and reduced sedimentary CH_4 retention. The presence of extensive sulfur bacterial mats, which are often associated with zones of elevated methane flux and incomplete consumption during AOM, supports this interpretation. These patterns are consistent with previously described flux

regimes and their impact on AOM efficiency (Boetius & Suess, 2004; Torres et al., 2002; Treude et al., 2003). Across all three sites, CH_4 oxidation rates peaked primarily ~10–30 m above the seafloor (in some instances higher in the water column) and coincided with modest increases (~0.5–1 log) in *pmoA* gene abundance, forming a narrow layer of enhanced microbial activity. Depth-resolved qPCR data revealed increasing *pmoA* gene abundance with decreasing distance from the seafloor at Sanak and Edge, consistent with methanotroph accumulation near the zone of peak CH_4 availability. However, limited vertical resolution precludes robust conclusions about trends higher in the water column. Despite low CH_4 concentrations in the upper water column (<200 m), CH_4 oxidation was still detectable. While these signals are unlikely to originate from deep-sea seep emissions, given physical constraints on CH_4 transport (McGinnis et al., 2006), they may reflect *in situ* CH_4 cycling processes that link aerobic CH_4 production (Karl et al., 2008) with simultaneous oxidation.

The horizontal transect at Sanak further revealed spatial heterogeneity in CH_4 oxidation, consistent with near-bottom transport of CH_4-enriched waters driven by local circulation or plume dispersion. Along an ~325 m near-bottom track (CTD11), oxidation rates were lowest at adjacent stations near hydrate-bearing features and increased toward the distal end of the transect (WP9), where both CH_4 concentrations and *pmoA* gene abundances were highest. This spatial pattern suggests that bottom currents (from WP1 to WP10) may redistribute CH_4 and methanotrophs away from active seep points, similar to what was observed in this thesis (chapter 3), decoupling microbial activity from seepage. Related hydrodynamic controls have been observed at other seep systems, where strong bottom flow suppresses oxidation by displacing CH_4 before microbial communities can respond (Sauter et al., 2006; van Aken et al., 1995). Despite uniform O_2 concentrations along the transect, oxidation was patchy, indicating that CH_4 availability and

microbial positioning, not necessarily O_2 gradients, are the primary controls. These observations suggest that the methanosphere extends beyond active seeps, even in deep, high-O_2 seeps, and is dynamically structured by physical transport processes that modulate both CH_4 delivery and microbial access.

4.2 Inter- and intra-seep heterogeneity of CH_4, CH_4 oxidation, and community composition

We observed both inter- and intra-seep variation in CH_4 oxidation dynamics across the study sites. Inter-seep differences included site-wide contrasts in CH_4 flux, oxidation rates, and methanotroph gene abundance, associated with distinct seafloor geochemistry and seep characteristics such as the presence or absence of bubble plumes, bacterial mats, or clam beds. At finer scales, intra-seep variation reflected spatial heterogeneity within individual seep fields, including variation within bubble plumes and along local gradients in CH_4 availability, O_2 concentration, and microbial activity. These spatial patterns underscore the tight coupling between seep structure, microbial community dynamics, and the physical environment in regulating CH_4 turnover.

At Edge, CH_4 dynamics were investigated using *Alvin*-collected near-bottom water samples from depths ranging between 4812 and 4908 m. CH_4 concentrations (5.4–53 nM) and oxidation rates (0 to 3.9×10^{-2} nmol L^{-1} d^{-1}) were generally low and spatially variable. Nonetheless, some seafloor-associated habitats supported active methanotrophic communities. For example, one sample collected above a clam bed exhibited moderate CH_4 concentrations, detectable oxidation activity, and elevated *pmoA* gene abundance. A nearby sample collected over frenulate tubeworms showed higher CH_4 concentrations but lower *pmoA* abundance, illustrating that microbial responses did not consistently scale with local CH_4 availability. Interestingly, the highest oxidation rate at

Edge was measured in an off-seep sample with relatively low *pmoA* abundance, suggesting lateral CH_4 transport or localized mixing effects.

At Shumagin, *Alvin* samples collected between 4820 and 4874 m depth revealed elevated CH_4 concentrations (11–70 nM) and oxidation rates, with notable variability across sites. One sample collected from a hillside clam bed showed moderate CH_4 levels and oxidation activity but exhibited the highest *pmoA* gene abundance observed across all sites. In contrast, an off-seep sample with similar CH_4 concentrations displayed a substantially higher oxidation rate but lower gene abundance. These patterns suggest that microbial activity may be shaped by differences in community structure, CH_4 exposure history, or local environmental conditions such as O_2 availability.

Alvin-collected water samples at Sanak (2010 to 2046 m depth) revealed the strongest CH_4 signals across all sites, with concentrations reaching up to 2.2×10^4 nM and oxidation rates ranging from 1.2×10^{-1} to 2.4×10^2 nmol L^{-1} d^{-1}. However, *pmoA* gene abundance did not consistently scale with CH_4 availability. For example, the sample with the highest CH_4 concentration and oxidation rate, collected above a gas hydrate, exhibited only moderate *pmoA* abundance (log = 5.26). In contrast, a nearby sample from an orange bacterial mat with lower CH_4 (3.5×10^3 nM) and oxidation activity (11.54 nmol L^{-1} d^{-1}) showed higher *pmoA* levels (log = 5.51). These patterns suggest that intense CH_4 flux may outpace microbial growth or that physical transport processes decouple CH_4 availability from the established methanotrophic biomass.

These contrasts, particularly differences in bottom water CH_4 availability, and the presence or absence of focused CH_4 discharge, highlight the role of localized geochemical and physical gradients in shaping CH_4 transport and oxidation. Such variability also structures methanotrophic communities. Methanotrophic taxa exhibited vertical stratification, with greater diversity and

abundance near the seafloor, while members of the Methylomonadaceae clade IheB2-23 were detected throughout the water column at seep sites along the Southern California margin, including Del Mar and Santa Monica Mound (this thesis, chapter 3). A similar pattern was observed at the Alaska sites, where near-bottom *Alvin* samples contained the highest diversity of aerobic methanotrophs and Milano-WF1B-03 (another Methylomonadaceae lineage) were present throughout the water column. These observations underscore how environmental gradients across and within seep fields influence not only CH_4 oxidation rates but also the vertical and spatial organization of key methanotrophic lineages.

Across the *Alvin* sampling sites in the Gulf of Alaska, microbial CH_4 oxidation appeared to be influenced not only by CH_4 availability, but also by spatial variation in O_2 supply, CH_4 flux, and microbial community structure. At lower CH_4 flux sites like Edge and Shumagin, where no gas flares, plumes, or extensive bacterial mats were observed, oxidation was generally lower and concentrated in specific seep-associated habitats. In contrast, Sanak exhibited stronger CH_4 signals, higher oxidation rates, and broader distribution of methanotrophic activity, consistent with higher CH_4 flux and visible hydrates and expansive carbonates outcrops/faunal communities (e.g., tubeworm field). In several cases, we observed decoupling between CH_4 oxidation rates and *pmoA* gene abundance, which may reflect time lags in microbial response, differences in community structure, or physical–biological decoupling (Steinle et al., 2015).

Importantly, the spatial patterns in CH_4 oxidation described here have ecological implications that extend beyond CH_4 removal alone. Aerobic methanotrophs not only act as biogeochemical filters but also form the base of chemosynthetic food webs, supporting higher trophic levels through carbon transfer or symbiotic associations. Symbioses between aerobic methanotrophs and seep-dwelling fauna, such as bathymodiolin mussels, enable these animals to

exploit CH_4-rich habitats. Variability in methanotrophic activity and abundance, particularly in near-bottom waters and over clam beds, may therefore influence the structure, distribution, and productivity of symbiont-bearing communities. Where aerobic CH_4 oxidation is sustained and CH_4 supply is elevated, these communities may thrive; in contrast, patchy or limited oxidation may constrain the ecological footprint of CH_4-based symbioses. Understanding these patterns is essential for evaluating how CH_4 seeps function as integrated biological and geochemical hotspots (Levin, 2005; Levin et al., 2016).

4.3 CH_4 turnover and environmental controls in deep oxygenated seeps

To further identify the environmental factors regulating the CH_4 oxidation rate constant (k), a Spearman Rank Correlation analysis was conducted across the three seep sites (Edge, Shumagin, and Sanak; **Fig. 8**). The analysis only incorporated the CTD samples that contained CH_4, O_2, temperature, depth, and *pmoA* gene abundance measurements (log copies L^{-1}). Turnover time was omitted from the analysis as it is the reciprocal of k, and several samples had $k = 0$, resulting in undefined values. Details are provided in **Suppl. Table 2**. As CH_4 oxidation follows first-order kinetics, CH_4 concentration inherently influences oxidation rate, while variation in k reflects methanotroph efficiency under prevailing conditions, making correlations between k and environmental variables informative for understanding biogeochemical controls on methanotrophy.

At Edge Seep (**Fig. 8a**), k showed a moderate positive correlation with CH_4 ($\rho = 0.53$), consistent with first-order reaction kinetics. However, other correlations were relatively weak or inconsistent. k showed only a mild positive relationship with temperature ($\rho = 0.38$) and a weak negative correlation with O_2 ($\rho = –0.21$), suggesting that temperature may modestly enhance oxidation while O_2 is not limiting. Notably, k and pmoA were negatively correlated ($\rho = –0.25$), and

pmoA also declined with increasing temperature ($\rho = -0.58$), implying that the presence of methanotrophs was not a strong driver of oxidation rate. The absence of sulfur-oxidizing bacterial mats during seafloor surveys suggests that aerobic CH_4 oxidation may be spatially limited or carried out by low-biomass communities not forming conspicuous benthic assemblages. Anaerobic oxidation of CH_4 may still occur in the sediment, but its presence is not easily inferred from surface features alone.

At Shumagin Seep (**Fig. 7b**), correlations revealed a more coherent system. *k* was positively correlated with CH_4 ($\rho = 0.66$), pmoA ($\rho = 0.77$), and depth ($\rho = 0.43$), and strongly negatively correlated with temperature ($\rho = -0.89$), consistent with previous findings (Ruff et al., 2019). These trends suggest that CH_4 oxidation and methanotroph abundance are highest in deeper water layers where CH_4 is more abundant. The very weak correlation between *k* and O_2 ($\rho = 0.03$) suggests that O_2 is not a primary limiting factor for oxidation at this site. The positive covariation of CH_4, pmoA, and *k* indicates that methanotrophic communities are spatially aligned with CH_4 availability and responsive to its distribution. However, despite elevated CH_4 concentrations indicative of active seepage, no sulfur-oxidizing bacterial mats were observed during seafloor surveys. This suggests that sulfide production via AOM may be confined to deeper sediment layers or occur at rates insufficient to support conspicuous mat formation.

At Sanak Seep (**Fig. 8c**), CH_4 oxidation patterns deviated from typical expectations based on aerobic methanotrophy. *k* was positively correlated with CH_4 ($\rho = 0.31$) and O_2 ($\rho = 0.77$), indicating that CH_4 oxidation was more active in shallower, O_2-rich waters. However, *k* was negatively correlated with pmoA ($\rho = -0.83$), and pmoA also decreased with both O_2 ($\rho = -0.94$) and CH_4 ($\rho = -0.60$). This pattern is counterintuitive: higher CH_4 and O_2 concentrations are typically associated with greater MOB abundance, yet here oxidation appears to occur without a

corresponding increase in *pmoA* abundance. One possibility is that CH_4 oxidation was stimulated in a pre-existing water column methanotrophic community upon encountering a CH_4-rich environment, preceding detectable increases in cell density or *pmoA* gene abundance. In addition, physical mixing or recent shifts in water mass position may have displaced active populations from the sampling locations, contributing to the observed spatial decoupling between oxidation rates and methanotroph abundance (Steinle et al., 2015; Tavormina et al., 2013). These results suggest that vertical CH_4 oxidation above Sanak is O_2-dependent and may be strongly influenced by physical transport processes, highlighting a potential decoupling between microbial activity and methanotroph abundance.

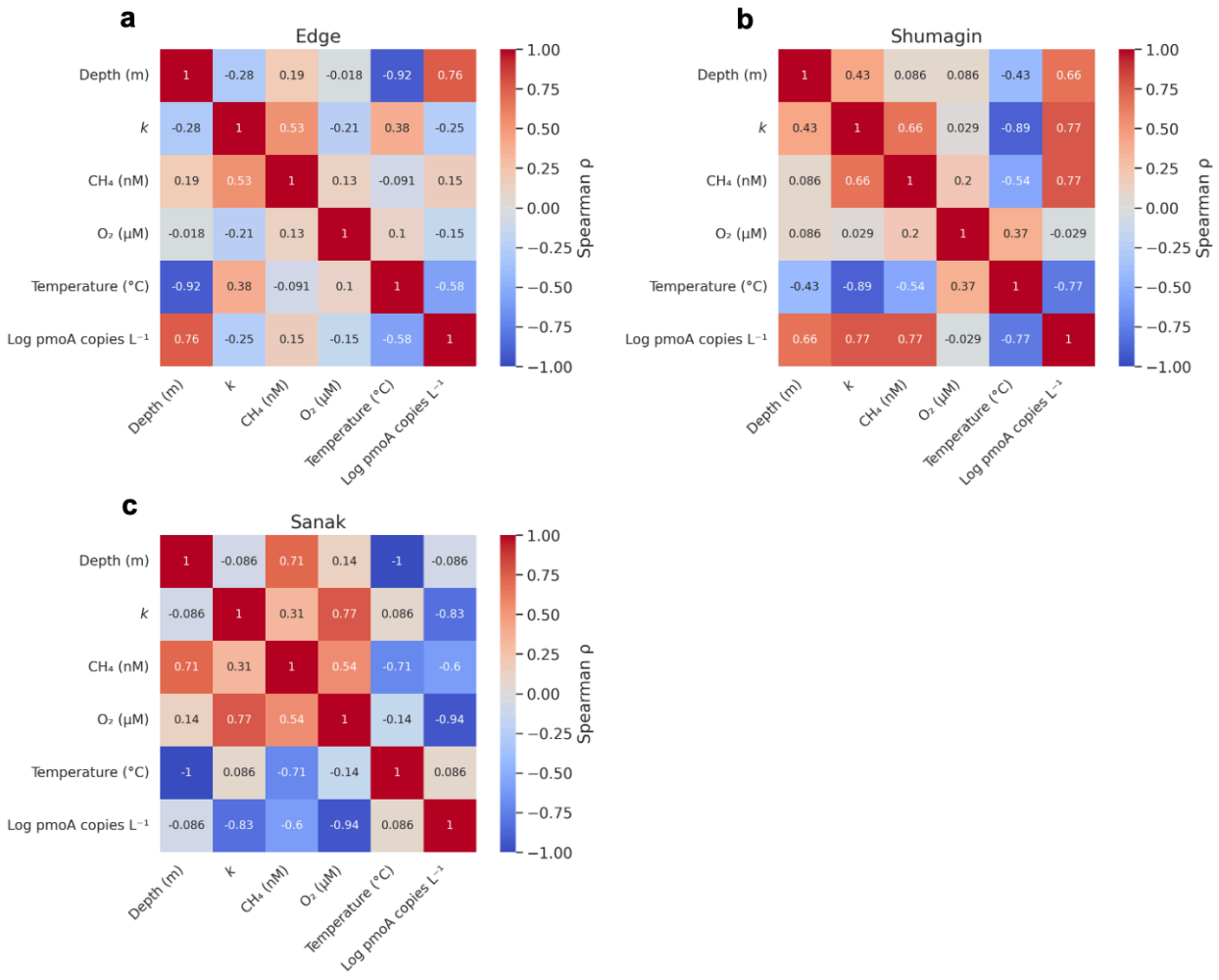

Figure 8. Spearman correlation heatmaps showing relationships among environmental and chemical variables at three CH_4 seep sites: (**a**) Edge, (**b**) Shumagin, and (**c**) Sanak seeps. Correlation matrices include depth, CH_4 oxidation rate constant (*k*), methane (CH_4), oxygen (O_2), temperature, and *pmoA* gene concentration (log copies L^{-1}). Warmer colors (red) represent stronger positive correlations, while cooler colors (blue) represent stronger negative correlations. Note that Spearman's rank correlation detects monotonic associations but does not imply causality and may be sensitive to outliers or small sample sizes.

4.4 Enhanced surface CH_4 oxidation during algal bloom indicates possible aerobic CH_4 production

An expansive algal bloom was visually observed during the AT50-24 expedition in late May 2023, consistent with the well-documented spring bloom period in the Gulf of Alaska, which typically begins in late April to early May (Strom et al., 2016). At Sanak, fluorescence data indicated a subsurface chlorophyll maximum of ~11 µg/L at 14 m depth, consistent with a surface algal bloom. Supporting this, significant phytodetritus aggregates were observed at their highest visual density below 1900 m based on *Alvin* dive footage, where they were both suspended in the water column and deposited on the seafloor. Fluorescence measurements were not available at Shumagin or Edge; however, the timing and regional oceanographic context suggest that these sites may also have experienced a bloom. Spring and early summer blooms in this region have become more frequent and persistent in recent years, likely due to increasing ocean stratification, warming surface temperatures, and enhanced nutrient delivery from eddy activity and coastal upwelling (Bond et al., 2015; Lomas et al., 2020; Strom et al., 2016). These blooms can restructure surface biogeochemistry by modifying O_2 availability, producing labile organic matter, and influencing microbial community dynamics.

While a direct mechanistic link remains to be established, elevated CH_4 concentrations (compared to midwater) and detectable CH_4 oxidation in the upper 25 m of the water column at all three Alaska seep sites coincided with evidence of a surface algal bloom, particularly at Sanak. The presence of CH_4 oxidation in surface waters, despite lower CH_4 concentrations relative to near-seafloor concentrations, suggests a cryptic CH_4 cycle potentially driven by *in situ* CH_4 production and rapid microbial consumption. This process may be fueled by the degradation of algal-derived organic matter (Damm et al., 2010; Klintzsch et al., 2019) and supported by cyanobacterial lineages

notionally capable of aerobic CH_4 production (Mao et al., 2024; Perez-Coronel & Michael Beman, 2022). Amplicon sequence data from surface waters revealed the presence of cyanobacteria previously implicated in this pathway (including Synechococcus; **Fig. 5**) (Bižić et al., 2020), further supporting the possibility of biologically mediated surface CH_4 production. Surface *pmoA* gene abundances confirmed methanotroph presence, albeit at lower levels (<2 log pmoA copies L^{-1}) than in bottom waters. Surface CH_4 concentrations exceeded atmospheric equilibrium at all three sites, with maximum values of 49 nM at 20 m (Shumagin CTD8), 21 nM (Sanak CTD10), and 22 nM (Edge CTD4). These findings are consistent with prior observations of surface CH_4 production, associated with phytoplankton blooms and support the hypothesis that cryptic CH_4 cycling may occur in productive marine surface waters (this thesis, chapter 3). In addition, the elevated surface CH_4, compared to mid-water, was observed in prior expeditions (Suess et al., 1998).

4.5 Influence of O_2 and CH_4 availability on water column CH_4 oxidation at Alaska and Southern California seeps

Patterns of CH_4 transport and oxidation observed at Alaska seeps show striking parallels to those documented in the Southern California Margin (this thesis, chapter 3; AT50-12 expedition, June–July 2023), while also revealing important contrasts driven by differences in seep flux, physical setting, and O_2 availability. In both regions, vertical and lateral redistribution of CH_4 and methanotrophs expands the extent of seep influence beyond visibly active venting zones, forming a diffuse methanosphere. These distributions appear shaped by physical transport processes, including stratification and bubble-mediated flux, although water-mass properties and circulation likely also play a role.

During the Alaska and Southern California expeditions, CH_4 oxidation rates peaked within 10–30 m of the seafloor (when sampled via CTD/rosette system) and were accompanied by increases in *pmoA* gene abundance, suggesting the presence of a near-seafloor microbial oxidation layer. These layers often persisted even in the absence of visible seepage, indicating lateral redistribution of CH_4 and associated microbial communities. At Sanak and Santa Monica Mound in southern California, high CH_4 concentrations, vigorous bubble plumes, and elevated oxidation rates suggest that bubble-mediated transport promoted oxidation well above the seafloor. In contrast, Edge and Shumagin exhibited more limited oxidation and weaker seep signals. At Lasuen Knoll in southern California, while there were observations of sulfur mats, CH_4 oxidation was more spatially constrained during our sampling, potentially reflecting temporal variability in seep activity.

Both regions exhibited fine-scale spatial heterogeneity in CH_4 concentrations, oxidation rates, and *pmoA* gene abundances, even among similar seep habitats. This patchiness may reflect localized control by CH_4 and O_2 gradients, physical transport processes (e.g., bottom currents), or microbial community composition. In Alaska, for example, water samples with elevated CH_4 (e.g., AD5279-C at Sanak) displayed relatively low *pmoA* gene abundance despite high oxidation rates, paralleling patterns observed at Santa Monica Mound. One possible explanation is the presence of pmoA-negative methanotrophs, aerobic methanotrophs that oxidize CH_4 without the pmoA gene, instead relying on alternative monooxygenases such as soluble MMO, and thereby eluding detection by conventional pmoA-based molecular surveys (Guerrero-Cruz et al., 2021). Alternatively, gene abundance may not have yet responded to transient CH_4 input due to rapid microbial turnover, delayed growth, or advective displacement of methanotrophs from CH_4-rich waters (Heintz et al., 2012; Steinle et al., 2015; Ussler III et al., 2013). The absence of ANME and

the presence of fully oxygenated waters in these profiles further support aerobic, rather than anaerobic, CH_4 oxidation.

Surface CH_4 oxidation also appears in both regions, while under lower CH_4 concentrations than measured near-seafloor, likely fueled by phytoplankton-derived precursors such as dimethylsulfoniopropionate and methylated amines (Damm et al., 2010; Karl et al., 2008). However, surface water *pmoA* gene concentrations were consistently higher in Southern California than in Alaska (both surface and near-seafloor), suggesting a more abundant or responsive methanotrophic population, supported by a higher CH_4 concentration (~32–*98 nM)* in the upper water column of the Southern California Margin, potentially reflecting regional differences in productivity, precursor supply, or microbial adaptation. In the Southern California seep water column, the methanotrophic community included multiple members of the Methylomonadaceae, including IheB2–23, Marine Methylotrophic Group 2, *Methyloprofundus*, Milano–WF1B–03, and pltb–vmat–59. In contrast, the Alaska seeps contained only IheB2–23 and Milano–WF1B–03. These differences suggest distinct regional methanotrophic assemblages likely shaped by variations in geochemistry, seepage style, or water column structure.

Despite these broad similarities, regional differences shape how these processes manifest. Southern California seeps in the Santa Monica Basin exhibit persistently low bottom-water O_2 concentrations (<5 μM), which may increase water column CH_4 oxidation (Heintz et al., 2012) compared to the more oxygenated conditions observed at Alaskan seeps. Additionally, the semi-enclosed Santa Monica Basin may retain CH_4 and support prolonged oxidation activity due to limited bottom-water ventilation, whereas the Gulf of Alaska's more open and advective hydrography, characterized by northward inflow through the Aleutian Passes and eastward flow

along the Aleutian North Slope Current, likely promotes greater dispersal of CH_4 and methanotrophs (Stabeno et al., 2002; Stabeno et al., 2009).

5. Conclusion

This study expands the ecological scope of the methanosphere in high-latitude, oxygenated waters by demonstrating that aerobic CH_4 oxidation is not confined to discrete seep zones but forms a vertically structured and spatially diffuse system. Across three contrasting Alaskan seep environments, Edge, Shumagin, and Sanak, we observed oxidation layers 10–30 m above the seafloor, supported by elevated CH_4 concentrations and measurable oxidation rates, even in waters with relatively low *pmoA* gene abundance. Oxidation was also detected in surface and near-surface waters during a seasonal algal bloom, suggesting the potential for cryptic CH_4 cycling in the upper water column, potentially fueled by phytoplankton-derived precursors.

Seep-specific differences in CH_4 oxidation reflect how physical transport and CH_4 delivery shape microbial activity. At the shallower Sanak site, bubble plumes and vertical fluxes of organic matter supported oxidation throughout the water column. In contrast, oxidation at the deeper Edge and Shumagin sites was more spatially localized, with activity concentrated in intermediate and bottom waters. At Edge, a distinct oxidation peak near 2000 m, at the base of the OMZ, coincided with elevated CH_4 concentrations and moderate *pmoA* gene copy numbers, indicating a zone of enhanced methanotrophic activity under low-O_2 conditions. The presence of oxidation activity beyond zones of active seepage in all three settings underscores the importance of water column CH_4 gradients and likely the hydrographic structure in controlling the extent and persistence of methanotrophic activity. These observations suggest the water column forms a vertically distributed methanotrophic network, with activity spanning surface productivity zones, midwater CH_4

oxidation layers, and an expanded methanosphere associated with benthic methane release. The detection of oxidation across vertical profiles and lateral transects, even where methanotrophic gene markers were reduced, suggests the influence of lateral CH_4 transport and tidal currents (supported by an observed curvature in the EM124 dual Sanak CH_4 plumes during sampling). Compared to the Gulf of Alaska sites, Southern California seeps exhibit lower bottom-water O_2 concentrations, higher CH_4 fluxes (excluding Sanak), and elevated *pmoA* gene copy numbers, conditions that coincide with more sustained and spatially extensive CH_4 oxidation in those systems. Collectively, these findings reveal that the methanosphere is not a static feature anchored to the seafloor, but a flexible microbial scaffold shaped by the distribution of CH_4 and O_2 and by physical transport dynamics. Rather than passively following CH_4 release, methanotrophic communities exhibit spatial plasticity and compositional resilience across regions, remaining active under both oxic and hypoxic conditions and in the presence or absence of focused venting. The methanosphere thus emerges as a diffuse but functionally cohesive biogeochemical layer that regulates CH_4 cycling and links benthic and pelagic microbial processes in the ocean.

Funding

This project was supported by the U.S. National Science Foundation (Award Nos. 2048597 to T.T., 2048720 to L.A.L., 2048666 to V.J.O., 2205998 to K.H., and 2126631 to D.U.). We would like to thank UNOLS, the crew of R/V *Atlantis*, the HOV *Alvin* team, and the shipboard scientific party for their logistical, technical, and scientific support during expedition AT50-24.

Acknowledgements

We thank the captain and crew of the *R/V Atlantis*, the *Alvin* operations team, the Shipboard Scientific Services Group (SSSGs), and the supporting personnel from the Woods Hole Oceanographic Institution (WHOI) for their outstanding support during the AT50-24 cruise. Their expertise and dedication were essential to the success of this research. We are also thankful to S. Martinez for her assistance with water sampling and filtration. We also gratefully acknowledge S. Connon at the California Institute of Technology for her invaluable guidance in microbial sample processing.

References

Bižić, M., Klintzsch, T., Ionescu, D., Hindiyeh, M., Günthel, M., Muro-Pastor, A. M., Eckert, W., Urich, T., Keppler, F., & Grossart, H.-P. (2020). Aquatic and terrestrial cyanobacteria produce methane. *Science Advances*, *6*(3), eaax5343.

Boetius, A., Ravenschlag, K., Schubert, C. J., Rickert, D., Widdel, F., Gieseke, A., Amann, R., Jørgensen, B. B., Witte, U., & Pfannkuche, O. (2000). A marine microbial consortium apparently mediating anaerobic oxidation of methane. *Nature*, *407*(6804), 623-626.

Boetius, A., & Suess, E. (2004). Hydrate Ridge: a natural laboratory for the study of microbial life fueled by methane from near-surface gas hydrates. *Chemical Geology*, *205*(3-4), 291-310.

Bohrmann, G., Greinert, J., Suess, E., & Torres, M. (1998). Authigenic carbonates from the Cascadia subduction zone and their relation to gas hydrate stability. *Geology*, *26*(7), 647-650.

Bond, N. A., Cronin, M. F., Freeland, H., & Mantua, N. (2015). Causes and impacts of the 2014 warm anomaly in the NE Pacific. *Geophysical Research Letters*, *42*(9), 3414-3420.

Bussmann, I., Matousu, A., Osudar, R., & Mau, S. (2015). Assessment of the radio 3H-CH4 tracer technique to measure aerobic methane oxidation in the water column. *Limnology and Oceanography: Methods*, *13*(6), 312-327.

Callahan, B. J., McMurdie, P. J., Rosen, M. J., Han, A. W., Johnson, A. J. A., & Holmes, S. P. (2016). DADA2: High-resolution sample inference from Illumina amplicon data. *Nature methods*, *13*(7), 581-583.

Childress, J. J., Fisher, C., Brooks, J., Kennicutt, M., Bidigare, R., & Anderson, A. (1986). A methanotrophic marine molluscan (Bivalvia, Mytilidae) symbiosis: mussels fueled by gas. *Science*, *233*(4770), 1306-1308.

Ciais, P., Sabine, C., Bala, G., Bopp, L., Brovkin, V., & House, J. I. (2014). Carbon and other biogeochemical cycles. In *Climate Change 2013: The Physical Science Basis. Contribution of Working Group I to the Fifth Assessment Report of the Intergovernmental Panel on Climate Change Change* (pp. 465-570). Cambridge University Press.

Conrad, R. (2009). The global methane cycle: recent advances in understanding the microbial processes involved. *Environmental Microbiology Reports*, *1*(5), 285-292.

Cordova-Gonzalez, A., Birgel, D., Wisshak, M., Urich, T., Brinkmann, F., Marcon, Y., Bohrmann, G., & Peckmann, J. (2023). A carbonate corrosion experiment at a marine methane seep: The role of aerobic methanotrophic bacteria. *Geobiology*, *21*(4), 491-506.

Crémière, A., Lepland, A., Chand, S., Sahy, D., Condon, D. J., Noble, S. R., Martma, T., Thorsnes, T., Sauer, S., & Brunstad, H. (2016). Timescales of methane seepage on the Norwegian margin following collapse of the Scandinavian Ice Sheet. *Nature communications*, *7*(1), 11509.

Crespo-Medina, M., Meile, C., Hunter, K., Diercks, A., Asper, V., Orphan, V., Tavormina, P., Nigro, L., Battles, J., & Chanton, J. P. (2014). The rise and fall of methanotrophy following a deepwater oil-well blowout. *Nature Geoscience*, *7*(6), 423-427.

Cuellar, S. (2023). Project Instructions: EX-23-02, Seascape Alaska: Aleutians Explorations 1.

Damm, E., Helmke, E., Thoms, S., Schauer, U., Nöthig, E., Bakker, K., & Kiene, R. (2010). Methane production in aerobic oligotrophic surface water in the central Arctic Ocean. *Biogeosciences*, *7*(3), 1099-1108.

Deines, P., Bodelier, P. L., & Eller, G. (2007). Methane-derived carbon flows through methane-oxidizing bacteria to higher trophic levels in aquatic systems. *Environmental Microbiology*, *9*(5), 1126-1134.

Eitel, E. M., Utter, D., Connon, S., Orphan, V. J., & Murali, R. (2024). CABO-16S: A Combined Archaea, Bacteria, Organelle 16S database for amplicon analysis of prokaryotes and eukaryotes in environmental samples. *bioRxiv*, 2024.2010. 2023.619938.

Elvert, M., Suess, E., Greinert, J., & Whiticar, M. J. (2000). Archaea mediating anaerobic methane oxidation in deep-sea sediments at cold seeps of the eastern Aleutian subduction zone. *Organic Geochemistry*, *31*(11), 1175-1187.

Fuchs, A., Lyautey, E., Montuelle, B., & Casper, P. (2016). Effects of increasing temperatures on methane concentrations and methanogenesis during experimental incubation of sediments from oligotrophic and mesotrophic lakes. *Journal of Geophysical Research: Biogeosciences*, *121*(5), 1394-1406.

Goffredi, S. K., Tilic, E., Mullin, S. W., Dawson, K. S., Keller, A., Lee, R. W., Wu, F., Levin, L. A., Rouse, G. W., & Cordes, E. E. (2020). Methanotrophic bacterial symbionts fuel dense populations of deep-sea feather duster worms (Sabellida, Annelida) and extend the spatial influence of methane seepage. *Science Advances*, *6*(14), eaay8562.

Greinert, J., Bohrmann, G., & Elvert, M. (2002). Stromatolitic fabric of authigenic carbonate crusts: result of anaerobic methane oxidation at cold seeps in 4,850 m water depth. *International Journal of Earth Sciences*, *91*, 698-711.

Grey, J. (2016). The incredible lightness of being methane-fuelled: stable isotopes reveal alternative energy pathways in aquatic ecosystems and beyond. *Frontiers in Ecology and Evolution*, *4*, 8.

Guerrero-Cruz, S., Vaksmaa, A., Horn, M. A., Niemann, H., Pijuan, M., & Ho, A. (2021). Methanotrophs: discoveries, environmental relevance, and a perspective on current and future applications. *Frontiers in microbiology*, *12*, 678057.

Hanson, R. S., & Hanson, T. E. (1996). Methanotrophic bacteria. *Microbiological reviews*, *60*(2), 439-471.

Heintz, M., Mau, S., & Valentine, D. (2012). Physical control on methanotrophic potential in waters of the Santa Monica Basin, Southern California. *Limnology and Oceanography*, *57*(2), 420-432.

Hoy, S. (2023). Project Instructions: EX2304: Seascape Alaska 3-Aleutians Remotely Operated Vehicle Exploration and Mapping.

Jahnke, R. A. (2010). Global synthesis1. In *Carbon and nutrient fluxes in continental margins: A global synthesis* (pp. 597-615). Springer.

Janvier, M., Frehel, C., Grimont, F., & Gasser, F. (1985). Methylophaga marina gen. nov., sp. nov. and Methylophaga thalassica sp. nov., marine methylotrophs. *International Journal of Systematic and Evolutionary Microbiology*, *35*(2), 131-139.

Jimenez-Infante, F., Ngugi, D. K., Vinu, M., Alam, I., Kamau, A. A., Blom, J., Bajic, V. B., & Stingl, U. (2016). Comprehensive genomic analyses of the OM43 clade, including a novel species from the Red Sea, indicate ecotype differentiation among marine methylotrophs. *Applied and Environmental Microbiology*, *82*(4), 1215-1226.

Jordan, S., Treude, T., Leifer, I., Schulz-Vogt, H., & Schmale, O. (2019). Bubble Shuttle: A bubble-mediated bentho-pelagic transport mechanism of methanotrophs and a first study at the Coal Oil Point seep field to identify the controlling parameters. EGU General Assembly Conference Abstracts,

Jordan, S. F., Treude, T., Leifer, I., Janßen, R., Werner, J., Schulz-Vogt, H., & Schmale, O. (2020). Bubble-mediated transport of benthic microorganisms into the water column: Identification

of methanotrophs and implication of seepage intensity on transport efficiency. *Scientific reports*, *10*(1), 4682.

Jørgensen, B. B., & Boetius, A. (2007). Feast and famine—microbial life in the deep-sea bed. *Nature Reviews Microbiology*, *5*(10), 770-781.

Kalyuzhnaya, M. G., Gomez, O. A., & Murrell, J. C. (2019). The methane-oxidizing bacteria (methanotrophs). *Taxonomy, genomics and ecophysiology of hydrocarbon-degrading microbes*, 245-278.

Karl, D. M., Beversdorf, L., Björkman, K. M., Church, M. J., Martinez, A., & Delong, E. F. (2008). Aerobic production of methane in the sea. *Nature Geoscience*, *1*(7), 473-478.

Klintzsch, T., Langer, G., Nehrke, G., Wieland, A., Lenhart, K., & Keppler, F. (2019). Methane production by three widespread marine phytoplankton species: release rates, precursor compounds, and potential relevance for the environment. *Biogeosciences*, *16*(20), 4129-4144.

Kutterolf, S., Liebetrau, V., Mörz, T., Freundt, A., Hammerich, T., & Garbe-Schönberg, D. (2008). Lifetime and cyclicity of fluid venting at forearc mound structures determined by tephrostratigraphy and radiometric dating of authigenic carbonates. *Geology*, *36*(9), 707-710.

Leifer, I., Luyendyk, B. P., Boles, J., & Clark, J. F. (2006). Natural marine seepage blowout: Contribution to atmospheric methane. *Global Biogeochemical Cycles*, *20*(3).

Levin, L. A. (2005). Ecology of cold seep sediments: interactions of fauna with flow, chemistry and microbes. In *Oceanography and Marine Biology* (pp. 11-56). CRC Press.

Levin, L. A., Baco, A. R., Bowden, D. A., Colaco, A., Cordes, E. E., Cunha, M. R., Demopoulos, A. W., Gobin, J., Grupe, B. M., & Le, J. (2016). Hydrothermal vents and methane seeps: rethinking the sphere of influence. *Frontiers in Marine Science*, *3*, 72.

Levin, L. A., & Mendoza, G. F. (2007). Community structure and nutrition of deep methane-seep macrobenthos from the North Pacific (Aleutian) Margin and the Gulf of Mexico (Florida Escarpment). *Marine Ecology*, *28*(1), 131-151.

Lomas, M. W., Eisner, L. B., Gann, J., Baer, S. E., Mordy, C. W., & Stabeno, P. J. (2020). Time-series of direct primary production and phytoplankton biomass in the southeastern Bering Sea: responses to cold and warm stanzas. *Marine Ecology Progress Series*, *642*, 39-54.

Mao, Y., Lin, T., Li, H., He, R., Ye, K., Yu, W., & He, Q. (2024). Aerobic methane production by phytoplankton as an important methane source of aquatic ecosystems: Reconsidering the global methane budget. *Science of the Total Environment*, *907*, 167864.

Martin, M. (2011). Cutadapt removes adapter sequences from high-throughput sequencing reads. *EMBnet. journal*, *17*(1), 10-12.

McGinnis, D., Greinert, J., Artemov, Y., Beaubien, S. E., & Wüest, A. (2006). Fate of rising methane bubbles in stratified waters: How much methane reaches the atmosphere? *Journal of Geophysical Research: Oceans*, *111*(C9).

Niemann, H., Steinle, L., Blees, J., Bussmann, I., Treude, T., Krause, S., Elvert, M., & Lehmann, M. F. (2015). Toxic effects of lab-grade butyl rubber stoppers on aerobic methane oxidation. *Limnology and Oceanography: Methods*, *13*(1), 40-52.

Orata, F. D., Meier-Kolthoff, J. P., Sauvageau, D., & Stein, L. Y. (2018). Phylogenomic analysis of the gammaproteobacterial methanotrophs (order Methylococcales) calls for the

reclassification of members at the genus and species levels. *Frontiers in Microbiology*, *9*, 3162.

Orphan, V. J., House, C. H., Hinrichs, K.-U., McKeegan, K. D., & DeLong, E. F. (2001). Methane-consuming archaea revealed by directly coupled isotopic and phylogenetic analysis. *science*, *293*(5529), 484-487.

Pasulka, A. L., Goffredi, S. K., Tavormina, P. L., Dawson, K. S., Levin, L. A., Rouse, G. W., & Orphan, V. J. (2017). Colonial tube-dwelling ciliates influence methane cycling and microbial diversity within methane seep ecosystems. *Frontiers in Marine Science*, *3*, 276.

Paul, B. G., Ding, H., Bagby, S. C., Kellermann, M. Y., Redmond, M. C., Andersen, G. L., & Valentine, D. L. (2017). Methane-oxidizing bacteria shunt carbon to microbial mats at a marine hydrocarbon seep. *Frontiers in Microbiology*, *8*, 186.

Paull, C. K., Hecker, B., Commeau, R., Freeman-Lynde, R., Neumann, C., Corso, W., Golubic, S., Hook, J., Sikes, E., & Curray, J. (1984). Biological communities at the Florida Escarpment resemble hydrothermal vent taxa. *Science*, *226*(4677), 965-967.

Perez-Coronel, E., & Michael Beman, J. (2022). Multiple sources of aerobic methane production in aquatic ecosystems include bacterial photosynthesis. *Nature communications*, *13*(1), 6454.

Pohlman, J. W., Greinert, J., Ruppel, C., Silyakova, A., Vielstädte, L., Casso, M., Mienert, J., & Bünz, S. (2017). Enhanced CO2 uptake at a shallow Arctic Ocean seep field overwhelms the positive warming potential of emitted methane. *Proceedings of the National Academy of Sciences*, *114*(21), 5355-5360.

Reeburgh, W. S. (2007). Oceanic methane biogeochemistry. *Chemical reviews*, *107*(2), 486-513.

Rubin-Blum, M., Antony, C. P., Sayavedra, L., Martínez-Pérez, C., Birgel, D., Peckmann, J., Wu, Y.-C., Cardenas, P., MacDonald, I., & Marcon, Y. (2019). Fueled by methane: deep-sea sponges from asphalt seeps gain their nutrition from methane-oxidizing symbionts. *The ISME journal*, *13*(5), 1209-1225.

Ruff, S. E., Felden, J., Gruber-Vodicka, H. R., Marcon, Y., Knittel, K., Ramette, A., & Boetius, A. (2019). In situ development of a methanotrophic microbiome in deep-sea sediments. *The ISME journal*, *13*(1), 197-213.

Sauter, E. J., Muyakshin, S. I., Charlou, J.-L., Schlüter, M., Boetius, A., Jerosch, K., Damm, E., Foucher, J.-P., & Klages, M. (2006). Methane discharge from a deep-sea submarine mud volcano into the upper water column by gas hydrate-coated methane bubbles. *Earth and Planetary Science Letters*, *243*(3-4), 354-365.

Stabeno, P., Reed, R., & Napp, J. (2002). Transport through Unimak Pass, Alaska. *Deep Sea Research Part II: Topical Studies in Oceanography*, *49*(26), 5919-5930.

Stabeno, P. J., Schumacher, J. D., & Ohtani, K. (2009). The physical oceanography of the Bering Sea: A summary of physical, chemical, and biological characteristics, and a synopsis of research on the Bering Sea. *Geography*, *24*, 1-22.

Steinle, L., Graves, C. A., Treude, T., Ferré, B., Biastoch, A., Bussmann, I., Berndt, C., Krastel, S., James, R. H., & Behrens, E. (2015). Water column methanotrophy controlled by a rapid oceanographic switch. *Nature Geoscience*, *8*(5), 378-382.

Steinle, L., Maltby, J., Treude, T., Kock, A., Bange, H. W., Engbersen, N., Zopfi, J., Lehmann, M. F., & Niemann, H. (2017). Effects of low oxygen concentrations on aerobic methane oxidation in seasonally hypoxic coastal waters. *Biogeosciences*, *14*(6), 1631-1645.

Strom, S. L., Fredrickson, K. A., & Bright, K. J. (2016). Spring phytoplankton in the eastern coastal Gulf of Alaska: Photosynthesis and production during high and low bloom years. *Deep Sea Research Part II: Topical Studies in Oceanography*, *132*, 107-121.

Suess, E. (2010). Marine cold seeps. In. Springer.

Suess, E., Bohrmann, G., Von Huene, R., Linke, P., Wallmann, K., Lammers, S., Sahling, H., Winckler, G., Lutz, R. A., & Orange, D. (1998). Fluid venting in the eastern Aleutian subduction zone. *Journal of Geophysical Research: Solid Earth*, *103*(B2), 2597-2614.

Takeuchi, M., Katayama, T., Yamagishi, T., Hanada, S., Tamaki, H., Kamagata, Y., Oshima, K., Hattori, M., Marumo, K., & Nedachi, M. (2014). Methyloceanibacter caenitepidi gen. nov., sp. nov., a facultatively methylotrophic bacterium isolated from marine sediments near a hydrothermal vent. *International Journal of Systematic and Evolutionary Microbiology*, *64*(Pt_2), 462-468.

Tavormina, P. L., Ussler III, W., & Orphan, V. J. (2008). Planktonic and sediment-associated aerobic methanotrophs in two seep systems along the North American margin. *Applied and Environmental Microbiology*, *74*(13), 3985-3995.

Tavormina, P. L., Ussler III, W., Steele, J. A., Connon, S. A., Klotz, M. G., & Orphan, V. J. (2013). Abundance and distribution of diverse membrane-bound monooxygenase (C u-MMO) genes within the C osta R ica oxygen minimum zone. *Environmental Microbiology Reports*, *5*(3), 414-423.

Thamdrup, B., Steinsdóttir, H. G., Bertagnolli, A. D., Padilla, C. C., Patin, N. V., Garcia-Robledo, E., Bristow, L. A., & Stewart, F. J. (2019). Anaerobic methane oxidation is an important sink for methane in the ocean's largest oxygen minimum zone. *Limnology and Oceanography*, *64*(6), 2569-2585.

Torres, M. E., McManus, J., Hammond, D., De Angelis, M., Heeschen, K., Colbert, S., Tryon, M., Brown, K., & Suess, E. (2002). Fluid and chemical fluxes in and out of sediments hosting methane hydrate deposits on Hydrate Ridge, OR, I: Hydrological provinces. *Earth and Planetary Science Letters*, *201*(3-4), 525-540.

Treude, T., Boetius, A., Knittel, K., Wallmann, K., & Jørgensen, B. B. (2003). Anaerobic oxidation of methane above gas hydrates at Hydrate Ridge, NE Pacific Ocean. *Marine Ecology Progress Series*, *264*, 1-14.

Tunnicliffe, V., Juniper, S. K., & Sibuet, M. (2003). Reducing environments of the deep-sea floor. *Ecosystems of the World*, 81-110.

Ussler III, W., Preston, C., Tavormina, P., Pargett, D., Jensen, S., Roman, B., Marin III, R., Shah, S. R., Girguis, P. R., & Birch, J. M. (2013). Autonomous application of quantitative PCR in the deep sea: in situ surveys of aerobic methanotrophs using the deep-sea environmental sample processor. *Environmental science & technology*, *47*(16), 9339-9346.

van Aken, H. M., Budeus, G., & Hähnel, M. (1995). The anatomy of the Arctic frontal zone in the Greenland Sea. *Journal of Geophysical Research: Oceans*, *100*(C8), 15999-16014.

Vekeman, B., Kerckhof, F. M., Cremers, G., De Vos, P., Vandamme, P., Boon, N., Op den Camp, H. J., & Heylen, K. (2016). New Methyloceanibacter diversity from North Sea sediments includes methanotroph containing solely the soluble methane monooxygenase. *Environmental microbiology*, *18*(12), 4523-4536.

Wallmann, K., Linke, P., Suess, E., Bohrmann, G., Sahling, H., Schlüter, M., Dählmann, A., Lammers, S., Greinert, J., & von Mirbach, N. (1997). Quantifying fluid flow, solute mixing, and biogeochemical turnover at cold vents of the eastern Aleutian subduction zone. *Geochimica et Cosmochimica Acta*, *61*(24), 5209-5219.

Welte, C., & Deppenmeier, U. (2014). Bioenergetics and anaerobic respiratory chains of aceticlastic methanogens. *Biochimica et Biophysica Acta (BBA)-Bioenergetics*, *1837*(7), 1130-1147.

Yamamoto, S., Alcauskas, J. B., & Crozier, T. E. (1976). Solubility of methane in distilled water and seawater. *Journal of Chemical and Engineering Data*, *21*(1), 78-80.

Supplementary Material: Klonicki et al. Methane Oxidation and the Distribution of Methane-Oxidizing Bacteria above Cold Seeps in the Eastern Aleutian Subduction Zone

Supplementary Table 1. Geographic coordinates, depths, and two-dimensional distances between sequential waypoints for the Sanak horizontal CTD (CTD11). The last waypoint in each section does not have a distance to the next waypoint, as it is the final point in the survey sequence.

Location	Waypoint	Latitude (dec. deg.)	Longitude (dec. deg.)	Depth (m)	Approximate Distance to next Waypoint (m)
Sanak	1	53.749036	-162.590273	2019	34.66
Sanak	2	53.748863	-162.589796	2011	51.76
Sanak	3	53.748613	-162.589132	2010	51.82
Sanak	4	53.748407	-162.588425	2005	39.6
Sanak	5	53.748171	-162.587974	2003	39.73
Sanak	6	53.747991	-162.587452	2003	34.66
Sanak	7	53.747824	-162.587007	2010	35.9
Sanak	8	53.747642	-162.586556	2005	35.05
Sanak	9	53.747437	-162.586151	1999	N/A

Supplementary Table 2. Environmental and microbiological characteristics at different depths across the three seep sites: Edge, Shumagin and Sanak. Variables include depth, first-order rate constant (*k*), methane turnover time, methane (CH_4) and oxygen (O_2) concentrations, temperature, and *pmoA* gene copy abundance (log scale).

Site	Depth (m)	*k*	Turnover Time (y)	CH_4 (nM)	O_2 (μM)	Temp. °C	Log copies pmoA L^{-1}
Edge	11	0	N/A	8.6	320	6.2	2.54
Edge	3000	0	N/A	12	106	1.6	5.4
Edge	3501	0	N/A	16	125	1.5	N/A
Edge	4000	0	N/A	8.4	139	1.5	N/A
Edge	4250	8.50×10^{-5}	32.2	10	143	1.5	N/A
Edge	4500	0	N/A	12	148	1.5	N/A
Edge	4600	5.28×10^{-5}	51.8	11	149	1.5	N/A
Edge	4701	0	N/A	13	150	1.5	4.64
Edge	4801	6.49×10^{-5}	42.2	9.4	150	1.6	N/A
Edge	4850	0	N/A	28	150	1.6	5.44
Edge	4901	7.73×10^{-5}	35.4	28	150	1.6	5.44
Edge	4960	0	N/A	30	153	1.6	5.37
Edge	50	8.23×10^{-5}	33.2	33	303	5.0	2.45
Edge	100	2.89×10^{-5}	94.9	40	126	5.9	N/A
Edge	200	1.39×10^{-4}	19.7	40	73	4.8	4.93
Edge	400	2.33×10^{-5}	117	17	29	4.2	N/A
Edge	600	0	N/A	9.1	19	3.8	4.72
Edge	800	0	N/A	8.3	16	3.3	N/A
Edge	1000	0	N/A	8.2	17	3.0	N/A
Edge	1500	8.39×10^{-4}	3.27	21	31	2.3	4.52
Edge	2000	7.04×10^{-4}	3.89	43.5	59	1.9	N/A
Edge	20.8	1.55×10^{-4}	17.7	49	314	0.1	0.0997
Edge	660	1.17×10^{-4}	23.4	36	16	3.5	5.25
Shumagin	3001	9.20×10^{-5}	29.8	40	112	1.6	N/A
Shumagin	4000	6.54×10^{-4}	4.19	35	144	1.5	N/A
Shumagin	4501	1.16×10^{-3}	2.36	50	151	1.5	5.36
Shumagin	4601	2.66×10^{-4}	10.3	45	153	1.5	N/A
Shumagin	4700	3.81×10^{-4}	7.19	51	153	1.5	5.46
Shumagin	4749	2.97×10^{-4}	9.21	52	154	1.5	N/A
Shumagin	4800	7.49×10^{-4}	3.66	59	154	1.5	5.49
Shumagin	4823	3.36×10^{-4}	8.15	23	154	1.5	5.31
Shumagin	30	1.98×10^{-3}	1.38	21	312	1.9	1.86
Shumagin	651	4.03×10^{-4}	6.80	19	15	3.5	5.12
Sanak	1001	3.81×10^{-4}	7.19	5.4	17	2.9	5.18
Sanak	1501	4.40×10^{-3}	0.623	10	34	2.3	N/A
Sanak	1700	1.93×10^{-4}	14.2	10	42	2.1	N/A
Sanak	1800	3.24×10^{-4}	8.46	20	47	2.1	N/A
Sanak	1900	3.17×10^{-4}	8.64	72	54	2.0	4.97
Sanak	1972	4.50×10^{-4}	6.09	85	60	1.9	N/A
Sanak	1991	5.27×10^{-4}	5.20	322	63	1.9	4.93
Sanak	2010	6.73×10^{-4}	4.07	178	64	1.9	4.67

Chapter 5: Conclusions and Future Directions

This thesis explores how microbial methane oxidation shapes redox gradients, controls methane flux, and links biogeochemical processes across diverse aquatic settings, ranging from a Proterozoic Ocean analog to modern cold seeps. Chapter 2 examines the water column of Fayetteville Green Lake under low oxygen and euxinic conditions to show how methane oxidation interacts with sulfur, nitrogen, and iron cycles and to infer its potential role in Mesoproterozoic oxygen dynamics. Chapters 3 and 4 focus on water column methane oxidation in modern cold seep environments, where methanotrophic communities and activity define a spatially distributed methanosphere, refining the broader ecological and biogeochemical influence of these dynamic ecosystems. My primary contribution is elucidating how water column methanotroph abundance and activity are governed by vertical and lateral transport and by oxygen and methane availability within the environment. In this chapter, I synthesize the major outcomes of each research chapter, identify emergent cross-system themes, discuss methodological insights, and propose future work that extend beyond the individual manuscripts.

For Chapter 2, the Fayetteville Green Lake study revealed that metabolically flexible aerobic methanotrophs can likely oxidize methane under strongly reducing, euxinic conditions, a finding that challenges conventional redox constraints on aerobic methane oxidation. Methane oxidation co-occurred with high sulfate-reduction rates and monomethylamine-based methanogenesis, forming a dynamic methane cycle under euxinic conditions. Aerobic methanotrophs, including *Crenothrix* and members within *Methylacidiphilales*, were detected in euxinic water, consistent with potentially denitrification- or fermentation-linked methane oxidation

(Awala et al., 2024; Oswald et al., 2017; Schorn et al., 2024). Although aerobic methanotrophy accounted for only ~4% of total oxygen demand, its targeted consumption in this narrow redox interface played a disproportionate role in limiting vertical methane transport. This methane oxidation, in concert with high microbial sulfate reduction rates that generated substantial sulfide flux, helped maintain the vertical redox structure of the lake. The accumulation of sulfide created a chemically reduced barrier that suppressed oxygen penetration, such that microbial activity not only controlled methane availability but also reinforced euxinic conditions by buffering the water column against oxygen intrusion through sustained reductant production.

These findings advance current models of the Mesoproterozoic Ocean by revealing how tightly coupled microbial processes, particularly involving sulfur, nitrogen, and methane, may have actively structured redox stratification and stabilized oxygen-deficient conditions. Rather than viewing the mid-Proterozoic solely as a consequence of nutrient scarcity or slow oxygen production, this work highlights the role of microbial feedbacks in reinforcing and maintaining geochemical gradients over time. The detection of metabolically versatile aerobic methanotrophs within the euxinic water column, where high rates of methane oxidation coincided, extends the functional reach of the aerobic methane filter beyond traditional oxic boundaries and highlights the potential for alternative metabolic strategies that bridge redox transitions. This expands the conceptual framework for methane cycling in ancient oceans and suggests that steep, fluctuating redox gradients may have exerted selective pressure on early methanotrophs. Such conditions may have favored the evolution of non-classical metabolic pathways, that enabled survival and activity in transitional redox zones. Supporting this view, genomic evidence suggests that aerobic methanotrophs evolved from methylotrophs, a transition thought to have occurred independently

multiple times (Kang et al., 2019; Khadka et al., 2018; Osborne & Haritos, 2018), likely indicating strong evolutionary plasticity in response to environmental pressures.

The co-occurrence of methane oxidation and methylotrophic methanogenesis below the chemocline points to the potential for cryptic methane cycling in the euxinic water column, although the predominance of methane oxidation indicates that most methane is rapidly consumed *in situ* (Krause & Treude, 2021; Maltby et al., 2016; Maltby et al., 2018; Xiao et al., 2017; Xiao et al., 2018). In Green Lake, this tightly coupled internal loop likely constrains methane build-up and vertical flux, acting as a self-regulating buffer that stabilizes water column redox structure. Water column cryptic cycles remain poorly characterized compared with their sedimentary counterparts, particularly in meromictic, low sulfate, lakes where non-competitive pathways such as monomethylamine-based methanogenesis may flourish. Future work should employ ^{14}C-labelled monomethylamine incubations combined with biomass filtration to quantify assimilation versus oxidation of methylated substrates; when paired with parallel nucleic-acid extraction and taxon-specific molecular assays, such experiments can pinpoint the microbes actively driving this hidden methane source. Clarifying the environmental triggers, spatial extent, and turnover rates of water column cryptic cycling will refine methane budget estimates for both modern systems and Proterozoic analogs.

As the Proterozoic likely encompassed both iron-rich and sulfide-rich basins, dependent on spatial and temporal scales (Lyons et al., 2024), future work should explore whether similar mechanisms operate under ferruginous conditions, and whether methane oxidation coupled to iron or nitrate reduction could have reinforced redox stability in those settings. Integrating metatranscriptomics and stable isotope labeling in modern analogs like Lake Cadagno (Philippi et al., 2021) or ferruginous lakes such as Lake Montano (Crowe et al., 2011) may help confirm novel

methane oxidation pathways and quantify their energetics. The availability of methane oxidation rate data, geochemical concentrations, and electron-equivalent fluxes from Green Lake also offers an opportunity to incorporate microbial methane cycling into Earth system models of the Proterozoic Ocean. Such work would provide essential constraints on the resilience, flexibility, and biogeochemical significance of methane-oxidizing microbial communities in early Earth environments on the biosphere. Moreover, integrating these empirically constrained methane-oxidation dynamics into coupled climate–photochemistry frameworks will improve predictions of redox-disequilibrium biosignatures (e.g., CH_4–O_2 coexistence) and thereby refine habitability assessments for exoplanetary atmospheres.

The Southern California Borderland seep study (Chapter 3) demonstrates that aerobic methane oxidation in cold seep-impacted waters is not confined to discrete benthic vent fields but extends vertically and laterally into the water column, forming a diffuse and dynamic oxidation zone. Elevated methane oxidation rates observed 0.5 m above targeted microbial mats and bubble plumes, as well as 10–30 m above the seafloor in CTD/rosette system casts, indicate that localized methane inputs stimulate microbial activity both directly at the seafloor and within the overlying water column. This vertical layering likely reflects the upward transport of methane via bubble-mediated flux (Jordan et al., 2020) and advection, generating localized methane maxima that intersect with low-oxygen bottom waters, promoting methanotrophic activity. At Santa Monica Mound, where bottom waters were persistently hypoxic (<5 µM), methane concentrations, oxidation rates, and *pmoA* gene abundance were strongly aligned, pointing to an active, substrate-responsive methanotrophic community. In contrast, the weaker coupling between methane, oxidation, and *pmoA* at Del Mar and Lasuen Knoll points to physical decoupling between microbial communities and geochemical gradients, possibly driven by episodic seepage, variable bottom

currents, or time lags in methanotroph or methane accumulation. These patterns indicate that the methanosphere is not a static feature, but a dynamic, transport-influenced system whose structure and activity are modulated by both physical processes and microbial ecological response time. In more transient systems, oxidation potential may lag methane delivery, temporarily constrain the biological filter and permit greater methane escape. Yet, the observation that oxidation rates can remain elevated even when *pmoA* gene abundance is low suggests that methanotrophs may maintain activity during dispersal or persist in a low-abundance or potentially dormant state capable of rapid metabolic activation upon methane exposure (Roslev & King, 1994). Additionally, indications of elevated oxidation and methane concentrations at off-seep locations support the notion of geochemical and microbial seeding, where methane and methanotrophs are redistributed laterally from active vent zones. This pattern underscores the spatial flexibility of the methanosphere, suggesting that methane oxidation is not solely constrained by microbial standing stock at seep sources, but can extend into surrounding waters through dispersal and localized activation, shaped by methane delivery, oxygen gradients, and physical transport. Similarly, studies have demonstrated that while methane concentrations decrease with distance from the Santa Monica Mound, methanotroph gene abundance and expression do not show a corresponding decline, implying the persistence of the methanotrophic community (Ussler III et al., 2013).

Chapter 4 reveals that aerobic methane oxidation at high-latitude seeps occurs across well-oxygenated, and in many instances, low-methane water masses. At Edge, Shumagin, and Sanak seeps in the Gulf of Alaska, methane oxidation exhibited a vertically layered structure, echoing patterns observed off the Southern California margin. However, unlike the Southern California sites, where bottom-water hypoxia likely enhances oxidation efficiency, Alaskan seeps demonstrate that methane oxidation can remain robust, and in some occurrences, positively corelated with

oxygen even under fully oxygenated conditions. Notably, at Edge, a midwater methane oxidation maximum occurred around 2000 m depth, near the base of the oxygen minimum zone. This feature likely reflects localized methane enrichment or delivery of labile organic substrates via sinking phytodetritus, diverging from the more typical seafloor-associated oxidation signal. Such midwater activity highlights the influence of vertical carbon fluxes and particle-driven methane transport in fueling oxidation at depth, independent of benthic seepage. More broadly, these findings suggest that methanotrophy at high-latitude seeps is not constrained by oxygen or gene abundance alone, but instead reflects a spatially flexible, transport-modulated system shaped by dynamic methane inputs and microbial dispersal.

Across both systems, the Southern California Margin and the Gulf of Alaska, methane oxidation was not confined to the benthic zone but instead occurred in vertically stratified envelopes that extended tens of meters above the seafloor. Between seeps, these oxidation layers, varied in thickness, intensity, and lateral extent depending on physical transport processes and local methane and oxygen concentrations. Oxidation efficiency was not governed solely by the absolute concentrations of methane or oxygen, but more likely by their ratio, the rate and mode of methane delivery, and the ecological and physiological history of the methanotrophic community. Notably, methane oxidation also persisted in low-methane surface waters at both Southern California and Alaska seep sites, driven by the consumption of methane produced aerobically from algal-derived compounds (Damm et al., 2010; Karl et al., 2008; Klintzsch et al., 2019). These observations support the presence of a cryptic methane cycle in productive surface waters, potentially widespread globally but underrecognized.

In parallel, consistent differences in bacterial methanotroph community composition were observed between the two regions. Southern California seeps hosted a more diverse suite of known

or putative methanotrophic genera, including members within Methylomonadacaeae (IheB2–23, Marine Methylotrophic Group 2, *Methyloprofundus*, Milano-WF1B-03, and pitb-vmat-59) that were absent from the Alaskan water column. In contrast, Alaskan seeps were dominated by a narrower set of MOB taxa (IheB2–23, and Milano-WF1B-03). This reduced diversity may reflect regional differences in physical constraints (temperature and pressure), water mass history, or biogeochemical structure, but it also raises broader questions about the ecological flexibility and resilience of methanotrophic assemblages.

Although methane concentrations and oxidation rates at Edge and Shumagin were generally lower than those at the Southern California seeps, the Sanak site displayed methane levels and microbial activity comparable to Santa Monica Mound, albeit with more pronounced spatial heterogeneity. These patterns suggest that biogeographic divergence is not easily explained by methane concentration or oxidation alone. Instead, differences in methanotroph diversity and structure likely arise from a combination of environmental selection, dispersal limitation, and functional redundancy (Hanson et al., 2012). Future comparative studies spanning gradients in oxygen, methane, temperature, depth, and circulation dynamics will be critical to disentangling the environmental and ecological controls on methanotroph distribution and adaptation.

In future work, a critical challenge is to determine how methanotrophic communities will respond to an ocean with stronger stratification, episodic deoxygenation, and elevated methane or organic-matter inputs. The ability of methanotrophs to function across heterogeneous and dynamic environments will be important to sustaining the marine methane filter. However, the idiosyncratic behavior of individual seeps, even among those with similar depths or fluxes, underscores the limitations of extrapolating broadly across systems. Constraining the full extent of the methanosphere will require fine-scale vertical sampling (<5 m intervals), systematic lateral

sampling to track dilution and dispersal, and autonomous sensing technologies capable of capturing transient methane and oxygen fluctuations. These tools will help resolve the spatial and temporal variability of methanotrophic activity and improve our predictive understanding of how the methanosphere mediates marine carbon cycling and ecosystem functioning under changing environmental conditions.

From a methodological perspective, this work also highlighted important limitations in standard microbial community surveys. Amplicon-based 16S rRNA sequencing often failed to detect aerobic methanotrophs, even in samples with positive methane oxidation rates and elevated *pmoA* gene copy numbers. This likely reflects both the low relative abundance of methanotrophs in bulk microbial assemblages, since their transcriptional activity can exceed their representation in 16S rRNA amplicon data (Galambos et al., 2019), and the limited taxonomic resolution of short-read amplicons. In contrast, qPCR targeting the functional marker gene pmoA provided a higher-resolution, more sensitive proxy for methanotroph abundance and was more strongly correlated with measured oxidation rates. These results emphasize the value of pairing functional gene assays with activity measurements to detect low abundance but biogeochemically impactful microbial groups. Moving forward, integrating metagenomic, metatranscriptomic, and single-cell genomic approaches will further improve the taxonomic and functional resolution of methane-cycling communities and help identify novel or pmoA-negative aerobic methanotrophs whose contributions remain poorly constrained (Tchawa Yimga et al., 2003).

Collectively, this dissertation demonstrates that water column methane oxidation is a resilient and ecologically integrative process that shapes the redox structure of stratified water columns, modulates methane fate, and contributes to the organization of aquatic ecosystems across a wide range of environmental regimes. Through investigations of a permanently stratified, sulfidic

lake and of fully oxygenated and low-oxygen marine seeps, this work reveals that bacterial methanotrophs persist across steep redox gradients, adapt to diverse metabolic niches, and influence biogeochemical processes beyond the sediment–water interface. These findings reframe water column methane oxidation not as a passive sink, but as a dynamic ecological scaffold that structures microbial communities and biogeochemical processes across aquatic ecosystems from Earth's deep past to its present oceans.

References

Awala, S. I., Gwak, J.-H., Kim, Y., Jung, M.-Y., Dunfield, P. F., Wagner, M., & Rhee, S.-K. (2024). Nitrous oxide respiration in acidophilic methanotrophs. *Nature communications*, *15*(1), 4226.

Crowe, S., Katsev, S., Leslie, K., Sturm, A., Magen, C., Nomosatryo, S., Pack, M., Kessler, J., Reeburgh, W., & Roberts, J. (2011). The methane cycle in ferruginous Lake Matano. *Geobiology*, *9*(1), 61-78.

Damm, E., Helmke, E., Thoms, S., Schauer, U., Nöthig, E., Bakker, K., & Kiene, R. (2010). Methane production in aerobic oligotrophic surface water in the central Arctic Ocean. *Biogeosciences*, *7*(3), 1099-1108.

Galambos, D., Anderson, R. E., Reveillaud, J., & Huber, J. A. (2019). Genome-resolved metagenomics and metatranscriptomics reveal niche differentiation in functionally redundant microbial communities at deep-sea hydrothermal vents. *Environmental Microbiology*, *21*(11), 4395-4410.

Hanson, C. A., Fuhrman, J. A., Horner-Devine, M. C., & Martiny, J. B. (2012). Beyond biogeographic patterns: processes shaping the microbial landscape. *Nature Reviews Microbiology*, *10*(7), 497-506.

Jordan, S. F., Treude, T., Leifer, I., Janßen, R., Werner, J., Schulz-Vogt, H., & Schmale, O. (2020). Bubble-mediated transport of benthic microorganisms into the water column: Identification of methanotrophs and implication of seepage intensity on transport efficiency. *Scientific reports*, *10*(1), 4682.

Kang, C. S., Dunfield, P. F., & Semrau, J. D. (2019). The origin of aerobic methanotrophy within the Proteobacteria. *FEMS microbiology letters*, *366*(9), fnz096.

Karl, D. M., Beversdorf, L., Björkman, K. M., Church, M. J., Martinez, A., & Delong, E. F. (2008). Aerobic production of methane in the sea. *Nature Geoscience*, *1*(7), 473-478.

Khadka, R., Clothier, L., Wang, L., Lim, C. K., Klotz, M. G., & Dunfield, P. F. (2018). Evolutionary history of copper membrane monooxygenases. *Frontiers in Microbiology*, *9*, 2493.

Klintzsch, T., Langer, G., Nehrke, G., Wieland, A., Lenhart, K., & Keppler, F. (2019). Methane production by three widespread marine phytoplankton species: release rates, precursor compounds, and potential relevance for the environment. *Biogeosciences*, *16*(20), 4129-4144.

Krause, S. J., & Treude, T. (2021). Deciphering cryptic methane cycling: Coupling of methylotrophic methanogenesis and anaerobic oxidation of methane in hypersaline coastal wetland sediment. *Geochimica et Cosmochimica Acta*, *302*, 160-174.

Lyons, T. W., Tino, C. J., Fournier, G. P., Anderson, R. E., Leavitt, W. D., Konhauser, K. O., & Stüeken, E. E. (2024). Co-evolution of early Earth environments and microbial life. *Nature Reviews Microbiology*, *22*(9), 572-586.

Maltby, J., Sommer, S., Dale, A. W., & Treude, T. (2016). Microbial methanogenesis in the sulfate-reducing zone of surface sediments traversing the Peruvian margin. *Biogeosciences*, *13*(1), 283-299.

Maltby, J., Steinle, L., Löscher, C. R., Bange, H. W., Fischer, M. A., Schmidt, M., & Treude, T. (2018). Microbial methanogenesis in the sulfate-reducing zone of sediments in the Eckernförde Bay, SW Baltic Sea. *Biogeosciences*, *15*(1), 137-157.

Osborne, C. D., & Haritos, V. S. (2018). Horizontal gene transfer of three co-inherited methane monooxygenase systems gave rise to methanotrophy in the Proteobacteria. *Molecular phylogenetics and evolution*, *129*, 171-181.

Oswald, K., Graf, J. S., Littmann, S., Tienken, D., Brand, A., Wehrli, B., Albertsen, M., Daims, H., Wagner, M., & Kuypers, M. M. (2017). Crenothrix are major methane consumers in stratified lakes. *The ISME journal*, *11*(9), 2124-2140.

Philippi, M., Kitzinger, K., Berg, J. S., Tschitschko, B., Kidane, A. T., Littmann, S., Marchant, H. K., Storelli, N., Winkel, L. H., & Schubert, C. J. (2021). Purple sulfur bacteria fix N2 via molybdenum-nitrogenase in a low molybdenum Proterozoic ocean analogue. *Nature communications*, *12*(1), 4774.

Roslev, P., & King, G. M. (1994). Survival and recovery of methanotrophic bacteria starved under oxic and anoxic conditions. *Applied and Environmental Microbiology*, *60*(7), 2602-2608.

Schorn, S., Graf, J. S., Littmann, S., Hach, P. F., Lavik, G., Speth, D. R., Schubert, C. J., Kuypers, M. M., & Milucka, J. (2024). Persistent activity of aerobic methane-oxidizing bacteria in anoxic lake waters due to metabolic versatility. *Nature communications*, *15*(1), 5293.

Tchawa Yimga, M., Dunfield, P. F., Ricke, P., Heyer, J. r., & Liesack, W. (2003). Wide distribution of a novel pmoA-like gene copy among type II methanotrophs, and its expression in Methylocystis strain SC2. *Applied and Environmental Microbiology*, *69*(9), 5593-5602.

Ussler III, W., Preston, C., Tavormina, P., Pargett, D., Jensen, S., Roman, B., Marin III, R., Shah, S. R., Girguis, P. R., & Birch, J. M. (2013). Autonomous application of quantitative PCR in the deep sea: in situ surveys of aerobic methanotrophs using the deep-sea environmental sample processor. *Environmental science & technology*, *47*(16), 9339-9346.

Xiao, K.-Q., Beulig, F., Kjeldsen, K. U., Jørgensen, B. B., & Risgaard-Petersen, N. (2017). Concurrent methane production and oxidation in surface sediment from Aarhus Bay, Denmark. *Frontiers in microbiology*, *8*, 1198.

Xiao, K. Q., Beulig, F., Røy, H., Jørgensen, B. B., & Risgaard-Petersen, N. (2018). Methylotrophic methanogenesis fuels cryptic methane cycling in marine surface sediment. *Limnology and Oceanography*, *63*(4), 1519-1527.